

Non-invasive Assessment of Small Airway Obstruction in Asthma

**Thesis submitted for the degree of
Doctor of Philosophy
at the University of Leicester**

by

**Sherif Gonem BM BSc MRCP
Department of Infection, Immunity and Inflammation
University of Leicester**

February 2015

Non-invasive Assessment of Small Airway Obstruction in Asthma

Sherif Gonem

Abstract

Small airway inflammation and remodelling occurs in asthma and may underpin disease persistence, since conventional inhaled treatments do not penetrate to the small airway compartment. There is an important unmet need for reliable and non-invasive methods to measure small airway obstruction. This thesis describes the development and validation of such methods, with a particular focus on the multiple breath inert gas washout (MBW) technique. *In vitro* validation of the sulphur hexafluoride wash-in technique for performing MBW demonstrated that the method yields accurate and repeatable results. We developed novel methods for analysing inert gas washout curves, and showed that the parameters derived are repeatable, capture the full information content of the curve, and may be superior to standard parameters in distinguishing between subphenotypes of airway diseases. MBW and impulse oscillometry (IOS) parameters were found to be repeatable within-visit, but IOS parameters displayed greater stability over time. IOS parameters were independent predictors of asthma symptoms, quality of life and exacerbation frequency, suggesting that IOS may add value to spirometry in the assessment of patients with asthma. The response of small airway biomarkers to an intervention was assessed within a clinical trial of a novel anti-eosinophilic agent. Significant treatment effects were observed with respect to spirometric airflow obstruction and air trapping, as well as with a number of MBW parameters. The structural correlates of ventilation heterogeneity in asthma were examined using hyperpolarised ³helium magnetic resonance and quantitative computed tomography. There was evidence for a structural abnormality in the pulmonary acinus in patients with asthma causing subtle alterations in diffusion within this compartment. Future studies should seek to further understand the structural basis of IOS and MBW parameters through computational modelling and the coupling of physiological measurements and functional imaging. Longitudinal studies are also required to assess the long-term significance of small airway biomarkers.

Acknowledgements

I would like to thank the patients and healthy volunteers who willingly gave up their time to make this work possible.

I would like to thank my supervisors Dr. Salman Siddiqui and Prof. Chris Brightling for their mentoring and support over the past three years, and for encouraging me to develop my own research ideas.

This work could not have been carried out without the help of many people both within and outside the Department. I would like to thank the research nurses who were involved in my studies, Beverley Hargadon, Kate Hadley, Marcia Soares, and in particular Amisha Singapuri and Michelle Bourne for going above and beyond the call of duty on countless occasions to help deliver our interventional trial.

I would like to thank my colleagues Rachid Berair, without whose help the interventional trial would not have been the success it was, and Ruth Hartley for performing the CT analysis. I would also like to thank Sushiladevi Natarajan, Alys Scadding, Steven Corkill and Dhananjay Desai for their help with patient characterisation and physiological measurements, and Nisha Rana for performing the induced sputum cell counts.

I would like to thank the many external collaborators I have worked with over the past three years, in particular Per Gustafsson for his help with multiple breath inert gas washout, and for kindly accommodating me at his house in Skövde while we validated our system; Florian Singer for his help with the lung phantom validation experiments; John Owers-Bradley and his team Iain Ball, Steven Hardy and Niels Buhl for performing the magnetic resonance measurements reported in this thesis; and Alex Horsley for kindly providing me with his multiple breath washout data in cystic fibrosis patients.

I would like to acknowledge the funding I have received from the AirPROM consortium, Novartis, Chiesi and Roche, and to thank our industry contacts Richard Kay and Rino Costanza.

Finally, I would like to thank my family for their love, encouragement and support, in particular my parents Nabil and Hoda, my sisters Sarah and Rania, my wife Shaymaa and my daughter Mariam.

Statement of work personally performed

I have been intellectually involved in the development of all the studies reported in this thesis, including writing scientific protocols and assisting with ethics applications and amendments. I performed all statistical analysis of data presented in this thesis, interpreted the data and wrote the resulting manuscripts. I travelled to Skövde, Sweden to undertake validation of our multiple breath washout system using a lung model built by Dr. Per Gustafsson. I performed these validation experiments under Dr. Gustafsson's supervision and carried out all the data extraction and analysis. I independently developed novel multiple breath washout parameters and validated these using our own multiple breath washout data and raw data kindly provided to me by Dr. Alex Horsley in patients with cystic fibrosis. I performed 50% of our multiple breath washout tests and analysed 100% of the washout curves reported in this thesis. I took a major role in the clinical characterisation of patients in each of my studies, including the collection of clinical and demographic details, physical examination, and the performance of spirometry, impulse oscillometry, sputum induction, and measurement of exhaled nitric oxide. I was the main sub-investigator on the clinical trial of a CRTH2 receptor antagonist, and was in charge of the day-to-day running of the trial, together with the research nurses, and coordinated the recruitment effort.

Publications arising from this thesis

Original research articles

Gonem S et al. Randomized controlled trial of the prostaglandin D2 receptor antagonist QAW039 in persistent eosinophilic asthma. *Manuscript in preparation*.

Gonem S, Hardy S, Buhl N, Hartley R, Soares M, Kay R, Costanza R, Gustafsson P, Brightling CE, Owers-Bradley J, Siddiqui S. Characterisation of acinar airspace involvement in patients with asthma using non-invasive methods. *Manuscript in preparation*.

Gonem S, Singer F, Corkill S, Singapuri A, Siddiqui S, Gustafsson P. Validation of a photoacoustic gas analyser for the measurement of functional residual capacity using multiple breath inert gas washout. *Respiration*. 2014; 87(6): 462-8.

Gonem S, Scadding A, Soares M, Singapuri A, Gustafsson P, Ohri C, Range S, Brightling CE, Pavord I, Horsley A, Siddiqui S. Lung clearance index in adults with non-cystic fibrosis bronchiectasis. *Respir Res*. 2014 May 18; 15: 59.

Gonem S, Natarajan S, Desai D, Corkill S, Singapuri A, Bradding P, Gustafsson P, Costanza R, Kajekar R, Parmar H, Brightling CE, Siddiqui S. Clinical significance of small airway obstruction markers in patients with asthma. *Clin Exp Allergy*. 2014; 44(4): 499-507.

Gonem S, Corkill S, Singapuri A, Gustafsson P, Costanza R, Brightling CE, Siddiqui S. Between-visit variability of small airway obstruction markers in patients with asthma. *Eur Respir J*. 2014; 44(1): 242-4.

Review articles

Gonem S, Raj V, Wardlaw AJ, Pavord ID, Green R, Siddiqui S. Phenotyping airways disease: An A to E approach. *Clin Exp Allergy*. 2012; 42(12): 1664-83.

Siddiqui S, **Gonem S**, Wardlaw AJ. Advances in the management of severe asthma. *Semin Respir Crit Care Med*. 2012; 33(6): 666-84.

Brightling CE, Gupta S, **Gonem S**, Siddiqui S. Lung damage and airway remodelling in severe asthma. *Clin Exp Allergy*. 2012; 42(5): 638-49.

Gonem S, Desai D, Siddiqui S, Brightling CE. Evidence for phenotype-driven treatment in asthmatic patients. *Curr Opin Allergy Clin Immunol*. 2011; 11(4): 381-5.

Abstracts and prizes

As a result of the work presented in this thesis I have presented 13 abstracts at European Respiratory Society and British Thoracic Society meetings. In 2014 I was awarded the ERS Excellence Grant in Clinical Physiology and Exercise, and won the Best Abstract Competition award.

Contents

1 Introduction

1.1	Overview.....	18
1.2	Small airway disease in asthma.....	20
1.3	Non-invasive physiological tests of small airway obstruction	
1.3.1	<i>Spirometry</i>	24
1.3.2	<i>Lung volumes</i>	27
1.3.3	<i>Forced oscillation technique</i>	28
1.3.4	<i>Multiple breath inert gas washout</i>	34
1.4	Imaging techniques for the assessment of small airway structure	
1.4.1	<i>Morphometry of the human airway tree</i>	43
1.4.2	<i>Quantitative computed tomography</i>	44
1.4.3	<i>Hyperpolarised noble gas magnetic resonance imaging</i>	45
1.5	Aims and hypotheses.....	48

2 Methods

2.1	Spirometry.....	51
2.2	Measurement of lung volumes using body plethysmography.....	51
2.3	Single breath determination of carbon monoxide uptake in the lung.....	52
2.4	Impulse oscillometry.....	52
2.5	Multiple breath inert gas washout.....	54
2.6	Validation of multiple breath washout technique using a lung model.....	61
2.7	Development of novel multiple breath washout parameters.....	65
2.8	Quantitative computed tomography.....	78
2.9	Hyperpolarised ³ helium diffusion magnetic resonance.....	78

3 Studies

3.1	Validation of a photoacoustic gas analyser for the measurement of functional residual capacity using multiple breath inert gas washout.....	86
3.2	Specific ventilation inequality and dead space components of lung clearance index in patients with cystic fibrosis and non-cystic fibrosis bronchiectasis.....	100
3.3	Between-visit variability of small airway obstruction markers in patients with asthma.....	125
3.4	Clinical significance of small airway obstruction markers in patients with asthma.....	133
3.5	Characterisation of acinar airspace involvement in patients with asthma using hyperpolarised ³ He magnetic resonance and quantitative computed tomography.....	160
3.6	Randomised controlled trial of the prostaglandin D2 receptor antagonist QAW039 in persistent eosinophilic asthma.....	179

4 Conclusions

4.1	Summary of findings.....	204
4.2	Future work.....	206

List of tables

3.1	List of multiple breath washout validation experiments performed with results.....	93
3.2	Demographic and physiological data across healthy controls, cystic fibrosis patients and non-cystic fibrosis bronchiectasis patients.....	107
3.3	Correlations between multiple breath washout parameters.....	113
3.4	Physiological parameters in patients with and without chronic bacterial colonisation.....	115
3.5	Within-visit repeatability of multiple breath washout parameters in cystic fibrosis and non-cystic fibrosis bronchiectasis.....	116
3.6	Between- and within-visit variability of physiological variables in patients with asthma.....	130
3.7	Sample size calculations for impulse oscillometry and inert gas washout parameters.....	132
3.8	Physiological interpretation of airway obstruction markers.....	137
3.9	Demographic and clinical data across asthma severity groups.....	143
3.10	Physiological data across asthma severity groups.....	144
3.11	Correlations between clinical outcome measures and physiological variables.....	146
3.12	Linear regression models assessing the contributions of physiological variables to ACQ-6 and AQLQ(S) scores.....	148

3.13	Demographic and physiological variables in exacerbation-prone and non-exacerbation-prone patients with asthma.....	149
3.14	Demographic and clinical characteristics of participant groups in magnetic resonance study.....	167
3.15	Physiological data across participant groups in magnetic resonance study.....	169
3.16	Baseline Characteristics of Subjects in the Intention-to-Treat Population.....	188
3.17	Outcome Measures at Baseline and Post-Treatment in the Per-Protocol Population.....	195
3.18	Outcome Measures at Baseline and Post-Treatment in the Intention-to-Treat Population.....	198

List of figures

1.1	Resistance and reactance within the frequency and time domains.....	30
1.2	Inert gas washout curve from a healthy subject.....	36
1.3	Graph of SF ₆ concentration against expired volume during a single exhalation.....	40
2.1	Innocor photoacoustic gas analyser.....	56
2.2	Patient interface for the performance of multiple breath inert gas washout.....	56
2.3	Calculation of phase III slope parameters.....	60
2.4	Schematic diagram of lung model for the validation of multiple breath washout technique.....	62
2.5	Photograph of lung model for the validation of multiple breath washout technique.....	63
2.6	Exponential decay curves.....	67
2.7	Washout curves from a healthy subject and a patient with cystic fibrosis fitted to a two-phase exponential decay model.....	69
2.8	Simulated washout curves.....	71
2.9	Magnetic resonance pulse sequences for measuring diffusion in the lungs.....	83
3.1	Inert gas washout curve of an acrylic glass lung model.....	90

3.2	Bland-Altman plots of calculated versus measured functional residual capacity.....	94
3.3	Error in lung clearance index against calculated functional residual capacity.....	96
3.4	Multiple breath washout parameters across groups.....	109
3.5	Correlations between lung clearance index and FEV ₁ (% predicted).....	112
3.6	Receiver operating characteristic curves of lung clearance index and FEV ₁ (% pred.) for distinguishing between control subjects and bronchiectasis patients.....	117
3.7	Scatterplots of forced expiratory volume in one second standardised residuals against multiple breath washout parameters in patients with non-cystic fibrosis bronchiectasis.....	118
3.8	Scatterplots of forced expiratory volume in one second standardised residuals against small airway obstruction markers in patients with asthma.....	151
3.9	Pie charts showing proportions of patients with concordance or discordance between forced expiratory volume in one second and small airway obstruction markers.....	154
3.10	Quantitative computed tomography densitometry between groups.....	171
3.11	Apparent diffusion coefficients (ADC) across groups.....	172
3.12	Correlations between ³ He-MR, CT and physiological variables in patients with asthma.....	173

3.13	Change in apparent diffusion coefficient (%) against change in volume of gas in the lungs (%) in healthy subjects and patients with asthma.....	174
3.14	QAW039 study protocol.....	183
3.15	Number of patients who were screened, randomised and completed the study up to the post-treatment visit.....	187
3.16	Changes from baseline to mid-treatment, post-treatment and post-washout visits with respect to main outcomes in the per protocol population.....	193
3.17	Changes from baseline to post-treatment and post-washout visits with respect to lung clearance index and resistance at 5Hz in the per protocol population.....	194

Abbreviations

ACQ	Asthma Control Questionnaire
ADC	Apparent diffusion coefficient
AHR	Airway hyperresponsiveness
AQLQ	Asthma Quality of Life Questionnaire
ATS	American Thoracic Society
AX	Reactance area
BDP	Beclometasone dipropionate
BMI	Body mass index
BTPS	Body temperature and pressure, saturated
CDI	Convection-dependent inhomogeneity
C_{et}	End-expiratory inert gas concentration
CEV	Cumulative expired volume
CF	Cystic fibrosis
COPD	Chronic obstructive pulmonary disease
CoV	Coefficient of variation
CRTH2	Chemoattractant Receptor-homologous molecule expressed on Th2 cells
CT	Computed tomography
DCDI	Diffusion-convection-dependent inhomogeneity
DLCO	Diffusing capacity of the lung for carbon monoxide
DS_{eq}	Equipment dead space
EPAP	Expiratory positive airway pressure
ERS	European Respiratory Society
FAO	Fixed airflow obstruction
$FeNO_{50}$	Fractional exhaled nitric oxide at 50ml/s
FEV_1	Forced expiratory volume in one second
FEV_3	Forced expiratory volume in three seconds
FID	Free induction decay
FOT	Forced oscillation technique
FRC	Functional residual capacity

FRC _{calc}	Functional residual capacity calculated from dimensions of lung model
FRC _{mbw}	Functional residual capacity calculated using multiple breath inert gas washout
FRC _{pleth}	Functional residual capacity measured with body plethysmography
fSAD	Functional small airway disease
FVC	Forced vital capacity
GINA	Global Initiative for Asthma
HU	Hounsfield Units
ICC	Intraclass correlation coefficient
ICS	Inhaled corticosteroid
IOS	Impulse oscillometry
IPAP	Inspiratory positive airway pressure
KCO	Carbon monoxide transfer coefficient
LABA	Long-acting β -agonist
LCI	Lung clearance index
LCI _{ds}	Dead space component of lung clearance index
LCI _{ideal}	Ideal lung clearance index
LCI _{vent}	Specific ventilation inequality component of lung clearance index
MBW	Multiple breath inert gas washout
MCID	Minimal clinically important difference
MLD E/I	Mean lung density expiratory/inspiratory ratio
MMEF	Maximal mid-expiratory flow
MRI	Magnetic resonance imaging
P ₁₅	Fifteenth lower percentile of inspiratory lung density
PG	Prostaglandin
PRM	Parametric response map
PsA	Pseudomonas aeruginosa
R20	Resistance at 20Hz
R5	Resistance at 5Hz
RB1	Right upper lobe apical segmental bronchus
Rc	Central airway resistance

RF	Radiofrequency
RL	Total lung resistance
RMS	Respiratory mass spectrometer
ROC	Receiver operating characteristic
Rp	Peripheral airway resistance
RV	Residual volume
S_{acin}	Acinar ventilation heterogeneity
SAO	Small airway obstruction
S_{cond}	Conductive ventilation heterogeneity
SD	Standard deviation
SE	Spin echo
SIII	Phase III slope
SnIII	Concentration-normalised phase III slope
SR	Standardised residual
STE	Stimulated echo
SVC	Slow vital capacity
TH ₂	T-helper 2
TLC	Total lung capacity
TO	Turnover
V _A	Alveolar volume
VC	Vital capacity
V _{D_{anat}}	Anatomical dead space
V _{D_{resp}}	Effective respiratory dead space
VH	Ventilation heterogeneity
V _T	Tidal volume
X5	Reactance at 5Hz

1 Introduction

1.1 Overview

Asthma is a chronic inflammatory airway disease that is estimated to affect 300 million people worldwide¹. The reported prevalence has been increasing for a number of decades, in association with worldwide trends towards urbanisation and the adoption of Western lifestyles¹. Asthma is estimated to cause 250,000 deaths² and the loss of 15 million disability-adjusted life years each year¹. The economic burden of asthma is no less severe, with direct and indirect costs totalling approximately €17.7 billion each year in Europe³. Severe asthma imposes a disproportionate economic burden, accounting for 50% of these costs but only 10-20% of patients with asthma³.

The Global Initiative for Asthma (GINA, 2012) defines asthma as follows²:

'Asthma is a chronic inflammatory disorder of the airways in which many cells and cellular elements play a role. The chronic inflammation is associated with airway hyperresponsiveness that leads to recurrent episodes of wheezing, breathlessness, chest tightness and coughing, particularly at night or in the early morning. These episodes are associated with widespread, but variable, airflow obstruction within the lung that is often reversible either spontaneously or with treatment.'

This definition emphasises the variable nature of airflow obstruction in asthma. However, it is known that patients with asthma may manifest incompletely reversible airflow obstruction akin to that seen in chronic obstructive pulmonary disease (COPD), and that this is associated with increased morbidity⁴. Indeed, it was suggested in 1961 that asthma and COPD were variants of the same disease⁵, a proposition that was later termed the 'Dutch hypothesis'. Whilst this view is controversial^{6,7}, it is increasingly recognised that a number of patients cannot be easily categorised into classical asthma and COPD groups, and that a significant overlap exists between the conditions, particularly with respect to airway physiology⁸. Bronchodilator responsiveness, a classical feature of asthma, occurs in a significant proportion of patients with a diagnosis of COPD⁹, as does airway hyperresponsiveness¹⁰. Conversely, many patients with asthma manifest a degree of fixed airflow obstruction (FAO) and accelerated lung function decline, traits that are usually associated with COPD^{4,11,12}. The mechanisms of

airflow limitation in asthma may include airway smooth muscle hypertrophy and airway remodelling^{13,14}, obstruction of the airways with mucus and inflammatory debris¹⁵, airway closure due to surfactant dysfunction¹⁶, or loss of alveolar attachments causing reduced lung elastic recoil¹⁷. Risk factors for FAO in asthma include cigarette smoking¹², severe exacerbations¹¹, duration of asthma¹⁸, and either eosinophilic¹⁹ or neutrophilic²⁰ airway inflammation.

It is widely recognised that asthma is a heterogeneous disorder rather than one single well-defined condition, a concept that dates back to the description by Rackemann in 1941 of a group of patients whose asthma did not appear to be driven by an extrinsic allergen, and who were therefore labelled as having ‘intrinsic asthma’²¹. In the past decade there has been a concerted effort to understand the subtypes of asthma, based upon observable clinical characteristics (phenotypes) or underlying biological mechanisms (endotypes)^{8,22-27}. This has been driven to a large extent by the emergence of high-cost asthma therapies that appear to be effective only in subgroups of asthma patients. For example, the anti-IL-5 monoclonal antibody mepolizumab did not produce statistically significant clinical benefits in an unselected asthma population²⁸, but was subsequently found to significantly reduce exacerbation frequency in patients with eosinophilic asthma^{29,30}. Similarly, in a trial of the anti-IL-13 monoclonal antibody lebrikizumab, patients with high serum periostin, a marker of T-helper 2 (TH₂) cell inflammation, had a significantly greater improvement in forced expiratory volume in one second (FEV₁) than those with low serum periostin³¹.

A clinical phenotype has been defined as:

‘a single or combination of disease attributes that describe differences between individuals as they relate to clinically meaningful outcomes (symptoms, exacerbations, response to therapy, rate of disease progression, or death.)’³²

According to this definition, to qualify as a clinical phenotype, a group of observable characteristics must be related to clinically important outcomes. Characteristics that do not fulfil this criterion are referred to as ‘phenotypic traits’. Well-described clinical phenotypes of asthma include early-onset atopic, late-onset eosinophilic, aspirin-intolerant and obesity-related⁸.

The small airways are usually defined as airways with an internal diameter of less than 2mm³³, comprising both the smaller conducting airways and the intra-acinar airways. The morphometry of the human airway tree is discussed in detail in Section 1.4.1. Whilst asthma has traditionally been thought of a disease of the larger airways, there is increasing interest in the role of small airway disease in this condition³³⁻³⁹. The potential importance of the small airways in asthma is two-fold: Firstly, since in health the small airways contribute only a small proportion of total airway resistance⁴⁰, disease in the small airways may be widespread before abnormalities are detectable using spirometry. Therefore, tests of small airway obstruction may provide a sensitive measure of early airway damage in asthma, and may allow intervention to be instituted before the development of FAO, with its associated morbidity. Secondly, small airway disease may underlie disease persistence in asthma, since standard inhaled corticosteroids (ICS) are deposited mainly in the larger conducting airways and do not penetrate to the more peripheral regions of the lung⁴¹. Persistent asthma, in which symptoms and/or airway inflammation are inadequately controlled despite topical therapy, imposes a disproportionate burden on individual patients and society, and is relatively common. Indeed, a large randomised controlled trial comparing ICS with combination ICS and long-acting β -agonist (LABA) only achieved total control of asthma at one year in 28% and 41% of patients respectively⁴². The causes of persistence are not completely understood but include poor patient adherence^{43,44}, inadequate inhaler technique⁴⁵ and corticosteroid resistance⁴⁶. A further possibility is that patients with persistent asthma have pathology in the small airways that standard topical therapy cannot reach³⁶. Thus, the detection of small airway disease may indicate the need for systemic therapies and/or small particle inhalers to be introduced.

1.2 Small airway disease in asthma

It has been suggested that small airway disease may define a distinct clinical phenotype of asthma³⁴. Evidence for small airway involvement in asthma comes from post-mortem specimens, lung biopsies (surgical or transbronchial), and direct measurement of peripheral airway resistance using semi-invasive physiological methods such as the wedged bronchoscope technique. Carroll *et al* examined post-mortem lung specimens from patients who had died of asthma (fatal asthma), those who had a history of asthma

but died of a non-respiratory cause (non-fatal asthma) and control subjects who died suddenly with no history of respiratory disease^{47,48}. They found that airway remodelling occurred throughout the bronchial tree in both fatal and non-fatal asthma cases⁴⁷. In particular, airway wall areas in the small membranous bronchioles (perimeter < 2mm) were significantly greater in both fatal and non-fatal asthma cases than in control subjects. Airway inflammation was also observed in both large and small airways⁴⁸. Lymphocytes were distributed within both large and small airway walls, in both fatal and non-fatal asthma cases, to a significantly greater extent than in controls. Eosinophils were distributed within both large and small airway walls, but to a greater extent in fatal asthma compared to non-fatal asthma or controls. Similarly, Faul *et al* observed an inflammatory infiltrate of CD8⁺ T-cells, eosinophils and macrophages in both the proximal and distal airways of patients who died suddenly of asthma⁴⁹. However, it is possible that the pathology seen in fatal asthma, which is relatively uncommon, may not be representative of the majority of asthma cases.

Surgical lung biopsies taken from patients with asthma showed increased numbers of T-cells and eosinophils in both large and small airway walls compared to non-asthmatic controls⁵⁰. Moreover, in patients with asthma, the number of activated eosinophils was greater in airways with an internal perimeter of < 2mm compared with those with an internal perimeter > 2mm, suggesting that eosinophilic airway inflammation in asthma is more severe in the peripheral than the central airways. Using transbronchial biopsies obtained at 4:00 am and 4:00 pm, Kraft *et al* showed that patients with nocturnal asthma exhibited greater numbers of alveolar tissue eosinophils⁵¹ and CD4⁺ T-cells⁵² at 4:00 am than patients with non-nocturnal asthma. Moreover, patients with nocturnal asthma had greater numbers of tissue eosinophils and macrophages at 4:00 am compared to 4:00 pm⁵¹. Wenzel *et al* observed greater numbers of neutrophils in transbronchial biopsies from patients with oral glucocorticoid-dependent severe asthma than in healthy control subjects⁵³. Balzar *et al* reported a significantly higher density of inflammatory cells in small airways compared to medium or large airways, in an analysis of paired endobronchial and transbronchial samples from 12 patients with severe oral corticosteroid-dependent asthma⁵⁴. Hauber *et al* showed that treatment with a small-particle ICS could attenuate eosinophilic inflammation in both the central and peripheral airways, with a concomitant increase in neutrophils⁵⁵. The same group subsequently showed that a 6-week course of small-particle ICS reduced expression of

alpha-smooth muscle actin in the peripheral airways, but did not attenuate collagen deposition or transforming growth factor- β expression⁵⁶. However, assessing small airway disease using transbronchial biopsies is not without limitations, most notably that non-diagnostic biopsies (ie. not containing viable small airways) are relatively common. From a total of 29 transbronchial biopsies performed by Balzar *et al*⁵⁴, only 45% contained airway tissue, and 28% contained small airways. Moreover, transbronchial biopsy carries a small but significant risk of causing bleeding or pneumothorax⁵⁷.

Peripheral airway resistance (R_p) was first measured by Macklem and Mead in 1967, using a retrograde catheter, in open-chested living dogs and excised lungs from a variety of species including humans⁵⁸. Their results suggested that R_p constitutes a relatively small proportion of total lung resistance (RL) in health. However, the retrograde catheter technique is too invasive to be used in living humans. The wedged bronchoscope technique for measuring R_p was introduced by Wagner *et al* in 1990⁵⁹. These investigators wedged a flexible bronchoscope into a segmental right upper lobe bronchus and passed a double-lumen catheter through the instrument port of the bronchoscope. Air was passed through one lumen of the catheter at three different flow rates, whilst pressure was measured using a transducer positioned within the second lumen. R_p was defined as pressure divided by flow, averaged over the three flow rates measured. Since the bronchoscope was tightly wedged, air could not escape proximally, and therefore must have been exiting the lung segment distal to the bronchoscope via collateral channels leading to adjacent lung segments. R_p measured using this technique therefore represents the resistance of both the airways distal to the bronchoscope and the collateral pathways leading out of the lung segment. The procedure was performed in six healthy volunteers and nine patients with asthma. The patients with asthma were found to have markedly raised R_p compared to healthy subjects, despite only minor differences in spirometry. The same technique was later used to show that peripheral airway responsiveness to histamine is increased in patients with asthma compared to normal subjects⁶⁰, and that the peripheral airways in patients with exercise-induced asthma are responsive to cool dry air⁶¹. These results suggested that the small airways make a significant contribution to airway hyperresponsiveness in asthma. Kaminsky *et al* later refined the wedged bronchoscope technique by analysing the decay in pressure that occurred upon cessation of airflow, as well as the plateau pressure that was reached

once this decay ceased⁶². They reasoned that cessation of airflow would cause a sudden pressure drop which would be reflective of the resistance of the small airways distal to the wedged bronchoscope, and that the subsequent slow decay in pressure would reflect the passive emptying of the distal lung segment through collateral channels. The plateau pressure would be indicative of the volume of air that was trapped in the lung segment by closure of collateral channels. In fact, the initial sudden drop in pressure was not observed in either normal or asthmatic subjects, leading the authors to conclude that R_p was related almost entirely to the resistance of collateral channels, and that the resistance of these channels was increased in patients with asthma. A subsequent study showed that in patients with nocturnal asthma, plateau pressure was higher at 4:00 am than at 4:00 pm, suggesting that there was diurnal variation in the patency of collateral channels in this group of patients⁶³. Three distinct types of collateral channel have been identified in human lungs⁶⁴, namely the alveolar pores of Kohn, and the epithelium-lined channels of Lambert and Martin, which respectively connect terminal bronchioles to alveoli or to other terminal bronchioles. These channels would potentially allow the movement of gas molecules by both convection and diffusion, and they may constitute important alternative pathways for ventilation in patients with emphysema⁶⁴. However, there have been no histological studies investigating how collateral channels are altered in asthma in order to account for their increased resistance.

A different technical approach to the same problem was taken by Yanai *et al*⁶⁵, who wedged a catheter-tipped micromanometer of 3mm diameter into a right lower lobe segmental bronchus. Pressure changes in the central airways during tidal breathing were recorded by a transducer lying proximal to the wedged portion of the catheter, and were used to calculate central airway resistance (R_c). RL was calculated using the oesophageal balloon technique of Mead and Whittenberger⁶⁶, and R_p was obtained by subtracting R_c from RL. The procedure was performed in 5 healthy controls, 20 patients with asthma (10 of whom had $FEV_1 < 70\%$ predicted), and 15 patients with COPD. The authors found that in patients with COPD, and in those with asthma and low FEV_1 , both RL and R_p were significantly higher compared to healthy controls, and that R_p was disproportionately raised. Specifically, R_p was approximately 25% of RL in healthy controls, and 50% of RL in patients with COPD, or asthma with low FEV_1 . The authors concluded that the peripheral airways were the major site of development of obstructive airway diseases. In a subsequent study using the same technique, the RL response to

methacholine was partitioned into Rc and Rp components in 10 patients with asthma⁶⁷. A variety of patterns of response were observed, with most patients manifesting a combination of Rc and Rp responses.

The methods described in this section may be useful for small-scale mechanistic research studies, but are too complex and invasive for routine clinical or research use. The development of methods for reliably and non-invasively measuring small airway obstruction is therefore an important unmet need in clinical respiratory physiology. A number of candidate tests have been proposed to fulfil this purpose, as discussed in the following section, with the forced oscillation technique (FOT) and multiple breath inert gas washout (MBW) being the strongest contenders at present. These methods have in common the fact that they may be influenced not only by the site of obstruction but also by the degree of heterogeneity of airway obstruction. Thus it may be predicted on theoretical grounds that the results obtained from these tests may be related to a certain extent.

1.3 Non-invasive physiological tests of small airway obstruction

1.3.1 Spirometry

Vital capacity (VC) measurements were first reported in 1846 by John Hutchinson⁶⁸, who observed in a study of 2130 individuals that VC was proportional to height and inversely related to age. The introduction of the timed spirometer by Gaensler in 1951⁶⁹ allowed dynamic ventilatory capacity to be reliably measured, and the ratio of forced expiratory volume in one second (FEV_1) to forced vital capacity (FVC) has stood the test of time as a measure of airflow obstruction. Flow during a forced expiration is largely effort-independent, other than during the brief period before peak flow is achieved⁷⁰, a phenomenon that contributes to the remarkable reproducibility and clinical utility of spirometric indices. The shape of a volume-time curve or flow-volume loop during a forced expiration is thus determined almost entirely by the mechanical (resistive and elastic) properties of the airways and lung parenchyma. Two physical mechanisms of expiratory flow limitation have been described⁷¹:

- i) Wave speed limitation⁷²: Flow through an airway cannot exceed the speed of wave propagation through the airway walls.
- ii) Frictional and turbulent dissipation of gas energy

A recent mathematical modelling study⁷³ has shown that wave speed limitation appears approximately 0.1 seconds after the onset of a forced expiration, and is the primary flow-limiting mechanism during the first 1.5 seconds of the manoeuvre. The site of flow limitation moves distally from the 4th generation at 0.1 seconds to the 9th generation at 1.0 seconds. Flow limitation due to frictional energy dissipation becomes the dominant mechanism from approximately 1.8 seconds, occurring in the distal airways, whilst turbulent energy losses may play a role in the transition between wave-speed and frictional flow limitation. These simulations suggest that FEV₁ may largely reflect the calibre of the central airways, whereas alternative spirometric indices that particularly assess events late in a forced expiration may provide an insight into small airway obstruction.

A number of investigators have studied the potential utility of alternative indices derived from volume-time curves or flow-volume loops recorded during forced expiration. The maximal mid-expiratory flow (MMEF) was formerly considered a marker of small airway obstruction⁷⁴, but its usefulness has since been called into question by its wide normal range and poor discriminatory ability⁷⁵. Indeed, since MMEF mainly reflects events occurring within the first second of a forced expiration, it would be unlikely to provide significant additional information to FEV₁. More recently, it has been suggested by Morris *et al* that the ratio FEV₃/FVC may represent a marker of early lung injury⁷⁶. These authors investigated the physiological characteristics of patients who had an isolated reduction in FEV₃/FVC but with normal FEV₁/FVC. They found that, compared with patients who had both normal FEV₁/FVC and normal FEV₃/FVC, this group exhibited significantly higher residual volume (RV) and RV to total lung capacity (TLC) ratio, and significantly lower diffusing capacity of the lung for carbon monoxide. However, the group with an isolated reduction in FEV₃/FVC was relatively small, comprising just 6.3% of the study population, suggesting that this pattern of lung function abnormality is relatively uncommon. Cohen *et al* investigated the potential role of FVC to slow inspiratory vital capacity (SVC) ratio as a marker of small airway obstruction. In a group of lung transplant recipients, the FVC/SVC ratio

was found to fall significantly from baseline in patients who developed bronchiolitis obliterans syndrome, a classical small airway disease⁷⁷. However, the median (interquartile range) percentage change in FVC/SVC in this group was only -4.4 (-1.2 to -7.5), compared to -39.0 (-36.4 to -42.1) for FEV₁, calling into question the discriminatory ability of FVC/SVC as a marker of small airway obstruction. Moreover, there is no *a priori* reason to suppose that the FVC/SVC ratio, being a general marker of expiratory air trapping, would selectively measure obstruction of the small airways.

A further method of analysing forced expiratory spirometry was proposed by Fish *et al*⁷⁸, who postulated that each lung unit that emptied during a forced expiration could be considered to have a 'transit time', or emptying time, measured from the start of the expiration. If these transit times followed a given probability distribution, then a spirometry would simply represent the cumulative distribution function of this probability distribution. A number of authors investigated indices derived from the moments of the spirometry, of which the simplest was the mean transit time⁷⁹⁻⁸². However, a disadvantage of these indices was that they required the spirometry to be truncated at an arbitrary proportion of VC (eg. 75% or 90%) in order to allow comparison between individuals, thus leading to loss of information from the terminal portion of the spirometry^{83,84}.

Permutt *et al*⁸⁵ found that transit times tended to follow a log-normal distribution, such that log-transformed transit times were normally distributed, with a mean and standard deviation of μ and σ , respectively. Thus μ was interpreted as a measure of the 'typical' transit time, whilst σ was considered to be a measure of the dispersion of transit times around this typical value. This approach is attractive since the information content contained within the shape of a spirometry can be condensed to just two parameters, from which, with the addition of a scaling parameter such as the theoretical maximum FVC, any other index can in theory be derived. Reference values for the parameters μ and σ have been derived⁸⁶, and longitudinal changes in these indices over a four-year period were reported in a group of 225 healthy men⁸⁷. In a study of 484 male factory workers, Nakadate *et al* showed that σ was significantly raised in asymptomatic smokers compared to non-smokers, whereas conventional spirometric parameters such as FEV₁ did not differ between the groups⁸⁸. Miller *et al* showed that both μ and σ were significantly related to pack-years smoked in a linear regression analysis⁸⁹. However,

there is no evidence that the parameters μ and σ can be used to distinguish between large and small airway obstruction.

1.3.2 Lung volumes

Whilst spirometry may be used to measure the vital capacity, the determination of absolute lung volumes requires an alternative method such as body plethysmography, helium dilution or nitrogen washout⁹⁰. The ratio of residual volume (RV) to total lung capacity (TLC) is a commonly utilised marker of expiratory air trapping⁹¹. Although it has been suggested that air trapping may be a specific marker of small airway disease³³, this assertion does not have a strong theoretical basis, and it is possible that large airway obstruction may also contribute. Nevertheless, a number of studies have shown that air trapping is associated with increased asthma disease expression. Sorkness *et al* found that at any given level of airflow obstruction, as measured by FEV₁/FVC (% pred.), patients with severe asthma had more prominent air trapping, as measured by increased RV/TLC (% pred.)⁹². Mahut *et al* found that children who had suffered an asthma exacerbation within the previous 3 months had higher values of RV/TLC than those who had not⁹³. The oral leukotriene receptor antagonist montelukast has been shown to reduce air trapping, as measured using RV or RV/TLC, in both adults^{94,95} and children⁹⁶ with asthma. Kraft *et al* found that improvements in asthma symptoms in patients treated with montelukast correlated with reductions in RV, but not with increases in FEV₁ or FEV₁/FVC ratio⁹⁴. Filippelli *et al* utilised optoelectronic plethysmography to investigate the relationship between breathlessness (measured on the Borg scale) and changes in both FEV₁ and lung volumes during a methacholine challenge test⁹⁷. They found that FEV₁ and chest wall volume were independent predictors of Borg score, but that chest wall volume was a stronger predictor, suggesting that hyperinflation and air trapping have a major influence on the sensation of breathlessness in patients with asthma.

The ratio of alveolar volume (VA) derived from a single breath helium dilution technique to TLC measured using an alternative method such as multiple breath helium dilution or body plethysmography represents the proportion of the lung volume that is unventilated following a single deep inspiration. The VA/TLC ratio is a marker of airway obstruction and gas mixing inefficiency^{98,99}, and has been found to have similar sensitivity and specificity for detecting obstructive airway disease (asthma or COPD) as

FEV₁⁹⁸. VA/TLC is likely to be reflective of the extent of patchy ventilation defects, as may be visualised using techniques such as hyperpolarised ³He magnetic resonance imaging (MRI). As such, it is probable that this parameter represents obstruction of both the large and small airways.

1.3.3 Forced oscillation technique

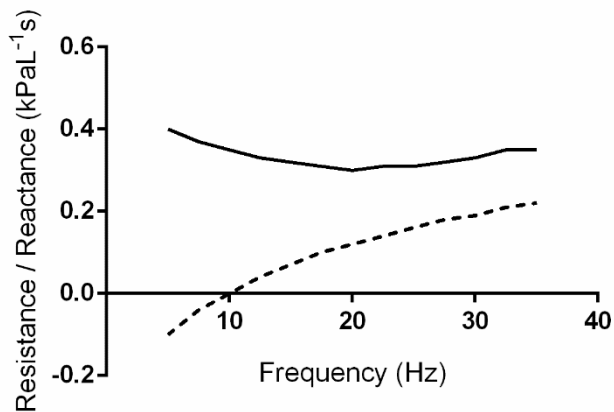
The forced oscillation technique, introduced by DuBois *et al* in 1956¹⁰⁰, is a method for non-invasively assessing lung mechanics by examining the relationship between pressure and flow whilst forced oscillations are delivered to the respiratory system by a loudspeaker or piston¹⁰¹. The waveform delivered may be a sine wave at a single frequency, a combination of sine waves at multiple discrete frequencies, or an impulse which is mathematically decomposed to a continuous spectrum of frequencies (a variant known as impulse oscillometry [IOS])¹⁰². The waveform delivered determines the frequencies at which the mechanical impedance of the respiratory system is measured. However, it should be noted that the impedance at a given frequency measured using different devices may not be exactly comparable, as was demonstrated in a recent multicentre study performed by Oostveen *et al.*¹⁰³ FOT is typically performed using a frequency range of approximately 5Hz to 35Hz, since at lower frequencies than this the subject's breathing harmonics are prone to interfere with the measurement. However, FOT has been successfully performed at lower frequencies during short voluntary apnoeas in well-trained participants¹⁰⁴⁻¹⁰⁷. In the steady state, the amplitude and phase relationships between pressure and flow waves produced by a forced oscillator depend upon the mechanical impedance (incorporating resistance and reactance) of the system being oscillated. In particular, a pure resistance will cause a reduction in the amplitude of flow with respect to pressure, but pressure and flow will remain in phase with each other. A negative reactance (known as an elastance) will cause pressure to lag behind flow, whereas a positive reactance (known as an inertance) will cause pressure to lead flow. Reactance naturally increases from being negative (predominantly elastive) at low frequencies to positive (predominantly inertive) at high frequencies, whereas resistance is always positive, and in an ideal linear system is equal across all frequencies. The resonant frequency of a given mechanical system is the oscillation frequency at which reactance is zero, so that flow and pressure are perfectly in phase. Figure 1.1 shows an illustrative trace of resistance and reactance against frequency, as might be measured

using IOS (Panel A), and a plot of resistance against time in a patient with asthma (Panel B).

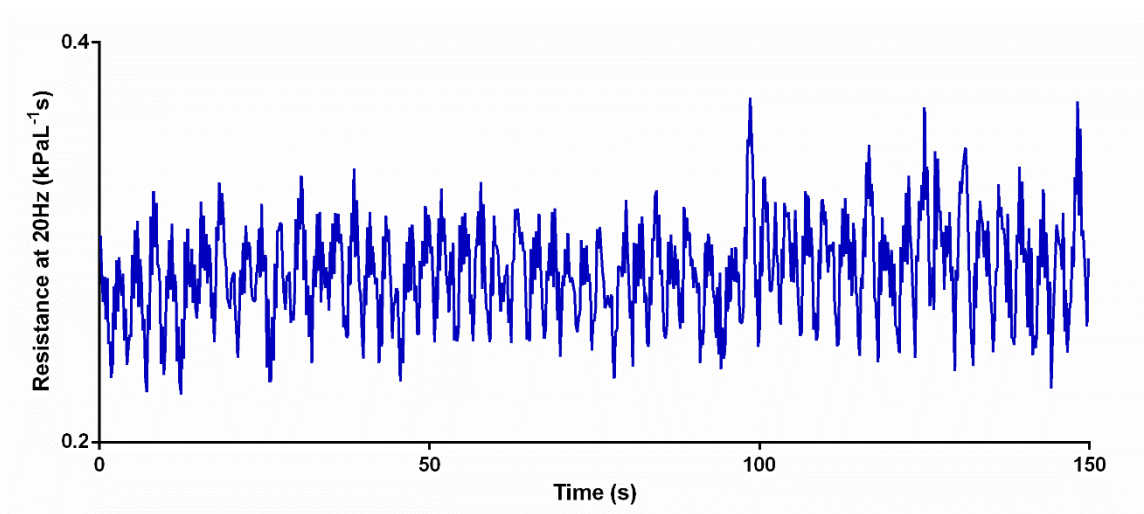
Figure 1.1: Resistance and reactance within the frequency and time domains

Panel A shows a schematic diagram of a typical trace of resistance (continuous line) and reactance (dashed line) against frequency as might be measured using impulse oscillometry. Resistance is positive at all frequencies, whereas reactance is negative at low frequencies and positive at high frequencies. The reactance curve crosses the x-axis at the resonant frequency, which is 10 Hz in this example. Panel B shows an example trace of resistance at 20 Hz against time measured using impulse oscillometry in a patient with asthma, showing typical oscillations in resistance during the respiratory cycle.

Panel A



Panel B



Examination of the resistance spectrum across a range of frequencies often reveals that resistance is disproportionately raised at low frequencies in patients with airway obstruction, a phenomenon known as frequency-dependence of resistance¹⁰¹⁻¹⁰². From a theoretical point of view, this may arise due to unequal ventilation time constants between parallel lung units¹⁰⁸, or non-linear viscoelastic properties of the airways and surrounding tissues¹⁰⁹. Computational models of lung impedance have shown that heterogeneous constriction of the peripheral airways would be expected to cause marked frequency-dependence of resistance between 0.1Hz and 3Hz, but that these effects are far less prominent if constriction is homogeneous or confined to the central airways¹¹⁰. This suggests that low frequency FOT may be essential to detect the effects of peripheral airway constriction. However, it should be noted that this study was based upon the branching structure of a canine lung, and frequency-dependence of resistance was observed only if extreme constriction (>80% reduction in diameter) was imposed upon randomly distributed airways.

Tissue and chest wall mechanical properties may also impact upon frequency-dependence of resistance, particularly at frequencies below 5Hz. Hantos *et al* used the oesophageal balloon technique to partition low-frequency respiratory resistance into pulmonary and chest wall components. They found that frequency-dependence of resistance was present in healthy subjects at low frequencies (0.25Hz to 5Hz), and that this was largely attributable to non-linear mechanical properties of the chest wall¹⁰⁴. Navajas *et al* investigated the mechanical properties of isolated strips of dog lung parenchyma, and observed that lung tissue resistance displayed prominent frequency-dependence, dropping close to zero at oscillation frequencies above 2Hz¹⁰⁹.

A further effect of airway constriction and closure on FOT measurements is that airways distal to the site of obstruction ‘move into the shadow’ so that their capacitive properties become hidden, thus making the respiratory system appear to be stiffer¹¹¹. For this reason, airway obstruction causes low-frequency reactance to become more negative. This is commonly expressed using the reactance at 5Hz (X5), or the reactance area (AX), which is the integrated low-frequency reactance between 5Hz and the resonant frequency. Distal airway obstruction may also cause diversion of forced oscillations across the upper airway and pharyngeal walls, so that the measured resistance and reactance spectra partly reflect the viscoelastic properties of these

structures. In support of this concept, FOT performed in patients with upper airway obstruction due to tracheostenosis revealed striking frequency-dependence of resistance and a marked reduction in low-frequency reactance¹¹². Furthermore, the resistance at 5Hz minus the resistance at 20 Hz (R5-R20) and AX are known to be closely correlated¹¹³, suggesting that these parameters may relate to similar structural abnormalities.

In order to remove the influence of the upper airways on FOT measurements, Kaminsky *et al* delivered forced oscillations to a single segment of the lung by means of a wedged bronchoscope, in a group of healthy subjects and patients with mild asthma¹¹⁴. At baseline, the mechanical impedance of the groups overlapped, although the asthma patients appeared to show a more pronounced response to methacholine than the healthy controls. In contrast, measurement of the resistance of collateral channels using a wedged bronchoscope technique with a constant flow showed clear differences between healthy and asthma groups at baseline⁵⁹. These results suggested that asthma may be characterised by abnormalities of the most peripheral respiratory bronchioles and alveolar ducts, where collateral pathways are located¹¹⁴. However, there is currently no direct histological evidence of abnormalities of collateral channels in patients with asthma.

The structural interpretation of FOT data is not straightforward because it may be affected by multiple factors including heterogeneous airway constriction, non-linear viscoelastic tissue properties and airway closure causing central airway shunting. In order to disentangle these effects, attempts have been made to fit FOT data to inverse models of lung impedance, in which the lungs are modelled using idealised electrical analogues with a small number of parameters. The most widely-used of these is the ‘constant phase model’¹¹⁵, which consists of a Newtonian resistance (R) and inertance (I) in series with a viscoelastic tissue compartment described by tissue damping (G) and elastance (H) parameters. However, such inverse models are not without limitations, primarily because the behaviour of an organ as complex as the lung cannot be easily captured by a small number of parameters with simple physiological interpretations¹¹⁶. For instance, the constant phase model described above assumes that frequency-dependence of resistance arises solely due to tissue viscoelastic properties and does not take into account the effect of heterogeneous airway constriction, as originally

described by Otis *et al*¹⁰⁸. Whilst more complex models have been proposed to take these and other effects into account^{117,118}, reliable parameter estimation would most likely be challenging in a clinical setting.

One promising approach to developing an understanding of the physiological basis of inverse model parameters is to utilise a combination of forward and inverse modelling. Whereas an inverse model seeks to explain measurements recorded *in vivo* in terms of a simple idealised lung model, forward modelling simulates a respiratory measurement such as FOT based upon a computational model of the respiratory system which is limited in complexity only by the computational power available. The properties of the computational model may be modified at will, and the output can then be entered into the inverse model. In this way, the effects of alterations in the respiratory system upon inverse model parameters can be readily investigated, and inferences about the physiological interpretation of the parameters made. Using this approach, Lutchen *et al*¹¹⁹ showed that heterogeneous peripheral airway constriction caused a disproportionate rise in the constant phase parameter G compared to the parameter H. A further innovative development in the field has been the coupling of computational modelling with FOT measurements and imaging data simultaneously, an approach known as image-functional modelling¹²⁰⁻¹²³. Image-functional modelling is a procedure by which a computational model of the respiratory system is tailored so as to reproduce a given combination of ventilation defects (for instance on positron emission tomography or ³He-MRI images) and FOT measurements. Using this approach, Tgavalekos *et al*¹²⁰ and Campana *et al*¹²¹ showed that ventilation defects and mechanical data from patients with asthma could not be accounted for by central airway constriction alone, and that the small airways must be involved. Other studies using image-functional modelling have highlighted the importance of network behaviour within the airway tree in producing observed ventilation defects and alterations in oscillatory lung mechanics^{122,123}. Computational modelling of airway networks has confirmed that the complex interactions between serial and parallel airways may cause catastrophic shifts in regional ventilation^{124,125}.

Despite uncertainties about their structural interpretation, a number of studies have examined the clinical significance of FOT parameters in patients with asthma, often making use of a commercially available IOS device. Shi *et al* reported that AX and R5-

R20 were significantly higher in children with uncontrolled asthma compared to those with controlled asthma¹²⁶. Similarly, Takeda *et al* investigated cross-sectional associations between asthma health status, using patient-reported outcome measures such as the Asthma Control Questionnaire, and IOS parameters¹²⁷. Using stepwise linear regression models, they ascertained that IOS parameters such as R20, R5-R20 and X5 were independent predictors of asthma health status over and above FEV₁.

1.3.4 Multiple breath inert gas washout

Multiple breath inert gas washout is a technique for quantifying ventilation heterogeneity (VH), the uneven distribution of ventilation, through analysis of the efficiency and pattern with which an inert non-absorbed tracer gas is washed out of the lungs during tidal breathing¹²⁸. MBW was introduced in 1950 by Robertson *et al*¹²⁹, and is steadily progressing from being a research tool to a clinical test of pulmonary function, particularly in the fields of paediatric respiratory medicine and cystic fibrosis (CF). A comprehensive standardisation document for the performance of inert gas washout has been recently published¹³⁰. MBW may be performed using an exogenous tracer gas, such as helium or sulphur hexafluoride (SF₆), in which case a wash-in phase is required followed by washout with room air, or alternatively resident lung nitrogen is utilised as the tracer gas, in which case no wash-in phase is required and the nitrogen is washed out using 100% oxygen. The technique requires that expired inert gas concentration and respiratory flows are measured accurately and with good temporal resolution, and that these signals are precisely aligned. A number of MBW methods have been reported, using either custom setups or commercially available devices. Inert gas concentration may be measured directly using a respiratory mass spectrometer¹²⁹, nitrogen analyser¹³¹ or photoacoustic gas analyser¹³², or indirectly using measurements of molar mass¹³³, or O₂ and CO₂ concentrations¹³⁴, to derive N₂ concentrations. Respiratory flows may be measured using a pneumotachometer^{131,132} or an ultrasonic flow sensor^{133,134}.

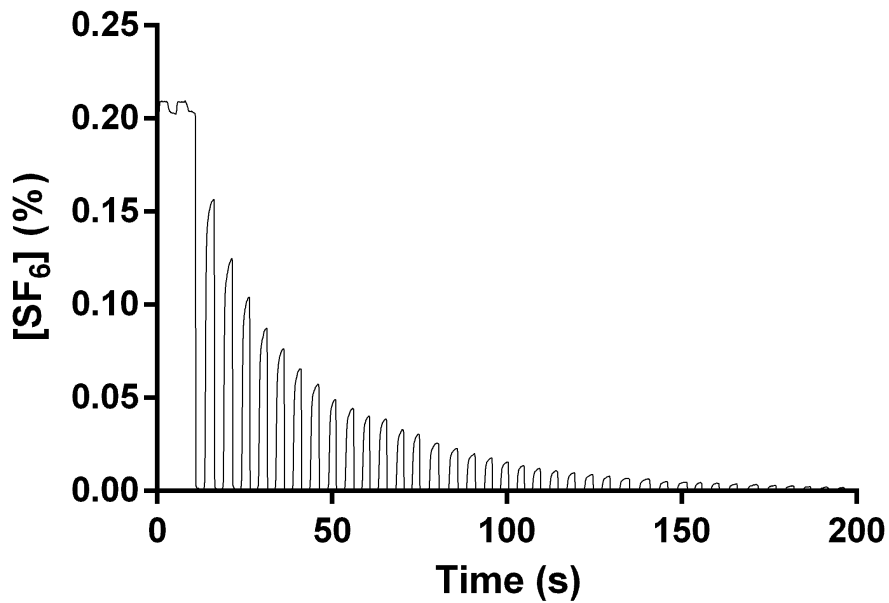
Figure 1.2 shows a typical washout curve in a healthy subject, using 0.2% SF₆ as the inert tracer gas. Panel A shows the raw trace of SF₆ concentration against time, while Panel B shows the end-expiratory SF₆ concentration (C_{et}) of each breath of the washout. As the washout proceeds, C_{et} decays in a roughly exponential manner until it reaches

1/40th of the initial SF₆ concentration (ie. 0.005%), at which point the washout experiment is by convention stopped. The units of the x-axis in Panel B are ‘turnover number’ (TO), where TO is the cumulative expired volume (CEV) measured in multiples of the functional residual capacity (FRC). The TO unit is used since it corrects for variations in both tidal volume and FRC. The most commonly reported MBW parameter is the lung clearance index (LCI)¹³⁵, which is the number of lung turnovers taken to wash out the inert gas to 1/40th of its initial concentration. Gas mixing inefficiency caused by VH results in a prolongation of the washout curve and hence an increase in LCI.

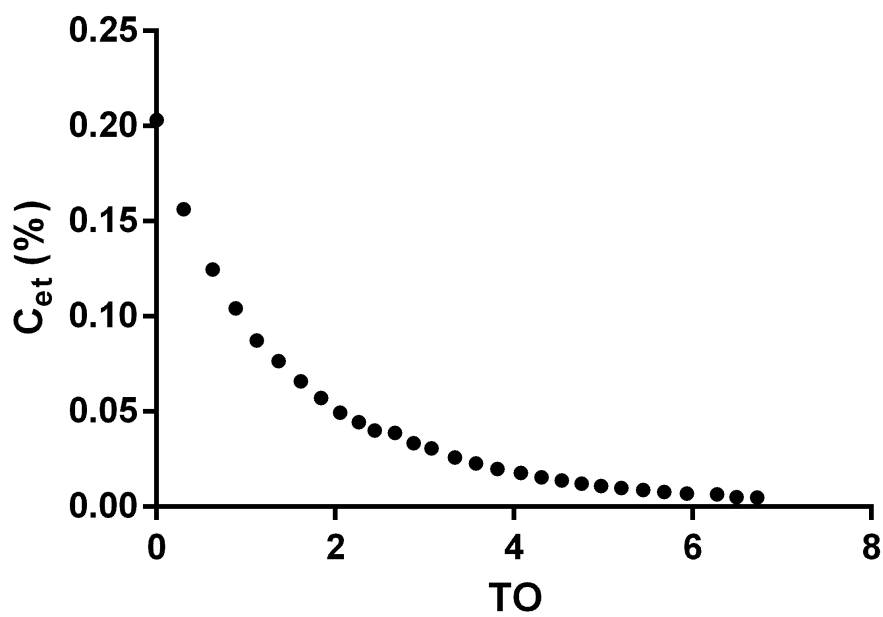
Figure 1.2: Inert gas washout curve from a healthy subject

Panel A shows a raw plot of measured SF_6 concentration against time, with each vertical peak representing a single expiration. Panel B shows the end-expiratory SF_6 concentration (C_{et}) of each breath of the same washout test.

Panel A



Panel B



Whilst LCI has the virtue of simplicity, it is biased to a certain extent by variations in tidal volume (V_T), anatomical dead space ($V_{D_{\text{anat}}}$) and FRC¹³⁶, and therefore the ‘ideal LCI’ for any given patient is not a fixed value, but instead varies between approximately 4.5 and 6, depending on the FRC, V_T and $V_{D_{\text{anat}}}$. An alternative index, the mixing ratio¹³⁶, is the ratio of the actual number of breaths taken to wash out the inert gas to $1/40^{\text{th}}$ of its initial concentration to the ideal number of breaths assuming perfect gas mixing. This is equivalent to the ratio of the actual value of LCI to its ideal value, since LCI and breath number are related to each other by a constant term in any given patient. Therefore, the ideal value of mixing ratio is always 1, with values higher than this indicating increasing VH. Despite its theoretical advantages, mixing ratio has not been widely used, most likely due to its increased complexity. Mixing ratio is calculated using the following formula:

$$\text{Mixing ratio} = \frac{n \times \ln\left(\frac{\text{FRC}}{\text{FRC} + V_T - V_{D_{\text{anat}}}}\right)}{\ln(0.025)}$$

Where n = number of breaths taken for C_{et} to reach $1/40^{\text{th}}$ of its initial value.

The mechanisms of VH have been elucidated largely on the basis of mathematical modelling studies, pioneered by Paiva and Engel in the 1970s and 1980s¹³⁷⁻¹⁴⁰. As air is drawn into the lungs during inspiration it moves through the larger conducting airways by bulk flow (convection). As the inspired air reaches more distal airways and the total cross-sectional area of the airways rises, the convective velocity falls and the movement of gas molecules by diffusion becomes more significant. The convection-diffusion front is that region of the airway tree at which convective and diffusive flows are of approximately equal magnitude. More distal to the convection-diffusion front, convective flows are negligible, and equilibration of concentration gradients occurs primarily by diffusion. In healthy lungs, the convection-diffusion front is thought to occur in the region of the acinar entrance¹⁴¹. However, the precise location is dependent upon the inert tracer gas used. In particular, gas diffusion rate is inversely proportional to the square root of the molar mass, and therefore the convection-diffusion front is more proximal for lighter gases such as helium, compared to heavier gases such as SF_6 ¹²⁹.

VH occurs due to two primary mechanisms¹⁴²:

- i) Convection-dependent inhomogeneity (CDI) – This refers to unequal ventilation between relatively large lung units subtended by conducting airways, with associated flow asynchrony such that the least well ventilated lung units empty later in expiration.
- ii) Diffusion-convection-dependent inhomogeneity (DCDI) – This refers to asymmetries of airway volume or cross-sectional area occurring in the region of the convection-diffusion front, and arises due to a complex interaction between convection and diffusion involving ‘diffusive pendelluft’.

Two-compartment model simulations of gas mixing have shown that LCI may be increased by either CDI or increased respiratory dead space¹⁴³. As a point of clarification, the respiratory dead space in the setting of inert gas washout has a different physiological significance compared to the normal situation in which the exchange of O₂ and CO₂ across the alveolar-capillary membrane is being considered. In both settings, a component of the respiratory dead space is the anatomical dead space, the volume of the conducting airways that do not participate in gas mixing or gas exchange. In the context of normal gas exchange, the remainder of the respiratory dead space (often referred to as the alveolar dead space) comprises the theoretical volume of ventilated gas (per tidal breath) that is wasted due to ventilation-perfusion mismatch. However, in the context of inert gas washout, ventilation-perfusion relationships are of no significance, since the gas of interest is by definition not absorbed across the alveolar-capillary membrane. Intriguingly, analysis of LCI washout curves suggests that even in this context, the effective respiratory dead space ($V_{D_{resp}}$) can be increased over and above the anatomical dead space. The origin of this additional dead space is poorly understood, but it is believed to be related to complex interactions between convection and diffusion occurring in the region of the convection-diffusion front¹⁴³. The construction of a computational model of convection and diffusion within a simulated human acinus that could explain this phenomenon would be an important advance in the field. Throughout this thesis, the term ‘respiratory dead space’, or its abbreviation $V_{D_{resp}}$, is used to signify the perfusion-independent effective respiratory dead space that occurs within the context of inert gas washout. $V_{D_{resp}}$ may be estimated from the SF₆ expirogram using the Bohr equation¹³⁰, but one disadvantage of this method is that a

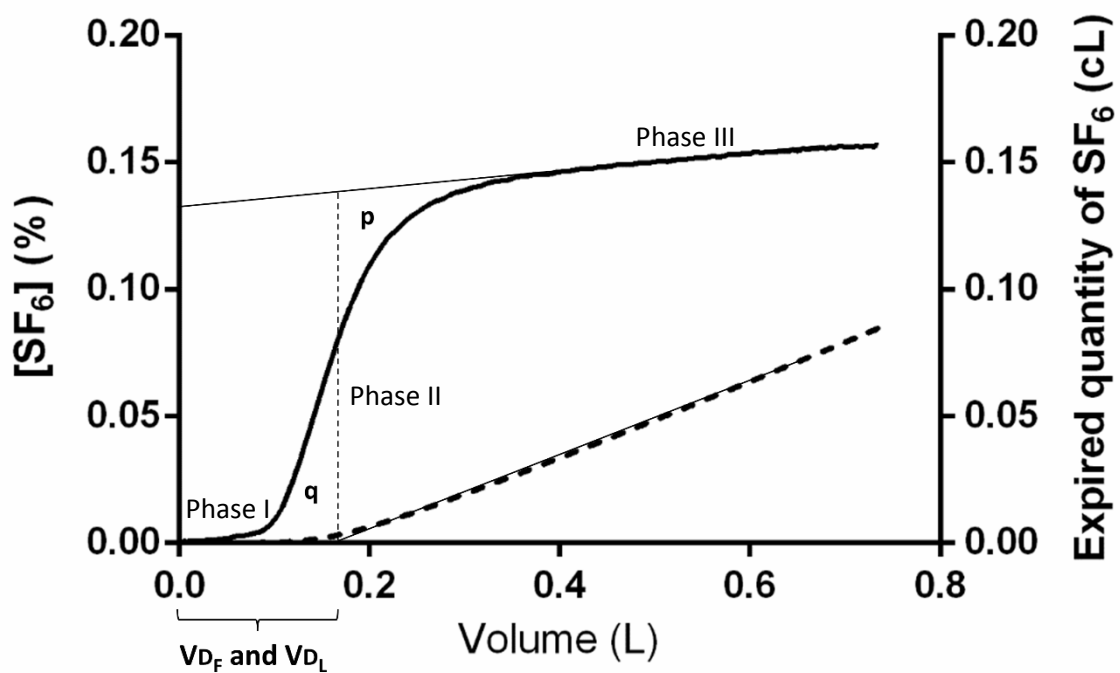
different value may be obtained on each expiration. In Section 2.7, an alternative method for determining $V_{D_{resp}}$ using a two-compartment lung model is described.

The CDI component of increased LCI may be estimated by measures of the so-called ‘curvilinearity’ of the curve, or the degree to which it deviates from the single exponential decay pattern that would be expected if all lung compartments were homogeneously ventilated. Examples of such indices include the slope index¹⁴² and *Curv*^{143,144}. Verbanck *et al*¹⁴³ utilised *Curv* because this parameter was thought to be relatively independent of $V_{D_{resp}}$, in contrast to LCI. They did not attempt to isolate the respiratory dead space effect from LCI.

An alternative method of analysing washout curves is to examine changes in expired inert gas concentration *within* breaths, rather than simply treating each breath as a single point. Figure 1.3 shows an expirogram of inert gas concentration against expired volume over the course of a single exhalation during a MBW test in a healthy subject. Phase I represents expired air from the anatomical dead space that does not take part in gas mixing, and thus the inert gas concentration during this phase is negligible. Phase II represents the arrival at the mouth of the first portions of alveolar air, with a corresponding sharp increase in inert gas concentration. Phase III (alveolar phase) represents pure alveolar air, following the complete clearance of the anatomical dead space. In some cases, a sharp increase in inert gas concentration is seen at the end of phase III, which is thought to correspond to the onset of airway closure in the basal lung segments, and is designated phase IV¹⁴⁵. The expirogram can also be utilised to calculate the anatomical dead space using the Fowler or Langley methods¹³⁰, as illustrated in Figure 1.3.

Figure 1.3: Graph of SF₆ concentration against expired volume during a single exhalation

Expirogram of SF₆ concentration against volume in a healthy subject. SF₆ concentration is indicated by the heavy continuous line and cumulative expired quantity of SF₆ is indicated by the heavy dashed line. Thin continuous lines indicate linear extrapolations through phase III and through the linear portion of the graph of expired quantity of SF₆. The Langlely dead space is the volume indicated by the intersection of the latter line with the x-axis. The thin vertical dashed line is positioned such that areas p and q are equal. The Fowler dead space is the volume indicated by the intersection of this line with the x-axis. Figure redrawn from Reference 130 using data collected in our laboratory.



In the absence of VH, the phase III segment would be expected to be horizontal. An increased phase III slope indicates VH due to either CDI or DCDI. Specifically, mathematical modelling studies have predicted that CDI should cause a progressive linear increase in the phase III slope (normalised to the mean inert gas concentration over the course of phase III), whilst DCDI should cause an increase in the phase III slope of the first breath of the washout test, reaching a maximum after approximately five breaths¹⁴². This model underlies the derivation of the indices S_{cond} and S_{acin} ¹³¹, which represent VH due to CDI and DCDI, respectively.

Verbanck *et al*¹³¹ performed MBW using a fixed tidal breathing protocol, in which subjects were encouraged to maintain a constant V_T of 1 litre, using a visual guide. Since not all groups of patients are able to achieve this (eg. children, or patients with severe airways disease), and because phase III slopes may be influenced by V_T , Aurora *et al* have proposed an empirical correction to account for within- and between-subject variability in V_T , namely that phase III slopes should be multiplied by the tidal volume of the corresponding breath before calculating S_{cond} and S_{acin} ¹⁴⁶. These tidal volume-corrected values may be designated $S_{\text{cond}V_Tc}$ and $S_{\text{acin}V_Tc}$, respectively¹⁴⁷. The Aurora correction is recommended for use in children, or in patients who cannot maintain a constant tidal volume of 1 litre¹³⁰, although it is not yet fully validated. Such validation would require detailed studies of the effect of tidal volume changes on the phase III slope, in both health and disease.

Whilst phase III slope parameters are widely used, they have a number of disadvantages. Determination of the phase III slope for each breath is labour intensive, and can be challenging in some cases due to cardiogenic oscillations, or ambiguity with respect to the transitions between phase II and III, and between phase III and IV. Therefore, phase III slope parameters are subject to inter-observer variability, and although automated phase III slope detection has been reported¹⁴⁸, manual confirmation of computer-specified slopes is still required¹³⁰. Horsley *et al*¹⁴⁷ found that tidal volume-corrected $S_{\text{cond}V_Tc}$ was poorly reproducible in healthy controls, and that the median goodness of fit (R^2) of the regression line upon which $S_{\text{cond}V_Tc}$ is based was only 0.14 in healthy controls and 0.64 in patients with CF. Furthermore, in CF patients with severe VH, phase III slopes often reach an asymptote before the 6th turnover, thus artificially reducing S_{cond} ¹⁴⁷. The occurrence of this asymptote was in fact predicted by

Paiva in 1975¹⁴⁹. Partly in response to these findings, Verbanck *et al* proposed modified phase III slope parameters (S_{cond}^* and S_{acin}^*), which are calculated analogously to S_{cond} and S_{acin} , except that S_{cond}^* is based upon S_{nIII} values between 0 and 3 turnovers, excluding the first breath of the washout, instead of between 1.5 and 6 turnovers¹⁵⁰. The clinical and analytical validity of these parameters, in particular their repeatability and discriminatory ability, has not yet been determined.

A number of studies have demonstrated evidence of VH in patients with asthma¹⁵¹⁻¹⁵⁵. Verbanck *et al*¹⁵¹ found that adults with asthma manifested partially reversible increases in S_{acin} , but no abnormality in carbon monoxide diffusing capacity. They suggested that this combination of findings could be due to an intra-acinar process that spared the alveolar airspaces. The same group also found that S_{acin} correlated with modelled alveolar nitric oxide in patients with asthma, suggesting a link between peripheral airway function and inflammation¹⁵². In contrast, mild asthma¹⁵³ and asthma in children¹⁵⁴ appeared to be associated mainly with conductive airway disease. MacLeod *et al*¹⁵⁵ showed that children with well-controlled asthma and normal spirometry manifested an increase in LCI compared to healthy controls, and that this was not reversible following bronchodilator administration. The authors concluded that LCI may be a marker of structural remodelling in children with asthma.

The clinical significance of VH in asthma has been investigated by a number of authors. Bourdin *et al* found that single breath nitrogen phase III slope correlated with ACQ scores¹⁵⁶ but these authors did not control for possible associations between nitrogen phase III slope and forced expiratory volume in one second (FEV_1). Subsequently, Farah *et al* found that S_{cond} correlated positively with five-point ACQ score (ACQ-5) at baseline, but in a multivariate analysis only FEV_1 was an independent predictor of baseline ACQ-5, since both S_{cond} and S_{acin} correlated negatively with FEV_1 ¹⁵⁷. The same group have also shown that S_{acin} , but not S_{cond} , is correlated with asthma severity, as measured using the Global Initiative for Asthma (GINA) treatment steps¹⁵⁸, and that asthma exacerbations are associated with increases in both S_{cond} and S_{acin} . Markers of VH have also been shown to predict response to inhaled corticosteroid dose titration¹⁵⁹, and S_{acin} has been found to improve following the replacement of standard corticosteroid inhalers with a small particle inhaler, in those patients who had a raised S_{acin} at baseline¹⁶⁰.

1.4 Imaging techniques for the assessment of small airway structure

1.4.1 Morphometry of the human airway tree

The human airway tree is an asymmetrical dichotomously branching structure of approximately 23 generations, of which the first 14 generations comprise purely conducting airways (trachea, bronchi, bronchioles, terminal bronchioles), and the final 9 generations comprise airways that are alveolated and thus participate in gas exchange (transitional bronchioles, respiratory bronchioles, alveolar ducts and alveolar sacs)¹⁶¹. The pulmonary acinus is the basic gas exchanging unit, and is a portion of lung that is ventilated by a single terminal bronchiole.

Information about the morphometry of the larger conducting airways has been obtained by analysis of resin casts of whole lungs^{162,163}. Weibel and Gomez¹⁶² found that the diameters of the first 10 generations of airways reduce by a fixed ratio with each generation, approximately equal to the cube root of $\frac{1}{2}$, which from a functional point of view is ideal with respect to minimising both the work needed to overcome flow resistance and the dead space volume¹⁶¹. Horsfield and Cumming undertook a similar study, measuring the length and diameter of all airways with diameter exceeding 0.07cm in a resin cast of a single pair of human lungs, fixed at an inflation volume of 5 litres¹⁶³. The number of divisions between the trachea and the lobular branches ranged between 8 and 25, with a mean of 14.6, and the path length from the carina to the lobular branches ranged from 7.5cm to 21.5cm. Therefore, the proximal portion of the human bronchial tree was found to be asymmetrically dichotomous, meaning that there was wide variation in the number of divisions between the stem branch and the terminal branches.

The structure of the acinar airways has been investigated using a number of different techniques. In the study of Horsfield and Cumming¹⁶³, a sample of 313 'lobules' (arbitrarily defined as segments of lung subtended by 'lobular branches', airways with diameter 0.07cm or less) was examined under a binocular dissecting microscope. The number of divisions between the lobular branches and the most distal respiratory

bronchioles ranged from 2 to 7, whilst the intralobular path length ranged from 0.2 to 0.9cm. The branching pattern within lobules was found to be appreciably more symmetrical than that seen in more proximal airways. In a later study, the same group confirmed that the branching pattern of the intralobular airways up to the distal respiratory bronchioles closely approximated to symmetrical dichotomy, with the number of branches in each generation increasing by a factor of 2 with each division¹⁶⁴, as compared to the factor of 1.38 that was observed in more proximal airways¹⁶³. An alternative method of investigation utilised histological sections to form inferences about the three-dimensional structure of the acinar airways, including the alveolar ducts and sacs, a technique known as stereology¹⁶⁵. Using this technique, Weibel *et al*¹⁶² showed that the diameters of these airways reduce to a much lesser extent with each generation than do those of the conducting airways. From a functional point of view, this reflects the fact that diffusion rather than convection begins to play a more prominent role in gas transport once the acinar airways are reached. More detailed information about the structure of the human pulmonary acinus has been recently obtained using micro-computed tomography (CT) imaging of resected lung specimens¹⁶⁶. This study showed that intra-acinar airways branched over up to 11 generations, with the mean airway internal diameter reducing from 0.66 mm at the terminal bronchioles to 0.34 mm at the seventh acinar generation, thereafter remaining constant. The lengths of each branch ranged from 0.52 to 0.93 mm, with no significant difference between generations. The branching angle between daughter branches ranged from 113 to 134 degrees, again with no difference between generations.

1.4.2 Quantitative computed tomography

Quantitative analysis of CT scans is an emerging technique for assessing both the large and small airways in patients with asthma and other airway diseases¹⁶⁷. Airway remodelling in asthma may be visualised and quantified based upon standard metrics such as the percentage wall area of the right upper lobe apical segmental bronchus¹⁶⁸. This bronchus is often utilised since it is usually visualised end-on on transverse CT slices, thus allowing the wall area to be accurately determined. However, a potential drawback to this method is that a single bronchus may not be representative of remodelling throughout the airway tree. More recently, simulations of airflow in CT-derived airway trees has been performed using computational fluid dynamics¹⁶⁹,

although, the current resolution of CT is such that only the first six airway generations may be directly visualised.

A number of CT indices of air trapping have been devised, including the percentage of voxels with attenuation < -850 Hounsfield units (HU) on expiratory CT¹⁷⁰, the ratio of mean lung density at expiration to inspiration (MLD E/I)¹⁷¹, and the difference in lung attenuation between inspiration and expiration¹⁷². Air trapping on CT in patients with asthma has been shown to be associated with airflow limitation^{170,171,173,174}, as well as an increased risk of asthma-related hospitalisations and intensive care admissions¹⁷⁰. In one study, treatment with inhaled corticosteroids attenuated air trapping on CT, although there was no significant difference between large and small particle inhalers¹⁷². Montelukast has also been found to reduce air trapping on CT following a four-week treatment period¹⁷⁵. CT imaging has recently been utilised to classify patients with asthma into clusters that may represent distinct patterns of airway remodelling¹⁷⁶. Galbán *et al* have described a novel CT biomarker based upon the parametric response map (PRM) technique, in which individual voxels were tracked between inspiratory and expiratory CT images using image registration techniques to determine their change in attenuation, in a group of patients with COPD¹⁷⁷. Voxels were classified as being indicative of functional small airway disease (fSAD) if their attenuation was > -950 HU on inspiration, but < -856 HU on expiration. In contrast, emphysematous voxels had an attenuation of < -950 HU on inspiration and < -856 HU on expiration. The authors suggested that patients with COPD may progress from predominant fSAD to predominant emphysema. Studies utilising the PRM technique in asthma are currently awaited.

1.4.3 Hyperpolarised noble gas magnetic resonance imaging

Whilst the small airways lie beyond the resolution of current CT scanners, hyperpolarised ³He and ¹²⁹Xe MRI techniques have been developed in the past 15 years that show considerable potential to detect microstructural abnormalities at the level of the acinar airways and alveoli¹⁷⁸. Hyperpolarisation of ³He and ¹²⁹Xe is the process by which the atoms of these noble gases are imparted with a nuclear polarisation approximately 10,000 times higher than that which would be present at thermal equilibrium, thus allowing them to act as gaseous contrast media for lung MRI¹⁷⁹. The principal methods for hyperpolarising noble gases are spin-exchange optical pumping

and metastability exchange optical pumping. Although the majority of studies in humans have thus far utilised ^3He , it is likely that in the future ^{129}Xe will be more widely used, firstly because it is cheaper and more abundant, and secondly because, unlike ^3He , it is absorbed across the alveolar-capillary membrane, and can therefore be utilised to study gas exchange as well as ventilation¹⁷⁹.

The diffusivity of any gas in an unenclosed space may be described by its free diffusion coefficient, which is approximately $0.86\text{ cm}^2/\text{s}$ for ^3He and $0.14\text{ cm}^2/\text{s}$ for ^{129}Xe ¹⁸⁰. However, when enclosed within a structure such as an alveolus or acinar airway, diffusion is impeded, so that the apparent diffusion coefficient (ADC) of a gas is reduced from its theoretical maximum value, the free diffusion coefficient. ^3He - or ^{129}Xe -MRI may be utilised to measure the ADC at either short timescales of a few milliseconds ($\text{ADC}_{\text{short}}$) or longer timescales of up to ten seconds (ADC_{long}). Short timescale ADC measurements correspond to diffusion mostly within alveoli and individual acinar airways, and appear to be sensitive markers of pulmonary emphysema, a condition that is characterised pathologically by the destruction and enlargement of alveolar airspaces¹⁷⁸. Several studies have shown that short-range ^3He or ^{129}Xe ADC is elevated in both patients with emphysema¹⁸¹⁻¹⁸⁷, and in animal models of emphysema¹⁸⁸⁻¹⁹¹, in comparison with values obtained in healthy lungs. Moreover, in a number of these studies $\text{ADC}_{\text{short}}$ was found to correlate with quantitative histological measures of emphysema such as the mean linear intercept (L_m), mean alveolar internal area and mean chord length^{184,186,188-191}. $\text{ADC}_{\text{short}}$ correlated negatively with FEV_1/FVC in patients with emphysema¹⁸³ and in asymptomatic smokers¹⁹². The structural significance of long timescale ADC measurements is less well understood, but they may reflect the extent of collateral ventilation pathways that bypass the normal branching structure of the acinar airways¹⁹³. However, Verbanck and Paiva have argued that collateral ventilation may not be necessary to explain measured long timescale ADC values, and that the pattern of intra-acinar branching may be a more important factor¹⁹⁴.

A small number of studies have reported ADC measurements in patients with asthma^{184,195}. Wang *et al* found that both long (1.5 s) and short (1 ms) timescale ADC was markedly elevated in patients with COPD compared to healthy controls, whereas in patients with asthma, $\text{ADC}_{\text{short}}$ was only mildly elevated and ADC_{long} was moderately

elevated compared to controls¹⁸⁴. Since asthma is not known to be associated with alveolar destruction, the authors suggested that the modest elevations in ADC_{short} and ADC_{long} observed in asthma may be due to lung hyperinflation, causing a generalised increase in alveolar airspace size. This conclusion is supported by a subsequent study which examined the effect of methacholine inhalation on ADC values in 25 patients with asthma and 8 healthy controls¹⁹⁵. Methacholine inhalation resulted in the formation of ventilation defects in both patients with asthma and healthy controls. Whole-lung ADC increased in patients with asthma following methacholine inhalation (0.204 cm²/s to 0.211 cm²/s), although this change was not statistically significant, and subsequently returned to baseline following treatment with salbutamol (0.211 cm²/s to 0.202 cm²/s, $p < 0.01$). The authors concluded that the observed changes in ventilation defect percentage and ADC_{short} were due to bronchoconstriction and air trapping. Indeed, it is known that there is a strong relationship between ADC_{short} and the degree of lung inflation¹⁹⁶, a factor that needs to be borne in mind when interpreting the structural significance of ADC in obstructive airway diseases.

Whilst ADC provides a general index of the diffusivity of ³He within the alveoli and acinar airspaces, it does not have a direct morphometric interpretation¹⁷⁸. Thus, more complex MR pulse sequences have been devised that allow the derivation of modelled values for parameters such as the alveolar duct outer radius and alveolar sleeve width¹⁹⁷. These parameters are based upon an idealised theoretical model of the acinar airways comprising a dichotomously branching network of cylindrical structures decorated by circumferential rings of alveoli, with eight alveoli per annular ring. From the values of R and h, a number of further parameters may be calculated that can be directly compared with histological measurements, including the alveolar surface area, lung volume per alveolus, number of alveoli per unit lung volume and L_m . This model has been validated in explanted human lungs with varying degrees of emphysema, with a strong correlation observed between histological and ³He-MRI-derived L_m measurements¹⁹⁷. Quirk *et al* utilised the same methodology to detect microstructural changes in smokers and ex-smokers, including those with normal lung function¹⁹⁸. In this study, FEV₁/FVC was positively correlated with alveolar sleeve width and negatively correlated with alveolar duct outer radius, suggesting that emphysema progression is associated with alveolar shallowing and alveolar duct enlargement. Studies in asthma using this technique are currently awaited.

In addition to studying the microstructure of the acinar airways, as described above, ^3He - and ^{129}Xe -MRI may also provide insight into regional lung ventilation. Several studies have reported the detection of ventilation defects in patients with asthma using these techniques¹⁹⁹⁻²⁰⁷. The number of ventilation defects correlates with spirometric airflow obstruction^{200,201}, and increases following methacholine or exercise challenge^{195,200,202}. Moreover, their location in any given patient with asthma is remarkably consistent over time^{202,204}, suggesting that they are associated with long-term structural remodelling of specific airways rather than being a consequence of random variability in airway smooth muscle tone. Recent studies have shown that ventilation defects are associated with areas of air trapping²⁰³ and airway wall thickening²⁰⁷ detected by CT. Tzeng *et al* quantified the heterogeneity of regional lung ventilation in healthy subjects and patients with asthma before and after a methacholine challenge²⁰⁸. They found that methacholine challenge elevated VH in both groups, and that this could be reversed by a deep inspiration in healthy subjects, but not in asthmatics. ^3He -MRI washout experiments have been performed in rodents²⁰⁹ and humans²¹⁰, providing a regionalised analogue of standard MBW techniques. The coupling of imaging techniques and computational modelling approaches is likely to yield important insights into the structural basis of VH²¹¹⁻²¹⁴.

1.5 Aims and hypotheses

1.5.1 Validation of multiple breath washout technique

This thesis presents the results of MBW measurements performed using the non-resident inert tracer gas 0.2% SF_6 , and a modified Innocor photoacoustic gas analyser, as described by Horsley *et al*¹³². It is recommended in current guidelines that MBW systems should be validated using a realistic lung model across the range of respiratory rates, tidal volumes and lung volumes likely to be encountered in clinical practice¹³⁰. I therefore aimed to:

- i) Validate our MBW system using an acrylic glass lung phantom with realistic body temperature and pressure, saturated (BTPS) conditions.

- ii) Determine the variability of repeated MBW measurements performed *in vivo* and *in vitro* in order to estimate the relative importance of biological and instrument noise.

1.5.2 Development of novel indices of ventilation heterogeneity

LCI may be increased by (i) unequal convective ventilation between larger lung units, or (ii) increased respiratory dead space. I aimed to develop novel MBW parameters (LCI_{vent} and LCI_{ds}) that would quantify the relative contributions of these mechanisms towards observed increases in LCI, particularly in patients with severe VH. With this aim in mind, I re-analysed raw washout data from 40 patients with CF, kindly provided to me by Dr. Alex Horsley (Manchester, UK). In addition, I analysed washout data from 43 patients with non-CF bronchiectasis, since VH in this patient group has not been the subject of a large number of previous studies.

I hypothesised that:

- i) LCI_{vent} and LCI_{ds} are repeatable in patients with CF and non-CF bronchiectasis.
- ii) CF and non-CF bronchiectasis are characterised by increased LCI_{vent} and LCI_{ds} compared to healthy control subjects.
- i) LCI, LCI_{vent} and LCI_{ds} are related to other measures of disease severity in CF and non-CF bronchiectasis, namely the degree of spirometric airflow obstruction and the presence or absence of chronic bacterial colonisation.

1.5.3 Repeatability of small airway biomarkers

Before small airway biomarkers enter into widespread clinical use, it is necessary to be assured of their repeatability and stability over time. I therefore aimed to determine the within-visit and between-visit repeatability of a range of IOS and MBW parameters. Furthermore, I aimed to calculate the standard deviation of between-visit differences for each parameter, in order to facilitate sample size calculations for future interventional trials.

1.5.4 Clinical significance of small airway obstruction markers in asthma

A number of studies have examined the clinical significance of various putative markers of small airway obstruction. However, there has as yet been no study examining the contributions of each of these markers to clinical outcomes in a single well-characterised group of adults with asthma.

I hypothesised that small airway obstruction markers are associated with (i) increased asthma severity, as evidenced by higher treatment requirements, (ii) impaired asthma control and quality of life, and (iii) frequent exacerbations.

1.5.5 Structural correlates of acinar ventilation heterogeneity

The structural and anatomical correlates of MBW indices in health and disease have not been determined, and our current understanding is based largely on simplified mathematical models¹³⁷⁻¹⁴². I aimed to utilise ³He-MR to shed light upon the structural correlates of S_{acin} , a putative marker of acinar airspace disease, in patients with asthma.

I hypothesised that asthma patients with raised S_{acin} would manifest evidence of altered diffusion within the acinar airways compared to asthma patients with normal S_{acin} and healthy controls.

1.5.6 Modification of small airway obstruction with treatment

A small number of studies have suggested that ventilation heterogeneity in asthma may be partially reversible with treatment¹⁵⁸⁻¹⁶⁰. I aimed to assess whether small airway obstruction in stable asthma is modifiable by a systemically active agent. With this objective in mind, we undertook a randomised, double-blind, placebo-controlled trial of QAW039, a chemoattractant receptor-homologous molecule expressed on Th2 cells (CRTH2) receptor antagonist with anti-eosinophilic properties, in patients with persistent eosinophilic asthma. The primary outcome measure was sputum eosinophil count, and a panel of putative small airway obstruction markers were incorporated into the study design as exploratory outcome measures.

I hypothesised that treatment with QAW039 would result in improvements in markers of small airway obstruction in patients with eosinophilic asthma.

2 Methods

2.1 Spirometry

Spirometry was performed according to standard American Thoracic Society / European Respiratory Society (ATS/ERS) guidelines²¹⁵, using a Vitalograph rolling seal spirometer, connected to a mouthpiece incorporating a bacterial filter. Participants were tested in a comfortable seated position, wearing a noseclip. Following a period of quiet tidal breathing, participants were instructed to inspire to TLC and then to immediately place their lips around the mouthpiece with a good seal and expire as forcefully as possible. The operator encouraged participants to continue the forced expiration until RV was reached. At least three forced expirations were performed. Repeatability was considered acceptable if the two largest FEV₁ values, and the two largest FVC values differed by no more than 150 ml. If the repeatability criterion was not met, additional manoeuvres, up to a maximum of eight, were performed until the criterion was met. The largest FEV₁ and FVC values were recorded, even if they occurred during different manoeuvres. Predicted values for FEV₁ and FVC were calculated using the European Coal and Steel Community regression equations²¹⁶.

2.2 Measurement of lung volumes using body plethysmography

Body plethysmography was performed according to standard ATS/ERS guidelines⁹⁰, using a constant volume plethysmograph. Participants were tested in a comfortable seated position, wearing a noseclip, and breathing exclusively through a rubber mouthpiece connected to a pneumotachometer. Following a period of quiet tidal breathing, participants were instructed to pant gently against a closed shutter, which automatically closed at the onset of a tidal inspiration at FRC, and automatically opened following the performance of an acceptable panting manoeuvre. Thoracic gas volume and plethysmographic FRC (FRC_{pleth}) were calculated automatically by the on-board software, using Boyle's Law, from pressure changes in the box and at the mouth. A minimum of three technically satisfactory panting manoeuvres were performed, with acceptable repeatability criteria being a difference of no more than 5% between the highest and lowest FRC_{pleth} values obtained. Immediately following completion of the panting manoeuvres, and without coming off the mouthpiece, participants were

instructed to inspire to TLC and then immediately perform a forced expiratory manoeuvre to RV. This was then used to calculate absolute values for TLC and RV.

2.3 Single-breath determination of carbon monoxide uptake in the lung

Carbon monoxide uptake in the lung was determined using the single-breath method, according to standard ATS/ERS guidelines²¹⁷. Participants were tested in a comfortable seated position, wearing a noseclip, and breathing exclusively through a rubber mouthpiece connected to a pneumotachometer. Following a period of quiet tidal breathing, participants were asked to perform a relaxed expiration to residual volume, at which point the inspired gas was switched, under the control of the operator, from room air to a gas mixture containing 0.3% carbon monoxide and 10% helium (balance air). Participants were instructed to rapidly inspire to TLC and then hold their breath at TLC for nine seconds, followed by a relaxed exhalation. Following the exhalation of 0.75 – 1L of air, so as to exclude dead space gas, a sample of alveolar gas was automatically collected for analysis of the helium and carbon monoxide concentrations. Alveolar volume (V_A) was calculated automatically by the on-board software from the dilution of helium, since this is not absorbed across the alveolar-capillary membrane. The carbon monoxide transfer coefficient (KCO), effectively a rate constant for the reduction in alveolar carbon monoxide concentration during the breath-hold period, was calculated based on the combined effect of dilution and absorption on the final concentration of carbon monoxide. The diffusing capacity of the lung for carbon monoxide (DLCO) was calculated as V_A multiplied by KCO.

2.4 Impulse oscillometry

2.4.1 Theoretical background

IOS is a variant of the forced oscillation technique (FOT), a method of determining the mechanical impedance of the respiratory system. FOT involves imposing an oscillatory waveform on the respiratory system at the mouth and determining the relationship between pressure and flow waves at the same location with respect to amplitude and

phase. This allows the resistance (R) and reactance (X) of the respiratory system to be determined:

$$R = \frac{A^1}{A^2} \cos(\varphi^1 - \varphi^2)$$

$$X = \frac{A^1}{A^2} \sin(\varphi^1 - \varphi^2)$$

Where A^1 and A^2 represent the amplitudes of the pressure and flow waves, respectively. The quantity $(\varphi^1 - \varphi^2)$ represents the phase difference between pressure and flow, and may range from $-\frac{\pi}{2}$ to $\frac{\pi}{2}$ radians (or -90° to 90°), with a positive value indicating that pressure leads flow, and a negative value indicating that pressure lags flow. Resistance is always positive, whereas reactance is negative if $\varphi^1 < \varphi^2$, positive if $\varphi^1 > \varphi^2$, and is equal to zero if $\varphi^1 = \varphi^2$.

The phase difference between pressure and flow depends upon the frequency of the forced oscillations. This is because there are two opposing properties of the respiratory system at work, namely (i) elastance, which causes pressure to lag behind flow (negative phase shift), and (ii) inertance, which causes pressure to lead flow (positive phase shift). Elastance is an expression of the elastic properties of the respiratory system, as measured at the mouth, and is analogous to the spring constant of an elastic body. In the current context, the elastic body under study is the ‘spring’ composed of tissue and air, comprising the airways, lung parenchyma and chest wall. In the context of asthma and COPD, elastance is thought to be affected mainly by airway closure, rather than changes in the elastic properties of the lung parenchyma¹¹¹. Inertance is an expression of the ‘inertia’ of the respiratory system, its resistance to acceleration. At low oscillation frequencies, inertia does not have a major effect, and the effect of elastance is therefore dominant, resulting in a negative reactance. At the resonant frequency, elastance and inertance are in balance, so that there is no phase difference between pressure and flow, and reactance is zero. Above the resonant frequency, inertia becomes the dominant force, and reactance is therefore positive.

If the forcing waveform delivered to the respiratory system is a simple sinusoid at a single frequency, then resistance and reactance will only be determined at this frequency. In order to obtain information about more than one frequency simultaneously, more complex waveforms incorporating multiple sinusoids at different frequencies may be used. The pressure and flow signals may be decomposed into their discrete component frequencies using a mathematical technique known as a Fourier transform, and the impedance may then be calculated at each frequency. The waveform employed in IOS consists of alternative positive and negative impulses, which are each analysed separately to obtain a resistance and a reactance at that time point, across a frequency range spanning 5Hz – 35Hz.

2.4.2 Patient testing procedure

IOS was performed in triplicate according to standard guidelines¹⁰¹ using the Jaeger MasterScreen Impulse Oscillometry System (Viasys Healthcare GmbH, Hoechberg, Germany). A volume calibration was performed daily using a 3 L syringe, and the accuracy of resistance measurements was confirmed daily using a standard 0.2 kPaL⁻¹s resistance mesh. The ambient temperature and atmospheric pressure was checked daily and entered into the system. Participants wore a nose clip and supported their cheeks whilst an impulse waveform was delivered to their respiratory system via a loudspeaker connected to a mouthpiece incorporating a bacterial filter (MicroGard, CareFusion, Basingstoke, UK) during 60 seconds of tidal breathing. Resistance at 5Hz (R5), resistance at 20Hz (R20), R5-R20, reactance at 5Hz (X5) and AX were automatically calculated by the IOS device from pressure and flow measurements recorded throughout the 60-second period. The mean value for each parameter across the triplicate measurements was recorded.

2.5 Multiple breath inert gas washout

2.5.1 Hardware specifications

MBW was performed using a modified Innocor photoacoustic gas analyser (Innovision A/S, Odense, Denmark), with 0.2% SF₆ as the inert tracer gas, as described by Horsley *et al*¹³², and according to standard guidelines¹³⁰. The Innocor device is a small, portable

unit which weighs approximately 8 kilograms and has dimensions of $35 \times 29 \times 26$ cm. It was originally designed to measure cardiac output at rest and during exercise, by measuring the difference in absorption between N_2O , which crosses the alveolar-capillary membrane, and SF_6 , which does not. In addition, the device can simultaneously measure oxygen uptake and carbon dioxide production. At the heart of the Innocor device is a photoacoustic gas analyser, which is capable of measuring the concentrations of CO_2 , SF_6 and N_2O at high accuracy and temporal resolution. It is sensitive to low concentrations of SF_6 within an operating range of $0 - 0.5\%$ ²¹⁸. The photoacoustic gas analyser works by exposing the gas sample to a beam of infra-red light at three separate frequencies, each of which is absorbed by one of the three compounds measured, and converted to heat. The beam of light is pulsed at three separate frequencies, resulting in cyclical heating and cooling of the measured gases, which in turn produces pressure (sound) waves at a specific frequency for each compound. These sound waves are detected by a microphone and used to determine the concentration of each compound. A separate oxygen analyser is placed in series before the photoacoustic analyser, since the photoacoustic principle cannot be used to detect monoatomic species. A photograph of the device is shown in Figure 2.1.

A number of modifications were made to the Innocor device to facilitate the performance of MBW. Firstly, the commercially supplied patient interface has an excessive dead space for inert gas washout, and was therefore replaced with a mesh-type pneumotachometer (3700 series, Hans Rudolph Inc., Kansas City, Missouri, USA), heated to $37^\circ C$ using a 3850A series pneumotachometer heater (Hans Rudolph Inc., Kansas City, Missouri, USA). The patient interface, shown in Figure 2.2, comprised a rubber mouthpiece connected to a bacterial filter (Clear-Guard Midi, Intersurgical, Wokingham, Berkshire, UK), which was in turn connected to the pneumotachometer. The gas sample needle was positioned distal to the pneumotachometer mesh, resulting in a minimal post-capillary dead space of 2.65 ml. The pre-capillary dead space was calculated as 40 ml for *in vitro* tests and 54.6 ml for *in vivo* tests (due to the additional dead space of the rubber mouthpiece).

Figure 2.1: Innocor photoacoustic gas analyser

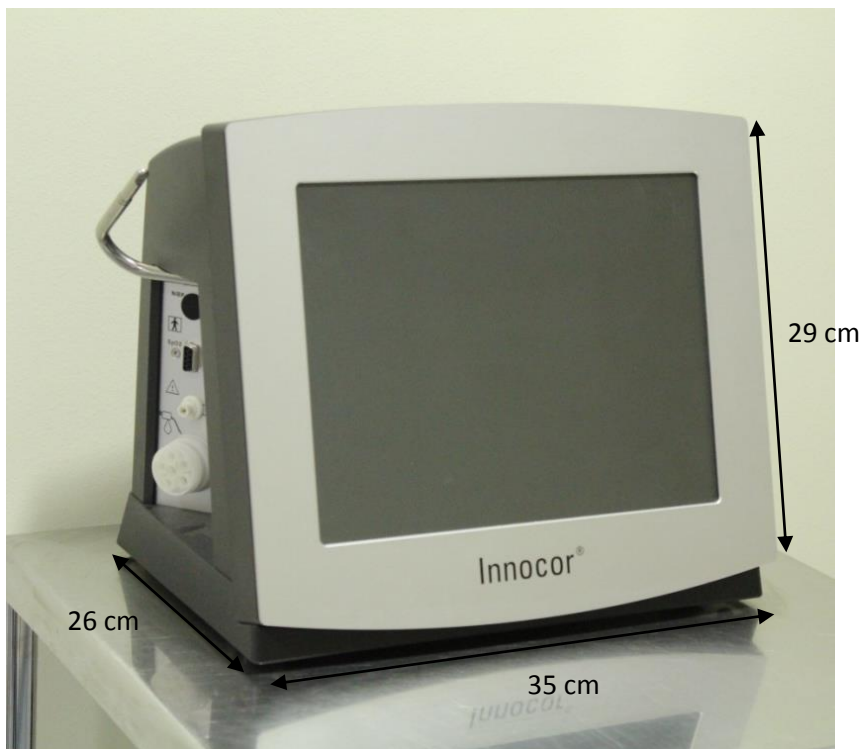
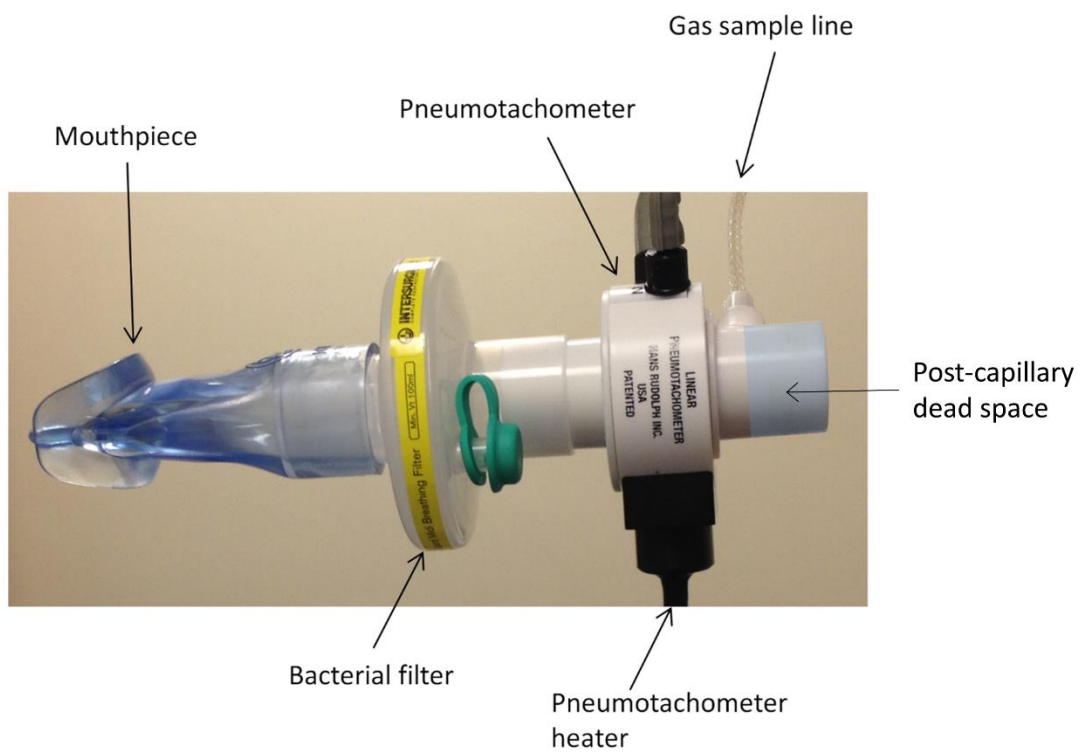


Figure 2.2: Patient interface for the performance of multiple breath inert gas washout



The flow signal was split between the Innocor device and a separate laptop computer, which was utilised to provide a visual guide to participants, so that they could adjust their tidal volume to approximately 1L. This was accomplished using a custom program, written using TestPoint (Measurement Computing Corporation, Norton, Massachusetts, USA) and provided to us by Dr. Per Gustafsson, Skövde, Sweden. A further modification made to the Innocor device was to manually bypass the oxygen analyser by diverting the internal Nafion tubing directly into the photoacoustic analyser. This had the effect of reducing both the gas analyser rise time and the flow-gas delay time.

Before the commencement of testing on each day, a volume calibration was performed using a 1L syringe at three different flow rates, in order to ensure accuracy of flow and volume measurements made by the Innocor device. A separate volume calibration, using the same 1L syringe, was performed to ensure accuracy of the TestPoint software used by participants to monitor their tidal volume.

2.5.2 Patient testing procedure

Participants were tested in a comfortable seated position, wearing a noseclip, and breathing exclusively through the rubber mouthpiece. Throughout the test, care was taken to ensure a good seal was maintained around the mouthpiece, and participants were encouraged to maintain a steady respiratory rate of approximately 12 breaths per minute, and a constant tidal volume of 1L¹³¹, using a real-time visual display of inspired volume as a guide. The first stage of the test was the wash-in phase, during which participants breathed an air mixture containing 0.2% SF₆, via an open-circuit bypass flow system. This comprised a Douglas bag, which acted as a reservoir for the SF₆ air mixture, connected to a valve, such that subjects inspired from the bag, but expired air was vented to the atmosphere. During the wash-in phase, the flow of SF₆ air mixture was adjusted to ensure that the Douglas bag remained approximately half-full, and participants were given instructions as appropriate to ensure that they maintained the required tidal volume and respiratory rate. Wash-in was continued until the expired SF₆ concentration was within 0.004% of the inspired concentration for at least three consecutive breaths. Participants were then switched to breathing room air during an expiration, by swiftly removing the Douglas bag from the end of the patient interface, and asked to continue breathing at the same respiratory rate and tidal volume. The end-

tidal concentration of SF₆ in exhaled breath (C_{et}) was recorded during this washout phase until it fell below 1/40th of the original concentration (0.005%) for three consecutive breaths, at which point the test was terminated.

MBW tests were performed in triplicate for each participant. In order to ensure consistency of results, a preliminary analysis was performed to verify that measured FRC values for the three tests did not differ by more than 10%¹²⁹. If no two tests were consistent then further washout runs were performed (to a maximum of five tests) until at least two tests were consistent. The final results reported for each participant comprised the average of the two or three consistent tests performed. If two consistent tests could not be obtained then this was recorded, and the results for that participant were not used.

2.5.3 Analysis of multiple breath washout data

The raw MBW data consisted of a flow and SF₆ signal, sampled at a rate of 100Hz. These data were transferred from the Innocor device to a laptop computer, where they were processed and analysed using custom software written with TestPoint (Measurement Computing Corporation, Norton, Massachusetts, USA), provided by Dr. Per Gustafsson. The first step in the process was to calculate the flow-gas delay time for each washout test, which was subsequently used to synchronise the flow and SF₆ concentration signals. The flow-gas delay time arises due to a combination of the gas analyser response time, which is approximately 154ms¹³⁰, and the time taken for gas to be drawn down the Nafion tubing from the patient interface to the photoacoustic analyser, at a sampling flow rate of 120 ml/minute¹³⁰. The flow-gas delay time was calculated using the method based upon re-inspiration of SF₆ from the post-capillary dead space¹³⁰. Specifically, the time point at which the post-capillary dead space had been inspired was aligned with the time point at which the inspired SF₆ concentration fell to 50% of its initial value. FRC was calculated by dividing the total volume of SF₆ expired by the difference between C_{et} at the beginning and end of the washout period²¹⁹. The end of the washout period for this purpose was taken to be the first expired breath in which C_{et} fell below 1/40th of the original SF₆ concentration. The total volume of expired SF₆ was calculated by integrating flow and SF₆ concentration over the course of each expiration, and subtracting the re-inspired SF₆ volume, which was in turn calculated by integrating flow and SF₆ concentration over the course of each

inspiration. LCI was defined as the cumulative expired volume (CEV) at the point at which C_{et} fell to $1/40^{\text{th}}$ of its initial value, divided by the FRC¹³⁵. Both FRC and CEV were corrected for equipment dead space (DS_{eq}) by subtracting this volume (54.6 ml) from the calculated FRC, and from the expiratory volumes used to calculate CEV. The anatomical dead space (VD_{anat}) was calculated using the method of Langley¹³⁰.

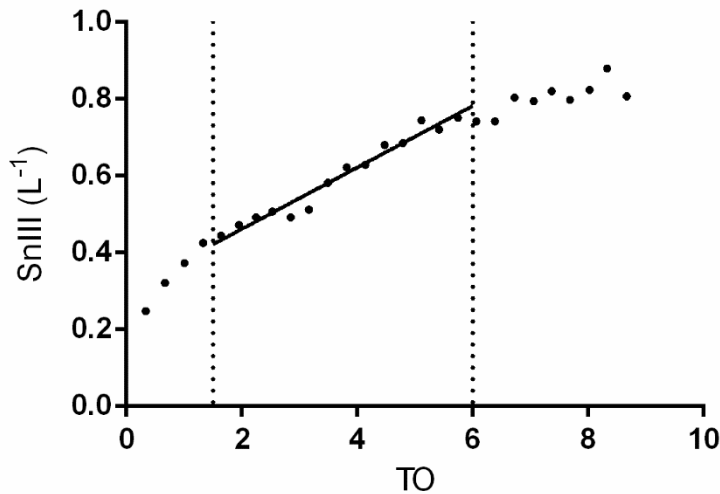
Phase III slope parameters were calculated by first determining the raw phase III slopes (SIII) of each expiration of the washout, as illustrated in Figure 1.3. The start and end points of the phase III slope were adjusted manually for each breath, to ensure that phases II and IV were not included. The TestPoint program automatically produced a linear regression line of the selected portion of the expirogram, and the slope for each breath was recorded. The data were then exported as an Excel file and further analysed using Excel 2007 (Microsoft Corporation, Redmond, Washington, USA). SIII values were concentration-normalised by dividing them by the mean expired SF_6 concentration over the course of phase III, to yield SnIII values for each breath. The tidal volume correction of Aurora *et al*¹⁴⁶ was not used, since most patients successfully adhered to the 1L tidal volume protocol, thus making this correction unnecessary. SnIII was then plotted against turnover number for each expiration, as illustrated in Figure 2.3. S_{cond} was calculated as the rate of increase of SnIII between 1.5 and 6 turnovers, whilst S_{acin} was the SnIII of the first breath minus a small correction factor to account for the CDI component of the first breath. S_{cond}^* and S_{acin}^* were calculated analogously to S_{cond} and S_{acin} , except that S_{cond}^* was based upon SnIII values between 0 and 3 turnovers, excluding the first breath of the washout, instead of between 1.5 and 6 turnovers¹⁴⁹. Phase III slope parameters may be calculated for each washout test separately (Figure 2.3, Panel A), or alternatively three washout tests may be analysed in combination (Figure 2.3, Panel B). In this thesis each washout was analysed separately.

Figure 2.3: Calculation of phase III slope parameters

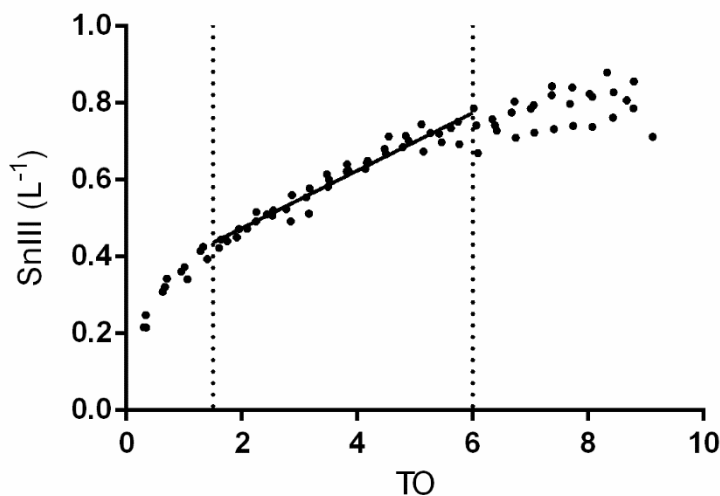
Panels A and B show plots of normalised phase III slopes (S_{nIII}) against turnover number (TO) in a patient with asthma. Panel A shows data from a single washout test, while Panel B shows data from three washout tests combined. S_{cond} is the slope of the best-fit regression line of the points between TO numbers 1.5 and 6. S_{acin} is given by the following equation:

$$S_{acin} = \text{First breath } S_{nIII} - (S_{cond} \times \text{TO number of first breath})$$

Panel A



Panel B



2.6 Validation of multiple breath washout technique using a lung model

Validation was performed using a simple one-compartment model of the lung consisting of an enclosed clear acrylic glass tank (Soloplex, Tidaholm, Sweden), partly filled with water at 37°C, as recommended in current guidelines¹³⁰. The lung model was designed by Dr. Per Gustafsson, and had previously been used to validate an alternative MBW system¹³⁴. In order to achieve BTPS conditions within the phantom lung, it was enclosed within a further acrylic glass tank containing water that was kept at a constant temperature of 37°C by a thermostat. The dimensions of the outer and inner tanks are shown in Figure 2.4, Panels A and B, respectively.

The inner tank was fitted with an off-centre vertical partition that divided it into a larger and a smaller section. The partition did not reach the base of the tank, thus allowing the two sides to communicate, but the water level was always kept above the lower end of the partition. The lid of the larger section was connected to a bi-level positive airway pressure ventilator (Vivo 30, Breas Medical AB, Mölnlycke, Sweden) which exerted alternating high and low pressures on the water surface, designated inspiratory and expiratory positive airway pressures (IPAP and EPAP), respectively. Due to the communication below the partition, this caused the water level in the smaller section to alternately rise and fall, simulating diaphragmatic movement. The IPAP setting on the ventilator determined the FRC of the phantom lung, whilst the difference between the IPAP and EPAP settings determined the tidal volume (V_T). The lid above the smaller section was modified to fit the patient interface described in Section 2.5, with the exception that the rubber mouthpiece was omitted and the lung model attached directly to the bacterial filter. A photograph of the lung model whilst in use is shown in Figure 2.5.

Figure 2.4: Schematic diagram of lung model for the validation of multiple breath washout technique

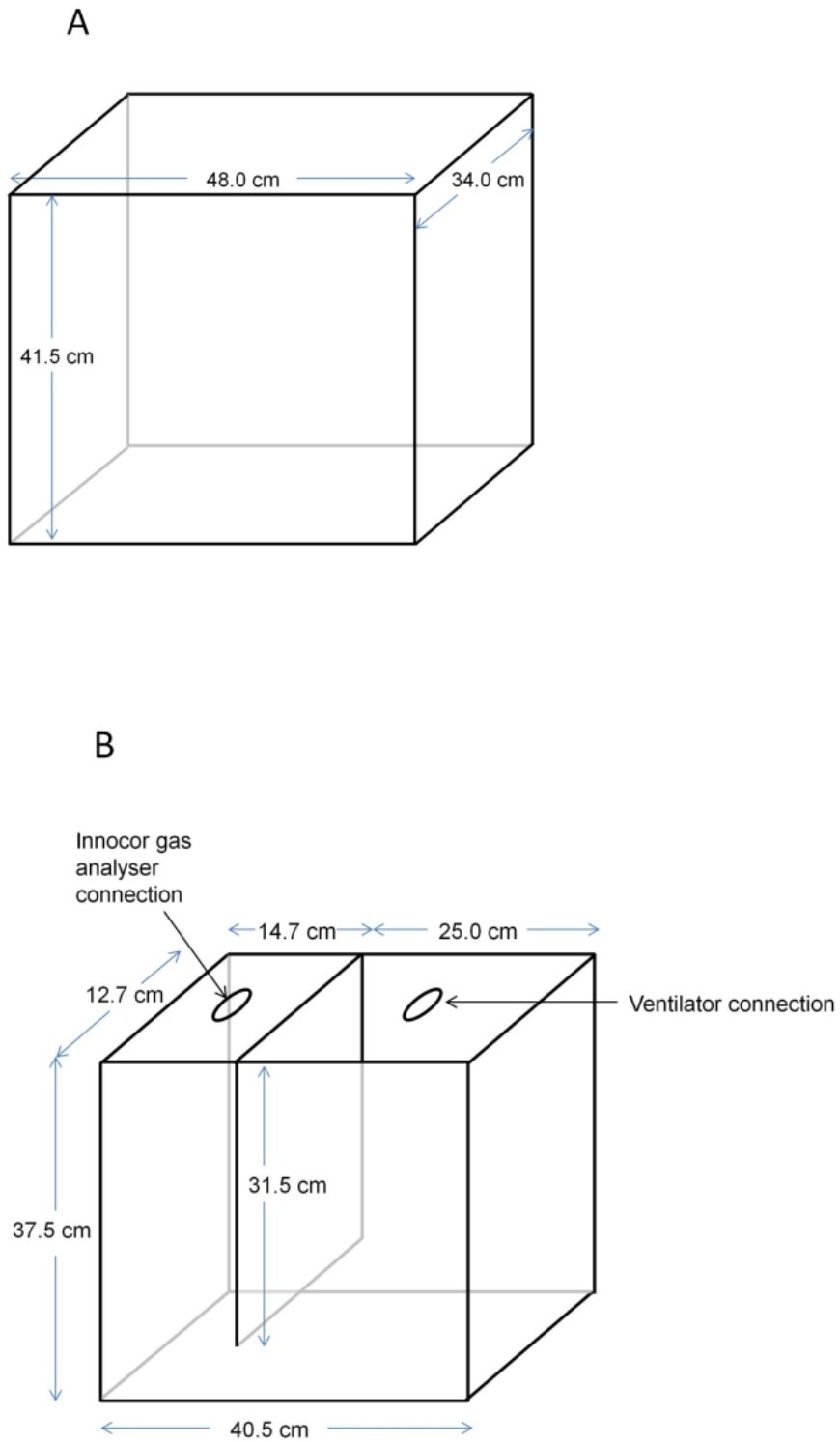
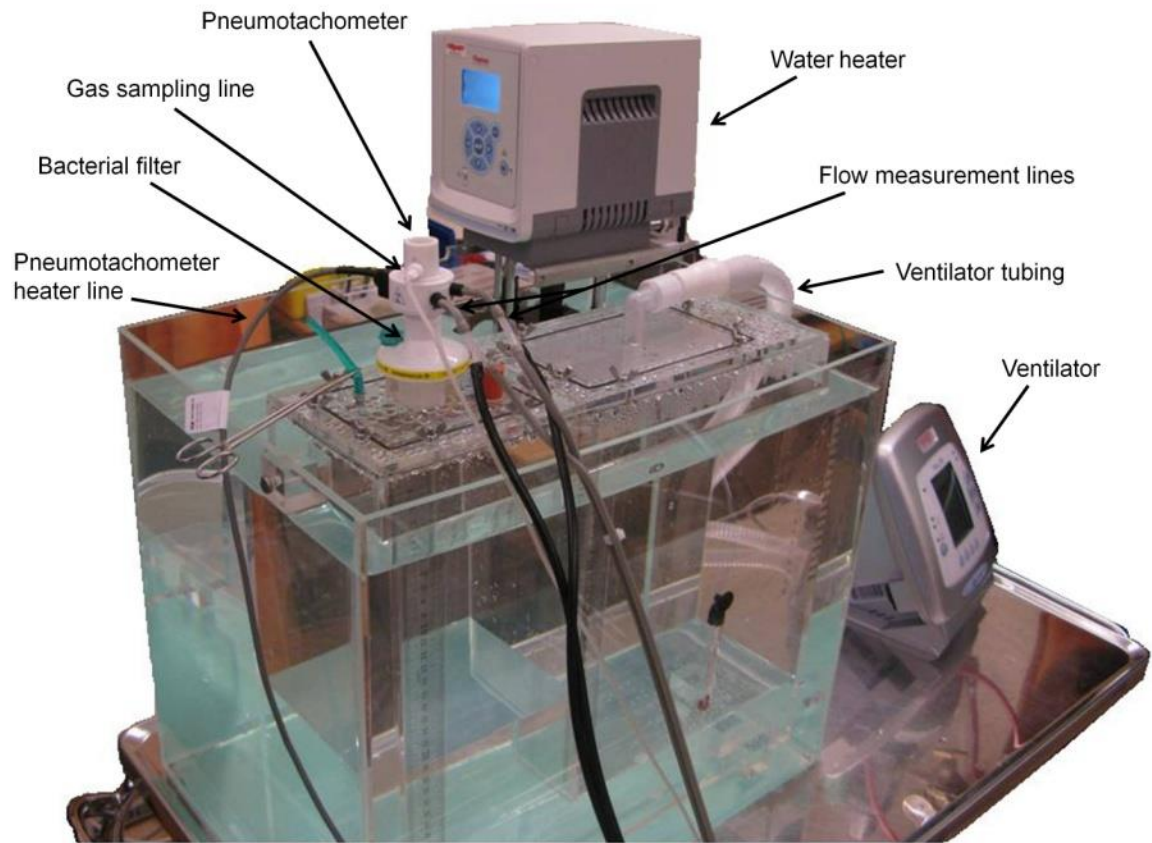


Figure 2.5: Photograph of lung model for the validation of multiple breath washout technique



The testing procedure consisted of the following steps:

- i) The water level, IPAP setting and EPAP setting were adjusted to achieve the required FRC and V_T within the lung model. This was facilitated by a measuring scale affixed to the inside of the lung model, which was utilised to measure the water level at its highest and lowest points during the respiratory cycle. Respiratory rate was set using the ventilator controls.
- ii) An air mixture containing 0.2% SF_6 was passively insufflated into the lung phantom via an open-circuit bypass flow system, and expiratory SF_6 concentration was monitored online using the Innocor gas analyser. The flow rate of SF_6 through the open circuit was increased sufficiently to allow complete wash-in of SF_6 .
- iii) Once complete equilibration (wash-in) had occurred, meaning that the inspired and expired SF_6 concentrations were equal, the bypass flow system was removed so that the lung model inspired from ambient air. Expiratory SF_6 concentration continued to be monitored during the wash-out phase, and the experiment was terminated once the expired SF_6 concentration fell below 0.005% ($1/40^{\text{th}}$ initial value) for three consecutive breaths.
- iv) Washout data were exported to a separate laptop computer, where they were analysed to derive the FRC and LCI.

2.7 Development of novel multiple breath washout parameters

2.7.1 Derivation of the novel parameters

Gustafsson *et al* recently reported a method for estimating the size of the “fast” (well-ventilated) and “slow” (poorly-ventilated) compartments in patients with CF using inert gas washout²²⁰. However, their method was not specifically indexed to the LCI, and in particular did not allow estimation of the relative contributions of specific ventilation inequality and increased respiratory dead space. This section describes the development of novel MBW parameters that estimate the contributions of each of these mechanisms to increased LCI in a given patient.

In order to simulate washout curves incorporating specific ventilation inequality between lung units, it is clear that an anatomical model with at least two compartments will be required. However, before introducing the two-compartment model, it is useful to briefly describe the even simpler one-compartment model of the lung. Consider the washout of a single uniformly ventilated alveolar compartment subtended by a conducting airway. The FRC is the sum of the alveolar volume (V_A) at end expiration and the conducting airway volume, or anatomical dead space ($V_{D_{\text{anat}}}$), which is considered to be fixed and to not take part in gas mixing.

Let FRC = functional residual capacity

$V_{D_{\text{anat}}}$ = anatomical dead space

V_T = tidal volume

With each successive inspiration, the SF_6 concentration in the alveolar compartment will be diluted by a fixed ratio. This dilution ratio was derived by Fowler *et al.*²²¹, and is equal to:

$$\frac{FRC}{FRC + V_T - V_{D_{\text{anat}}}}$$

Therefore, the SF_6 concentration in the alveolar compartment following the n^{th} inspiration will be equal to the initial SF_6 concentration (0.2%) multiplied by the dilution ratio raised to the power of n :

$$0.2 \times \left(\frac{FRC}{FRC + V_T - V_{D_{\text{anat}}}} \right)^n$$

This is an exponential decay curve, of which the standard form is:

$$y = a \times e^{-kx}$$

Where a = y-intercept of the curve

k = rate constant

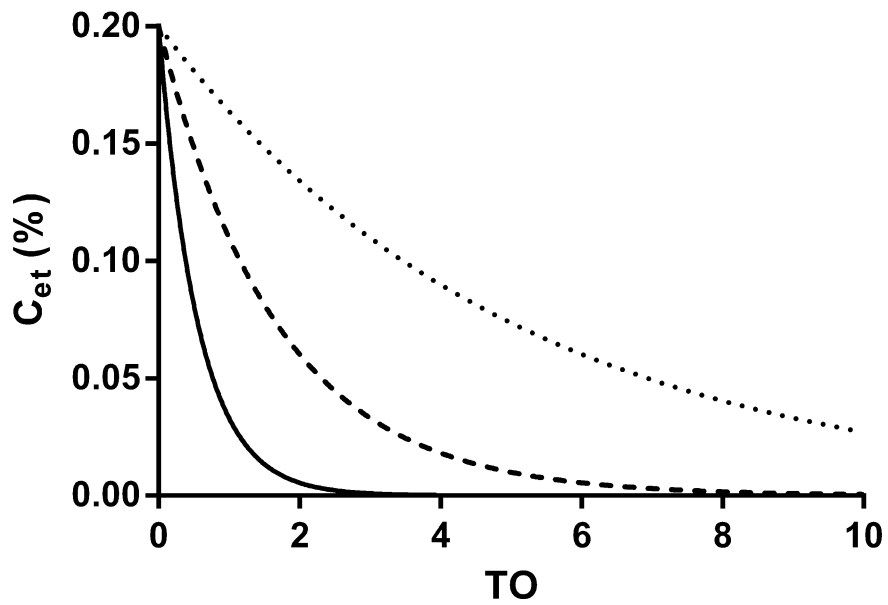
e = the base of natural logarithms ≈ 2.718

Assuming that the initial SF₆ concentration is 0.2%, the y-intercept parameter will be set at 0.2, and thus the only parameter that may vary is the rate constant k . The x-axis units may be breath number or TO number, but TO is preferred since it smoothes irregularities in the washout curve caused by variations in tidal volume. Figure 2.6 shows example exponential decay curves with different rate constants, illustrating that a higher rate constant results in a more rapid decay.

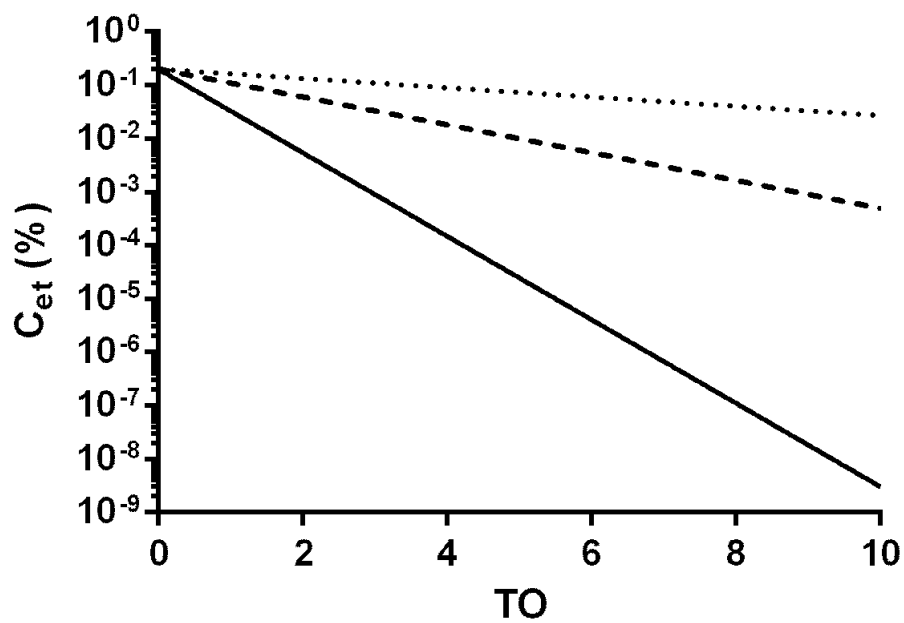
Figure 2.6: Exponential decay curves

Exponential decay curves are shown with rate constants of 0.2 (dotted line), 0.6 (dashed line) and 1.8 (continuous line), using linear (Panel A) and semilog (Panel B) scales.

Panel A



Panel B



In order to simulate the washout of a two-compartment lung model we require a two-phase exponential decay curve, which has the following general form:

$$y = (a \times e^{-jx}) + (b \times e^{-kx})$$

Where j = fast rate constant
 k = slow rate constant
 a = weighting of fast rate constant
 b = weighting of slow rate constant

The y-intercept of this curve is equal to $a + b$. Since in our case this is set at 0.2 (the initial SF₆ concentration), we can re-write the above equation as:

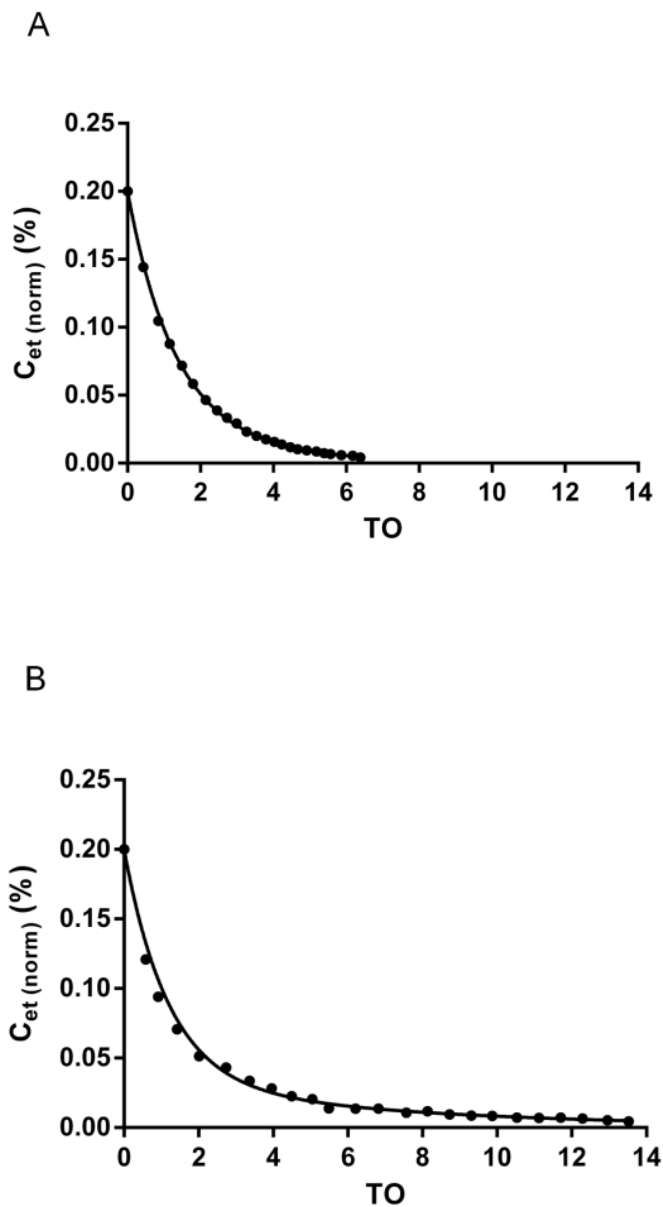
$$y = 0.2 \times (c \times e^{-jx} + [1 - c] \times e^{-kx})$$

Where c = proportionate weighting of fast-decaying component, and $0 < c < 1$

This curve therefore has three variable parameters (or degrees of freedom), namely the fast rate constant (j), the slow rate constant (k) and the proportionate weighting of the fast-decaying component (c). The curve-fitting software Prism 6 (GraphPad Software Inc., La Jolla, California, USA) was used to fit experimental washout curves (normalised to an initial SF₆ concentration of 0.2%) to the above model, which is also known as a two-phase decay model. This was performed using non-linear regression with a weighting of $1/y^2$ in order to minimise the sum of relative, rather than absolute, squared residuals. This was so that data points near the start of the washout curve (where absolute C_{et} values were higher) did not disproportionately impact upon the model fit. The initial values for j , k and c utilised in the curve fitting process were determined automatically by Prism 6, using in-built rules. Figure 2.7 shows washout curves from a healthy subject and a patient with CF fitted to a two-phase exponential decay model.

Figure 2.7: Washout curves from a healthy subject and a patient with cystic fibrosis fitted to a two-phase exponential decay model

Washout curves from a healthy subject (Panel A) and a patient with severe CF (Panel B) are fitted to a two-phase exponential decay curve, with a good model fit in both cases (goodness of fit [R^2] = 0.9973 and 0.9775, respectively). $C_{et(norm)}$ represents end-tidal SF₆ concentration, normalised to a starting concentration of 0.2%.



A natural anatomical model that would be expected to behave according to the equation above comprises two lung units in parallel, each consisting of an alveolar compartment subtended by a conducting airway. The constants j and k correspond to the rate constants for the washout of the over-ventilated (fast) and under-ventilated (slow) lung units respectively, which have resting (end-expiratory) volumes of V_{fast} and V_{slow} , respectively. The SF_6 concentration of the expired gas from this system is equal to the weighted mean of the SF_6 concentrations in each of the two alveolar compartments at end-inspiration, where the weighting is determined by the proportion of ventilation reaching each lung unit. Thus, the anatomical interpretation of the constant c , defined above, is the proportion of the tidal volume reaching the fast lung unit.

It is now possible to derive two anatomical parameters from the two-compartment model, one of which reflects specific ventilation inequality between the lung units, and the second of which reflects the effective respiratory dead space ($V_{D_{resp}}$). A natural measure of specific ventilation inequality is the ratio of the specific ventilation of the slow lung unit to that of the fast lung unit, which we refer to as the specific ventilation ratio (SVR).

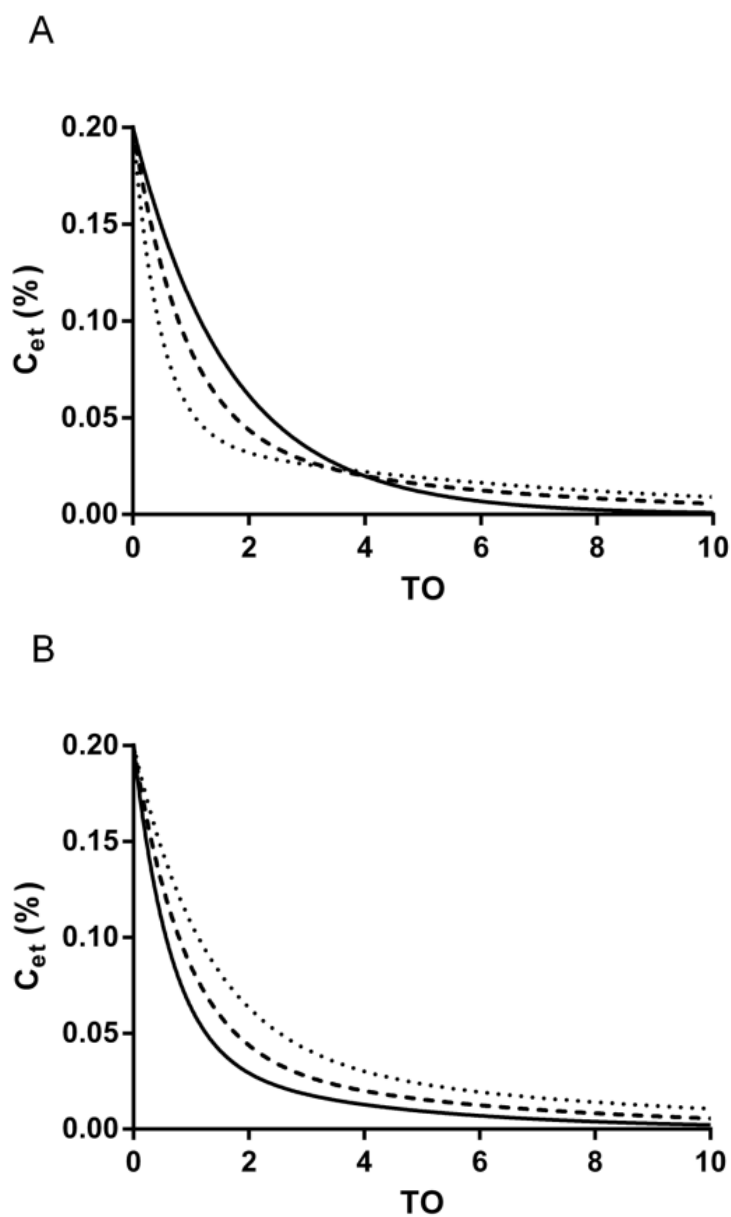
Figure 2.8 shows simulated washout curves based upon this two-compartment lung model, demonstrating the effect of alterations in SVR or $V_{D_{resp}}$. In these simulations, the proportion of ventilation reaching the fast lung unit (c) was kept constant at 0.8, and the anatomical dead space was kept constant at 0.2L. The expired SF_6 concentration measured at the mouth during the n^{th} expiration was calculated as the weighted mean of the washouts of the two compartments, and was given by the formula:

$$0.04 \times \left(\frac{V_{slow}}{V_{slow} + \frac{V_T}{5} - \frac{V_{D_{resp}}}{5}} \right)^n + 0.16 \times \left(\frac{V_{fast}}{V_{fast} + \frac{4 \times V_T}{5} - \frac{4 \times V_{D_{resp}}}{5}} \right)^n$$

Increasing SVR results in a change in the shape of the washout curve such that there is a rapid initial phase followed by a slow terminal phase, whereas increasing $V_{D_{resp}}$ results in a prolongation of the washout curve but without altering its shape. In both cases, the result is an increase in LCI.

Figure 2.8: Simulated washout curves

Panel A shows simulated washout curves with a fixed respiratory dead space of 0.4L and a specific ventilation ratio of 0.6 (continuous line), 0.15 (dashed line) and 0.05 (dotted line). Panel B shows simulated washout curves with a fixed specific ventilation ratio of 0.15 and a respiratory dead space of 0.1L (continuous line), 0.4L (dashed line) and 0.6L (dotted line).



From the definition of SVR as the ratio of the specific ventilation of the slow lung unit to that of the fast lung unit we may write:

$$SVR = \frac{\left(\frac{[1-c] \times V_T}{V_{slow}}\right)}{\left(\frac{c \times V_T}{FRC - V_{slow}}\right)} = \frac{(1-c)(FRC - V_{slow})}{c \times V_{slow}} = \frac{(1-c)(1-W)}{cW}$$

Where V_{slow} = volume of slow lung unit at FRC
 $W = V_{slow}/FRC$

$$SVR = \frac{(1-c)(1-W)}{cW}$$

$$W = \frac{1-c}{c \times SVR - c + 1}$$

As stated above, $C_{et(norm)}$ against TO curves can be accurately modelled by the following equation:

$$y = 0.2 \times (c \times e^{-jx} + [1-c] \times e^{-kx})$$

The subsequent analysis is simplified if this equation is expressed in terms of breath number (n) rather than TO. This change of scale is achieved by multiplying the rate constants j and k by a constant term to yield the new equation:

$$y = 0.2 \times (c \times e^{-rn} + [1-c] \times e^{-sn})$$

Where $r = j \times (V_T - DS_{eq})/FRC$, and $s = k \times (V_T - DS_{eq})/FRC$

DS_{eq} = equipment dead space between the patient's mouth and the gas sampling capillary, and was equal to 0.0546 L using our inert gas washout system.

Following the n^{th} inspiration, the SF_6 concentration is equal to $0.2 \times e^{-rn}$ in the fast compartment and $0.2 \times e^{-sn}$ in the slow compartment. Using the formula for the dilution ratio in a single compartment²²¹, and assuming that both tidal volume and respiratory dead space are distributed between the over-ventilated and under-ventilated lung units in a ratio of c to (1 - c), we may write the following equations:

$$0.2 \times e^{-rn} = 0.2 \times \left(\frac{FRC \times (1 - W)}{FRC \times (1 - W) + c \times V_T - c \times V_{D_{resp}}} \right)^n$$

$$0.2 \times e^{-sn} = 0.2 \times \left(\frac{FRC \times W}{FRC \times W + (1 - c) \times V_T - (1 - c) \times V_{D_{resp}}} \right)^n$$

Let $p = e^{-r}$ and $q = e^{-s}$

Then:

$$p = \frac{FRC \times (1 - W)}{FRC \times (1 - W) + c \times V_T - c \times V_{D_{resp}}}$$

$$q = \frac{FRC \times W}{FRC \times W + (1 - c) \times V_T - (1 - c) \times V_{D_{resp}}}$$

By solving these two equations in the two unknowns W and $V_{D_{resp}}$ the following formulae are derived:

$$V_{D_{resp}} = V_T + \frac{FRC \times (pq - p - q + 1)}{(pq - pc - q[1 - c])}$$

$$W = \frac{cpq - cq - pq + q}{cp - cq + q - pq}$$

Substituting:

$$W = \frac{1 - c}{c \times SVR - c + 1}$$

We obtain the following formula:

$$SVR = \frac{pq - p}{pq - q}$$

We may now utilise the values of c , $V_{D_{resp}}$ and SVR derived above to determine:

- i) LCI_{ideal} – The expected value of LCI assuming no specific ventilation inequality, and no additional respiratory dead space over and above $V_{D_{anat}}$.
- ii) LCI_{vent} – The proportional increase in LCI over and above LCI_{ideal} , taking into account specific ventilation inequality but assuming no additional respiratory dead space.
- iii) LCI_{ds} – The proportional increase in LCI over and above LCI_{ideal} , taking into account additional respiratory dead space, but assuming no specific ventilation inequality.

LCI_{ideal} and LCI_{ds} are calculated using the following formulae, which are based upon the dilution ratio in a single compartment²²¹:

$$LCI_{ideal} = \frac{\ln(0.025) \times (V_T - DS_{eq})}{FRC \times \ln\left(\frac{FRC}{FRC + V_T - V_{D_{anat}}}\right)}$$

$$LCI_{ds} = \frac{\ln\left(\frac{FRC}{FRC + V_T - V_{D_{anat}}}\right)}{\ln\left(\frac{FRC}{FRC + V_T - V_{D_{resp}}}\right)}$$

In order to determine LCI_{vent} , we utilise the values of c and SVR derived above, but set $V_{D_{resp}}$ to equal $V_{D_{anat}}$. We then reverse the algebraic steps described above in order to arrive at two new rate constants j' and k' . The values of c , j' and k' are then plugged into our original equation for the washout of a two-compartment model, with C_{et} on the y-axis and TO number on the x-axis:

$$y = 0.2 \times (c \times e^{-j'x} + [1 - c] \times e^{-k'x})$$

Setting $y = 0.005$ ($1/40^{\text{th}}$ of the original inert gas concentration of 0.2) yields the equation:

$$c \times e^{-j'x} + (1 - c) \times e^{-k'x} = 0.025$$

This equation may be solved numerically to any desired degree of accuracy in the unknown x . The solution is then divided by LCI_{ideal} to yield LCI_{vent} .

2.7.2 Step-by-step instructions for calculating LCI_{vent} and LCI_{ds}

This section summarises the calculation of LCI_{vent} and LCI_{ds} in a step-by-step fashion using Prism 6 (GraphPad Software Inc., La Jolla, California, USA):

Step 1

Choose an X-Y table format and enter the data with TO number on the x-axis and C_{et} on the y-axis. The initial SF_6 concentration (ie. the SF_6 concentration of expired air at the end of the wash-in phase) should be entered against a TO number of zero, and is thus the y-intercept of the curve. If a number of washout curves are to be analysed, it is convenient to normalise C_{et} values to a consistent initial SF_6 concentration such as 0.2% so that the y-intercept of the curve is always the same. For instance, if a given washout curve has an initial SF_6 concentration of 0.198%, the curve is normalised to a starting value of 0.2% by multiplying each C_{et} value by $0.2/0.198$.

Step 2

Choose the analysis method 'non-linear regression' and fit to the equation 'two phase decay'. In the Constrain tab, set:

Y0 – Constant equal to 0.2

Plateau – Constant equal to 0

PercentFast – Must be between zero and 100.0

KFast – No constraint

KSlow – Must be greater than 0

KFast must be greater than 1.0 times KSlow

In the Weights tab, choose: Weight by $1/y^2$

Press 'OK' to perform the analysis. This should produce values for PercentFast, KFast and KSlow. KFast and KSlow represent the rate constants for the washouts of the fast and slow lung units, respectively. These are represented as j and k respectively in the equations in Section 2.7.1. PercentFast represents the percentage of the tidal volume reaching the fast lung unit, and is equivalent to the parameter c in Section 2.7.1 (multiplied by a factor of 100, since PercentFast is a percentage while c is a proportion)

Step 3

Set:

$$KFast_{(b)} = \frac{KFast \times (V_T - DS_{eq})}{FRC}$$

$$KSlow_{(b)} = \frac{KSlow \times (V_T - DS_{eq})}{FRC}$$

Step 4

Set:

$$p = e^{-KFast_{(b)}}$$

$$q = e^{-KSlow_{(b)}}$$

$$c = \frac{PercentFast}{100}$$

Then:

$$SVR = \frac{pq - p}{pq - q}$$

$$V_{D_{resp}} = V_T + \frac{FRC \times (pq - p - q + 1)}{(pq - pc - q[1 - c])}$$

Step 5

LCI_{ideal} and LCI_{ds} are given by the following formulae:

$$LCI_{ideal} = \frac{\ln(0.025) \times (V_T - DS_{eq})}{FRC \times \ln\left(\frac{FRC}{FRC + V_T - V_{D_{anat}}}\right)}$$

$$LCI_{ds} = \frac{\ln\left(\frac{FRC}{FRC + V_T - V_{D_{anat}}}\right)}{\ln\left(\frac{FRC}{FRC + V_T - V_{D_{resp}}}\right)}$$

To calculate LCI_{vent} , utilise the values of c and SVR derived in step 4, and perform the following algebraic steps:

$$W = \frac{1 - c}{c \times SVR - c + 1}$$

$$p = \frac{FRC \times (1 - W)}{FRC \times (1 - W) + c \times V_T - c \times V_{D_{anat}}}$$

$$q = \frac{FRC \times W}{FRC \times W + (1 - c) \times V_T - (1 - c) \times V_{D_{anat}}}$$

$$r = -\ln p$$

$$s = -\ln q$$

$$j' = \frac{r \times FRC}{(V_T - DS_{eq})}$$

$$k' = \frac{s \times FRC}{(V_T - DS_{eq})}$$

Using the values of c , j' and k' derived above, solve the following equation numerically in the unknown x :

$$c \times e^{-j'x} + (1 - c) \times e^{-k'x} = 0.025$$

Divide the value of x obtained by LCI_{ideal} to yield LCI_{vent} .

2.8 Quantitative computed tomography

Volumetric whole lung scans were obtained using a Siemens Sensation 16 scanner using the following low dose protocol; 16 x 0.75 mm collimation, 1.5 mm pitch, 120 kVp, 40 mAs, 0.5 seconds rotation time and scanning field of view of 500 mm, dose modulation off. Scans were obtained at full inspiration and full expiration. Participants were coached in the breath holding technique immediately prior to scanning. Images were reconstructed with a slice thickness of 0.75 mm at a 0.5 mm interval using B35f kernel. VIDA Apollo image analysis software (VIDA Diagnostics, Coralville, Iowa) was used for quantitative analysis of lung densitometry, and the geometry of the major segmental bronchi. The main parameters extracted were:

- i) Ratio of mean lung density on expiration to inspiration (MLD E/I) – a marker of expiratory air trapping¹⁷¹
- ii) Fifteenth lower percentile of inspiratory lung density (P_{15}) – a marker of emphysema²²²
- iii) Right upper lobe apical segmental bronchus (RB1) wall area
- iv) RB1 wall percentage
- v) RB1 luminal area

Computed tomography was not performed in female patients under the age of 30, and the maximum allowed dose of radiation from research CT scans for any participant was 10 mSv over a three year period.

2.9 Hyperpolarised ³helium diffusion magnetic resonance

2.9.1 Theoretical background

Magnetic resonance techniques are based upon the physical principle that any spinning charged particle generates a magnetic field, effectively acting as a bar magnet²²³. The nucleus of a hydrogen atom comprises a single proton, and most clinical MR applications rely upon imaging protons in the body. However, proton imaging is not suitable for imaging the airways or measuring diffusive processes in the lungs, since the density of protons in ambient air is too low. For these applications, it is necessary for the subject to inhale a gas which acts as a magnetic dipole so that a measurable MR

signal can be produced and detected. The work presented in this thesis makes use of diffusion MR measurements using hyperpolarised ^3He . Hyperpolarisation is the process by which atoms are imparted with an increased nuclear polarisation¹⁷⁹, thus increasing the signal strength that may be obtained during MR measurements.

When placed in an external magnetic field such as that generated by an MRI scanner, ^3He nuclei will tend to line up in the direction of the external field (often designated B_0), which is assumed by convention to point longitudinally in the z-axis. The nuclei not only spin about their own axes, they also spin, or precess, around the axis of the external magnetic field. The angular frequency of this precession, known as the Larmor frequency (ω_0), is linearly related to the external magnetic field strength. However, because individual nuclei are not precessing in synchrony (phase) with each other at this point, the net magnetisation vector does not precess, but simply points in the direction of B_0 .

In order to generate a signal that may be used for imaging or other applications, it is necessary to transmit a radiofrequency (RF) pulse into the patient. The RF pulse is an electromagnetic wave, which comprises an electric and a magnetic component. The RF pulse generates a comparatively weak magnetic field along a new axis (designated B_1), perpendicular to B_0 . If the frequency of the RF pulse matches the frequency of precession of the ^3He nuclei around B_0 , resonance will be generated, and they will begin to precess around the new axis B_1 , a process known as flipping, while continuing to precess around the original axis at a much faster rate. This combined spiral motion is known as nutation. As the ^3He nuclei flip, they begin to precess in phase with each other, a phenomenon known as phase coherence. The rotating magnetic field they generate induces an alternating current in coils placed around the patient. This is the basic principle by which an RF pulse may produce a detectable signal from the patient.

The angle at which the ^3He nuclei flip (flip angle) is linearly related to both the power of the RF pulse and the duration of the pulse. A 90° pulse is one that causes the nuclei to flip fully into the transverse plane, resulting in a maximal signal. A 180° pulse causes the nuclei to flip from pointing in the direction of B_0 to pointing in the opposite direction, and thus does not generate an immediate signal, as there is no transverse

magnetisation. However, a 180° pulse also causes the direction of precession of the nuclei to reverse, a phenomenon that is made use of in spin echo pulse sequences.

Once the RF pulse is switched off the signal caused by transverse magnetisation begins to decay. This decaying sinusoidal signal is known as free induction decay (FID). The decay of transverse magnetisation (and thus signal) occurs at a much faster rate than the recovery of longitudinal magnetisation. This is because recovery of longitudinal magnetisation (T1 relaxation) occurs due to only one process, the relaxation of ^3He nuclei back to their equilibrium state, pointing in the direction of B_0 . However, decay of transverse magnetisation (T2* decay) is additionally brought about by loss of synchrony (dephasing) between precessing nuclei. This dephasing occurs due to (i) interactions between the magnetic fields of neighbouring nuclei (spin-spin interactions), and (ii) inhomogeneities (imperfections) in the external magnetic field B_0 .

Gradient coils are components of MRI scanners that allow the generation of additional gradients in the external magnetic field in the x, y or z directions. External magnetic field gradients may be utilised to perform spatial encoding, as well as to measure diffusive processes. The timing of RF and gradient pulses may be represented on a pulse sequence diagram. The top line of a pulse sequence usually indicates the timing and flip angle of each RF pulse. Immediately below this, one or more lines indicate the application of gradients (if applicable) along the x, y or z axes, in the positive or negative direction. The final line indicates the appearance of measurable signals.

2.9.2 Pulse sequences utilised to measure diffusion in the lungs

Figure 2.9a shows a simple pulse sequence that demonstrates the phenomenon of spin echoes. This pulse sequence comprises a 90° pulse which causes flipping of ^3He nuclei into the transverse plane, resulting in a rapidly decaying FID signal. This is followed, after a time period τ from the 90° pulse, by a 180° pulse, which causes the net magnetisation vector to flip into the direction opposite to B_0 . The 180° pulse also causes the direction of precession of ^3He nuclei to reverse, so that after a further time period τ a two-sided echo of the original FID is seen, as the nuclei come back into phase. For this reason, a 180° pulse is often referred to as a refocusing pulse. However, the echo is of smaller amplitude than the original FID, as the refocusing pulse can only reverse dephasing caused by fixed magnetic field inhomogeneities, but not spin-spin

interactions. It is possible to obtain repeated echoes (an echo train) by transmitting a series of 180° pulses, each of which will be followed by an echo. The amplitude of these echoes will decay in an exponential fashion, mainly due to spin-spin interactions. This is described as T2 decay, and is intermediate in speed between T1 relaxation and T2* decay.

The diffusion of atoms in an unrestricted space may be modelled as a ‘random walk’ process, in which atoms move a certain distance in a random direction after each small time increment. The constant of proportionality in this case is known as the free diffusion coefficient (D_0), and is measured in units of cm^2s^{-1} . If diffusion is restricted by a physical boundary such as the walls of the alveolar airspaces, the mean square displacement will be reduced, and D_0 is replaced by an apparent diffusion coefficient (ADC) with the same units. ADC may be measured at short timescales (measured in milliseconds) or long timescales (measured in seconds), with longer timescales corresponding to diffusion over greater distances. Two pulse sequences were utilised in the work presented in this thesis, namely spin echo (SE)²²⁴ and stimulated echo (STE)²²⁵, which measure diffusion at short and long timescales respectively.

Figure 2.9b shows the SE pulse sequence. This is similar to the sequence shown in Figure 2.9a, except that a gradient is applied in the cranio-caudal direction before and after each refocusing pulse. Diffusion of ^3He atoms in the time interval between the gradient pulses results in additional dephasing between spins so that the subsequent echo is attenuated. An echo train of 64 echoes is obtained, and an exponential decay curve is fitted to the envelope of the echo train, using MATLAB (Mathworks, Cambridge, UK). The rate constant of this decay curve is the ADC at 13ms.

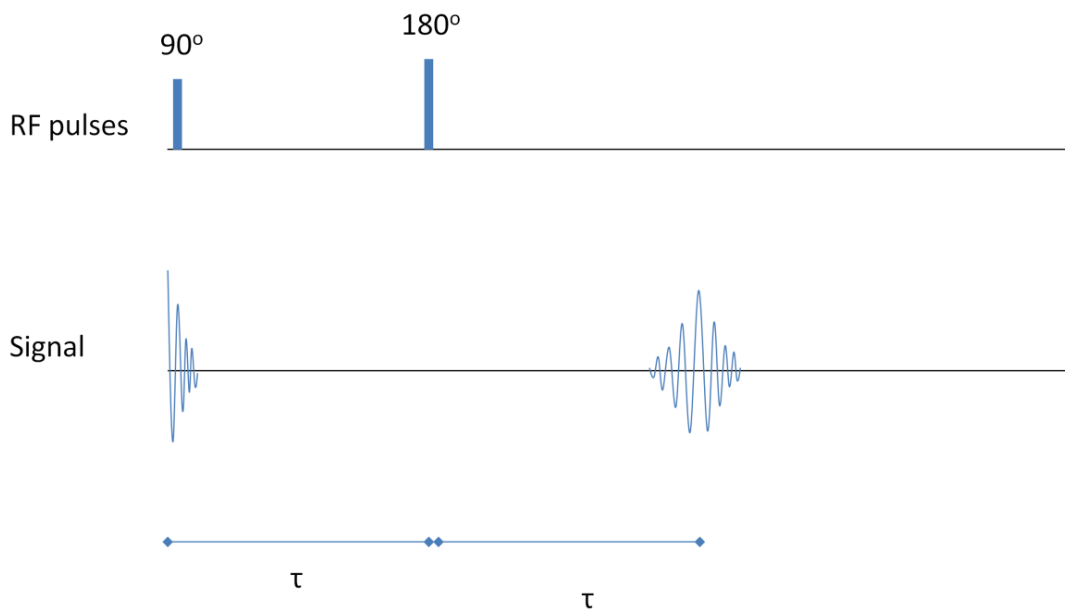
Figure 2.9c shows the STE pulse sequence with some simplifications for clarity. An initial 90° RF pulse is applied to induce phase coherence. This is followed by a gradient pulse, so that any subsequent diffusion of ^3He atoms results in dephasing. A second 90° pulse is applied, which causes the transverse spins to flip into the longitudinal axis. Once there, the spins maintain their phase relationships, and dephasing due to spin-spin interactions does not occur. This means that diffusion over much longer time scales can be measured. Following a time period of the order of 1s, a third 90° pulse is applied, which flips the spins that were ‘parked’ in the longitudinal axis back into the transverse

plane, but now spinning in the reverse direction. A refocusing gradient is applied, which results in an echo, the amplitude of which determines the degree of diffusion (and hence dephasing) that has occurred in the intervening period.

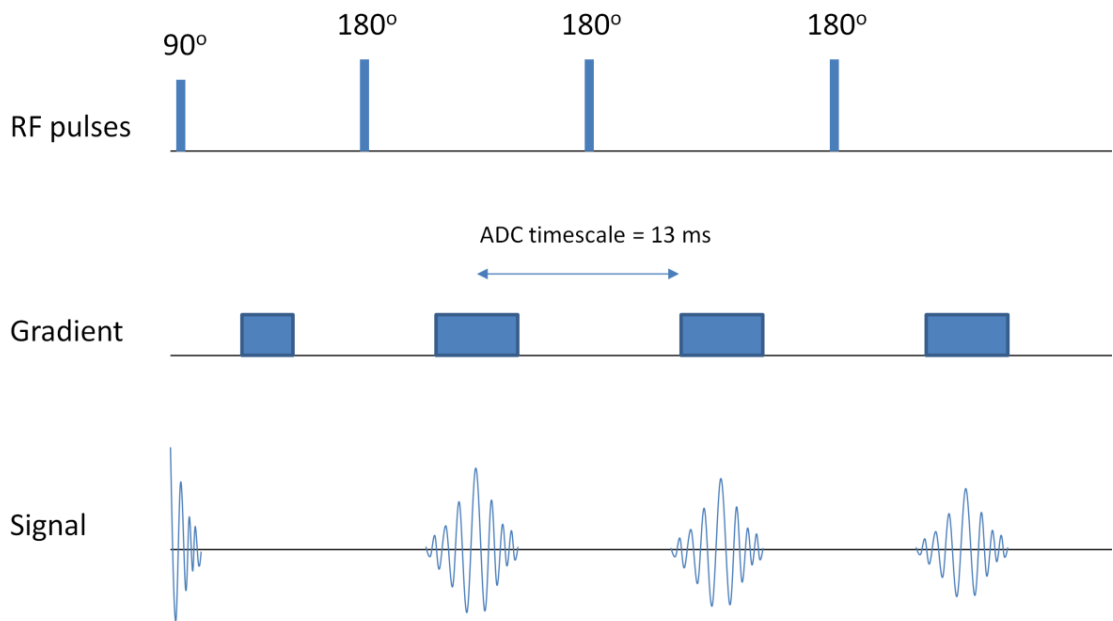
Figure 2.9: Magnetic resonance pulse sequences for measuring diffusion in the lungs

Panel A shows a simple spin echo pulse sequence, in which after an initial 90° pulse, a 180° refocusing pulse causes an echo of the original free induction decay. Panel B shows the spin echo diffusion pulse sequence, in which a series of refocusing pulses are applied following the initial 90° pulse. In between each refocusing pulse a diffusion-weighting gradient is applied. Panel C shows the stimulated echo diffusion pulse sequence, in which an initial 90° pulse is followed by a diffusion-weighting gradient and then a second 90° pulse, which has the effect of eliminating dephasing due to spin-spin interactions. Following a relatively long time period of the order of seconds, a third 90° pulse is applied, flipping the spins back into the transverse plane, followed by a refocusing gradient which causes an echo of the original free induction decay.

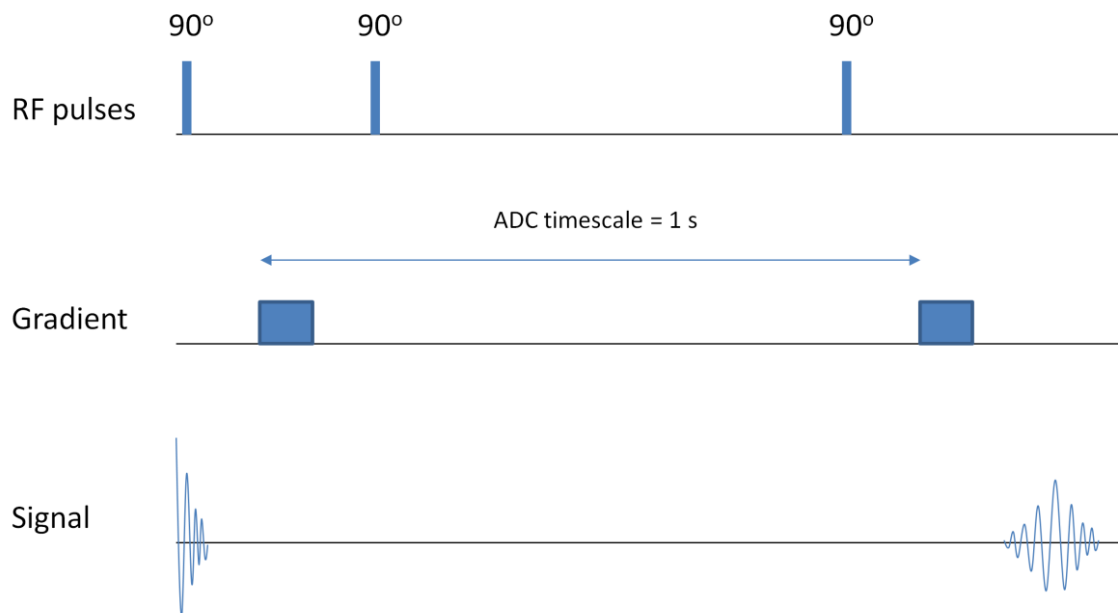
Panel A



Panel B



Panel C



2.9.3 Patient testing procedure

^3He gas was hyperpolarised via metastable exchange optical pumping²²⁶, using a custom-built polarisation system. Six hundred ml of gas comprising 15-30 ml hyperpolarised ^3He mixed in ^4He , was transported from the glass storage cell to the patient in a tedlar bag (SKC Limited, Blandford Forum, UK). MR measurements were made using a 0.15 T permanent magnet system (Intermagetics General Corporation, New York) with a Surrey Medical Imaging Systems console (Surrey, UK). Participants were positioned in a supine position within the magnet, with a custom-built induction coil around their chest. Following a period of relaxed tidal breathing, participants inhaled the contents of the tedlar bag from FRC and breath-held for 2 – 10 seconds whilst the MR measurement was performed.

3 Studies

3.1 Validation of a photoacoustic gas analyser for the measurement of functional residual capacity using multiple breath inert gas washout

Abstract

Background

The respiratory mass spectrometer is the current gold standard technique for performing multiple breath inert gas washout (MBW), but is expensive and lacks portability. A number of alternative techniques have recently been described.

Objectives

We aimed to validate, using an *in vitro* lung model, an open-circuit MBW system that utilises a portable photoacoustic gas analyser, with sulphur hexafluoride (SF₆) as the inert tracer gas.

Methods

An acrylic glass lung model was utilised to assess the accuracy of functional residual capacity (FRC) measurements derived from MBW. Measurements were performed in triplicate at 20 combinations of simulated FRC, tidal volume and respiratory rate. FRC measured using MBW (FRC_{mbw}) was compared to FRC calculated from the known dimensions of the model (FRC_{calc}). MBW was also performed in 10 healthy subjects and 14 patients with asthma.

Results

The MBW system measured FRC with high precision. The mean bias of FRC_{mbw} with respect to FRC_{calc} was -0.4% (95% limits of agreement of -4.6% and 3.9%). The mean coefficient of variation of triplicate FRC measurements was 4.0% *in vivo* and 1.0% *in vitro*. MBW slightly underestimated low lung volumes and overestimated high lung volumes, but this did not cause a significant error in lung clearance index except at lung volumes below 1500 ml.

Conclusions

The open-circuit MBW system utilising SF₆ as the inert tracer gas and a photoacoustic gas analyser is both accurate and repeatable within the adult range of lung volumes. Further modifications would be required before its use in young children or infants.

Introduction

Multiple breath inert gas washout (MBW) is a technique for assessing the non-uniformity of ventilation distribution in the lungs by measuring the efficiency with which an inert tracer gas is washed out of the lungs¹³⁰. The current gold standard MBW system is the respiratory mass spectrometer (RMS)¹³⁰, but this is expensive and lacks portability. An alternative system based upon a modified photoacoustic gas analyser (Innocor™, Innovision A/S, Odense, Denmark) and 0.2% sulphur hexafluoride (SF₆) as the tracer gas has been developed, and shown to be both repeatable and practical¹³², but its accuracy has not been formally validated. The functional residual capacity (FRC) may be derived from a MBW by dividing the total volume of inert gas expired by the difference between the inert gas concentrations at the beginning and end of the washout period²¹⁹. Current guidelines recommend that MBW systems are validated by determining FRC measurement accuracy, and in particular that measured FRC values should lie within 5% of known volumes, at least 95% of the time¹³⁰. Accurate FRC determination depends critically upon correct flow and gas concentration measurements, precise synchronisation of these signals, and adequate conversion of measured flows and volumes to body temperature, pressure and water vapour saturation (BTPS) conditions. These are the same technical factors that influence the accuracy of clinically relevant parameters such as the lung clearance index (LCI). FRC is a suitable end-point for quality control and methodological validation because measured values may be readily compared to a gold standard such as the known volume of an *in vitro* lung model. Current guidelines¹³⁰ recommend that MBW systems are validated using *in vitro* lung models incorporating realistic BTPS conditions, as previously described by Singer *et al*¹³⁴. We aimed to utilise this lung model to validate the MBW method of Horsley *et al*¹³², as well as to compare the variability of triplicate MBW tests performed *in vitro* and *in vivo*. The primary outcome of the study was the percentage difference between measured and calculated FRC measurements using the *in vitro* lung model, with satisfactory accuracy being defined as a percentage difference of between -5% and 5% for at least 95% of measurements. Secondary outcomes were the dependence, if any, of the measurement bias on absolute FRC values or the respiratory rate, as well as the difference in measurement variability between *in vitro* and *in vivo* measurements.

Materials and methods

The Innocor photoacoustic gas analyser setup, patient testing procedure and MBW data analysis methods are described in Section 2.5. The lung model utilised to perform the validation experiments and the methodology of these experiments are described in Section 2.6. Figure 3.1 shows an example trace of SF₆ concentration against time recorded using the lung model (Panel A), and the corresponding plot of end-expiratory SF₆ concentration against turnover number (Panel B).

***In vitro* testing procedure**

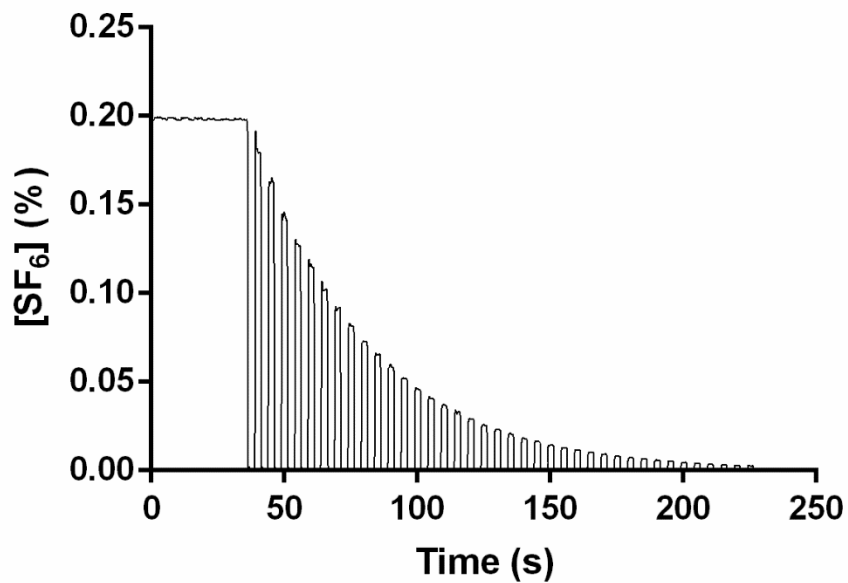
Before testing began, a volume calibration of the Innocor gas analyser was performed using a 1L syringe at low, medium and high flow rates. The gas analyser had recently been serviced, including a gas calibration. All tests were performed on the same day (17th December 2011), and the air temperature and relative humidity inside the phantom lung were measured on three occasions during the testing period to confirm that BTPS conditions in the lung compartment were maintained. This was performed using measuring probes that were inserted through a small hole in the lung phantom lid. The hole was then sealed prior to testing.

Testing using the lung phantom model was performed according to the method described in Section 2.6., at simulated FRC values between 500 ml and 4000 ml, at 500 ml intervals, in order to simulate lung volumes of young children through to large adults. Tidal volume (V_T) was set to approximately one third of FRC. Respiratory rate was set at between 12 and 24 breaths per minute; Larger respiratory rates were used with smaller lung volumes, in order to accurately simulate the physiology of young children. At FRC values of 500 ml, 1000 ml, 2000 ml, 3000 ml and 4000 ml, experiments were performed at three different respiratory rates in order to assess if accuracy was affected by changes in this parameter. Each of the 20 experiments was performed in triplicate, making a total of 60 washout runs.

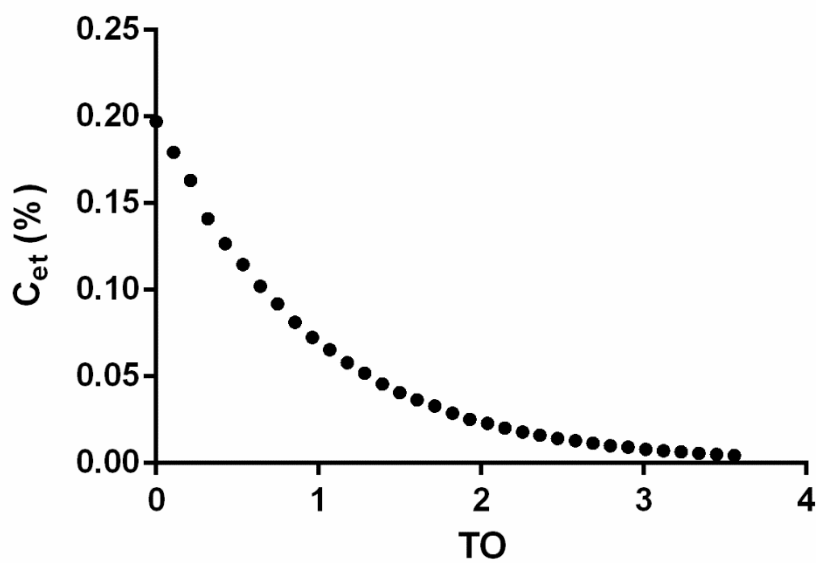
Figure 3.1: Inert gas washout curve of an acrylic glass lung model

Panel A shows a raw plot of measured SF_6 concentration against time, with each vertical peak representing a single expiration. Panel B shows the end-expiratory SF_6 concentration (C_{et}) of each breath of the same washout test.

Panel A



Panel B



***In vivo* testing procedure**

Ten healthy subjects with no history of respiratory disease and 14 patients with a clinical diagnosis of asthma were recruited. Subjects were aged over 18 years, and were never-smokers or ex-smokers with ≤ 10 pack years' smoking history. The study protocol was approved by the National Research Ethics Committee – East Midlands Leicester (approval number 08/H0406/189) and all subjects gave their written informed consent. Patients underwent MBW in triplicate using the method described in Section 2.5.

Statistical analyses were performed using Prism version 6 (GraphPad, San Diego, California, USA). Results from the *in vitro* lung model were displayed as a Bland-Altman plot²²⁷ of FRC measured using MBW (FRC_{mbw}) against FRC calculated using the measuring scale affixed to the lung model (FRC_{calc}). The percentage difference between FRC_{mbw} and FRC_{calc} was also compared between washout tests with low, intermediate and high respiratory rates, using one-way analysis of variance. The mean coefficient of variation (CoV) of triplicate values was compared across the three sets of measurements (lung model, healthy subjects and patients with asthma) using one-way analysis of variance with Bonferroni correction for multiple comparisons.

Results

The Innocor system measured FRC with high precision. Table 3.1 lists the 60 *in vitro* experiments that were performed, with the values of FRC_{calc} and FRC_{mbw} given in each case. Figure 3.2 shows Bland-Altman plots of FRC_{mbw} against FRC_{calc} , with the absolute and percentage difference between FRC_{mbw} and FRC_{calc} plotted on the y-axis in panels A and B. The mean absolute bias of FRC_{mbw} with respect to FRC_{calc} was 12.6 ml, and the 95% limits of agreement were -68.6 ml and 93.7 ml. The mean percentage bias of FRC_{mbw} with respect to FRC_{calc} was -0.4%, and the 95% limits of agreement were -4.6% and 3.9%. There was a significant positive correlation between the mean of FRC_{mbw} and FRC_{calc} and the percentage difference between these values (Pearson correlation coefficient = 0.82, $p < 0.0001$). The equation of the regression line was $y = 0.001462 * x - 3.653$. The regression line crossed the x-axis at a lung volume of 2499

ml, which was therefore the point of zero bias. The mean bias at a lung volume of 500 ml was -3.9% and at a lung volume of 4000 ml was 1.9%. Respiratory rate did not have an independent effect on the bias. The mean bias of FRC_{mbw} with respect to FRC_{calc} in washout runs with low, intermediate and high respiratory rates was -0.3%, -0.9% and -0.3% respectively, with no statistically significant difference between the sets of washout experiments.

Table 3.1: List of multiple breath washout validation experiments performed with results

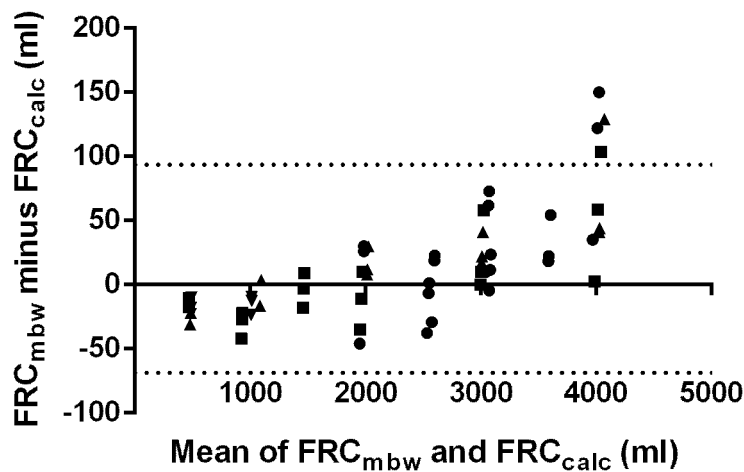
Experimental conditions			Results		
VT (ml)	Respiratory rate (min ⁻¹)	FRC _{calc} (ml)	FRC _{mbw} #1 (ml)	FRC _{mbw} #2 (ml)	FRC _{mbw} #3 (ml)
224	16	477	460	467	462
205	20	496	465	474	475
187	24	496	478	486	473
243	16	944	902	917	922
261	24	1019	1006	995	1009
336	20	1093	1077	1097	1077
448	16	1467	1449	1464	1476
523	12	1971	1925	1997	2001
504	16	1971	1936	1981	1960
467	20	2008	2020	2016	2038
541	12	2550	2512	2551	2543
1027	12	2587	2558	2606	2610
990	20	2998	3039	3020	3015
1046	16	2998	3056	3008	2998
485	12	3035	3045	3097	3108
1008	12	3072	3068	3084	3096
448	12	3577	3599	3631	3595
1008	12	3950	4100	3985	4072
971	16	3987	3990	4046	4091
952	20	4006	4047	4135	4050

VT = tidal volume; FRC_{mbw} = functional residual capacity measured using multiple breath washout; FRC_{calc} = functional residual capacity calculated from known dimensions of lung model.

Figure 3.2: Bland-Altman plots of calculated versus measured functional residual capacity

Bland-Altman plots of FRC_{mbw} against FRC_{calc} are shown, with absolute differences in Panel A and percentage differences in Panel B. % Difference is calculated as $100 * (FRC_{mbw} - FRC_{calc})$ divided by the mean of FRC_{mbw} and FRC_{calc} . Dotted lines represent 95% limits of agreement. Best-fit linear regression line is shown in Panel B (Pearson correlation coefficient = 0.82, $p < 0.0001$). Washout run respiratory rates are represented 12 (●), 16 (■), 20 (▲) and 24 (▼).

Panel A



Panel B

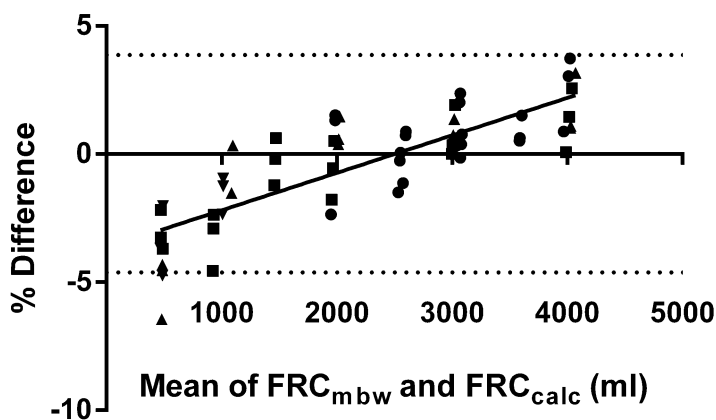


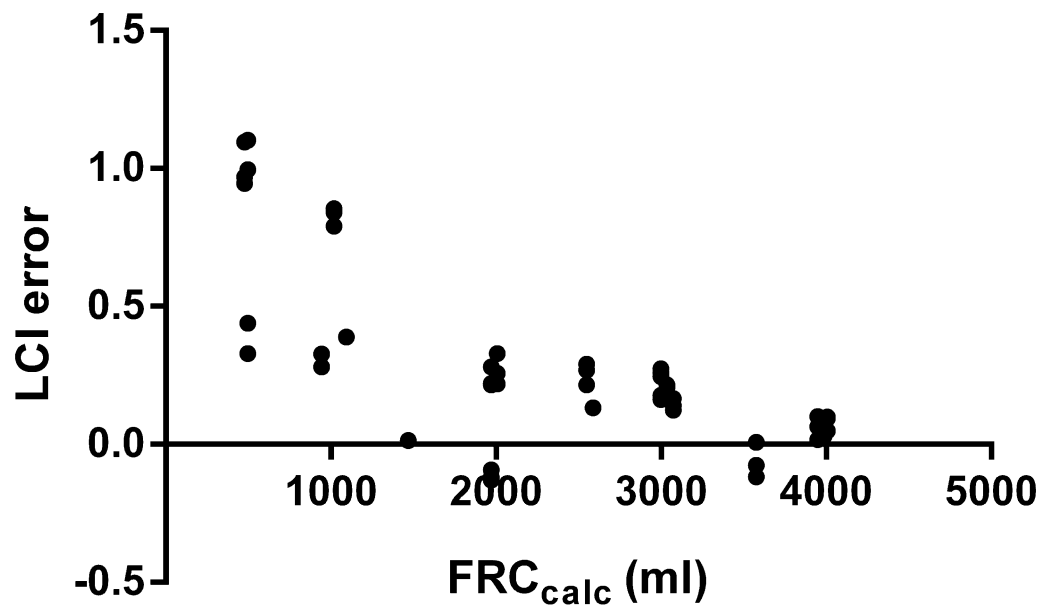
Figure 3.3 shows the error in LCI, defined as measured LCI minus calculated LCI (LCI_{calc}), against FRC_{calc} , where:

$$LCI_{calc} = \frac{((\text{calculated } V_T - \text{equipment dead space}) \times \text{number of breaths})}{FRC_{calc}}$$

LCI was measured accurately at lung volumes at or above 1500ml, with an error of less than 0.4 units in each case. However, at lung volumes of 500ml or 1000ml, LCI was in some cases over-estimated by up to 1.1 units.

The healthy participants comprised four women and six men with a mean (standard deviation [SD]) age of 46.4 (19.4) years, while the patients with asthma comprised seven women and seven men with a mean (SD) age of 59.0 (11.9) years. The mean (SD) FRC_{mbw} was 2796 (896) ml in healthy controls and 2555 (794) ml in patients with asthma. The mean (SD) LCI was 7.07 (1.07) in healthy controls and 8.12 (1.46) in patients with asthma. The mean (range) CoV of triplicate FRC_{mbw} measurements was 1.0% (0.4 – 2.2%) *in vitro*, 4.0% (1.9 – 5.3%) in healthy controls, and 2.9% (0.4 – 5.4%) in patients with asthma. These values were significantly different across the three sets of measurements ($p < 0.0001$). In particular, the mean CoV was significantly lower *in vitro* than in both healthy ($p < 0.0001$) and asthma ($p < 0.001$) groups, but did not differ significantly between the healthy and asthma groups. The difference in mean CoV between *in vitro* and healthy group measurements was 3.0% (95% confidence interval of difference: 2.5 – 3.5%), while the difference in mean CoV between *in vitro* and asthma group measurements was 1.9% (95% confidence interval of difference: 1.0 – 2.7%). The *in vitro* CoV of FRC_{mbw} was not significantly related to the respiratory rate. The mean (range) CoV was 1.1% (0.5 – 2.2%) with a respiratory rate of 12 breaths/minute, 1.0% (0.8 – 1.3%) with a respiratory rate of 16 breaths/minute, and 0.9% (0.4 – 1.4%) with a respiratory rate of 20 or 24 breaths per minute (no significant difference between groups of tests). The mean (range) CoV of triplicate LCI measurements was 1.2% (0.0 – 4.0%) *in vitro*, 4.6% (0.4 – 12.1%) in healthy controls, and 3.3% (0.3 – 7.0%) in patients with asthma.

Figure 3.3: Error in lung clearance index against calculated functional residual capacity



Discussion

In this study, we utilised a one-compartment acrylic glass lung model under BTPS conditions to validate a practical and portable MBW system that uses an Innocor photoacoustic gas analyser, with SF₆ as the inert tracer gas. Of note, this open-circuit system is distinct from the closed-circuit setup that was found to have poor intra-subject variability and patient acceptability by Pittman *et al*²²⁸. We found good agreement between FRC measured using Innocor (FRC_{mbw}) and FRC calculated from the known dimensions of the lung model (FRC_{calc}), with a mean bias of FRC_{mbw} with respect to FRC_{calc} of -0.4%, and 95% limits of agreement of -4.6% and 3.9%, comfortably below the recommended maximum error of 5%¹³⁰. An identical lung model has been previously used to validate a commercially available open-circuit nitrogen MBW system (Exhalyzer DTM, Eco Medics AG, Duernten Switzerland)¹³⁴. These authors found that for lung volumes above 500 ml, there was a mean bias of 0.4%, with 95% limits of agreement of -4.0% and 4.7% respectively. We therefore conclude that the accuracy of FRC measurements using Innocor and Exhalyzer D is similar within the FRC range of 500 ml to 4000 ml. We found that the mean coefficient of variation of triplicate FRC measurements was 1.0% *in vitro* and 4.0% *in vivo*, suggesting that the majority of between-measurement variability *in vivo* was caused by biological rather than technical factors. Singer *et al*¹³⁴ obtained similar values using the Exhalyzer D system, namely 1.4% and 4.5% respectively, suggesting that the two systems perform approximately equally with respect to within-visit repeatability.

The Innocor-based system appeared to slightly underestimate FRC when lung volumes were small and overestimate it when volumes were large. We speculated that this may have been due to cyclical heating and cooling of the pneumotachometer during the respiratory cycle, resulting in non-linearity of flow measurement. On closer examination of our data, we ascertained that the source of this FRC-dependent bias was the correction for re-inspired SF₆, which appeared to over-compensate at low lung volumes, resulting in artificially low FRC values. In particular, inspiratory flows were over-estimated at low lung volumes, particularly below an FRC of 1500 ml, resulting in an over-estimation of re-inspired SF₆ volume. Of note, this FRC-dependent bias was not seen with the Exhalyzer D¹³⁴, which utilises an ultrasonic flowmeter. However, the error in FRC measurements with Exhalyzer D increased with increasing respiratory

rate¹³⁴, an effect that we did not observe with the Innocor-based system. We furthermore examined the accuracy of LCI measurements performed using Innocor at different lung volumes and found that at lung volumes of 1500 ml or above, there was good agreement between measured and calculated LCI, whereas at lung volumes below 1500 ml, LCI was often over-estimated, by up to 1.1 units. This suggests that at lung volumes corresponding to older children or adults, the small bias observed in FRC does not significantly affect LCI measurements.

The open-circuit Innocor-based system described in this chapter is practical and convenient, and could potentially be utilised in clinical practice and multi-centre trials in both older children and adults. However, our *in vitro* results at low lung volumes suggest that the system would require further modification before it could be used reliably in young children and infants. Such modification would be likely to include the replacement of the pneumotachometer with a smaller model that has a lower flow range. Moreover, Innocor employs side-stream sampling of gas at a flow rate of 120 ml/minute¹³⁰, which may have a significant influence at low tidal volumes. Furthermore, the response time of the photoacoustic analyser is relatively slow (154 ms)¹³⁰, which may be particularly relevant at fast respiratory rates, as seen in young children. These latter two issues would require further technical development by the manufacturers of Innocor. There are a number of additional improvements that could be made relatively easily to further increase the general applicability of this technology to the performance of MBW. Foremost among these is that data analysis is currently performed off-line, which is relatively time consuming. It would however be straightforward to incorporate FRC and LCI calculations into the on-board Innocor software in the future. Ideally, this on-board software would also include a user-friendly patient interface to allow tidal volume to be targeted by the patient to a set value. Our current system requires the patient to target their tidal volume using a numerical display on a separate laptop computer. A further limitation of the current Innocor setup is the requirement of SF₆, which is restricted in some countries as it acts a greenhouse gas.

In conclusion, the open-circuit MBW system utilising SF₆ as the inert tracer gas and an Innocor photoacoustic gas analyser is both accurate and repeatable in adults, and is comparable in these respects to the Exhalyzer D MBW system. These results provide increased confidence in previous and future research studies conducted using the

Innocor-based system, and suggest its potential to develop into a commercially available MBW platform. Further modifications to the system would be required to facilitate its use in young children and infants.

3.2 Specific ventilation inequality and dead space components of lung clearance index in patients with cystic fibrosis and non-cystic fibrosis bronchiectasis

Abstract

Background

Lung clearance index (LCI) is a measure of abnormal ventilation distribution derived from the multiple breath inert gas washout (MBW) technique. We aimed to determine the clinical utility of LCI in non-CF bronchiectasis, and to assess two novel MBW parameters that distinguish between increases in LCI due to specific ventilation inequality (LCI_{vent}) and increased respiratory dead space (LCI_{ds}).

Methods

Forty-three patients with non-CF bronchiectasis and 18 healthy control subjects underwent MBW using the sulphur hexafluoride wash-in technique, and data from 40 adults with CF were re-analysed. LCI_{vent} and LCI_{ds} were calculated using a theoretical two-compartment lung model, and represent the proportional increase in LCI above its ideal value due to specific ventilation inequality and increased respiratory dead space, respectively.

Results

LCI was significantly raised in patients with non-CF bronchiectasis compared to healthy controls (9.99 versus 7.28, $p < 0.01$), and discriminated well between these two groups (area under receiver operating curve = 0.90, versus 0.83 for forced expiratory volume in one second [% predicted]). LCI, LCI_{vent} and LCI_{ds} were repeatable (intraclass correlation coefficient > 0.75), and correlated significantly with measures of spirometric airflow obstruction.

Conclusion

LCI is repeatable, discriminatory, and is associated with spirometric airflow obstruction in patients with non-CF bronchiectasis. LCI_{vent} and LCI_{ds} are a practical and repeatable alternative to phase III slope analysis and may allow a further level of mechanistic

information to be extracted from the MBW test in patients with severe ventilation heterogeneity.

Introduction

Non-cystic fibrosis (CF) bronchiectasis is a chronic suppurative lung disease caused by a range of underlying conditions, which is increasing in prevalence²²⁹, and which imposes a significant burden of morbidity and healthcare costs. In the United States alone, annual healthcare costs for bronchiectasis are estimated as \$630 million²³⁰. The causes of non-CF bronchiectasis are diverse, and include autoimmune disease, primary ciliary dyskinesia, allergic bronchopulmonary aspergillosis, immune deficiency and childhood respiratory infection²³¹. Regardless of the underlying cause, the pathogenesis is thought to involve a vicious cycle of bacterial colonisation, neutrophilic airway inflammation, airway damage and mucus stasis²³¹. The evidence base for the treatment of non-CF bronchiectasis lags well behind that of CF, but this is expected to change in the near future as a number of non-CF bronchiectasis research registries and clinical trials are actively enrolling patients at present²³². Such clinical trials will require robust physiological outcome measures in order to provide objective measures of improvement in lung function.

Multiple breath inert gas washout (MBW) is a technique for quantifying ventilation heterogeneity, the uneven distribution of ventilation¹²⁸. This is an early feature of obstructive airway diseases such as asthma¹⁵¹, chronic obstructive pulmonary disease¹⁵¹ and cystic fibrosis (CF)¹³². A comprehensive standardisation document for the performance of inert gas washout has been recently published¹³⁰. Lung clearance index (LCI)^{135,233} is the most commonly reported MBW parameter, and is defined as the cumulative expired volume at the point where end-tidal inert gas concentration falls below 1/40th of the original concentration, divided by the functional residual capacity (FRC). LCI has been shown to be both discriminatory and repeatable in patients with CF¹³², and is increasingly being used as an outcome measure in clinical trials of CF therapies²³⁴⁻²³⁶. A recent study has shown that LCI is repeatable in patients with non-CF bronchiectasis, and correlates with computed tomography bronchiectasis severity scores²³⁷.

Although LCI has been shown to be a robust and repeatable measurement in patients with CF and non-CF bronchiectasis, it also represents a simplification of the washout process since it is essentially determined by data points at the start and end of the

washout curve only. From a theoretical standpoint, LCI may be increased by two distinct mechanisms, namely (i) unequal convective ventilation between relatively large lung units subtended by proximal conducting airways (convection-dependent inhomogeneity), and (ii) increased respiratory dead space, which is thought to be underpinned by diffusion-dependent gas mixing inefficiencies (diffusion-convection-dependent inhomogeneity)¹⁴³. The only published method for separating out these mechanisms is the analysis of phase III slopes, yielding the parameters S_{cond} (conductive ventilation heterogeneity index) and S_{acin} (acinar ventilation heterogeneity index)¹³¹. This technique was developed from elegant clinical and modelling studies in healthy adult subjects¹⁴². However, the use of these parameters is problematic in patients with the most severe ventilation heterogeneity, such as those with advanced CF lung disease¹⁴⁷, both from a practical standpoint (the requirement for controlled 1L breaths), and because the modelling may not be directly applicable in those with severe ventilation heterogeneity. To overcome this, modified versions of these parameters (S_{cond}^* and S_{acin}^*) have recently been proposed for use in such patients¹⁴⁹. There remains a need however for a reliable and repeatable method of extracting mechanistic information from washout curves, which has been developed for, and can be applied in, those with more severe disease.

The aim of this study was firstly to determine whether or not ventilation heterogeneity is a significant feature of non-CF bronchiectasis, and whether LCI may have potential as an outcome measure in this group of patients. Furthermore, we aimed to extend currently available measures of ventilation heterogeneity by developing novel parameters that would distinguish between specific ventilation inequality (LCI_{vent}) and increased respiratory dead space (LCI_{ds}) as a cause of increased LCI. LCI_{vent} and LCI_{ds} would be expected to probe similar mechanisms of ventilation heterogeneity to S_{cond} and S_{acin} , respectively, but without the potential drawbacks of phase III slope analysis, and with the advantage of being directly linked to LCI.

We hypothesised that:

- i) Non-CF bronchiectasis is characterised by increased LCI, LCI_{vent} and LCI_{ds} compared to healthy control subjects.
- ii) LCI is related to other measures of disease severity in CF and non-CF bronchiectasis such as the presence or absence of chronic bacterial colonisation.

- iii) LCI is repeatable in patients with non-CF bronchiectasis, and is superior to spirometry for distinguishing between patients with non-CF bronchiectasis and healthy controls.

Methods

Subjects

Forty-three adult patients with non-CF bronchiectasis were recruited from the respiratory out-patient clinics at Glenfield Hospital. Bronchiectasis was diagnosed by high resolution computed tomography, and all scans were reported by a Consultant Radiologist to confirm the diagnosis. Eighteen healthy non-smoking control subjects with no history of respiratory symptoms were recruited through local advertising. The study was approved by the National Research Ethics Committee (East Midlands – Leicester), and all participants gave their written informed consent. As a disease comparator group, MBW data from 40 adults with CF who took part in a previous observational study¹³² were re-analysed. This study was approved by the Lothian Research and Ethics Committee and all participants gave their written informed consent.

Clinical characterisation of bronchiectasis patients

Demographic details and a full medical history were obtained from each patient. Sputum samples were obtained for bacterial culture, and sputum culture results during the previous year were recorded to assess for chronic bacterial colonisation, defined as isolation of the same microorganism on sputum culture on at least two occasions during the previous year. Participants underwent spirometry and measurement of lung volumes using helium dilution according to American Thoracic Society / European Respiratory Society guidelines^{90,215}.

Multiple breath washout test

MBW was performed in triplicate at a single visit, as described in Sections 2.5.1 and 2.5.2. Participants with non-CF bronchiectasis maintained a steady respiratory rate of

approximately 12 breaths per minute, and a constant tidal volume of 1L throughout the test. Patients with CF in the previously published cohort¹³² performed washout tests during relaxed tidal breathing. Washout curves were analysed as described in Section 2.5.3 to yield FRC, LCI, $S_{\text{cond}}/S_{\text{acin}}$ and $S_{\text{cond}}^*/S_{\text{acin}}^*$. The novel parameters LCI_{vent} and LCI_{ds} were calculated as described in Section 2.7.

Statistical analysis

Statistical analyses were performed using SPSS Version 20 (IBM Corporation, Somers, New York, USA) and Prism 6 (GraphPad Software Inc., La Jolla, California, USA). Between-group comparisons were performed using Student's T test or one-way analysis of variance for continuous data and the Chi-squared test for proportions, with the threshold for statistical significance set at $p < 0.05$. Repeatability of MBW parameters was assessed using the intraclass correlation coefficient (ICC) across triplicate measurements, using a two-way mixed model. Correlations between variables were assessed using Pearson's correlation coefficient (R). A generalised linear model was used to assess whether the relationship between LCI and spirometric airflow obstruction differed between the two disease groups. Areas under receiver operating characteristic (ROC) curves were used to assess the discriminatory ability of physiological parameters.

Results

Clinical characteristics

The cohort of patients with non-CF bronchiectasis comprised 19 men and 24 women with a mean (standard deviation [SD]) age of 67.4 (7.3) years. The group included 25 never smokers, 17 ex-smokers and 1 current smoker. The median (range) pack-year smoking history of the ex- and current smokers was 17.5 (1 – 140). Out of the 43 patients, a previous history of tuberculosis was elicited in 2 patients, childhood pneumonia in 14 patients and pertussis in 22 patients. Eleven patients had a history of asthma, and four had a formal diagnosis of allergic bronchopulmonary aspergillosis. Nineteen patients had symptoms of gastroesophageal reflux disease and two had inflammatory bowel disease. Twelve patients had an inflammatory arthritis and one had yellow nail syndrome. Twelve patients were chronically colonised with *Haemophilus*

influenzae, three patients with *Pseudomonas aeruginosa*, two patients with *Staphylococcus aureus* and two patients with coliforms.

The CF group comprised 20 men and 20 women with a mean (SD) age of 28.7 (9.8) years. Three CF patients were ex-smokers (pack-year histories of 5, 15 and 24 years). Fifteen patients had chronic *Pseudomonas aeruginosa* colonisation as defined by Lee *et al*²³⁸, 29 had pancreatic insufficiency and 6 had diabetes mellitus. Nineteen patients had a severe genotype, defined as having a class I or II mutation on both chromosomes, and 16 had a mild genotype, defined as having a class III, IV or V mutation on at least one chromosome. The genotype was incomplete in 5 patients.

Group comparisons

Table 3.2 shows physiological data across all three groups. Patients with bronchiectasis and CF both displayed spirometric airflow obstruction, with significantly reduced forced expiratory volume in one second/forced vital capacity (FEV₁/FVC) ratio compared to healthy controls. LCI, LCI_{vent} and LCI_{ds} were all significantly greater in bronchiectasis patients compared to controls, and significantly greater in CF patients compared to both controls and bronchiectasis patients, as shown in Figure 3.4 (Panels A, B and C respectively).

Table 3.2: Demographic and physiological data across healthy controls, cystic fibrosis patients and non-cystic fibrosis bronchiectasis patients

	Control subjects (n = 18)	CF patients (n = 40)	Non-CF bronchiectasis patients (n = 43)
Age (years) ^{††††}	48.3 (3.9)	28.7 (1.5) ^{####}	67.4 (1.1) ^{####, ¥¥¥}
Sex (% male)	50	50	44
BMI (kg/m ²) ^{††††}	26.8 (1.2)	22.9 (0.5) ^{##}	27.1 (0.7) ^{¥¥¥}
FEV ₁ (% pred.) ^{††††}	113.3 (4.8)	65.9 (3.4) ^{####}	82.0 (3.8) ^{####, ¥¥}
FVC (% pred.) ^{††††}	117.2 (5.6)	84.5 (3.0) ^{####}	96.1 (3.4) ^{##, ¥}
FEV ₁ /FVC (%) ^{††††}	80.9 (1.0)	65.9 (1.8) ^{####}	68.4 (1.7) ^{####}
FRC _{mbw} (L) ^{††}	2.52 (0.19)	1.99 (0.09) [#]	2.48 (0.10) ^{¥¥}
LCI ^{††††}	7.28 (0.27)	13.17 (0.56) ^{####}	9.99 (0.31) ^{##, ¥¥¥}
LCI _{vent} ^{††††}	1.20 (0.02)	1.65 (0.04) ^{####}	1.42 (0.03) ^{###, ¥¥¥}
LCI _{ds} ^{††††}	1.13 (0.01)	1.40 (0.03) ^{####}	1.27 (0.02) ^{###, ¥¥¥}
LCI _{vent} /LCI _{ds} ^{††††}	1.06 (0.02)	1.18 (0.01) ^{####}	1.12 (0.01) ^{#, ¥¥}
S _{cond} (L ⁻¹) ^{††††}	0.033 (0.007)	0.131 (0.010) ^{####}	0.064 (0.007) ^{¥¥¥}
S _{acin} (L ⁻¹) ^{††††}	0.118 (0.014)	0.509 (0.056) ^{####}	0.373 (0.036) ^{##}
S _{cond} * (L ⁻¹) ^{††††}	0.097 (0.009)	0.308 (0.034) ^{####}	0.107 (0.010) ^{¥¥¥}
S _{acin} * (L ⁻¹) ^{††††}	0.090 (0.012)	0.446 (0.054) ^{####}	0.355 (0.037) ^{##}

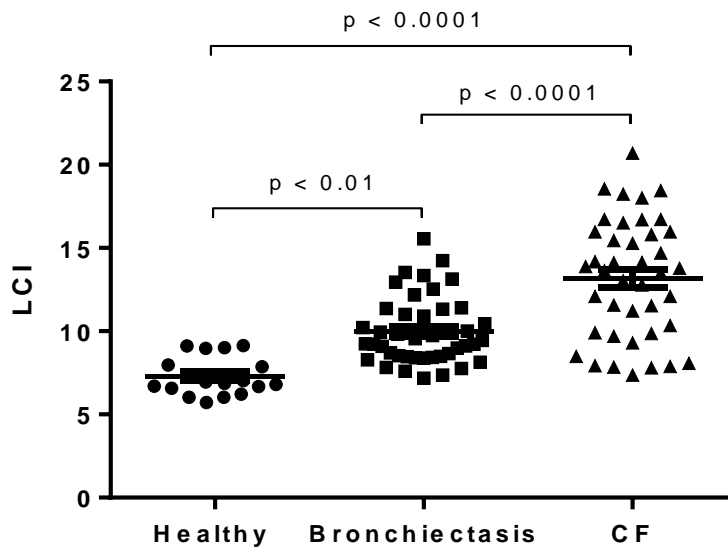
Legend for Table 3.2

CF = cystic fibrosis; BMI = body mass index; FEV₁ = forced expiratory volume in one second; FVC = forced vital capacity; FRC_{mbw} = functional residual capacity from multiple breath washout; LCI = lung clearance index; LCI_{vent} = specific ventilation inequality component of lung clearance index; LCI_{ds} = dead space component of lung clearance index. Data expressed as mean (standard error) or percentages. Groups compared using one-way analysis of variance with Bonferroni correction for multiple comparisons for parametric data, and the Chi-squared test for proportions. Significant differences across groups denoted †(p < 0.05), ††(p < 0.01), †††(p < 0.001) or ††††(p < 0.0001). Significant differences compared to control group denoted # (p < 0.05), ##(p < 0.01), ###(p < 0.001) or ####(p < 0.0001). Significant differences between bronchiectasis and CF groups denoted ¥(p < 0.05), ¥¥(p < 0.01), ¥¥¥(p < 0.001) or ¥¥¥¥(p < 0.0001).

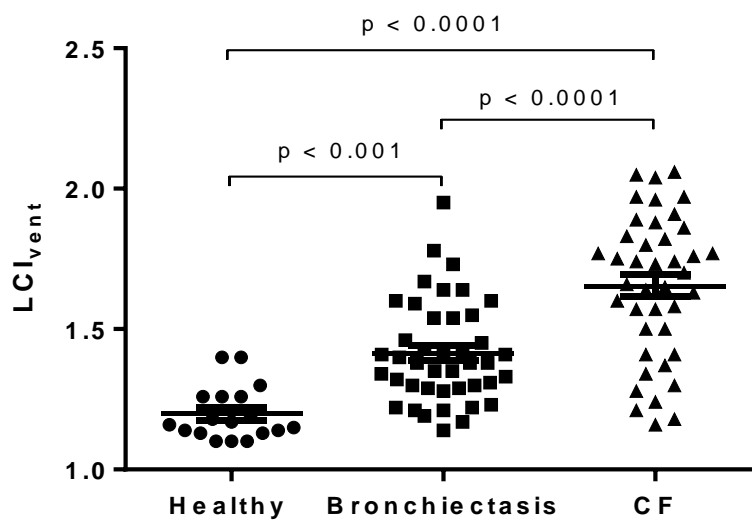
Figure 3.4: Multiple breath washout parameters across groups

Error bars indicate means \pm standard errors of the mean.

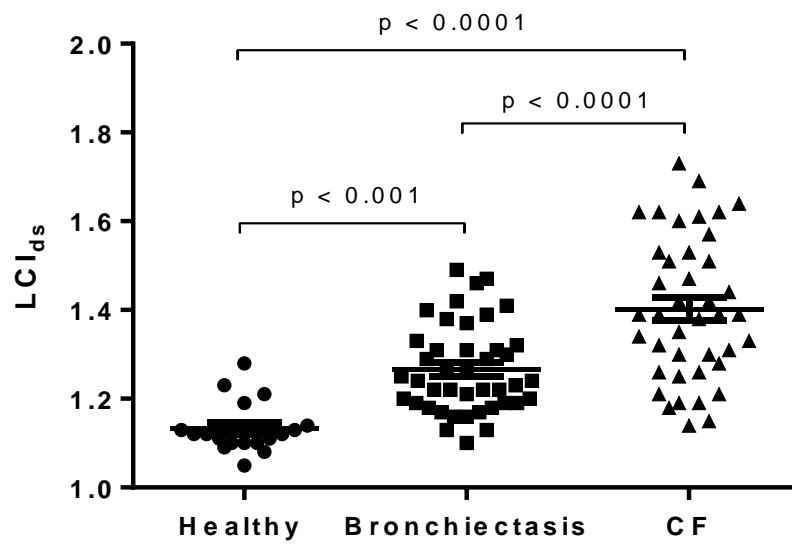
Panel A



Panel B



Panel C



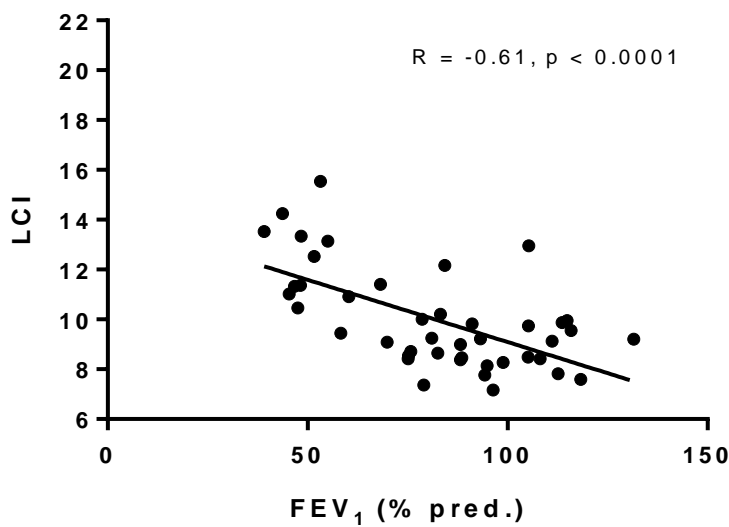
Correlations between spirometric and multiple breath washout parameters

Figure 3.5 shows correlations between the FEV₁ (% pred.) and LCI in patients with bronchiectasis (Panel A) and patients with CF (Panel B). In both cases, there was a highly significant ($p < 0.0001$) negative correlation between FEV₁ (% pred.) and LCI. However, the slope of the relationship between the two variables differed significantly between the groups. Patients with CF had a 0.13 unit increase in LCI for every 1 percentage point reduction in FEV₁ (% pred.), whereas patients with bronchiectasis had a 0.05 unit increase in LCI for every 1 percentage point reduction in FEV₁ (% pred.) ($p < 0.0001$). LCI_{vent} and LCI_{ds} correlated highly significantly with FEV₁ (% pred.) in both patients with non-CF bronchiectasis ($R = -0.63$ for LCI_{vent}, $R = -0.60$ for LCI_{ds}, $p < 0.0001$ for both analyses) and patients with CF ($R = -0.78$ for LCI_{vent}, $R = -0.76$ for LCI_{ds}, $p < 0.0001$ for both analyses). Table 3.3 shows correlations between MBW parameters in both patient groups. There were significant correlations between LCI_{vent} and LCI_{ds} in both patient groups ($R = 0.80$, $p < 0.0001$ for non-CF bronchiectasis; $R = 0.89$, $p < 0.0001$ for CF).

Figure 3.5: Correlations between lung clearance index and FEV₁ (% predicted)

Correlations are shown for patients with non-cystic fibrosis bronchiectasis (Panel A) and cystic fibrosis (Panel B). Best-fit linear regression lines are shown, together with Pearson correlation coefficients.

Panel A



Panel B

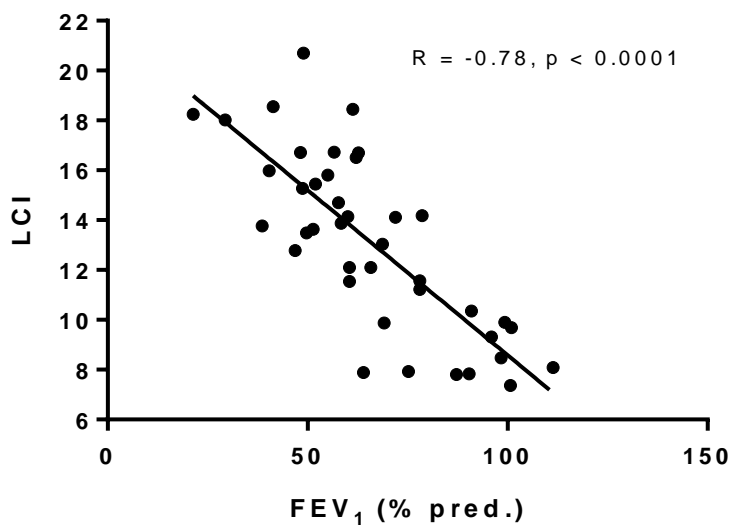


Table 3.3: Correlations between multiple breath washout parameters

	LCI	LCI _{vent}	LCI _{ds}	S _{cond}	S _{acin}	
LCI		.96**	.93**	-.11	.67**	Cystic fibrosis
LCI _{vent}	.95**		.89**	-.12	.65**	
LCI _{ds}	.90**	.80**		-.01	.68**	
S _{cond}	.14	.08	.15		-.11	
S _{acin}	.63**	.58**	.72**	.09		
Non-cystic fibrosis bronchiectasis						

LCI = lung clearance index; LCI_{vent} = specific ventilation inequality component of lung clearance index; LCI_{ds} = dead space component of lung clearance index. Pearson's correlation coefficients shown, for non-cystic fibrosis bronchiectasis patients in bottom triangle and cystic fibrosis patients in top triangle. Significant correlations denoted * (p < 0.05) or ** (p < 0.01).

Multiple breath washout parameters and chronic bacterial colonisation

Table 3.4 shows MBW and spirometric indices in patients with CF in the presence and absence of chronic *P. aeruginosa* colonisation, and in patients with non-CF bronchiectasis in the presence and absence of chronic bacterial colonisation. LCI_{ds} was significantly raised in CF patients with chronic *P. aeruginosa* colonisation compared to those without chronic colonisation (1.49 vs 1.34, $p = 0.004$).

Within-visit repeatability and discriminatory ability

Table 3.5 shows the repeatability of MBW parameters in patients with bronchiectasis and CF. Intraclass correlation coefficients exceeded 0.75 for LCI, LCI_{vent} and LCI_{ds} in both disease groups. S_{acin} and S_{acin}* displayed moderate or good repeatability, but S_{cond} and S_{cond}* were poorly repeatable in both disease groups. Figure 3.6 shows ROC curves illustrating the discriminatory ability of LCI and FEV₁ (% pred.) for distinguishing between healthy controls and patients with non-CF bronchiectasis. The area under the ROC curve was 0.90 for LCI and 0.83 for FEV₁ (% pred.). Areas under the ROC curve for other MBW parameters were: LCI_{vent} 0.88; LCI_{ds} 0.89; S_{cond} 0.76; S_{acin} 0.91; S_{cond}* 0.50; and S_{acin}* 0.92.

Figure 3.7 shows graphs of FEV₁ standardised residuals against LCI (Panel A), LCI_{vent} (Panel B) and LCI_{ds} (Panel C) in patients with non-CF bronchiectasis. The lower limit of normal for FEV₁ was defined as 1.645 standard deviations below the predicted value, while the upper limits of normal for LCI, LCI_{vent} and LCI_{ds} were defined as the mean + 1.645 standard deviations in the healthy control group. Thirty out of 43 patients had an FEV₁ within the normal range, and of these, LCI, LCI_{vent} and LCI_{ds} were high in 12, 10 and 10 patients, respectively. Conversely, there were no patients who had an FEV₁ below the normal range who did not also have a raised LCI and LCI_{vent}, and only one patient who had an FEV₁ below the normal range with a normal LCI_{ds}.

Table 3.4: Physiological parameters in patients with and without chronic bacterial colonisation

	Non-cystic fibrosis bronchiectasis		Cystic fibrosis	
	No chronic colonisation (n = 26)	Chronic colonisation (n = 17)	No chronic PsA colonisation (n = 25)	Chronic PsA colonisation (n = 15)
FEV ₁ (% pred.)	86.1 (5.3)	75.6 (4.9)	69.7 (4.5)	59.6 (4.5)
FVC (% pred.)	101.7 (4.6)	87.5 (4.1) [#]	86.9 (3.6)	80.6 (5.5)
FEV ₁ /FVC (%)	68.6 (2.4)	68.1 (2.4)	67.1 (2.5)	63.9 (2.5)
TLC (% pred.)	95.3 (3.1)	93.9 (4.0)	-	-
FRC _{mbw} (L)	2.38 (0.12)	2.62 (0.16)	1.87 (0.10)	2.18 (0.15)
LCI	10.02 (0.36)	9.95 (0.57)	12.29 (0.72)	14.44 (0.85)
LCI _{vent}	1.42 (0.03)	1.41 (0.05)	1.59 (0.05)	1.75 (0.05)
LCI _{ds}	1.27 (0.02)	1.26 (0.03)	1.34 (0.03)	1.49 (0.04) ^{##}
S _{cond} (L ⁻¹)	0.058 (0.010)	0.072 (0.010)	0.122 (0.010)	0.132 (0.018)
S _{acin} (L ⁻¹)	0.429 (0.053)	0.288 (0.038)	0.438 (0.070)	0.611 (0.093)
S _{cond} * (L ⁻¹)	0.102 (0.014)	0.115 (0.016)	0.284 (0.034)	0.294 (0.051)
S _{acin} * (L ⁻¹)	0.412 (0.053)	0.268 (0.041)	0.376 (0.068)	0.553 (0.092)

PsA = *Pseudomonas aeruginosa*; FEV₁ = forced expiratory volume in one second; FVC = forced vital capacity; TLC = total lung capacity; FRC_{mbw} = functional residual capacity using multiple breath washout; LCI = lung clearance index; LCI_{vent} = specific ventilation inequality component of lung clearance index; LCI_{ds} = dead space component of lung clearance index. Data expressed as mean (standard error). Colonised and non-colonised groups within each disease cohort compared using Student's T test. Significant differences between groups denoted [#](p < 0.05) or ^{##}(p < 0.01).

Table 3.5: Within-visit repeatability of multiple breath washout parameters in cystic fibrosis and non-cystic fibrosis bronchiectasis

	ICC in healthy controls	ICC in non-CF bronchiectasis	ICC in CF
LCI	0.90	0.86	0.93
LCI _{vent}	0.71	0.91	0.89
LCI _{ds}	0.47	0.79	0.88
S _{cond}	0.00 [#]	0.15	0.19
S _{acin}	0.69	0.63	0.88
S _{cond} *	0.56	0.10	0.41
S _{acin} *	0.44	0.65	0.90

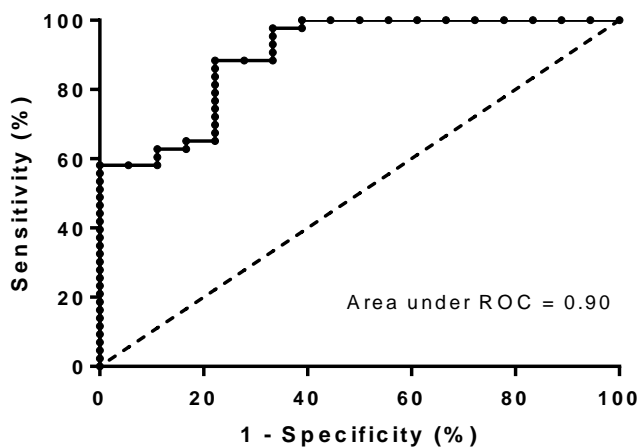
ICC = intraclass correlation coefficient; SD = standard deviation; CF = cystic fibrosis; LCI = lung clearance index; LCI_{vent} = specific ventilation inequality component of lung clearance index; LCI_{ds} = dead space component of lung clearance index.

[#]Negative ICC reported as zero.

Figure 3.6: Receiver operating characteristic curves of lung clearance index and FEV₁ (% pred.) for distinguishing between control subjects and bronchiectasis patients

Receiver operating characteristic (ROC) curves are shown for lung clearance index (LCI) (Panel A) and forced expiratory volume in one second percent predicted (FEV₁ [% pred.]) (Panel B). Areas under ROC curves are 0.90 for LCI and 0.83 for FEV₁ (% pred.).

Panel A



Panel B

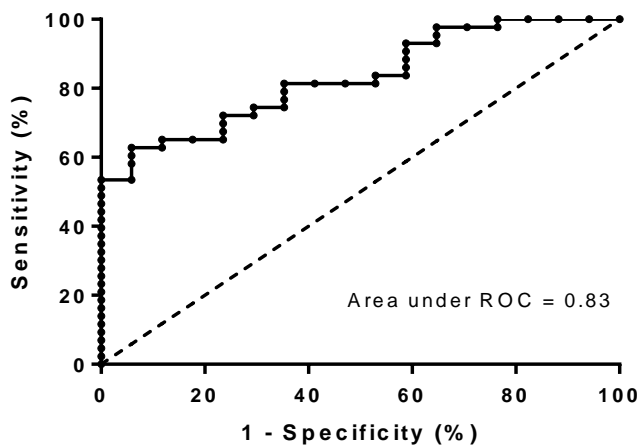
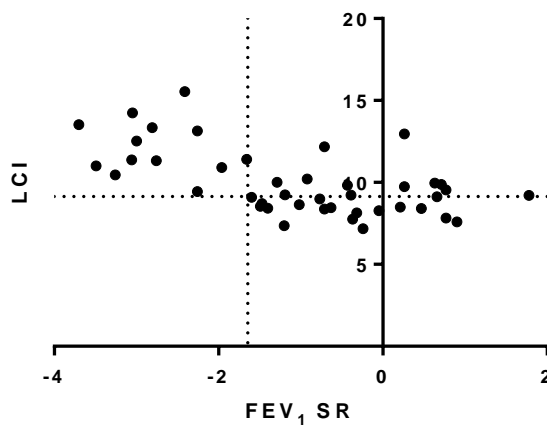


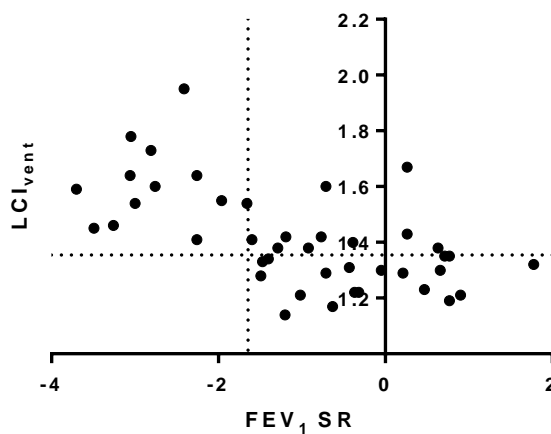
Figure 3.7: Scatterplots of forced expiratory volume in one second standardised residuals against multiple breath washout parameters in patients with non-cystic fibrosis bronchiectasis

LCI = lung clearance index; LCI_{vent} = specific ventilation inequality component of lung clearance index; LCI_{ds} = dead space component of lung clearance index; FEV_1 = forced expiratory volume in one second; SR = standardised residuals. Dotted lines denote the lower limit of normal for FEV_1 and upper limits of normal for LCI , LCI_{vent} and LCI_{ds} .

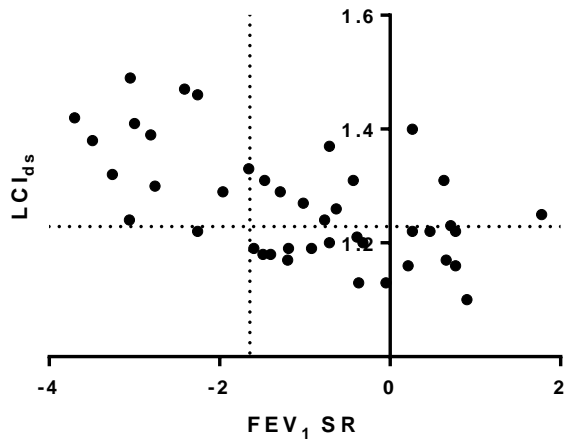
Panel A



Panel B



Panel C



Discussion

We have shown that LCI, and the novel parameters LCI_{vent} and LCI_{ds} , are significantly raised in patients with non-CF bronchiectasis compared to controls, and that these parameters correlate strongly with spirometric markers of airflow obstruction. LCI, LCI_{vent} and LCI_{ds} display good within-visit repeatability in patients with non-CF bronchiectasis, and superior discriminatory ability for distinguishing bronchiectasis patients from controls compared to FEV_1 . Moreover, these parameters are abnormally raised in a significant proportion of non-CF bronchiectasis patients with a normal FEV_1 . These findings suggest that MBW parameters may have potential as markers of disease severity in patients with non-CF bronchiectasis, and may be indicators of incipient airflow obstruction, although longitudinal studies are required to test this hypothesis. Further studies are also required to determine the between-visit variability and minimal clinically important difference of MBW parameters in patients with non-CF bronchiectasis, as well as their responsiveness to therapeutic interventions.

Interestingly, the relationship between FEV_1 and LCI differed significantly between patients with CF and non-CF bronchiectasis. Specifically, patients with CF had a 0.13 unit increase in LCI for every 1 percentage point reduction in FEV_1 (% pred.), whereas patients with bronchiectasis had a 0.05 unit increase in LCI for every 1 percentage point reduction in FEV_1 (% pred.) ($p < 0.0001$). In the asthma cohort presented in Study 3.4, the slope of the relationship was even shallower, with a 0.02 unit increase in LCI for every 1 percentage point reduction in FEV_1 (% pred.). We speculate that ventilation heterogeneity is most marked in suppurative lung diseases, in which there is patchy near-complete obstruction of airways by mucus hypersecretion. The degree of lung damage and bronchiectasis in the adult CF cohort was likely to be greater than in our non-CF bronchiectasis group, some of whom had mild or localised bronchiectasis. In contrast, the remodelling changes that occur in asthma appear to cause more subtle ventilation heterogeneity.

A major aim of this study was to develop novel markers of ventilation heterogeneity that would distinguish between the two possible mechanisms of increased LCI, namely specific ventilation inequality and increased respiratory dead space. Previous studies have used measures of the curvilinearity of the washout curve as markers of specific

ventilation inequality, but these methods did not provide a formal estimate of the respiratory dead space component^{143,149}. Although in healthy subjects it is thought that specific ventilation inequality is the only mechanism of ventilation heterogeneity operative at the level of the proximal conducting airways, the situation in disease is far more complex. Depending on the extent of airway damage and obstruction, diffusion may not be neatly compartmentalised to the distal airways. An advantage of the current method is that it does not pre-suppose an anatomical location for the observed abnormalities in ventilation heterogeneity, but concentrates on the underlying mechanisms. This is particularly relevant when dealing with those with more severe airflow obstruction and ventilation heterogeneity. Furthermore, since the proximal and distal airways are not independent of each other, and form a complex interacting network¹²⁴, it is also unsurprising that we noted a correlation between LCI_{vent} and LCI_{ds} in both patient groups. LCI_{vent} and LCI_{ds} may however allow subtle distinctions to be made in terms of mechanisms of disease in airway diseases such as CF and non-CF bronchiectasis. Indeed, we observed that CF patients with chronic *P. aeruginosa* colonisation had increased LCI_{ds} compared to those who did not, whereas LCI_{vent} did not differ significantly between the groups. This extends the findings of Belessis *et al.*²³⁹, who observed that LCI was higher in children with CF who had *P. aeruginosa* colonisation compared to those who did not. Our results suggest that this increase in LCI may be driven predominantly by an increased respiratory dead space. Interestingly, neither MBW parameters nor FEV_1 (% pred.) differed significantly between non-CF bronchiectasis patients with and without chronic bacterial colonisation. Chronic colonisation in our cohort was mainly with *H. influenzae* rather than *P. aeruginosa*, and our data therefore concord with previous observations that *H. influenzae*, unlike *P. aeruginosa*, is not associated with faster lung function decline in non-CF bronchiectasis²⁴⁰. The reduced FVC (% pred.) we observed in non-CF bronchiectasis patients with chronic colonisation was not associated with an abnormally low TLC (% pred.), and therefore did not represent a true restrictive deficit.

It is recognised that LCI may be influenced to a certain extent by the FRC, V_T and $V_{D_{anat}}$, and is therefore not a completely unbiased measure of VH ²⁴¹. We therefore derived a formula for the 'ideal' value of LCI for a given combination of FRC, V_T and $V_{D_{anat}}$, assuming no VH (LCI_{ideal}). We defined the novel parameters LCI_{vent} and LCI_{ds} as the proportional increase in LCI over and above LCI_{ideal} due to (i) convective

ventilation heterogeneity, and (ii) increased respiratory dead space, respectively. These parameters are based upon a simple two-compartment model of the lungs. The assumptions of this model will now be discussed:

i) We modelled washout curves using just two compartments, whereas in reality the lungs consist of many thousands of convection-dependent units, forming an almost continuous distribution of washout time constants. A number of authors have investigated the theoretical and practical limits on the information that may be extracted from an inert gas washout curve. Wagner *et al.* showed that under ideal theoretical conditions of error-free data, continuous distributions of washout rate constants with up to four modes could be distinguished²⁴². However, subsequent investigators simulated the effect of introducing experimental error into the data, and found that even with very low levels of error, the information that was recoverable dropped dramatically^{243,244}. These conclusions are in accordance with our own experience, in which we found that a two-compartment model was sufficient to capture the information content of experimental washout curves. The median (interquartile range) goodness of fit of the two-compartment model was 0.995 (0.991 – 0.997), 0.985 (0.975 – 0.993) and 0.959 (0.929 – 0.984) in the healthy, non-CF bronchiectasis and CF groups, respectively. We found that in the majority of cases it was not possible to fit a three-compartment model to experimental MBW data, except in the case of CF patients with the most severe ventilation heterogeneity.

ii) Our model did not take into account the effect of ‘sequencing’, whereby poorly-ventilated lung units empty later in expiration than well-ventilated units. Otis *et al.* showed that the phase shift in cyclical ventilation between lung units with different time constants could result in a curious phenomenon known as convective pendelluft¹⁰⁸, in which some lung units could continue to fill while others have started emptying, and vice versa. Safonoff *et al.* demonstrated that the effects of this phenomenon on estimates of FRC and ‘slow’ space volume derived from inert gas washout in patients with severe airway disease were likely to be modest²⁴⁵. However, our model could have been usefully extended by including this effect, particularly since we based our washout curves on end-tidal inert gas concentrations, which are disproportionately increased by sequencing compared to alternative points on the expirogram such as the mean expired concentration over the course of the phase III slope.

iii) Our model assumed that the respiratory dead space was distributed between the two compartments in the same proportion as the tidal volume. While it may be considered desirable to have allowed the dead space for each compartment to vary independently, it was necessary to fix the distribution of the dead space between the two compartments in some way, since otherwise it would not have been possible to distinguish between the slow washout of a compartment due to reduced ventilation or increased dead space. The assumption that dead space is distributed in the same proportion as tidal volume follows from the presumed independence of the convective and diffusive-convective mechanisms under investigation, and implies that a fixed proportion of the tidal volume in each of the two large compartments is ‘wasted’ due to anatomical dead space and diffusion-convection-dependent gas mixing inefficiencies. However, this work could have been extended by exploring the effect of different distributions of dead space, for instance by introducing a common dead space into the model.

A potential limitation of our study was that the disease groups were not matched for age with the control group. This was to a certain extent unavoidable, since patients with non-CF bronchiectasis are in general older than those with CF, and we therefore chose our control group to be approximately intermediate in age between the two disease groups. However, recently published regression equations²⁴⁶ indicate that the effects of this on our results were likely to be modest – in particular, LCI is expected to increase by 0.0223 units per year, so the 19-year difference in mean age between patients with bronchiectasis and healthy controls would be predicted to cause a relatively small 0.43 difference in LCI between the groups. Furthermore, the upper limit of normal of LCI derived from our healthy control data was slightly higher than that reported in previous studies using the same methodology¹³², a difference that may be explained by the older age of our healthy cohort. Similarly, the values for S_{cond} and S_{acin} that we obtained in healthy subjects were somewhat higher than those reported by Prisk *et al* in a small group of healthy participants who flew on the Spacelab Life Sciences (SLS) missions²⁴⁷. This may be explained by differences in both subject characteristics and methodology, since the SLS participants were younger than those in our study, and additionally washout tests in the Prisk study were performed using a mass spectrometer with 1.25% SF₆. Further studies are required to derive age- and sex-dependent

normative ranges for LCI and other MBW parameters using the SF₆ wash-in method, as have been published for nitrogen washout²⁴⁶.

In conclusion, we have shown that LCI, a marker of impaired gas mixing derived from the MBW test, is significantly raised in patients with non-CF bronchiectasis, and that this elevation correlates with spirometric airflow obstruction. LCI is repeatable and discriminatory in patients with non-CF bronchiectasis, and future studies are now required to assess the prognostic significance of a raised LCI in this patient group, as well as the potential utility of this marker as an outcome measure in interventional trials. The novel parameters LCI_{vent} and LCI_{ds} are an alternative to phase III slope analysis that may allow a further level of mechanistic information to be obtained from the MBW test without any additional demand on the patient.

3.3 Between-visit variability of small airway obstruction markers in patients with asthma

Abstract

Background and aims

The forced expiratory volume in one second is often utilised as an outcome measure in clinical asthma trials, but is thought to reflect mainly large airway obstruction. Putative markers of small airway disease include measures of respiratory system resistance using impulse oscillometry (IOS), and indices of ventilation heterogeneity derived from multiple breath inert gas washout (MBW). We aimed to determine the between-visit variability of these measurements in patients with asthma in the stable state.

Methods

Eighteen patients with asthma underwent IOS and MBW at baseline, and the tests were subsequently repeated using identical methodology two weeks and three months following baseline. The intraclass correlation coefficient (ICC) and standard deviation of between-visit within-subject differences (SD) was calculated for each physiological variable, for each of the two time intervals.

Results

ICC values ranged from 0.80 to 0.91 for IOS parameters, and from 0.63 to 0.91 for MBW parameters. The SD data we have provided may be utilised to perform sample size calculations for interventional trials.

Conclusion

We conclude that IOS parameters are stable over time, and have potential as outcome measures in clinical asthma trials. MBW indices are moderately stable, but require further investigation in patients with asthma.

Introduction

Clinical trials in patients with airway diseases often utilise the forced expiratory volume in one second (FEV₁) as the sole physiological outcome measure. However, FEV₁ is thought to be insensitive to obstruction of the smaller airways, which may be particularly relevant in asthma³⁷. Putative markers of small airway obstruction include measures of airway resistance using impulse oscillometry (IOS)¹¹³, and indices of ventilation heterogeneity derived from multiple breath inert gas washout (MBW)¹²⁸. Recently, Takeda *et al* have shown that IOS parameters such as R20, R5-R20 and X5 are independent predictors of asthma health status over and above FEV₁¹²⁷, and Farah *et al* have demonstrated that MBW parameters may be responsive to asthma therapy¹⁵⁷.

In order to conduct clinical trials using these alternative outcome measures, it is necessary to be assured of their repeatability and stability over time. Moreover, an estimate of between-visit variability in the stable state is required so that sample size calculations can be performed. Between-visit variability may arise from a number of sources including purely technical factors, differences in patient performance of the test, and true temporal variability in the degree of airway obstruction. We aimed to determine the between-visit variability of a range of IOS and MBW indices in a group of patients with asthma in the stable state. We investigated between-visit variability over two time intervals, namely two weeks and three months, in order to encompass the typical lengths of treatment period that are utilised in clinical trials.

Methods

We recruited 18 adults (age > 18) with moderate-to-severe asthma (Global Initiative for Asthma treatment steps 3-5), diagnosed by a specialist asthma physician in a secondary care setting, according to British Thoracic Society guidelines^{2,248}. The study was approved by the National Research Ethics Committee – East Midlands Leicester, and all participants gave their written informed consent. The participant group comprised nine men and nine women with a mean (standard deviation [SD]) age of 58 (11) years. All participants were treated with inhaled corticosteroids (1000 – 2000 µg per day, beclometasone dipropionate equivalent) and long-acting β₂ agonists. Eleven patients

received maintenance low-dose prednisolone (5 – 15mg per day). Mean (SD) post-bronchodilator FEV₁ (% pred.) was 80.5 (23.0) with mean (SD) bronchodilator reversibility of 13.5% (16.0%). A previous history of atopy was documented in nine patients. Geometric mean (95% confidence interval) sputum eosinophil percentage was 2.6 (1.1 – 6.3) (upper limit of normal 2.2%)²⁴⁹, and mean (SD) neutrophil percentage was 58.6 (28.2).

At each study visit, participants completed the six-point Asthma Control Questionnaire (ACQ-6)²⁵⁰. Following administration of a bronchodilator (400µg via a metered dose inhaler and spacer), IOS, MBW and spirometry were performed at baseline, then at two weeks and three months following baseline. All study visits took place in the stable state, at least six weeks following any exacerbation of asthma.

IOS was performed using a Jaeger MasterScreen Impulse Oscillometry System (Viasys Healthcare GmbH, Hoechberg, Germany), according to standard guidelines¹⁰¹, as described in Section 2.4.2. IOS was performed three times in succession at each visit, with each test lasting 60 seconds. R5, R20, R5-R20, X5 and AX values were obtained from each test by taking the mean value measured over the course of the 60 second test interval. MBW was performed according to current guidelines¹³⁰, using the sulphur hexafluoride (SF₆) wash-in method¹³², as described in Section 2.5. The novel parameters LCI_{vent} and LCI_{ds} were calculated as described in Section 2.7.

Results and discussion

The intraclass correlation coefficient (ICC, SPSS Version 20, IBM Corporation, Somers, New York, USA) was calculated for each physiological variable, for the two-week and three-month time intervals, as shown in Table 3.6. Between-visit repeatability was good at both time intervals for most IOS and MBW parameters, with ICC values exceeding 0.8 in the majority of cases. However, the repeatability of S_{cond} and S_{acin} at 3 months was only moderate, with ICC values of 0.63 and 0.71 respectively. Within-visit repeatability was also assessed using the ICC of triplicate tests performed at baseline. All physiological measurements had high within-visit repeatability (ICC > 0.85), with the exception of S_{cond}. Previous investigators have also noted the poor within-visit

repeatability of S_{cond}^{147} , suggesting that this parameter may be less reliable than LCI and S_{acin} using the current MBW methodology.

The mean, SD and 95% confidence intervals of between-visit differences are shown in Table 3.6. The SD data may be used, in conjunction with estimates of the minimal clinically important difference (MCID), to perform sample size calculations for interventional studies in patients with asthma. Given a parallel group study design in which the change in the variable of interest from baseline to follow-up is compared between an intervention and a control group using a parametric test, the required sample size may be calculated using a standard formula²⁵¹:

$$\text{Sample size} = \frac{2\sigma^2(u + v)^2}{d^2}$$

Where σ = standard deviation of between-visit changes
 u = one-sided percentage point of the normal distribution corresponding to 100% - power (eg. if power = 80%, $u = 0.84$)
 v = percentage point of the normal distribution corresponding to the (two-tailed) significance level (eg. if significance level = 5%, $v = 1.96$)
 d = difference in between-visit changes to be detected

Although the MCID has not been established for most small airway outcome measures, estimates can be made in some cases from previously published data. Yamaguchi *et al* compared the response to small-particle and standard corticosteroid inhalers in steroid-naïve asthmatics using IOS²⁵². They observed a reduction in R5-R20 of 0.05 kPa·L⁻¹·s in the small-particle group and 0.02 kPa·L⁻¹·s in the standard group, thus giving a difference between groups of 0.03 kPa·L⁻¹·s with respect to the change in R5-R20 from baseline to follow-up. The sample size required to detect this difference following a two-week treatment period with 80% power and 5% two-tailed significance would be 28 per treatment arm, which would be feasible in most clinical trial settings. Table 3.7 shows, for each of the IOS and MBW parameters, the minimum between-group

difference that could be detected with respect to baseline-to-follow-up change, at 80% power and 5% two-tailed significance, with 30 patients in each arm of the study.

A potential limitation of our study was the relatively high mean age of our participants. It is possible that younger patients with asthma manifest a greater degree of variability in airway function than older patients, and further studies are required to investigate this possibility. However, the relative preponderance of middle-aged patients in our participant group is typical of previously described refractory asthma cohorts²⁵³, and is thus representative of patients most likely to be enrolled in clinical trials. Most patients in this study had moderate or severe asthma, and the results therefore may not be generalisable to mild asthma. As expected, variability was greater at three months than at two weeks for most outcome measures. However, LCI, LCI_{vent} and LCI_{ds} were exceptions to this pattern. We therefore recommend that the two-week estimate of variability be used for all sample size calculations involving these indices, in order to mitigate the risk of being underpowered.

We conclude that IOS parameters are stable over time, and have potential as outcome measures in clinical asthma trials. MBW indices are moderately stable, but require further investigation in patients with asthma. Further studies are required to determine the longer-term variability of MBW and IOS parameters, as well as to establish the MCID for a number of small airway outcome measures.

Table 3.6: Between- and within-visit variability of physiological variables in patients with asthma

	Baseline values		Variability at two weeks		Variability at three months	
	Mean \pm SD	ICC*	Mean \pm SD change from baseline (95% confidence intervals)	ICC [†]	Mean \pm SD change from baseline (95% confidence intervals)	ICC [†]
ACQ-6 score	1.61 \pm 1.14	-	0.02 \pm 0.64 (-1.24 – 1.28)	0.83	0.04 \pm 0.85 (-1.63 – 1.71)	0.78
FEV ₁ (L)	2.21 \pm 0.82	0.99	-0.04 \pm 0.14 (-0.32 – 0.24)	0.98	0.04 \pm 0.18 (-0.33 – 0.40)	0.98
R5 (kPa·L ⁻¹ ·s)	0.52 \pm 0.18	0.94	-0.02 \pm 0.08 (-0.18 – 0.14)	0.89	-0.02 \pm 0.09 (-0.21 – 0.16)	0.86
R20 (kPa·L ⁻¹ ·s)	0.39 \pm 0.12	0.90	-0.01 \pm 0.06 (-0.12 – 0.10)	0.88	-0.02 \pm 0.06 (-0.14 – 0.10)	0.85
R5-R20 (kPa·L ⁻¹ ·s)	0.14 \pm 0.10	0.97	-0.02 \pm 0.04 (-0.09 – 0.06)	0.91	-0.01 \pm 0.05 (-0.12 – 0.10)	0.84
X5 (kPa·L ⁻¹ ·s)	-0.19 \pm 0.11	0.94	0.02 \pm 0.05 (-0.08 – 0.11)	0.88	0.03 \pm 0.06 (-0.08 – 0.15)	0.80
AX (kPa·L ⁻¹)	1.47 \pm 1.42	0.98	-0.25 \pm 0.59 (-1.40 – 0.91)	0.88	-0.23 \pm 0.67 (-1.54 – 1.09)	0.86
FRC _{mbw} (L)	2.50 \pm 0.79	0.98	-0.10 \pm 0.23 (-0.55 – 0.35)	0.95	0.06 \pm 0.65 (-1.22 – 1.34)	0.72
LCI	8.20 \pm 1.48	0.95	0.14 \pm 1.04 (-1.89 – 2.18)	0.78	-0.25 \pm 0.63 (-1.48 – 0.99)	0.91
LCI _{vent}	1.28 \pm 0.15	0.97	0.01 \pm 0.10 (-0.19 – 0.20)	0.78	-0.02 \pm 0.06 (-0.13 – 0.09)	0.91
LCI _{ds}	1.20 \pm 0.08	0.94	0.01 \pm 0.05 (-0.09 – 0.10)	0.83	-0.01 \pm 0.04 (-0.10 – 0.08)	0.84
S _{cond} (L ⁻¹)	0.066 \pm 0.081	0.23	0.004 \pm 0.038 (-0.072 – 0.079)	0.89	-0.007 \pm 0.057 (-0.119 – 0.104)	0.63
S _{acin} (L ⁻¹)	0.207 \pm 0.127	0.87	-0.024 \pm 0.067 (-0.156 – 0.108)	0.83	-0.027 \pm 0.068 (-0.16 – 0.11)	0.71

Legend for Table 3.6

SD = standard deviation; ICC = intraclass correlation coefficient; ACQ-6 = six-point Asthma Control Questionnaire; FEV₁ = forced expiratory volume in one second; R5/R20 = resistance at 5Hz/20Hz; X5 = reactance at 5Hz; AX = reactance area; FRC_{mbw} = functional residual capacity measured using multiple breath washout; LCI = lung clearance index; LCI_{vent} = specific ventilation inequality component of lung clearance index; LCI_{ds} = dead space component of lung clearance index.

*Denotes ICC of triplicate tests performed at baseline.

†Denotes ICC of tests performed at baseline versus follow-up visits.

Table 3.7: Sample size calculations for impulse oscillometry and inert gas washout parameters

	Δ following 2-week treatment period*	Δ following 3-month treatment period*
R5 (kPa·L ⁻¹ ·s)	0.06	0.07
R20 (kPa·L ⁻¹ ·s)	0.05	0.05
R5-R20 (kPa·L ⁻¹ ·s)	0.03	0.04
X5 (kPa·L ⁻¹ ·s)	0.04	0.05
AX (kPa·L ⁻¹)	0.43	0.49
LCI †	0.76	0.76
LCI _{vent} †	0.08	0.08
LCI _{ds} †	0.04	0.04
S _{cond} (L ⁻¹)	0.028	0.042
S _{acin} (L ⁻¹)	0.049	0.050

R5/R20 = resistance at 5Hz/20Hz; X5 = reactance at 5Hz; AX = reactance area; LCI = lung clearance index; LCI_{vent} = specific ventilation inequality component of lung clearance index; LCI_{ds} = dead space component of lung clearance index.

*Denotes the minimum between-group difference with respect to baseline-to-follow-up change that may be detected given a parallel-group study design, with 30 patients in each arm, at 80% power and 5% two-tailed significance.

†Two-week estimate of variability utilised for both two-week and three-month calculations, as discussed in the text.

3.4 Clinical significance of small airway obstruction markers in patients with asthma

Abstract

Background

The role of small airway obstruction in the clinical expression of asthma is incompletely understood.

Objective

We tested the hypotheses that markers of small airway obstruction are associated with (i) increased asthma severity, (ii) impaired asthma control and quality of life, and (iii) frequent exacerbations.

Methods

Seventy-four adults with asthma and 18 healthy control subjects underwent impulse oscillometry (IOS), multiple breath inert gas washout (MBW), body plethysmography, single-breath determination of carbon monoxide uptake and spirometry. Patients completed the six-point Asthma Control Questionnaire (ACQ-6) and standardised Asthma Quality of Life Questionnaire (AQLQ(S)). Asthma severity was classified according to the Global Initiative for Asthma (GINA) treatment steps.

Results

The putative small airway obstruction markers S_{acin} , resistance at 5Hz minus resistance at 20 Hz (R5-R20) and reactance area (AX) were not independently associated with asthma severity, control, quality of life or exacerbations. In contrast, markers of total (R5) and mean airway resistance of large and small airways (R20) were significantly higher in the severe asthma group compared to the mild-moderate group (0.47 vs 0.37, $p < 0.05$ for R5; 0.39 vs 0.31, $p < 0.01$ for R20). The strongest independent contributors to ACQ-6 score were R20 and forced expiratory volume in one second (% pred.), and the strongest independent contributors to AQLQ(S) score were R20 and forced vital

capacity (% pred.). A history of one or more exacerbations within the previous year was independently associated with R20.

Conclusions and Clinical Relevance

Previously reported markers of small airway obstruction do not appear to be independently associated with asthma disease expression. In contrast, the IOS parameter R20, a marker of mean airway resistance of both large and small airways, appears to have independent clinical significance. These observations require confirmation in prospective longitudinal studies.

Introduction

Asthma is a common inflammatory airway disease that is estimated to affect 300 million people worldwide¹. Inhaled corticosteroids (ICS) comprise the mainstay of asthma therapy, but deposition of most standard topical therapies is limited to the large conducting airways⁴¹. Persistent asthma, in which symptoms and/or airway inflammation are inadequately controlled despite topical therapy, imposes a disproportionate burden on individual patients and society, and is relatively common. Indeed, a large randomised controlled trial comparing ICS with combination ICS and long-acting β -agonist (LABA) only achieved total control of asthma at one year in 28% and 41% of patients respectively⁴². The causes of persistence are not completely understood but include poor patient adherence^{43,44}, inadequate inhaler technique⁴⁵ and corticosteroid resistance⁴⁶. A further possibility is that patients with persistent asthma have pathology in the small airways (usually defined as those with an internal diameter < 2mm) that standard topical therapy cannot reach³⁴.

The forced expiratory volume in one second (FEV₁) is often used to monitor asthma control, and as an outcome measure in clinical trials. However, FEV₁ is thought to be insensitive to small airway obstruction, and therefore a number of putative markers of small airway obstruction have been suggested, as summarised in Table 3.8. Measures of expiratory air trapping such as the forced vital capacity (FVC) and the ratio of residual volume (RV) to total lung capacity (TLC) are often assumed to represent small airway obstruction²⁵⁴, although conclusive evidence in support of this assertion is lacking. Impulse oscillometry (IOS), a variant of the forced oscillation technique (FOT), allows the non-invasive assessment of lung mechanics, and may provide novel insights into small airway obstruction¹¹³. The structural interpretation of IOS/FOT parameters is not fully understood, and has been the subject of much research, often based around computational models of lung impedance²⁵⁵. An additional complication is that values of resistance and reactance measured using different equipment may not be directly comparable¹⁰³. Resistance at 20Hz (R20) may be a marker of the general level of airway resistance throughout the airway tree, while the difference between R5 and R20 (R5-R20) may represent the heterogeneity of airway resistance. Measures of low-frequency reactance such as the reactance at 5Hz and reactance area (AX) are likely to reflect airway closure²⁵⁶. Multiple breath inert gas washout (MBW) is a test of gas

mixing efficiency and ventilation heterogeneity within the airway tree, with lung clearance index (LCI) being a general marker of ventilation heterogeneity^{130,233}. The specific ventilation inequality and respiratory dead space components of LCI may be extracted using the novel parameters LCI_{vent} and LCI_{ds} , respectively. The indices S_{cond} and S_{acin} derived from MBW are thought to represent ventilation heterogeneity arising due to convective and diffusive-convective mechanisms, respectively¹³¹, with convective mechanisms occurring in both the large and small conducting airways and diffusive-convective mechanisms occurring more distally in the airway tree, in the region of the acinar entrance. To summarise, while a number of physiological markers have been proposed that may provide greater insight into small airway obstruction than spirometry, these are unlikely to be completely specific to the small airways, as defined above. Moreover, it is known that the large and small airways are not independent of each other, but that they instead form a complex interacting network that may exhibit emergent properties such as catastrophic closure and re-opening¹²⁴. Therefore, the distinction between markers of large and small airway obstruction may be to a certain extent artificial.

Table 3.8: Physiological interpretations of airway obstruction markers

Variable	Interpretation of abnormal result
Forced expiratory volume in one second (FEV ₁)	Reduced ventilatory function
Forced vital capacity (FVC)	Air trapping
Ratio of forced expiratory volume in one second to forced vital capacity (FEV ₁ /FVC)	Expiratory flow limitation
Ratio of residual volume to total lung capacity (RV/TLC)	Air trapping
Ratio of alveolar volume by single breath helium dilution to total lung capacity (VA)	Abnormal convective ventilation distribution
Lung clearance index (LCI)	Ventilation heterogeneity
LCI _{vent}	Specific ventilation inequality component of lung clearance index
LCI _{ds}	Increased dead space component of lung clearance index
S _{cond}	Conductive ventilation heterogeneity
S _{acin}	Acinar ventilation heterogeneity
Resistance at 5Hz (R5)	General marker of airway resistance
Resistance at 20Hz (R20)	General marker of airway resistance
Resistance at 5Hz minus resistance at 20Hz (R5-R20)	Heterogeneity of airway resistance
Reactance at 5Hz (X5)	Airway closure
Reactance area (AX)	Airway closure

Nevertheless, there is some evidence that the putative markers of small airway obstruction described above may relate to disease expression in patients with asthma. Bourdin *et al* found that single breath nitrogen phase III slope correlated with Asthma Control Questionnaire (ACQ) score¹⁵⁶, although these authors did not control for possible associations between nitrogen phase III slope and FEV₁. Farah *et al* found that changes in S_{cond} and S_{acin} correlated significantly with changes in five-point ACQ scores following treatment with high-dose ICS¹⁵⁷. The same group showed that MBW parameters could predict the symptomatic response to ICS up- or down-titration¹⁵⁹. Moreover, Thompson *et al* found that S_{acin} was raised during asthma exacerbations and fell markedly as the exacerbation resolved¹⁵⁸. Shi *et al* reported that AX and R5-R20 were significantly higher in children with uncontrolled asthma compared to those with controlled asthma, and that this effect was more apparent with pre-bronchodilator than post-bronchodilator measurements¹²⁶. Similarly, Takeda *et al* found that R20, R5-R20 and X5 were independent predictors of patient-reported outcome measures such as ACQ score and Asthma Quality of Life Questionnaire (AQLQ) score in adults with asthma¹²⁷. Sorkness *et al* found that at any given level of airflow obstruction, as measured with the FEV₁/FVC (% pred.), patients with severe asthma had more severe air trapping, as measured by reduced FVC (% pred.) and increased RV/TLC (% pred.)⁹². However, there has as yet been no study examining the contributions of each of these putative small airway obstruction markers to clinical outcomes in a single well-characterised group of adults with asthma. Moreover, with the exception of the study by Bourdin *et al*¹⁵⁶, physiological measurements in the above studies were performed having withheld bronchodilator medications, and it is therefore possible that variations in large airway bronchial tone may have contributed to the associations that were observed. We therefore wished to specifically investigate post-bronchodilator measurements, in order to eliminate these variations and focus on the effects of long-term remodelling changes in the smaller airways.

In this study, we aimed to test the hypotheses that small airway obstruction markers are associated with (i) increased asthma severity, as evidenced by higher treatment requirements, (ii) impaired asthma control and quality of life, and (iii) frequent exacerbations.

Materials and methods

Subjects

Seventy-four patients with asthma and 18 healthy subjects with no history of respiratory disease were recruited. All participants were over 18 years of age. Current smokers (defined as people who have smoked within the previous year) and ex-smokers with a greater than 10 pack-year smoking history were excluded from the study. Asthma was diagnosed by a specialist asthma physician in a secondary care setting according to current British Thoracic Society guidelines²⁴⁸. Asthma severity was classified according to the current Global Initiative for Asthma (GINA) treatment steps². The study protocol was approved by the National Research Ethics Committee – East Midlands Leicester (approval number 08/H0406/189) and all subjects gave their written informed consent.

Study protocol

All participants attended a single visit in the stable state, not less than six weeks following any asthma exacerbation. Exacerbations were defined as worsening asthma symptoms for ≥ 3 days requiring additional therapy (short burst oral prednisolone and/or antibiotics) following either primary or secondary care consultation²⁵⁷. Clinical and physiological assessment was performed in the following sequence:

- i) Collection of demographic and clinical details
- ii) Completion of six-point ACQ (ACQ-6)²⁵⁰ and standardised AQLQ (AQLQ(S))²⁵⁸
- iii) Administration of salbutamol 400 micrograms via metered dose inhaler and spacer
- iv) Impulse oscillometry, using Jaeger MasterScreen Impulse Oscillometry System (Viasys Healthcare GmbH, Hoechberg, Germany)¹⁰¹
- v) Multiple breath washout, using sulphur hexafluoride (SF₆) wash-in method^{130,132}
- vi) Lung volumes using body plethysmography⁹⁰
- vii) Single-breath determination of carbon monoxide uptake²¹⁷
- viii) Spirometry²¹⁵

All physiological tests were performed in the seated position by individuals with appropriate training and accreditation. Physiological tests were performed 10 minutes

after administration of a short-acting bronchodilator (salbutamol 400 micrograms). This was administered via a metered dose inhaler and spacer, with each 100 microgram actuation being inhaled in a separate inhalation to TLC, followed by a 5-10 second breath-hold.

Statistical analysis

Statistical analyses were performed using SPSS 20 (IBM Corporation, Somers, New York, USA) and Prism 6 (GraphPad Software Inc., La Jolla, California, USA). A p value of < 0.05 was taken as the threshold for statistical significance. Comparisons between or across groups were performed using Student's T test or one-way analysis of variance for parametric data, the Mann-Whitney U test or Kruskal-Wallis test for non-parametric data, and Fisher's exact test or the Chi-squared test for proportions. Bonferroni/Dunn corrections for multiple comparisons were used as appropriate. Correlations between continuous variables were calculated using Pearson's correlation coefficient (R). Log-normally distributed variables were log-transformed as appropriate. Linear regression models were constructed (SPSS 20, stepwise algorithm, with probability for variable entry < 0.05 and probability for variable removal > 0.10) to determine the physiological determinants of ACQ and AQLQ scores. A logistic regression model (SPSS 20, forward conditional algorithm, with probability for variable entry < 0.05 and probability for variable removal > 0.10) was constructed to determine the physiological predictors of the exacerbation-prone phenotype, defined as having had at least one asthma exacerbation during the preceding year. The pool of variables that could potentially be entered into the linear or logistic regression models comprised FEV₁ (% pred.), FVC (% pred.), FEV₁/FVC, TLC (% pred.), RV/TLC (% pred.), alveolar volume using single breath helium dilution (V_A), V_A/TLC, LCI, LCI_{vent}, LCI_{ds}, S_{cond}, S_{acin}, R5, R20, log-transformed R5-R20, X5 and log-transformed AX. Predicted values and standardised residuals for FEV₁, FVC, TLC, RV/TLC, KCO and DLCO were calculated using published regression equations²¹⁶. The lower limit of normal for FEV₁ was defined as 1.645 standardised residuals below predicted, and the upper limit of normal for RV/TLC was defined as 1.645 standardised residuals above predicted. Upper limits of normal for R20, R5-R20, AX, LCI and S_{acin} were defined as the mean + 1.645 standard deviations in the healthy control group.

Results

Demographic, clinical and physiological data across groups are shown in Tables 3.9 and 3.10. The groups did not differ significantly with respect to age, sex or body mass index. The small airway obstruction markers S_{acin} , R5-R20 and AX did not differ significantly between the asthma severity groups. However, markers of total (R5) and mean large and small airway resistance (R20) were significantly higher in the GINA 4-5 group compared to the GINA 1-3 group (0.47 vs 0.37, $p < 0.05$ for R5; 0.39 vs 0.31, $p < 0.01$ for R20).

Table 3.11 shows correlations between physiological variables and both ACQ-6 and AQLQ(S) scores, as well as FEV₁ (% pred.). ACQ-6 score correlated significantly with FEV₁ (% pred.), RV/TLC (% pred.), TLC, VA, VA/TLC, diffusing capacity of the lung for carbon monoxide (DLCO) (% pred.), functional residual capacity from multiple breath washout (FRC_{mbw}), R5 and R20, but not with S_{acin} , log-transformed R5-R20 or log-transformed AX. The strongest correlation was with R20 ($R = 0.369$, $p < 0.01$). AQLQ(S) score correlated significantly with FEV₁ (% pred.), FVC (% pred.), RV/TLC (% pred.), TLC, VA, VA/TLC, DLCO (% pred.), FRC_{mbw}, R5, R20 and log-transformed R5-R20, but not with S_{acin} or log-transformed AX. The strongest correlation was again with R20 ($R = -0.430$, $p < 0.01$). Linear regression models, shown in Table 3.12, revealed that the strongest independent contributors to ACQ-6 score were R20 and FEV₁ (% pred.), and the strongest independent contributors to AQLQ(S) score were R20 and FVC (% pred.).

Table 3.13 shows physiological variables between patients with and without the exacerbation-prone phenotype, defined as having had at least one asthma exacerbation within the previous year. S_{acin} , R5-R20 and AX did not differ significantly between the groups. R5 and R20 were significantly higher in the exacerbation-prone group compared to the non-exacerbation-prone group, while FVC (% pred.), TLC, VA and DLCO (% pred.) were significantly lower. A logistic regression model revealed that the only independent predictor of the exacerbation-prone phenotype was R20. In particular, a 0.1 kPa·L⁻¹·s increase in R20 was associated with an odds ratio of 1.86 for having the exacerbation-prone phenotype (confidence interval of odds ratio 1.12 to 3.10, $p < 0.05$).

Figure 3.8 shows scatterplots of FEV₁ standardised residuals versus selected small airway obstruction markers. Patients were divided into four quadrants depending upon whether their FEV₁ was normal or low (fixed airflow obstruction negative or positive [FAO⁻ or FAO⁺], respectively), and whether the given small airway obstruction marker was normal or high (small airway obstruction negative or positive [SAO⁻ or SAO⁺], respectively). In each case, the majority of patients were concordant (FAO⁻/SAO⁻ or FAO⁺/SAO⁺). Figure 3.9 shows pie charts indicating the proportion of patients that were concordant (FAO⁻/SAO⁻ or FAO⁺/SAO⁺) or discordant (FAO⁻/SAO⁺ or FAO⁺/SAO⁻) for each small airway obstruction marker.

Table 3.9: Demographic and clinical data across asthma severity groups

	Healthy controls (n = 18)	Mild-moderate asthma [#] (n = 43)	Severe asthma [#] (n = 31)
Age (years)	48.3 (3.9)	57.2 (2.0)	53.8 (2.5)
Sex (% male)	50	51	39
BMI (kg/m ²)	26.8 (1.2)	27.0 (0.8)	30.0 (1.4)
Atopy (% atopic)	-	79	71
Duration of asthma (years)	-	18.7 (2.9)	25.3 (3.2)
Age of onset of asthma (years)*	-	38.4 (3.3)	28.3 (3.8)
ICS dose (BDP equivalent [mcg])****	-	547 (66)	1726 (118)
Oral prednisolone use (%)****	-	0	45
Leukotriene receptor antagonist use (%)**	-	5	35
Oral theophylline use (%)**	-	0	19
Exacerbations in past year****	-	1.0 (0.28)	3.5 (0.56)
ACQ-6 score***	-	0.99 (0.12)	1.82 (0.22)
AQLQ(S) score*	-	5.65 (0.16)	5.00 (0.23)

BMI = body mass index; ICS = inhaled corticosteroid; BDP = Beclometasone dipropionate; ACQ-6 = Six-point Asthma Control Questionnaire; AQLQ(S) = standardised Asthma Quality of Life Questionnaire. [#]Mild-moderate asthma refers to Global Initiative for Asthma (GINA) treatment steps 1-3; Severe asthma refers to GINA treatment steps 4-5. Data expressed as mean (standard error), †median (interquartile range) or proportions. Groups compared using Student's T test or one-way analysis of variance for parametric data, †Kruskal-Wallis test for non-parametric data, and Fisher's exact test or the Chi-squared test for proportions. Bonferroni/Dunn corrections for multiple comparisons used as appropriate. Significant differences across groups denoted *(p < 0.05), **(p < 0.01), ***(p < 0.001) or ****(p < 0.0001). Significant differences between GINA 1-3 and GINA 4-5 groups denoted †(p < 0.05) or ††(p < 0.01).

Table 3.10: Physiological data across asthma severity groups

	Healthy controls (n = 18)	Mild-moderate asthma [†] (n = 43)	Severe asthma [†] (n = 31)
FEV ₁ (% pred.)***	113.3 (4.8)	90.8 (3.4) ^{##}	86.9 (4.6) ^{###}
FVC (% pred.)*	117.2 (5.6)	101.1 (3.0) [#]	105.0 (4.2)
FEV ₁ /FVC (%)***	80.7 (1.0)	73.1 (1.5) [#]	68.4 (2.2) ^{###}
TLC (L)	6.39 (0.37)	6.14 (0.21)	6.00 (0.30)
TLC (% pred.)	104.3 (3.9)	104.9 (2.5)	107.8 (3.2)
RV/TLC (% pred.)***	89.2 (3.2)	110.4 (3.1) ^{###}	108.7 (2.7) ^{###}
VA (L)	5.58 (0.34)	5.07 (0.22)	4.88 (0.27)
VA/TLC (%)**	90.3 (1.7)	82.0 (1.6) ^{##}	80.8 (1.4) ^{##}
DLCO (% pred.)	89.3 (2.9)	91.2 (2.5)	89.5 (2.9)
KCO (% pred.)	97.4 (2.9)	107.4 (2.7)	104.6 (3.0)
FRC _{mbw} (L)	2.52 (0.19)	2.45 (0.11)	2.39 (0.17)
LCI	7.28 (0.27)	7.79 (0.20)	7.94 (0.22)
LCI _{vent}	1.20 (0.02)	1.23 (0.02)	1.25 (0.02)
LCI _{ds}	1.13 (0.01)	1.17 (0.01)	1.18 (0.02)
S _{cond} (L ⁻¹)	0.033 (0.007)	0.051 (0.006)	0.038 (0.005)
S _{acin} (L ⁻¹)	0.118 (0.014)	0.175 (0.019)	0.184 (0.020)
R5 (kPa·L ⁻¹ ·s)***	0.32 (0.03)	0.37 (0.02)	0.47 (0.03) ^{##, ¥}
R20 (kPa·L ⁻¹ ·s)***	0.29 (0.02)	0.31 (0.01)	0.39 (0.02) ^{##, ¥¥}
R5-R20 (kPaL ⁻¹ s) †*	0.03 (0.01 – 0.06)	0.05 (0.03 – 0.11)	0.05 (0.01 – 0.15)
X5 (kPa·L ⁻¹ ·s)	-0.10 (0.01)	-0.13 (0.01)	-0.15 (0.02)
AX (kPa·L ⁻¹) †*	0.23 (0.16 – 0.54)	0.41 (0.24 – 0.66)	0.47 (0.23 – 1.27) [#]

Legend for Table 3.10

FEV₁ = forced expiratory volume in one second; FVC = forced vital capacity; TLC = total lung capacity; RV = residual volume; VA = alveolar volume (single-breath helium dilution); DLCO = diffusing capacity of the lung for carbon monoxide; KCO = carbon monoxide transfer coefficient; FRC_{mbw} = functional residual capacity from multiple breath washout; LCI = lung clearance index; LCI_{vent} = specific ventilation inequality component of lung clearance index; LCI_{ds} = dead space component of lung clearance index; R5/R20 = resistance at 5Hz/20Hz; R5-R20 = resistance at 5Hz minus resistance at 20Hz; X5 = reactance at 5Hz; AX = reactance area. ¶Mild-moderate asthma refers to Global Initiative for Asthma (GINA) treatment steps 1-3; Severe asthma refers to GINA treatment steps 4-5. Data expressed as mean (standard error), †median (interquartile range) or proportions. Groups compared using Student's T test or one-way analysis of variance for parametric data, ‡Kruskal-Wallis test for non-parametric data, and Fisher's exact test or the Chi-squared test for proportions. Bonferroni/Dunn corrections for multiple comparisons used as appropriate. Significant differences across groups denoted *(p < 0.05), **(p < 0.01), *** (p < 0.001) or ****(p < 0.0001). Significant differences compared to healthy control group denoted #(p < 0.05), ##(p < 0.01) or ###(p < 0.001). Significant differences between GINA 1-3 and GINA 4-5 groups denoted ¥(p < 0.05) or ¥¥(p < 0.01).

Table 3.11: Correlations between clinical outcome measures and physiological variables

	ACQ-6 score	AQLQ(S) score	FEV ₁ (% pred.)
FEV ₁ (% pred.)	-.285*	.289*	-
FVC (% pred.)	-.230	.299*	.835**
FEV ₁ /FVC	-.166	.100	.657**
TLC	-.252*	.254*	.100
TLC (% pred.)	-.118	.154	.416**
RV/TLC (% pred.)	.268*	-.322**	-.573**
VA	-.300*	.322**	.214
VA/TLC	-.248*	.274*	.358**
DLCO (% pred.)	-.286*	.313**	.348**
KCO (% pred.)	-.084	.019	-.216
FRC _{mbw}	-.240*	.243*	.106
LCI	.151	-.202	-.406**
LCI _{vent}	.051	-.052	-.383**
LCI _{ds}	.104	-.142	-.352**
S _{cond}	.139	.025	-.196
S _{acin}	.160	-.168	-.200
R5	.341**	-.405**	-.340**
R20	.369**	-.430**	-.169
log R5-R20	.221	-.250*	-.379**
X5	-.070	.091	.402**
log AX	.173	-.202	-.492**

Legend for Table 3.11

ACQ-6 = Six-point Asthma Control Questionnaire; AQLQ(S) = standardised Asthma Quality of Life Questionnaire; FEV₁ = forced expiratory volume in one second; FVC = forced vital capacity; TLC = total lung capacity; RV = residual volume; VA = alveolar volume (single-breath helium dilution); DLCO = diffusing capacity of the lung for carbon monoxide; KCO = carbon monoxide transfer coefficient; FRC_{mbw} = functional residual capacity from multiple breath washout; LCI = lung clearance index; LCI_{vent} = specific ventilation inequality component of lung clearance index; LCI_{ds} = dead space component of lung clearance index; R5/R20 = resistance at 5Hz/20Hz; R5-R20 = resistance at 5Hz minus resistance at 20Hz; X5 = reactance at 5Hz; AX = reactance area.

Pearson's correlation coefficients are shown. Significant correlations are indicated * (p < 0.05) or ** (p < 0.01).

Table 3.12: Linear regression models assessing the contributions of physiological variables to ACQ-6 and AQLQ(S) scores

Dependent variable	Constant term	Independent variables	Unstandardised coefficient (B)	Standardised coefficient (β)	p value	Model R ²
ACQ-6 score	1.129	R20 (kPa·L ⁻¹ ·s)	3.276	0.330	0.005	0.187
		FEV ₁ (% pred.)	-0.010	-0.229	0.046	
AQLQ(S) score	5.459	R20 (kPa·L ⁻¹ ·s)	-4.355	-0.398	< 0.0005	0.229
		FVC (% pred.)	0.014	0.248	0.026	

ACQ-6 = Six-point Asthma Control Questionnaire; AQLQ(S) = standardised Asthma Quality of Life Questionnaire; R20 = resistance at 20Hz; FEV₁ = forced expiratory volume in one second; FVC = forced vital capacity.

Table 3.13: Demographic and physiological variables in exacerbation-prone and non-exacerbation-prone patients with asthma

	Non-exacerbation-prone[#] (n = 34)	Exacerbation-prone[#] (n = 40)
Age (years)*	59.9 (1.5)	52.2 (2.5)
Sex (% male)	59	35
BMI (kg/m ²)	27.3 (0.9)	29.0 (1.2)
FEV ₁ (% pred.)	94.0 (4.5)	85.1 (3.3)
FVC (% pred.)*	108.2 (3.7)	97.9 (3.1)
FEV ₁ /FVC (%)	70.1 (2.0)	72.1 (1.7)
TLC (L)**	6.59 (0.23)	5.66 (0.24)
TLC (% pred.)	109.8 (3.3)	103.1 (2.3)
RV/TLC (% pred.)	106.0 (3.4)	115.6 (3.9)
VA (L)**	5.48 (0.23)	4.58 (0.23)
VA/TLC (%)	82.8 (1.6)	80.3 (1.4)
DLCO (% pred.)**	96.1 (2.9)	85.8 (2.2)
KCO (% pred.)	108.4 (2.9)	104.4 (2.7)
FRC _{mbw} (L)	2.58 (0.13)	2.30 (0.13)
LCI	8.01 (0.24)	7.71 (0.19)
LCI _{vent}	1.25 (0.02)	1.23 (0.02)
LCI _{ds}	1.18 (0.02)	1.16 (0.01)
S _{cond} (L ⁻¹)	0.052 (0.007)	0.052 (0.009)
S _{acin} (L ⁻¹)	0.197 (0.023)	0.170 (0.018)
R5 (kPa·L ⁻¹ ·s)*	0.37 (0.03)	0.45 (0.02)
R20 (kPa·L ⁻¹ ·s)**	0.31 (0.02)	0.37 (0.02)
R5-R20 (kPa·L ⁻¹ ·s) †	0.04 (0.02 – 0.09)	0.06 (0.03 – 0.13)
X5 (kPa·L ⁻¹ ·s)	-0.14 (0.02)	-0.13 (0.01)
AX (kPa·L ⁻¹) †	0.33 (0.20 – 0.71)	0.51 (0.29 – 1.24)

Legend for Table 3.13

FEV₁ = forced expiratory volume in one second; FVC = forced vital capacity; TLC = total lung capacity; RV = residual volume; VA = alveolar volume (single-breath helium dilution); DLCO = diffusing capacity of the lung for carbon monoxide; KCO = carbon monoxide transfer coefficient; FRC_{mbw} = functional residual capacity from multiple breath washout; LCI = lung clearance index; LCI_{vent} = specific ventilation inequality component of lung clearance index; LCI_{ds} = dead space component of lung clearance index; R5/R20 = resistance at 5Hz/20Hz; R5-R20 = resistance at 5Hz minus resistance at 20Hz; X5 = reactance at 5Hz; AX = reactance area.

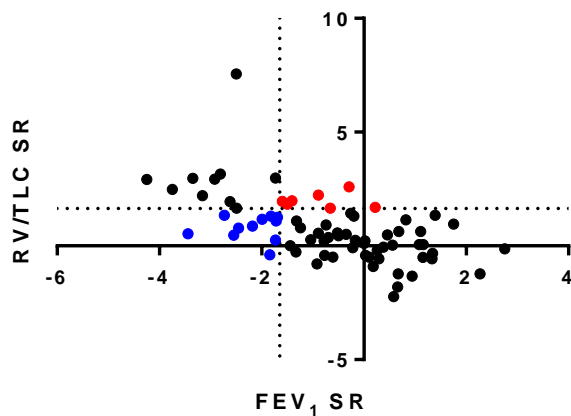
#Exacerbation-prone defined as having had at least one asthma exacerbation in the previous year.

Data expressed as mean (standard error), †median (interquartile range) or proportions. Groups compared using Student's T test for parametric data, †Mann-Whitney U test for non-parametric data or Fischer's exact test for proportions. Significant differences between groups denoted *(p < 0.05), **(p < 0.01), ***(p < 0.001) or ****(p < 0.0001).

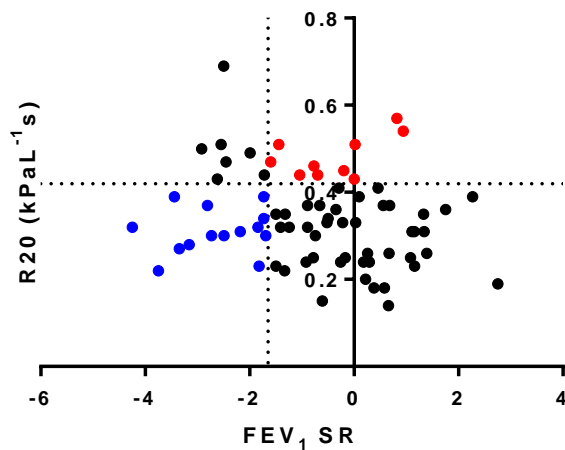
Figure 3.8: Scatterplots of forced expiratory volume in one second standardised residuals against small airway obstruction markers in patients with asthma

Scatterplots are shown of forced expiratory volume in one second (FEV_1) standardised residuals (SR) against residual volume to total lung capacity ratio SR (Panel A), resistance at 20Hz (Panel B), resistance at 5Hz minus resistance at 20Hz (Panel C), reactance area (Panel D), lung clearance index (Panel E) and S_{acin} (Panel F). Dotted lines indicate lower limits of normal for FEV_1 and upper limits of normal for small airway obstruction markers. Patients with normal FEV_1 and abnormal small airway obstruction markers are indicated in red, and patients with low FEV_1 but normal small airway obstruction markers are indicated in blue.

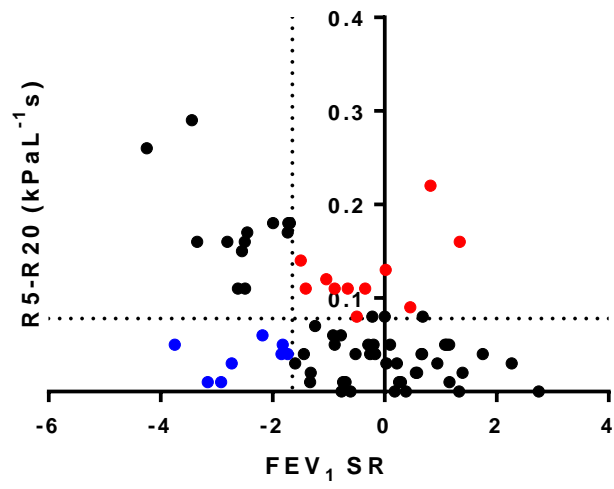
Panel A



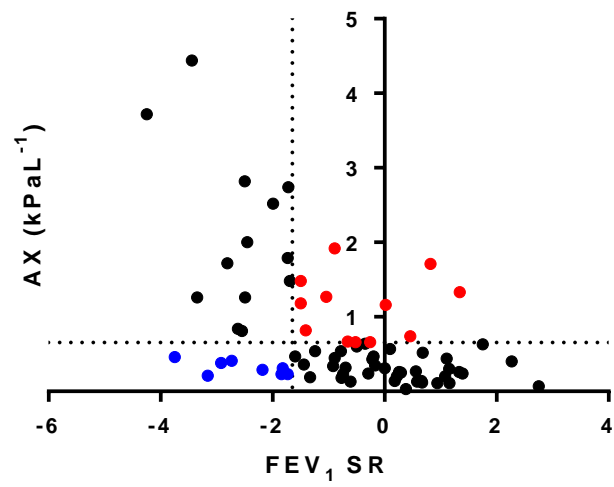
Panel B



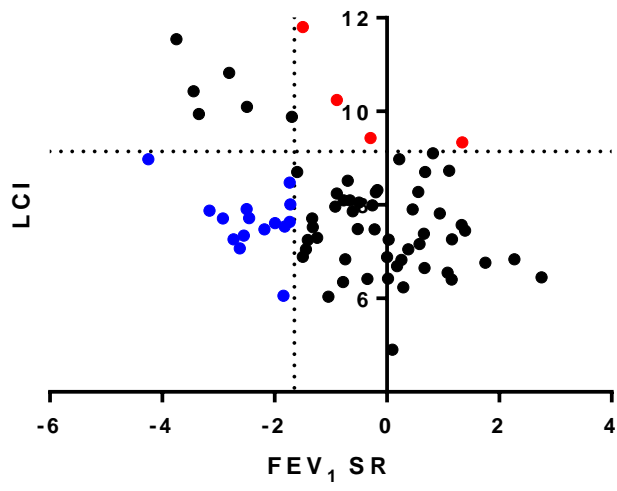
Panel C



Panel D



Panel E



Panel F

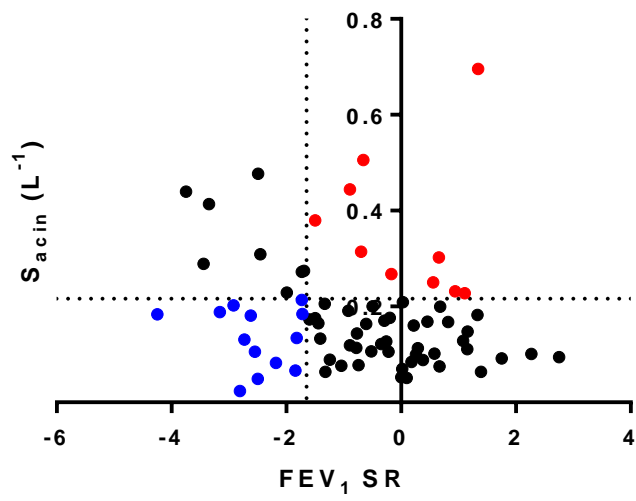
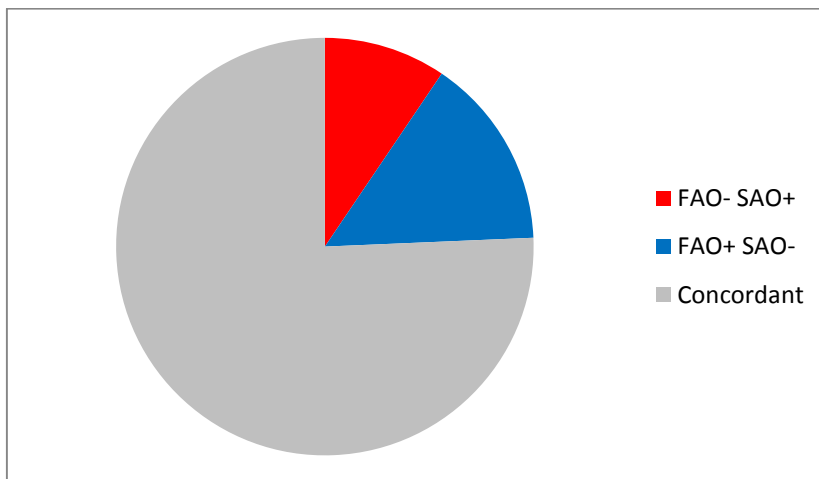


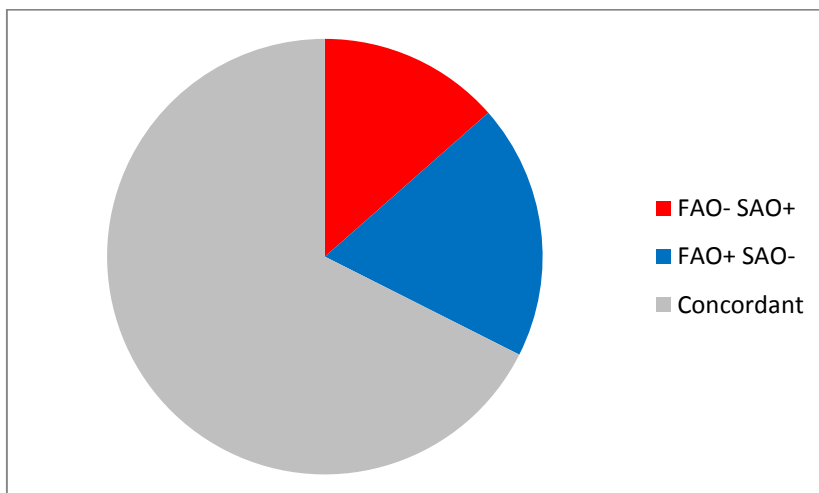
Figure 3.9: Pie charts showing proportions of patients with concordance or discordance between forced expiratory volume in one second and small airway obstruction markers

Pie charts are displayed showing the proportions of patients with (i) concordance between FEV₁ and small airway obstruction markers (ie. both normal or both abnormal), (ii) elevated small airway obstruction markers but normal FEV₁ (FAO⁻ SAO⁺), or (iii) low FEV₁ but normal small airway obstruction markers (FAO⁺ SAO⁻). The small airway obstruction markers analysed are residual volume to total lung capacity ratio (Panel A), resistance at 20Hz (Panel B), resistance at 5Hz minus resistance at 20Hz (Panel C), reactance area (Panel D), lung clearance index (Panel E) and S_{acin} (Panel F).

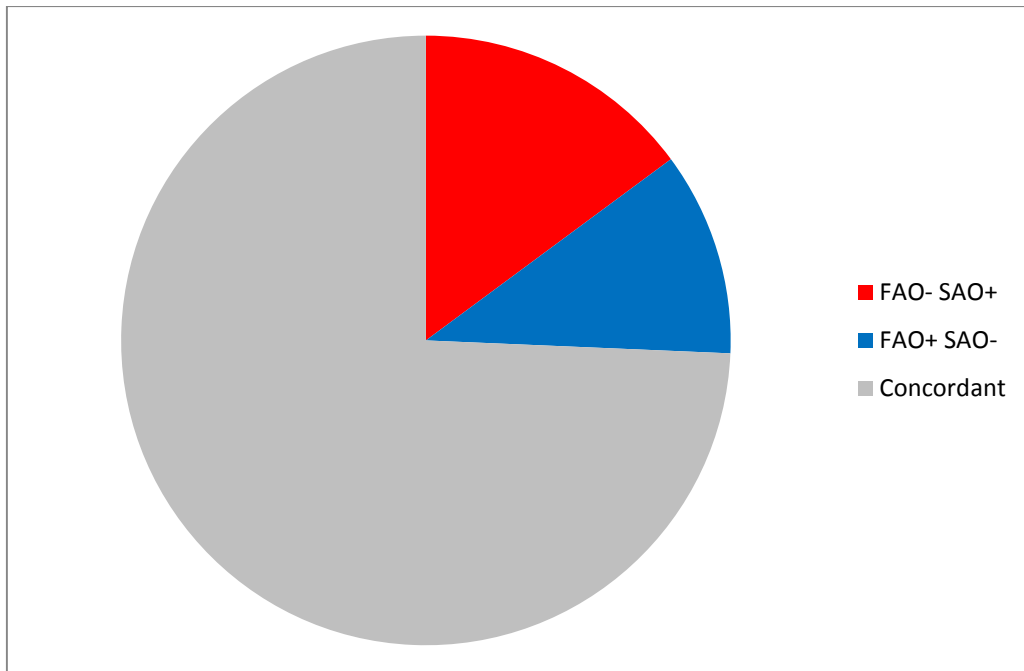
Panel A (RV/TLC)



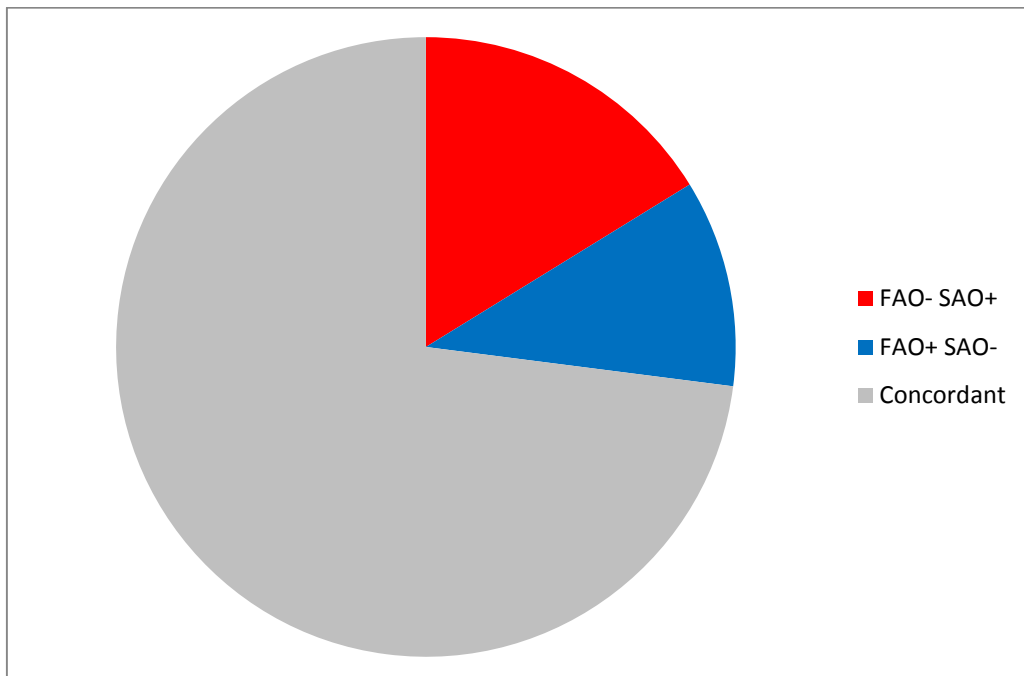
Panel B (R20)



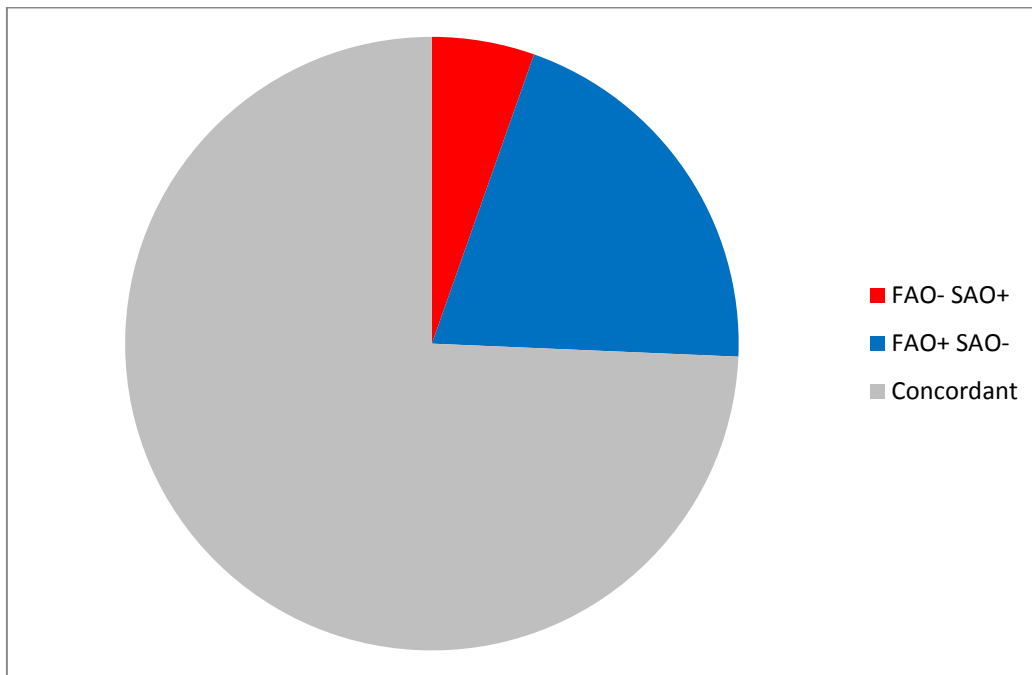
Panel C (R5-R20)



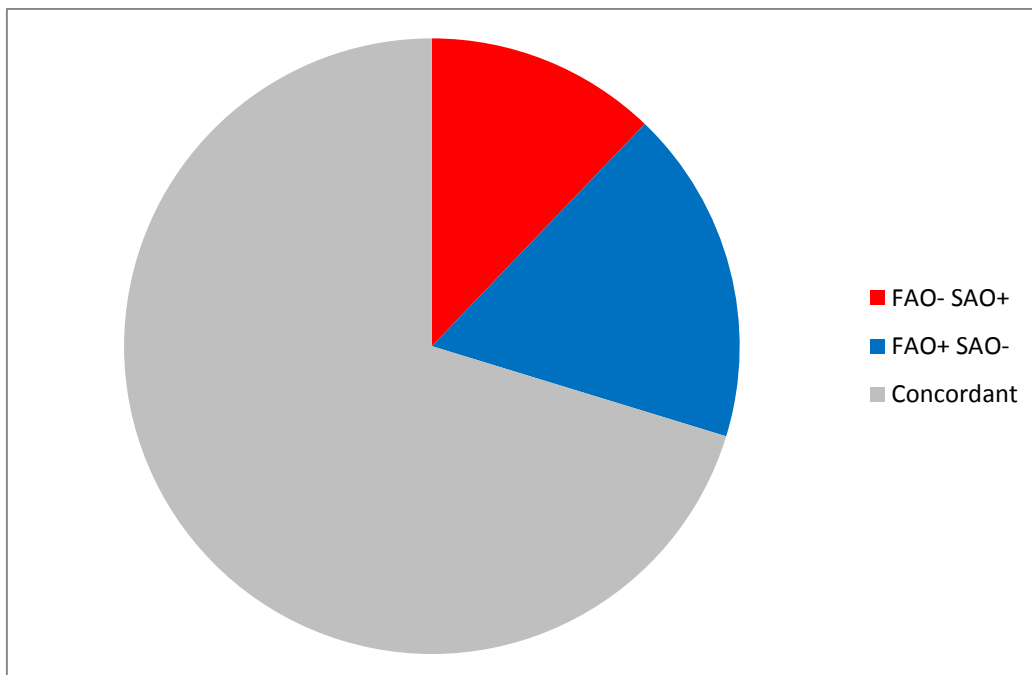
Panel D (AX)



Panel E (LCD)



Panel F (Sacin)



Discussion

In this study we investigated the relationship between clinical outcomes and a comprehensive panel of physiological measurements in a group of patients with asthma being managed in a secondary care setting, particularly focussing on measurements that are often considered to reflect small airway obstruction. We found that S_{acin} , R5-R20 and AX did not differ significantly between patients with mild-moderate asthma and those with severe asthma, nor did these parameters correlate significantly with asthma clinical outcomes. Our results on the surface appear to be discordant with those of previous studies^{126,127,157-159}, in which positive associations between these markers and clinical outcomes were reported. However, in these studies bronchodilators were withheld prior to the study visits, whereas we performed all physiological tests after the administration of a bronchodilator, in order to eliminate the effect of large airway smooth muscle tone, and thus accentuate as much as possible the effects of the distal small airways. It is therefore possible that the associations that were observed in previous studies were at least partly related to the effect of proximal airway tone impacting upon the heterogeneity of distal airway calibre. Indeed, it has previously been observed that pre-bronchodilator physiological measurements correlate more strongly with asthma outcomes than post-bronchodilator measurements¹²⁶.

An unexpected finding of our study was the striking relationship between the IOS parameter R20 and a number of clinically important outcome measures such as asthma control, quality of life and exacerbations. Moreover, in multivariate linear regression analyses, the contribution of R20 was additive to that of traditional spirometric outcome measures such as FEV₁ and FVC, suggesting that it may represent a distinct facet of asthma disease expression. Although the structural correlates of IOS parameters have not yet been defined, R20 is thought to reflect the mean level of airway resistance, including both the large and small airways, whereas R5-R20 represents the heterogeneity of airway resistance. Computational models and ex vivo prototypic models of lung impedance based upon realistic airway geometry may shed further light on this area in the near future²¹². Interestingly, the ACQ was significantly associated with FEV₁, whereas the AQLQ associated more with FVC. This suggests that asthma quality of life may be particularly affected by air trapping.

The association observed in this study between absolute lung volumes and asthma exacerbations is intriguing and, to our knowledge, has not been previously reported. In particular, we found that patients with a history of one or more exacerbations within the previous year had significantly lower TLC and VA than those without a history of recent exacerbations. This was contributed to partly by a lower TLC (% pred.) in the exacerbation-prone group, although this did not reach statistical significance, and partly by a greater proportion of females in the exacerbation-prone group, although this also did not reach statistical significance. The reduced DLCO (% pred.) seen in the exacerbation-prone group was driven primarily by the lower absolute lung volumes, since neither KCO (% pred.) nor the VA/TLC ratio differed significantly between the two groups. These observations suggest that a preserved TLC may have a protective effect against exacerbations of asthma, a possibility that merits further investigation. However, a limitation of this analysis is that exacerbations were recorded retrospectively, and it is therefore possible that the physiological associations observed were due to the after-effects of previous exacerbations, rather than being predictive of future exacerbations.

We found that physiological variables explained approximately one fifth of the variance of ACQ-6 and AQLQ(S) scores. The lack of a strong association between physiological variables and patient-reported outcome measures in patients with asthma has been previously documented^{259,260}, although the causes of this are poorly understood. One possible explanation is that patients with asthma become accustomed to a certain level of disease control, thus regarding this as their normal baseline state. Therefore, patient-reported measures of asthma control or quality of life may be related more strongly to changes in physiological variables, rather than to their absolute values. Moreover, it is likely that subjective measures of asthma control are influenced by a large number of factors other than the function of the lower airways, including obesity²⁶¹, deconditioning²⁶², dysfunctional breathing^{263,264}, vocal cord dysfunction²⁶⁴, and psychological factors²⁶⁵.

Our study was limited by its cross-sectional design, and a number of important questions remain about the role of small airway obstruction in the clinical expression of asthma. Most notably, it is not known whether small airway obstruction affects the long-term outcome of patients with asthma, and longitudinal studies are required to

address this issue. With this limitation in mind, we performed an exploratory analysis on our cross-sectional data to assess which small airway obstruction markers might hold promise as indicators of incipient airflow obstruction in patients with asthma and normal spirometry. We found that for R5-R20 and AX, a significant proportion of patients (15% and 16% respectively) displayed abnormally high values in the presence of normal FEV₁, whereas there were fewer patients who had low FEV₁ and normal R5-R20 and AX. This suggests that these indices may be sensitive early markers of airflow obstruction, but longitudinal follow-up would be required to determine whether this group of patients is at increased risk of developing spirometric airflow obstruction in the future. Interestingly, the MBW parameter LCI did not appear to be particularly sensitive in detecting asthma patients with airway obstruction, with only 5% of patients having a high LCI and normal FEV₁, compared to 20% of patients who had a low FEV₁ and normal LCI. These results contrast with observations made in cystic fibrosis (CF)¹³² and non-CF bronchiectasis (Section 3.2 of this thesis), in which LCI appeared to be a significantly more sensitive marker of airway obstruction than FEV₁. This suggests that ventilation heterogeneity is a relatively subtle phenomenon in patients with asthma, particularly when compared to suppurative lung diseases such as CF and non-CF bronchiectasis. Nevertheless, the alternative MBW parameter S_{acin} was abnormally raised in the presence of a normal FEV₁ in 12% of patients with asthma, and therefore merits investigation as an early marker of airway disease alongside the IOS parameters R20, R5-R20 and AX.

In conclusion, we have investigated the clinical correlates of a broad panel of physiological parameters in a well-characterised group of patients with asthma. Measurements that have traditionally been considered to represent small airway obstruction, such as S_{acin}, R5-R20 and AX, do not appear to be associated with impaired asthma control or quality of life cross-sectionally, although the long-term significance of these parameters requires further investigation. In contrast, the IOS parameter R20 is strongly and independently associated with adverse outcome. Further studies are required to confirm this novel finding and to investigate its clinical significance.

3.5 Characterisation of acinar airspace involvement in patients with asthma using hyperpolarised ^3He magnetic resonance and quantitative computed tomography

Abstract

Background

The multiple breath inert gas washout (MBW) parameter S_{acin} is thought to be a specific marker of acinar airway involvement, but has not been validated using quantitative imaging techniques in asthma. We aimed to utilise ^3He diffusion magnetic resonance (^3He -MR) and quantitative computed tomography (CT) densitometry to determine the nature of acinar airway involvement in patients with asthma.

Methods

Thirty-seven patients with asthma and seventeen age-matched healthy controls underwent spirometry, body plethysmography, MBW and ^3He -MR. A subset of patients with asthma ($n = 27$) underwent quantitative CT densitometry.

Results

The apparent diffusion coefficient (ADC) at 1s was significantly higher in patients with asthma and a high S_{acin} compared to healthy controls (0.024 vs 0.017, $p < 0.05$), but ADC at 13ms did not differ significantly between the groups. S_{acin} correlated strongly with ADC at 1s ($R = 0.65$, $p < 0.001$), but weakly with ADC at 13ms ($R = 0.38$, $p < 0.05$). ADC at both 13ms and 1s correlated strongly with the mean lung density expiratory / inspiratory ratio, a CT marker of expiratory air trapping ($R = 0.77$, $p < 0.0001$ for ADC at 13ms; $R = 0.72$, $p < 0.001$ for ADC at 1s). CT markers of emphysema did not differ significantly between control and asthma groups.

Conclusion

The MBW parameter S_{acin} is associated with subtle alterations in diffusion within the acinar airways in patients with asthma. The precise nature and clinical significance of the underlying structural abnormality requires further investigation.

Introduction

Asthma is a chronic inflammatory airway disease that is characterised by variable airflow obstruction, airway hyperresponsiveness and structural remodelling in both the large and small airways¹⁴. Inhaled corticosteroids (ICS) are the mainstay of asthma therapy, but optimal treatment requires that the drug is delivered adequately to the site of inflammation within the airway tree. In particular, the deposition of traditional large particle inhalers has often been limited to the larger conducting airways, and there has been increasing interest in targeting the small airways with extra-fine inhaled therapies³⁶.

While it is known that inflammatory and structural changes in asthma occur in the smaller conducting airways⁴⁷⁻⁵⁶, it is not known whether the lesion extends to the more distal intra-acinar airways. The acinar airways of the lung constitute the majority of the airway surface area and comprise respiratory bronchioles, alveolar ducts and alveoli¹⁶¹. Understanding the role and contribution of the acinar airways to asthma is important because currently available inhaled therapies are not designed to provide penetration to this compartment²⁶⁶. A number of tools are available to non-invasively probe the structure of the acinar airways in patients with asthma. These include the physiological assessment of gas mixing using multiple breath inert gas washout (MBW)¹²⁸, measurement of gas diffusion using hyperpolarised noble gas magnetic resonance techniques¹⁷⁸, and computed tomography (CT) densitometry to evaluate expiratory air trapping¹⁶⁷. However to date there has not been a comprehensive assessment of the acinar airways in asthma using these approaches.

There are thought to be two independent mechanisms of gas mixing inefficiency in the lungs, namely convection-dependent inhomogeneity (CDI) and diffusion-convection-dependent inhomogeneity (DCDI)^{140,142}. CDI arises due to unequal convective ventilation between relatively large lung units subtended by conducting airways. DCDI is a more complex mechanism that occurs due to an interaction between convective and diffusive gas flows at the convection-diffusion front, the region of the airway tree at which these flows are of approximately equal magnitude. The MBW parameters S_{cond} and S_{acin} were proposed by Verbanck *et al.* as measures of CDI and DCDI, respectively¹³¹. Since in health, the convection-diffusion front is thought to be located

within the pulmonary acinus, S_{acin} was proposed as a putative physiological marker of acinar airspace disease. Elevations in S_{acin} have been observed in patients with asthma, leading to the suggestion that this condition is characterised by a specific structural abnormality in the pulmonary acinus¹⁵⁰. However, the precise nature of this structural abnormality has not been elucidated.

Hyperpolarised ³helium diffusion magnetic resonance (³He-MR) is a technique that allows microstructural changes at the level of alveoli and acinar airways to be examined non-invasively, under resting physiological conditions¹⁷⁸. The apparent diffusion coefficient (ADC) of ³He within the pulmonary acinus may be measured across a wide range of timescales, from 1ms to 10s. Short timescales correspond to diffusion within a single alveolus or alveolar duct, while long timescales correspond to diffusion within the acinar airways, and possibly along collateral ventilation pathways¹⁷⁸. Air trapping may be assessed using physiological measurements of lung volumes⁹¹, or with imaging techniques such as quantitative CT densitometry¹⁶⁷.

We aimed to utilise ³He-MR at multiple diffusion timescales and quantitative CT densitometry to determine the structural correlates of the multiple breath washout marker S_{acin} in asthma. We hypothesised that asthma patients with an elevated S_{acin} would manifest altered long range diffusion suggestive of intra-acinar airway disease. We also hypothesised that the degree of acinar involvement in asthma would be independent of lung hyperinflation. We sought to test these hypotheses in a cohort of carefully phenotyped adults with asthma.

Methods

Thirty-seven patients with asthma and seventeen age-matched healthy control subjects were recruited. All participants were never smokers or ex-smokers with less than 5 pack years' smoking history. Asthma was diagnosed in a secondary care setting according to British Thoracic Society guidelines²⁴⁸. The study was approved by the National Research and Ethics Committee – East Midlands, Leicester, and all participants gave their written informed consent.

Patients with asthma completed the six-point Asthma Control Questionnaire (ACQ)²⁵⁰ and the standardised Asthma Quality of Life Questionnaire (AQLQ(S))²⁵⁸. Participants were administered 200 micrograms of salbutamol via a metered-dose inhaler and spacer, to minimise the confounding effects of airway smooth muscle tone on physiological and imaging assessments. Spirometry, body plethysmography and measurement of carbon monoxide diffusing capacity were performed according to American Thoracic Society / European Respiratory Society guidelines^{90,215,217}. Induced sputum inflammatory cell counts were obtained in patients with asthma using a previously published method²⁶⁷. MBW was performed according to current guidelines¹³⁰ using the sulphur hexafluoride (SF₆) wash-in method¹³², as described in Section 2.5.

³He-MR was performed using a 0.15 T permanent magnet system (Intermagetics General Corporation, New York, NY) and a Surrey Medical Imaging Systems console (Surrey, UK). Participants were scanned in the supine position, and inhaled 600ml of a ³He/⁴He mixture from functional residual capacity (FRC), followed by a breath-hold lasting between 2 and 10 seconds, depending upon the pulse sequence being performed. Short-timescale ADC (13ms) was measured using a diffusion-weighted Carr-Purcell-Meiboom-Gill technique²²⁴, and long-timescale ADC (1s) was measured using a stimulated echo sequence²²⁵. The first seven patients with asthma and the first two healthy controls to enter the study took part in a pilot phase in which only short timescale ADC measurements were made.

The effect of lung volume changes on short-timescale ADC have been previously reported, with a strong positive correlation observed between the degree of lung inflation and short-timescale ADC¹⁹⁶. In order to aid the interpretation of our results, we also investigated the relationship between lung volume and long-timescale ADC, in three healthy control subjects and three patients with asthma. Long-timescale ADC measurements were performed at specified lung volumes above either residual volume (RV) or FRC. The absolute values of RV and FRC were determined using body plethysmography.

A subset of patients with asthma (n = 27) were further characterised using quantitative computed tomography (CT) densitometry, as described in Section 2.8. Scans were

obtained at full inspiration and full expiration. VIDA Apollo image analysis software (VIDA Diagnostics, Coralville, Iowa) was used for quantitative analysis of lung densitometry. The main parameters extracted were the ratio of mean lung density on expiration to inspiration (MLD E/I), a marker of expiratory air trapping¹⁷¹, and the fifteenth lower percentile of the inspiratory lung attenuation curve (P₁₅), a marker of emphysema²²².

Statistical analyses were performed using SPSS 20 (IBM Corporation, Somers, New York, USA) and Prism 6 (GraphPad Software Inc., La Jolla, California, USA). Group comparisons were performed using the Student's *t* test, one-way analysis of variance with Tukey test for multiple comparisons, or the Mann-Whitney U test for continuous variables, and Fisher's exact test or the Chi-squared test for proportions. Relationships between continuous variables were investigated using Pearson's correlation coefficient. Previous data on the group standard deviation of ADC at 1s was not available for use in a sample size calculation. However, Wang *et al*¹⁸⁴ reported a 0.0051 cm²s⁻¹ difference in mean ADC at 1.5s between healthy and asthma groups, with a group standard deviation of 0.0026 cm²s⁻¹ in the healthy group and 0.0055 cm²s⁻¹ in the asthma group, using similar methodology to our own. We calculated that to detect this difference between healthy and asthma groups at 90% power, using a *t* test with a 5% significance level, we would require 15 patients in each group.

Results

Asthma patient-reported and clinical outcomes in patients with an elevated S_{acin}

Table 3.14 shows the demographic and clinical characteristics of the participant groups. Patients with asthma were divided into S_{acin}-normal and S_{acin}-high groups, with the upper limit of normal for S_{acin} being defined as the mean + 1.64 standard deviations in the age-matched control group (0.204 L⁻¹). The three groups were well-matched for age and sex. The S_{acin}-high group had evidence of suboptimal asthma control, quality of life, and greater treatment utilisation compared to patients with a normal S_{acin}. These observations were present despite similar levels of eosinophilic airway inflammation in both groups.

Physiological phenotyping of asthmatics with an elevated S_{acin}

Table 3.15 shows physiological parameters in the participant groups. The S_{acin} -high group exhibited significantly worse expiratory flow limitation and expiratory air trapping than the S_{acin} -normal group. FEV₁ (% pred.) was significantly lower in the S_{acin} -high group compared to the S_{acin} -normal group (69.3 vs 90.9, $p < 0.01$), and the ratio of residual volume to total lung capacity (RV/TLC) was significantly higher (48.3% vs 38.2%, $p < 0.01$), as was the FRC (% pred.) (131.5% vs 103.7%, $p < 0.01$). Carbon monoxide transfer coefficient (KCO) did not differ significantly between the groups.

Imaging-based phenotyping of asthmatics with an elevated S_{acin}

Figure 3.10 shows the CT densitometry data in the two asthma groups. There was evidence of expiratory air trapping in the S_{acin} -high group, with a significantly raised MLD E/I compared to the S_{acin} -normal group (0.89 vs 0.83, $p < 0.05$). However, the inspiratory P₁₅ did not differ between the groups, suggesting that a raised S_{acin} is not associated with emphysema in patients with asthma. Figure 3.11 shows the short and long timescale ADC measurements across the three groups. ADC at 1s was significantly higher in the S_{acin} -high group compared to the healthy control group (0.024 vs 0.017, $p < 0.05$), with a trend towards a significant difference between the S_{acin} -high and S_{acin} -normal asthma groups (0.024 vs 0.019, $p = 0.09$).

Evaluation of the contribution of lung volume to apparent diffusion coefficients

Figure 3.12 shows correlations between ADCs and S_{acin} (Panels A and B), FRC (% pred.) (Panels C and D) and MLD E/I (Panels E and F) in patients with asthma. S_{acin} correlated weakly with ADC at 13ms ($R = 0.38$, $p < 0.05$), but strongly with ADC at 1s ($R = 0.65$, $p < 0.001$). ADC at both 13ms and 1s correlated strongly with the functional residual capacity percent predicted ($R = 0.73$, $p < 0.0001$ for ADC at 13ms; $R = 0.68$, $p < 0.0001$ for ADC at 1s) and with the mean lung density expiratory / inspiratory ratio, a CT marker of expiratory air trapping ($R = 0.77$, $p < 0.0001$ for ADC at 13ms; $R = 0.72$, $p < 0.0001$ for ADC at 1s). However, in healthy subjects there were no significant correlations between ADC at 13ms / 1s and either S_{acin} or FRC (% pred.).

Figure 3.13 shows the relationship between lung inflation and ADC at 1s in three healthy volunteers (Panel A) and three patients with asthma (Panel B). The correlation

was positive but weak in both cases, only reaching statistical significance in the patients with asthma ($p < 0.05$). The slope of the lines was shallow, with a 50% increase in lung inflation resulting in a 3.7% increase in ADC in healthy volunteers, and a 4.5% increase in patients with asthma.

Table 3.14: Demographic and clinical characteristics of participant groups in magnetic resonance study

	Healthy controls (n = 17)	Asthma S_{acin} normal (n = 20)	Asthma S_{acin} high (n = 17)
Age (years)	53.4 (3.3)	54.2 (3.1)	61.2 (1.9)
Sex (% male)	47	40	65
Height (cm)	170.6 (2.6)	164.8 (2.5)	169.7 (1.9)
Weight (kg)*	75.0 (2.7)	78.1 (3.3)	90.4 (5.0) #
Body mass index (kg/m ²)*	25.8 (0.8)	28.9 (1.3)	31.2 (1.4) ##
Age of onset of asthma symptoms (years)	-	23.4 (5.0)	27.5 (5.3)
Duration of asthma (years)	-	30.9 (3.8)	33.7 (5.1)
Atopic status (% positive)	-	85	82
ACQ-6 score*	-	1.43 (0.26)	2.14 (0.22)
AQLQ(S) score [‡]	-	5.61 (0.23)	4.95 (0.31)
Sputum neutrophil count (%)	-	57.2 (6.0)	61.8 (7.1)
Sputum eosinophil count (%) [†]	-	2.69 (1.23 – 5.89)	1.76 (0.76 – 4.04)
Blood eosinophil count (×10 ⁹ /L)	-	0.33 (0.04)	0.34 (0.07)
Daily dose of inhaled corticosteroid (beclometasone dipropionate equivalent [μg]) Median Range	-	1000 0 – 2000	1600 200 – 2000
Use of long-acting beta-agonists (% of subjects)	-	75	94
Regular use of oral prednisolone (% of subjects)	-	20	35
Use of leukotriene receptor antagonist (% of subjects)	-	10	35
Use of a methylxanthine (% of subjects) [‡]	-	10	41
Asthma treatment step ^{‡, §}	-	1 : 6 : 9 : 4	1 : 0 : 9 : 7
Refractory asthma (% positive) ^{¶, §}	-	45	76

Legend for Table 3.14

ACQ-6 = six-point Asthma Control Questionnaire; AQLQ(S) = standardised Asthma Quality of Life Questionnaire.

† Expressed as geometric mean (95% confidence interval). Log-transformed data compared between groups using Student's *t* test.

‡ As defined by the Global Initiative for Asthma². Expressed as number of patients receiving treatment at step 2: step 3: step 4: step 5.

¶ Refractory asthma defined according to the American Thoracic Society Workshop definition²⁶⁸.

Data expressed as mean (standard error) or proportions, unless stated otherwise. Groups compared using one-way analysis of variance with Tukey test for multiple comparisons or Student's *t* test for parametric data, Mann-Whitney U test for non-parametric data, and Chi-squared test or Fisher's exact test for proportions. Significant differences across or between groups denoted *($p < 0.05$) with trends towards significance denoted †($p < 0.1$). Significant differences compared to healthy control group denoted #($p < 0.05$) or ##($p < 0.01$).

Table 3.15: Physiological data across participant groups in magnetic resonance study

	Healthy controls (n = 17)	Asthma S_{acin} normal (n = 20)	Asthma S_{acin} high (n = 17)
FEV ₁ (% pred.)****	104.5 (3.5)	90.9 (4.3)	69.3 (5.0) ####, ¥¥
FVC (% pred.)**	119.9 (3.8)	106.0 (3.5) #	100.1 (3.5) ##
FEV ₁ /FVC (%)****	72.1 (1.7)	70.6 (2.5)	55.6 (3.3) ###, ¥¥¥
FRC (L)**	3.67 (0.26)	3.08 (0.23)	4.28 (0.26) ¥¥
FRC (% pred.)*	114.4 (6.2)	103.7 (6.7)	131.5 (6.2) ¥¥
TLC (L)	6.92 (0.48)	5.70 (0.34)	6.77 (0.39)
TLC (% pred.)	109.8 (3.7)	103.3 (3.8)	109.5 (3.4)
RV/TLC (%)****	31.9 (2.2)	38.2 (1.9)	48.3 (2.3) ####, ¥¥
VA/TLC (%)****	88.2 (1.8)	82.0 (1.9)	74.3 (1.9) ####, ¥
KCO (mmol•min ⁻¹ •kPa ⁻¹ •L ⁻¹)	1.55 (0.06)	1.66 (0.06)	1.58 (0.07)
LCI****	7.34 (0.26)	7.43 (0.25)	9.59 (0.31) ####, ¥¥¥¥
LCI _{vent} ****	1.20 (0.02)	1.22 (0.03)	1.41 (0.03) ####, ¥¥¥¥
LCI _{ds} ****	1.14 (0.01)	1.14 (0.01)	1.25 (0.01) ####, ¥¥¥¥
S _{cond} (L ⁻¹)	0.029 (0.004)	0.054 (0.015)	0.068 (0.012)
S _{acin} (L ⁻¹)****	0.120 (0.012)	0.115 (0.011)	0.319 (0.026) ####, ¥¥¥¥

Legend for Table 3.15

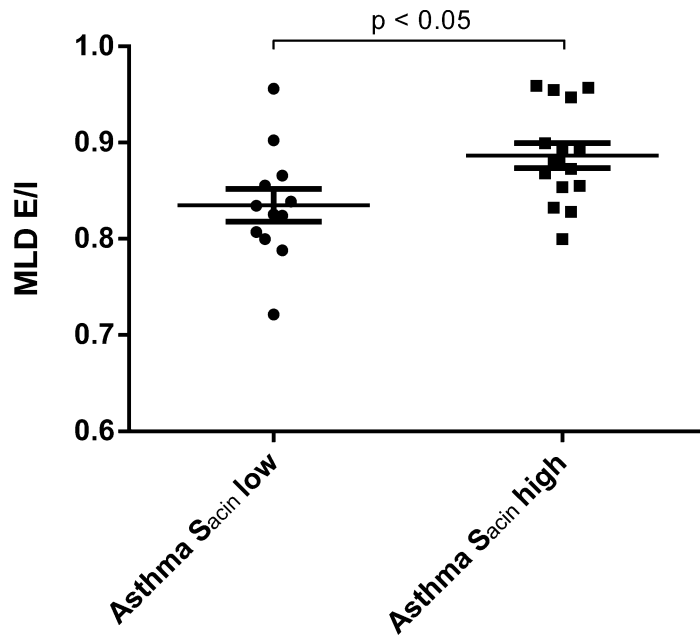
FEV₁ = forced expiratory volume in one second; FVC = forced vital capacity; FRC = functional residual capacity from body plethysmography; TLC = total lung capacity; RV = residual volume; VA = alveolar volume from single breath helium dilution; KCO = carbon monoxide transfer coefficient; LCI = lung clearance index; LCI_{vent} = specific ventilation inequality component of lung clearance index; LCI_{ds} = dead space component of lung clearance index.

Data expressed as mean (standard error). Groups compared using one-way analysis of variance with Tukey test for multiple comparisons or Student's *t* test. Significant differences across groups denoted *(*p* < 0.05), **(*p* < 0.01), ***(*p* < 0.001) or ****(*p* < 0.0001). Significant differences compared to healthy control group denoted #(*p* < 0.05), ##(*p* < 0.01), ###(*p* < 0.001) or ####(*p* < 0.0001). Significant differences between asthma S_{acin}-low and S_{acin}-high groups denoted ¥(*p* < 0.05), ¥¥(*p* < 0.01), ¥¥¥(*p* < 0.001) or ¥¥¥¥(*p* < 0.0001).

Figure 3.10: Quantitative computed tomography densitometry between groups

Error bars indicate means \pm standard errors of the mean.

A



B

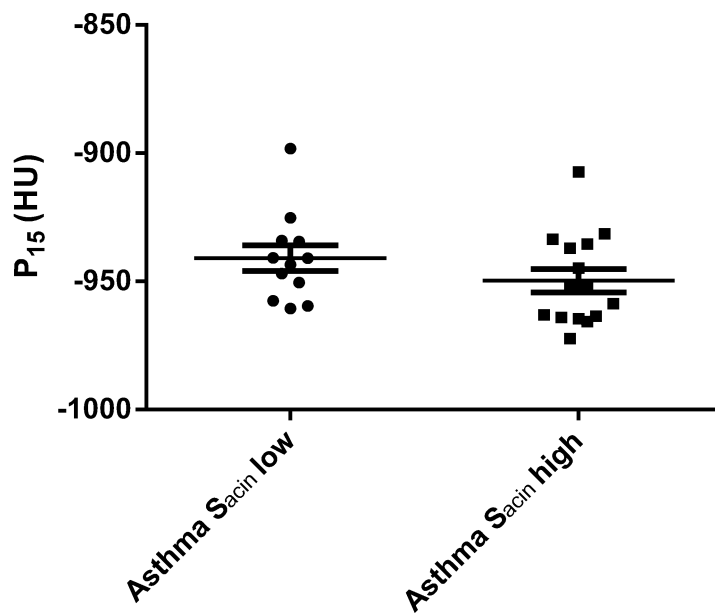
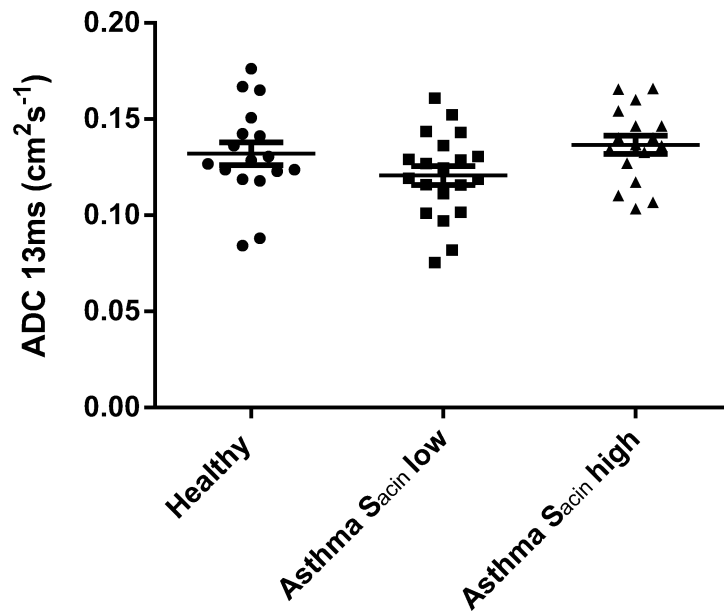


Figure 3.11: Apparent diffusion coefficients (ADC) across groups

Error bars indicate means \pm standard errors of the mean.

A



B

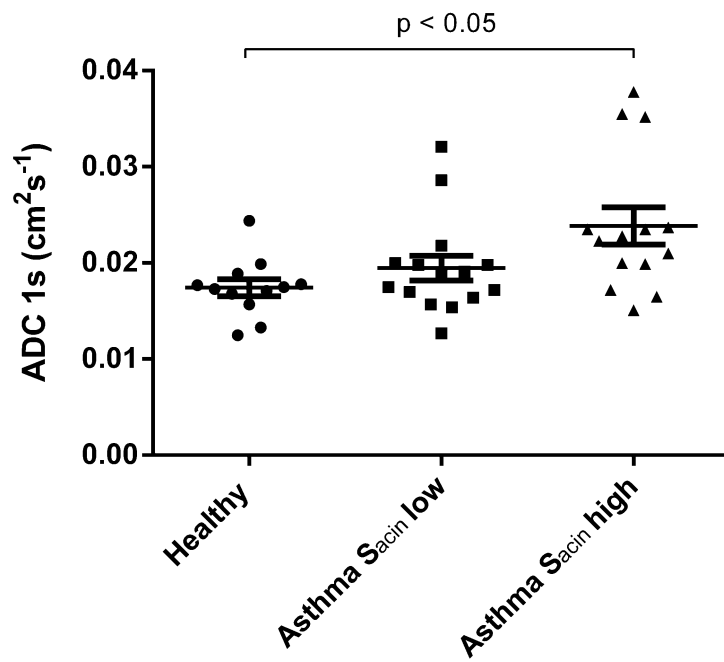


Figure 3.12: Correlations between ^3He -MR, CT and physiological variables in patients with asthma

Best-fit linear regression lines and Pearson correlation coefficients are shown.

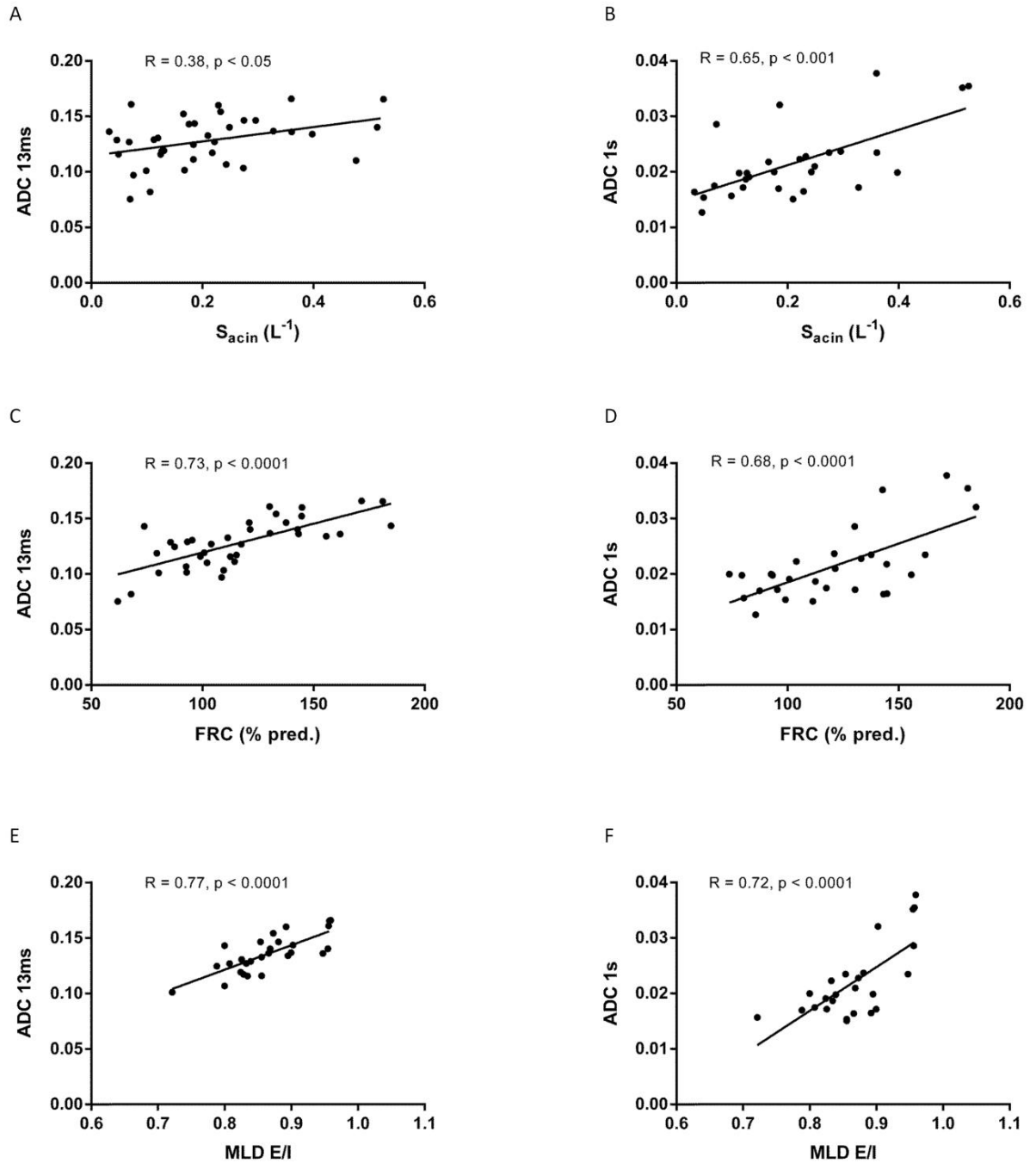
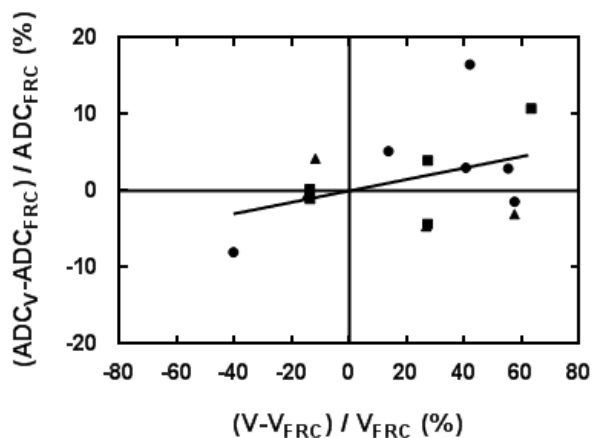


Figure 3.13: Change in apparent diffusion coefficient (%) against change in volume of gas in the lungs (%) in healthy subjects and patients with asthma

Correlations are shown between percentage change in ADC and percentage change in volume of gas in the lungs in three healthy subjects (Panel A) and three patients with asthma (Panel B). The three participants in each case are denoted with different symbols. V = volume of gas in lungs; V_{FRC} = volume of gas in lungs at functional residual capacity; ADC_V = ADC at lung volume V ; ADC_{FRC} = ADC at functional residual capacity (extrapolated).

Panel A



Discussion

The main finding of this study is that in patients with asthma, the MBW parameter S_{acin} is strongly associated with elevations in long-timescale ADC. However, this association is not observed in healthy subjects. Moreover, elevations in long timescale ADC cannot be reproduced purely by lung inflation, suggesting that such elevations result from a specific structural abnormality in the pulmonary acinus in patients with asthma.

A number of previous studies have investigated the clinical significance of the acinar lesion in asthma. Farah *et al* found that improvements in S_{acin} were independently associated with improvements in five-point ACQ score following the initiation of ICS treatment¹⁵⁷, and that markers of ventilation heterogeneity could predict the response to inhaled corticosteroid dose titration¹⁵⁹. Thompson *et al* found that S_{acin} correlated with asthma severity, as measured using the Global Initiative for Asthma treatment steps, and that asthma exacerbations were associated with increases in S_{acin} ¹⁵⁸. However, in the above studies MBW was performed using nitrogen as the inert tracer gas, which may probe less distal structures than SF₆¹³⁰, and additionally MBW was performed without the administration of a bronchodilator, so that the influence of large airway bronchial tone was not eliminated. Indeed it has been shown that bronchodilator administration results in complete or partial normalisation of a high baseline S_{acin} in both children and adults with asthma^{150,152,153}, suggesting that large airway bronchodilator tone may impact upon measurements of distal airway function. The study reported in Section 3.4 of this thesis found that S_{acin} , performed post-bronchodilator using the SF₆ wash-in method, was not independently associated with ACQ scores, AQLQ scores or asthma exacerbations, suggesting that a raised S_{acin} in asthma may be a marker of pre-symptomatic early remodelling in the distal airways. Longitudinal studies are required to assess whether this abnormality progresses to fixed airflow obstruction in asthma, as may be the case in other obstructive airway diseases such as cystic fibrosis¹³² and bronchiolitis obliterans post-allogeneic haematopoietic stem cell transplant²⁶⁹.

There is some evidence that treating the small airways with extra-fine inhaled therapies can improve asthma control. Barnes *et al* found in a retrospective cohort study that asthma control was more likely to be achieved in the year following the initiation or

step-up of an extra-fine ICS compared to a large particle formulation²⁷⁰. Verbanck *et al* found that S_{acin} improved following the replacement of standard corticosteroid inhalers with an extra-fine inhaler, in those patients who had a raised S_{acin} at baseline¹⁶⁰. However, while it is known that extra-fine ICS provide improved penetration into the smaller conducting airways²⁷¹⁻²⁷⁵, it is not clear whether or not this extends into the pulmonary acinus. In particular, there are few studies that have specifically measured drug deposition within this compartment, and theoretical models suggest that very small particles ($< 0.5 \mu\text{m}$ in diameter) may simply remain suspended in the air and be exhaled without depositing in the airways²⁶⁶.

The acinar airways form an asymmetrically dichotomous branching network in three-dimensional space that may be described in terms of its mean airway radius, branch length and branch angle. Short timescale ADC is mainly sensitive to changes in acinar airway radius, since an increase in this parameter reduces the restriction to transverse displacement of helium. Long timescale ADC is a measure of the network properties of the acinar airways, with higher values being associated with greater interconnectedness and reduced tortuosity of the acinus. Long timescale ADC is relatively insensitive to acinar airway radius, since at long diffusion times transverse displacement is negligible compared to longitudinal displacement along the airway axis. An increase in branch length would theoretically cause elevation of long-timescale ADC because a given helium atom would then encounter less branch points, each of which entails a change in direction in three-dimensional space, and would thus travel a greater distance in any given direction. Long timescale ADC may also be affected by the width of the alveolar sleeve surrounding the acinar airways, as well as the size of the alveolar mouth opening. Verbanck and Paiva simulated axial diffusion within an alveolar duct model, with the two main parameters of their model being (i) the ratio of luminal diameter to total diameter (s/S), where the total diameter includes the alveolar sleeve surrounding the duct, and (ii) the ratio of the alveolar mouth opening diameter to the mean alveolar width in the axial direction (AM/AW)²⁷⁶. The authors found that a low s/S ratio (ie. a relatively large alveolar sleeve width) was associated with reduced axial diffusion, due to the retarding effect of radial diffusion into the alveolar sleeve. The AM/AW ratio had a far more modest effect on axial diffusion, with a low ratio (ie. relatively narrow alveolar mouth openings) associated with a small reduction in axial diffusion. This may be explained by the fact that narrow alveolar mouth openings result in gas molecules

becoming trapped in the alveoli, thus retarding axial diffusion. However, narrow alveolar mouth openings also result in less gas molecules entering the alveoli in the first place, and it is likely that these two opposing effects accounted for the relatively modest dependence of axial diffusion on the AM/AW ratio. A further factor that may influence long timescale ADC is the presence of collateral channels. Simulations of long timescale ADC within an anatomically realistic asymmetrically dichotomous model of the acinus yielded values that were of the same order as those observed experimentally in healthy subjects²⁷⁷. The addition of intra-acinar collateral channels to the model produced significantly increased values of simulated long timescale ADC²⁷⁸.

An important question to address is whether the correlation between S_{acin} and long timescale ADC represents a true structural change in the pulmonary acinus, or whether the relationship is driven by the presence of expiratory air trapping and hyperinflation in patients with raised S_{acin} . Hajari *et al* utilised ³He MR lung morphometry to assess the changes that occur in the acinar airways during lung inflation in healthy subjects²⁷⁹. They concluded that lung inflation occurs primarily by alveolar recruitment, and to a lesser extent by the expansion of alveolar ducts. The alveolar sleeve width actually decreased with increasing lung inflation. The expansion of alveolar ducts would be expected to increase short timescale ADC, and indeed it is known that short timescale ADC has a strong linear relationship with lung inflation in healthy subjects¹⁹⁶. It might be expected that a reduction in alveolar sleeve width with increasing lung inflation would result in an increase in long timescale ADC, on the basis of the alveolar duct model alluded to above²⁷⁶. However, we observed only minor effects of lung inflation on long timescale ADC, suggesting that hyperinflation alone cannot account for the strong association between S_{acin} and long timescale ADC. Nevertheless, ADC did appear to fall somewhat when measurements were taken near residual volume, suggesting that airway closure could result in more restricted diffusion.

We observed strong correlations between the CT marker of expiratory air trapping MLD E/I and both short and long-timescale ADC, suggesting that there may be common structural abnormalities at the level of the acinar airways that result in both expiratory air trapping and altered diffusion in the distal airspaces. A possible method of elucidating these abnormalities in future studies may be micro-CT of surgical lung biopsies or resected lung specimens, as has been performed in patients with COPD²⁸⁰.

We found no evidence of emphysema in patients with asthma and a raised S_{acin} , with neither P_{15} nor KCO differing between the S_{acin} -normal and S_{acin} -high groups. Previous studies have also found no evidence of histological emphysema in patients with asthma, although a subtle loss of alveolar-parenchymal attachments has been observed, which could theoretically lead to loss of lung elastic recoil and dynamic airway collapse¹⁷.

We conclude that the MBW parameter S_{acin} appears to be associated with a structural abnormality in the pulmonary acinus in patients with asthma, causing subtle alterations in diffusion within the acinar airways. However, a number of questions remain to be answered. In particular, it is not known whether currently available small-particle inhalers provide significant deposition into the acinar airways, or what the benefits if any of acinar drug deposition would be. Longitudinal studies are required to determine whether acinar airway disease is a precursor to the development of fixed airflow obstruction in patients with asthma, and whether treatment with extra-fine ICS or systemic therapies could prevent this adverse outcome.

3.6 Randomised controlled trial of the prostaglandin D2 receptor antagonist QAW039 in persistent eosinophilic asthma

Abstract

Background

Asthma is a chronic inflammatory airway disease that imposes a substantial burden of morbidity and healthcare costs worldwide. There is evidence that eosinophils are a primary driver of asthma, and that control of eosinophilic airway inflammation reduces the frequency of asthma exacerbations.

Methods

We performed a single-centre, randomised, double-blind, placebo-controlled, parallel-group clinical trial of the prostaglandin D2 receptor antagonist QAW039 in 61 subjects with persistent eosinophilic asthma. The treatment phase lasted for three months, during which subjects received either QAW039 225mg twice per day orally, or placebo. The primary outcome was the change in sputum eosinophil percentage from baseline to post-treatment. Secondary and exploratory outcomes included changes in Asthma Control Questionnaire score (ACQ), Standardised Asthma Quality of Life Score (AQLQ(S)) and forced expiratory volume in one second (FEV₁).

Results

QAW039 was associated with a 5.2-fold reduction in geometric mean sputum eosinophil percentage, from 4.88 at baseline to 0.91 post-treatment, versus a 1.3-fold reduction in the placebo group ($p = 0.005$). Mean AQLQ(S) scores fell by 0.17 in the placebo group and increased by 0.27 in the QAW039 group ($p < 0.05$), but changes in ACQ score did not differ between the groups. Mean post-bronchodilator FEV₁ fell by 100 ml in the placebo group and increased by 110 ml in the QAW039 group ($p < 0.05$). QAW039 displayed a favourable side-effect profile, with no serious adverse events reported.

Conclusions

QAW039 is effective at attenuating eosinophilic airway inflammation in patients with persistent eosinophilic asthma, and has a favourable safety profile. There is evidence that QAW039 improves lung function and asthma-related quality of life.

Introduction

Asthma is a chronic inflammatory airway disease that is characterised by heterogeneity with respect to clinical phenotype and response to therapy²⁵. Eosinophilic airway inflammation, mediated by the T helper 2 (T_H2) axis, is a feature of the two most commonly recognised phenotypes of asthma, namely early-onset atopic and late-onset non-atopic asthma²⁵. Treatment strategies that specifically target eosinophilic airway inflammation have been shown to reduce exacerbations of asthma²⁸¹. Moreover, treatments such as anti-IL-5 and anti-IL-13 that modify the T_H2 axis are particularly effective in patients with uncontrolled eosinophilic airway inflammation²⁹⁻³¹, but may be less effective in an unselected population²⁸.

There is increasing evidence that the actions of prostaglandin D₂ (PGD₂) upon the chemoattractant receptor homologous molecule expressed on T_H2 cells (CRTH2) may play an important role in mediating eosinophilic airway inflammation in asthma and allergic diseases. The CRTH2 receptor mediates the migration of T_H2 cells, delays their apoptosis and stimulates them to produce the cytokines IL-4, IL-5 and IL-13²⁸²⁻²⁸⁴. Furthermore, CRTH2 is also expressed by eosinophils, and directly mediates their chemotaxis and degranulation^{282,285}. CRTH2 is therefore considered to be a highly promising novel drug target in the treatment of asthma, and a number of small molecule antagonists to this receptor are currently in clinical development. QAW039 is an orally active highly selective and potent antagonist of PGD₂ that binds to the CRTH2 receptor, but not to the more general homeostatic PGD₂ receptor DP1. QAW039 would therefore be expected to bind to CRTH2 receptors on T_H2 cells and eosinophils, and to inhibit their migration into airway tissues.

We tested the hypothesis that, in patients with a sputum eosinophilia ($\geq 2\%$) and persistent, moderate-to-severe asthma, 12-weeks treatment with QAW039 at a dose of 225mg twice per day (compared to placebo), on top of conventional treatment, reduces the levels of eosinophils in induced sputum. Secondary objectives were to determine the effects of QAW039 on asthma symptoms, as measured by the Asthma Control Questionnaire (ACQ), and to assess safety and tolerability of QAW039 as compared to placebo. Exploratory objectives included assessment of the effect of QAW039 (compared to placebo) on the forced expiratory volume in one second (FEV₁) and

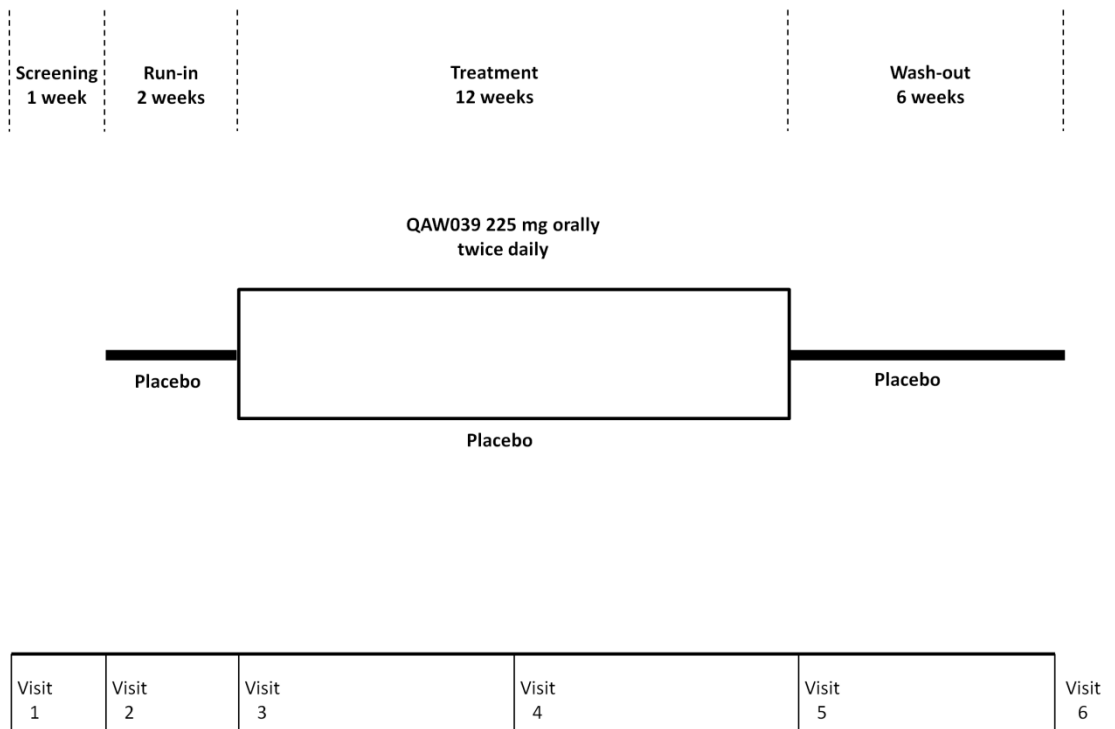
health-related quality of life as measured by the standardised Asthma Quality of Life Questionnaire (AQLQ(S)). A number of novel physiological and imaging outcome measures were incorporated into the study design in order to provide additional mechanistic information, and to assess their responsiveness in the context of an intervention.

Methods

Subjects

Participants were older than 18 years of age and had a clinical diagnosis of asthma that was supported by one or more of the following criteria: an increase in FEV₁ of $\geq 12\%$ and $\geq 200\text{ml}$ from its pre-bronchodilator value following the inhalation of 400 μg salbutamol, a provoked fall in FEV₁ of 20% by methacholine at $\leq 16\text{mg/ml}$ while on inhaled corticosteroids (ICS), or a change in FEV₁ of $> 12\%$ over two measurements during the previous year. Participants were recruited from a refractory asthma clinic providing tertiary care for a mixed urban and rural population of 4 million people, as well as from secondary care asthma and general respiratory clinics in the region. Suitable participants were also identified through the screening of local primary care databases. Inclusion criteria were current treatment with ICS, a sputum eosinophil count of $\geq 2\%$ at screening, and either an ACQ score ≥ 1.5 at randomisation or ≥ 1 exacerbations (requiring higher than the patient's normal dose of systemic corticosteroids for ≥ 3 days) in the past 12 months. Exclusion criteria included serious coexisting illness, pregnancy or lactation, the possibility of conception, a history of malignancy within the previous five years, recent (within 6 weeks of screening) lower respiratory tract infection or exacerbation of asthma requiring $> 10\text{mg}$ of oral prednisolone per day, the use of omalizumab within 6 months before randomisation into the study, and the use of immunosuppressive medication (except low-dose [$\leq 10\text{mg}$ prednisolone per day] oral corticosteroids) within 30 days before randomisation. All subjects provided written informed consent. The study protocol was approved by the National Research Ethics Committee (East Midlands) and the United Kingdom Medicines and Healthcare Products Regulatory Agency.

Figure 3.14: QAW039 study protocol



Design of the study

The study was a single-centre, randomised, double-blind, placebo-controlled, parallel-group clinical trial conducted from February 2012 through June 2013. The protocol of the study is summarised in Figure 3.14.

At a screening visit (Visit 1, Day -21), demographic and clinical details were collected, and inclusion and exclusion criteria were reviewed. An induced sputum sample was collected to assess eligibility based upon a sputum eosinophil count of $\geq 2\%$. Regular treatment was kept constant from this time until the end of the study. One week later, a two-week placebo run-in period was commenced (Visit 2, Day -14). Following this, patients attended a baseline visit (Visit 3, Day 0), at which they completed the ACQ, and eligibility based upon the inclusion and exclusion criteria was again assessed, taking into account the ACQ score. If patients fulfilled the criteria, they proceeded to undertake the remainder of the study visit tests, and were then randomised in a 50:50 ratio to receive either QAW039 at a dose of 225mg twice per day, or an identical placebo. Randomisation was performed by the trial pharmacist using previously generated treatment allocation cards, and was stratified by whether or not participants were receiving treatment with regular oral corticosteroids. Patients completed the ACQ and AQLQ(S). The fractional exhaled nitric oxide at 50ml/s (FeNO_{50}) was measured using a NIOX MINO device (Aerocrine AB, Solna, Sweden). Patients undertook impulse oscillometry using the Jaeger MasterScreen Impulse Oscillometry System (Viasys Healthcare GmbH, Hoechberg, Germany). Multiple breath inert gas washout was performed using the sulphur hexafluoride wash-in method¹³², followed by body plethysmography, measurement of carbon monoxide diffusing capacity and pre-bronchodilator spirometry. An induced sputum sample was then collected. Salbutamol (400 μg via a metered-dose inhaler and spacer) was administered, followed by the measurement of post-bronchodilator spirometry. A blood sample was drawn for the measurement of blood eosinophil count. Inspiratory and expiratory computed tomography (CT) was then performed. Six weeks following randomisation, patients attended a mid-treatment visit (Visit 4, Day 42), at which they completed the ACQ and AQLQ(S) questionnaires, pre- and post-bronchodilator spirometry was performed, an induced sputum sample was obtained, and a blood sample was drawn for the measurement of blood eosinophil count. Twelve weeks following randomisation, patients attended an end-of-treatment visit (Visit 5, Day 84), which incorporated the

same assessment schedule as Visit 3. Patients then began a six-week placebo washout period, in which all participants received placebo. Following this, patients attended an end-of-study visit (Visit 6, Day 126) and undertook the same assessments as at Visits 3 and 5, except that CT scans were not performed.

Criteria for withdrawal from the study were defined *a priori*, and included withdrawal of informed consent, asthma exacerbation, pregnancy and adverse events for which continued exposure to the study drug would be detrimental. Safety was assessed at each study visit on the basis of history and physical examination, vital signs, haematology, blood chemistry, urinalysis and an electrocardiogram. Because of the expected anti-eosinophilic effects of QAW039, results of sputum and blood eosinophil counts obtained during Visits 5 and 6 were not disclosed to the investigators during the study.

Statistical analysis

The primary outcome of the study was the change in sputum eosinophil percentage between the baseline visit (Visit 3) and the post-treatment visit (Visit 5). As sputum eosinophil percentage is known to follow a log-normal distribution, the analysis was based on a \log_{10} -transformed scale. Secondary outcomes included the change from baseline to post-treatment with respect to ACQ score. Exploratory outcomes included the change from baseline to post-treatment with respect to AQLQ(S) score and FEV₁. All participants who were randomised were included in the intention-to-treat population, and missing data due to withdrawals or otherwise were imputed using the last observation carried forward. Participants who completed the study up to the post-treatment visit (Visit 5) without major protocol deviations were included in the per-protocol population. The study was aimed to power for a 50% reduction in sputum eosinophil percentage, equivalent to an absolute reduction in \log_{10} sputum eosinophil percentage of 0.301²⁸⁶. In order to detect this difference between groups with 80% power, we required 21 patients in each group. With 30 patients per arm to be randomised, we expected 24 patients to complete the post-treatment assessments, assuming a 20% dropout rate during the course of the treatment phase. Statistical analyses were performed using SPSS 20 (IBM Corporation, Somers, New York, USA) and Prism 6 (GraphPad Software Inc., La Jolla, California, USA). Between-group comparisons at baseline were performed using unpaired t-tests for parametric data, the Mann-Whitney U test for non-parametric data and Fisher's exact test for proportions.

Between- and within-group comparisons of the change from baseline to post-treatment with respect to primary, secondary and exploratory outcomes were performed using unpaired and paired t-tests respectively.

Results

Enrolment and baseline characteristics

Figure 3.15 shows the numbers of subjects who attended a screening visit, were randomly assigned to a study group, and who completed the study up to the post-treatment visit. A total of 117 patients attended a screening visit, of which 61 fulfilled the inclusion and exclusion criteria and were randomised. Thirty-two patients were assigned to receive placebo and 29 to receive QAW039. Three patients withdrew in the placebo group and three patients in the QAW039 group. In each case, the reason for withdrawal was an exacerbation of asthma. One patient was assigned to QAW039 but was incorrectly dispensed placebo at the mid-treatment visit. This patient was excluded from the per-protocol analysis but included in the intention-to-treat analysis. The groups were well-matched for baseline characteristics (Table 3.16), with the only statistically significant difference between the groups being a higher proportion of patients using a methylxanthine in the QAW039 group.

Figure 3.15: Number of patients who were screened, randomised and completed the study up to the post-treatment visit

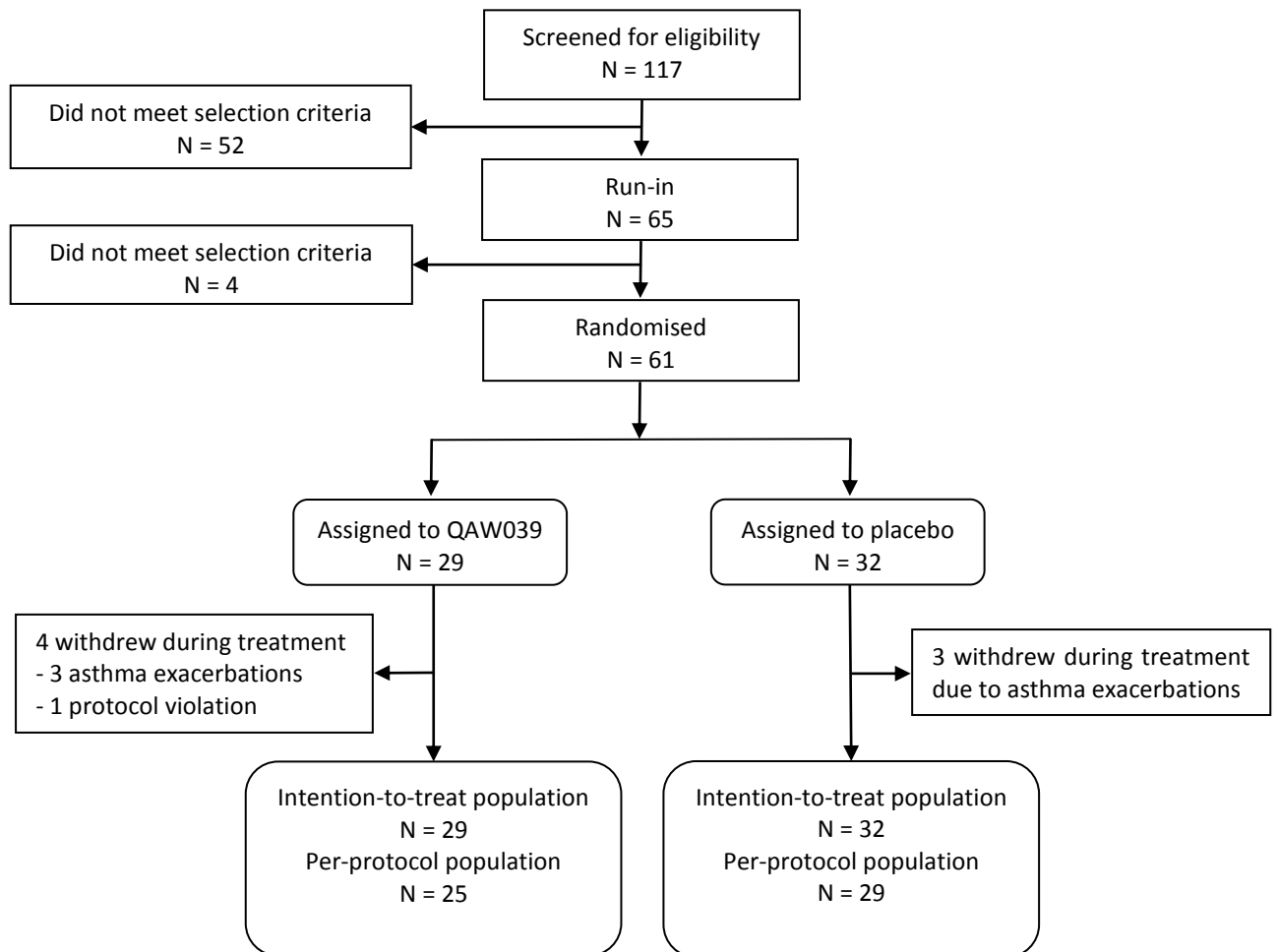


Table 3.16a Baseline Characteristics of Subjects in the Intention-to-Treat Population

Characteristic	QAW039 (n = 29)	Placebo (n = 32)	P value†
Sex (no. of subjects)			0.13
Male	18	13	
Female	11	19	
Age (yr)			0.98
Mean	50	50	
Range	20 – 80	19 – 69	
Age at onset of symptoms (yr)			0.46
Mean	18	21	
Range	2 – 46	2 – 57	
Body-mass index (kg/m ²)	31.1 ± 5.9	29.5 ± 5.9	0.30
Positive atopic status (% of subjects)‡	93	88	0.67
Total IgE (U/ml)			0.88
Median	167.3	163.4	
Interquartile range	81.9 – 450.7	78.9 – 489.1	
Presence of nasal polyps (% of subjects)	14	16	1.00
Severe exacerbations per subject in previous year (no.)	2	2	0.74
Previous admission to the intensive care unit for asthma (% of subjects)	21	16	0.74

Plus-minus values are means ± standard deviation (SD) unless otherwise stated.

† P values were calculated with the use of a two-sided unpaired t-test for parametrically distributed variables, Fisher's exact test for comparison of proportions, and the Mann-Whitney U test for comparison of non-parametric variables.

‡ Positive atopic status was defined as a positive skin test or radioallergosorbent test for any of a panel of specified aeroallergens.

Table 3.16b Baseline Characteristics of Subjects in the Intention-to-Treat Population

Characteristic	QAW039 (n = 29)	Placebo (n = 32)	P value†
FEV ₁ after bronchodilator use (% of predicted value)	79.6 ± 24.3	86.4 ± 26.1	0.30
FEV ₁ /FVC (%)	66.1 ± 14.7	69.3 ± 11.5	0.35
Improvement in FEV ₁ after bronchodilator use (%)			0.18
Median	8.9	11.4	
Interquartile range	5.2 – 14.0	5.8 – 28.5	
Eosinophil count in sputum (%) ¶	4.88 ± 1.27	5.11 ± 1.24	0.82
Eosinophil count in blood (×10 ⁹ /L)			
FENO ₅₀ (ppb)	30.5 ± 1.4	36.3 ± 1.6	0.41
Score on Juniper Asthma Control Questionnaire	1.90 ± 0.83	2.23 ± 0.90	0.14
Score on Asthma Quality of Life Questionnaire	5.42 ± 1.04	5.02 ± 0.95	0.13
Daily dose of inhaled corticosteroid – beclometasone dipropionate equivalent (µg)			0.57
Median	1600	1600	
Range	400 – 3000	200 – 2000	
Use of long-acting beta-agonists (% of subjects)	89.7	84.4	0.71
Use of oral prednisolone			
Regular use (% of subjects)	24.1	21.9	1.00
Daily maintenance dose (mg)			0.59
Mean	9	7	
Range	5 – 10	5 – 10	
Use of montelukast (% of subjects)	34.5	12.5	0.07
Use of a methylxanthine (% of subjects)	34.5	6.3	0.009

Legend for Table 3.16b

Plus-minus values are means \pm standard deviation (SD) unless otherwise stated. FENO₅₀ denotes the fraction of exhaled nitric oxide in exhaled air at a flow rate of 50 ml/s, FEV₁ forced expiratory volume in one second, and FVC forced vital capacity.

† P values were calculated with the use of a two-sided unpaired t-test for parametrically distributed variables, Fisher's exact test for comparison of proportions, and the Mann-Whitney U test for comparison of non-parametric variables.

¶ Values are geometric means \pm log₁₀ SD.

Efficacy

Figures 3.16 and 3.17 show the changes from baseline to the mid-treatment, end-of-treatment and end-of-study visits with respect to the primary outcome and the main secondary and exploratory outcomes, in the per-protocol population. Table 3.17 shows all efficacy outcome measures at baseline and post-treatment in the per-protocol population. Table 3.18 shows the equivalent data in the intention-to-treat population. All statistically significant differences between groups in the per-protocol analysis were also present in the intention-to-treat analysis.

Primary outcome

The geometric mean sputum eosinophil percentage fell from 4.88 at baseline to 0.91 post-treatment in the QAW039 group ($p < 0.0001$), and from 5.11 at baseline to 3.58 post-treatment in the placebo group ($p = 0.43$). The geometric mean fold change in sputum eosinophil percentage from baseline to post-treatment was 0.74 (1.3-fold reduction) in the placebo group and 0.19 (5.2-fold reduction) in the QAW039 group, with a statistically significant difference between the groups ($p = 0.005$).

Secondary and exploratory outcomes

The mean six-point ACQ score (ACQ-6), which included questions about asthma symptoms and bronchodilator use but excluded the pre-bronchodilator FEV₁ component, increased by 0.11 in the placebo group and fell by 0.25 in the QAW039 group, with the changes not reaching statistical significance within either group or between groups. The mean AQLQ(S) score fell by 0.17 in the placebo group and increased by 0.27 in the QAW039 group, with a statistically significant difference between groups ($p = 0.036$). The mean post-bronchodilator FEV₁ fell by 100 ml in the placebo group and increased by 110 ml in the QAW039 group, a statistically significant difference between groups ($p = 0.004$), and a statistically significant improvement from baseline within the QAW039 group ($p = 0.001$). The mean pre-bronchodilator FEV₁ also increased by 110 ml in the QAW039 group, a statistically significant change from baseline ($p = 0.022$), but the between-group comparison did not reach statistical significance. The mean ratio of residual volume (RV) to total lung capacity (TLC) increased by 0.3% in the placebo group and fell by 3.2% in the QAW039 group, a statistically significant change within the QAW039 group ($p = 0.019$) and between the groups ($p = 0.036$). The MBW parameters LCI, LCI_{vent} and LCI_{ds} fell significantly

following treatment in the QAW039 group, but the between-group comparisons did not reach statistical significance.

Safety

QAW039 had an acceptable side-effect profile throughout the study period. There were no serious adverse events reported, and no patient withdrawals due to side-effects of QAW039.

Figure 3.16: Changes from baseline to mid-treatment, post-treatment and post-washout visits with respect to main outcomes in the per protocol population

Orange lines represent the QAW039 group, blue lines represent the placebo group. Error bars denote 95% confidence intervals. P values are for between-group comparisons of the change from baseline.

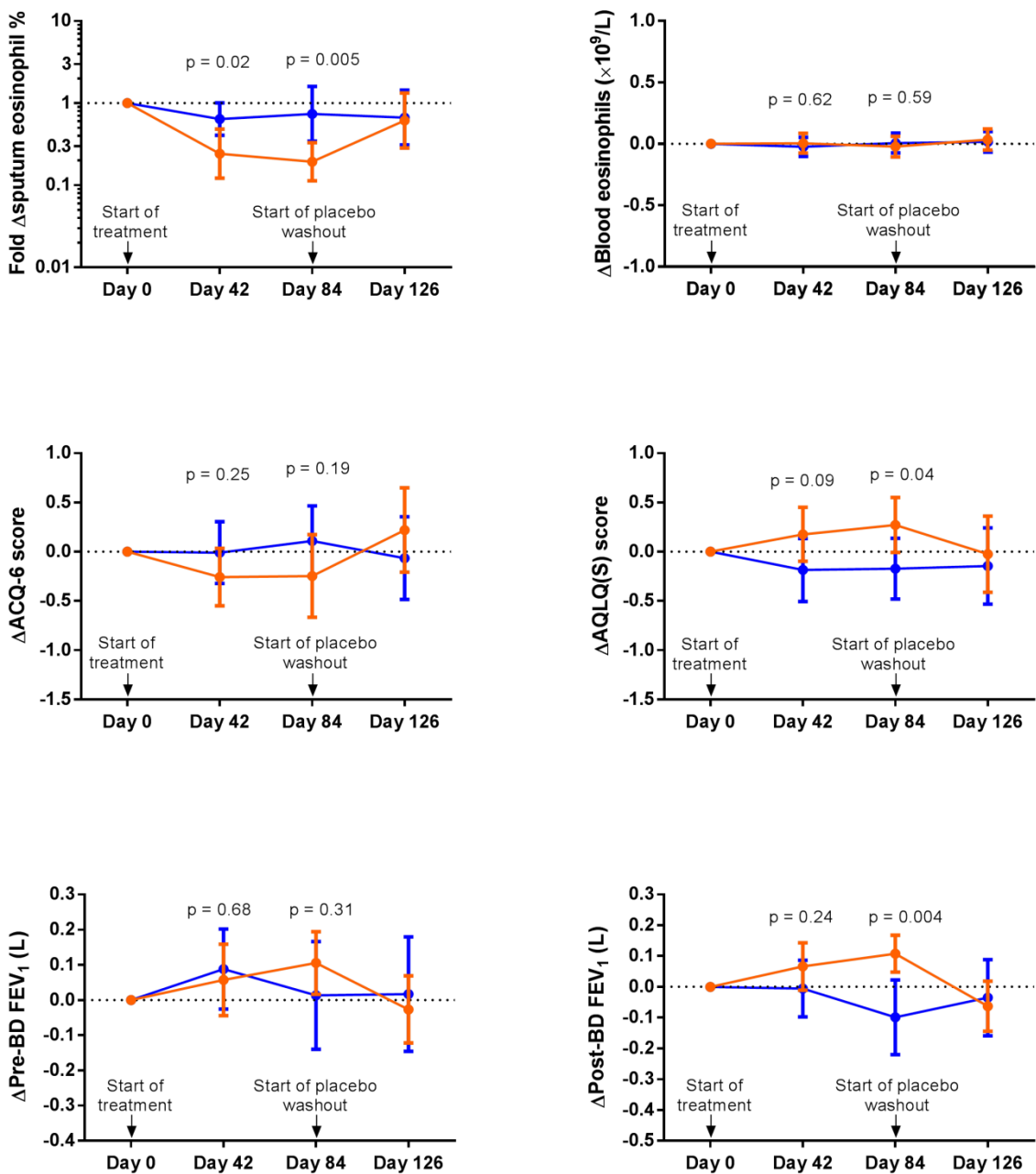


Figure 3.17: Changes from baseline to post-treatment and post-washout visits with respect to lung clearance index and resistance at 5Hz in the per protocol population

Orange lines represent the QAW039 group, blue lines represent the placebo group. Error bars denote 95% confidence intervals. P values are for between-group comparisons of the change from baseline.

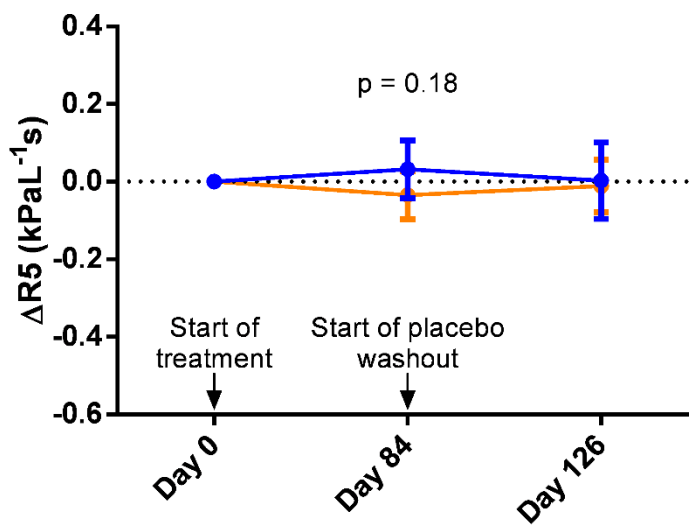
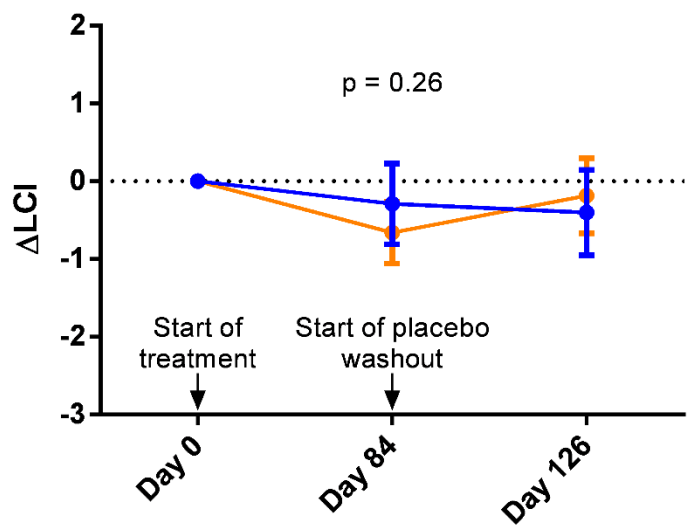


Table 3.17a: Outcome Measures at Baseline and Post-Treatment in the Per-Protocol Population

Outcome	Baseline values		Post-treatment values		Change from baseline to post-treatment values		
	QAW039 (n = 25)	Placebo (n = 29)	QAW039 (n = 25)	Placebo (n = 29)	QAW039 (n = 25)	Placebo (n = 29)	P value†
Eosinophil count in sputum (%) ‡	4.69 ± 1.21	4.97 ± 1.24	0.91 ± 0.68	3.58 ± 1.24	0.19 (0.11 – 0.33) §	0.74 (0.34 – 1.60)	0.005¶
Eosinophil count in blood (×10 ⁹ /L)	0.36 ± 0.26	0.35 ± 0.24	0.35 ± 0.28	0.36 ± 0.23	-0.02 (-0.11 – 0.06)	0.01 (-0.07 – 0.09)	0.59
FENO ₅₀ (ppb)	38.0 ± 25.5	43.7 ± 35.5	31.5 ± 20.2	42.1 ± 32.7	-6.5 (-13.9 – 0.9)	-4.3 (-14.2 – 5.6)	0.72
ACQ-6 score	1.71 ± 0.95	2.07 ± 0.93	1.47 ± 0.96	2.18 ± 1.29	-0.25 (-0.67 – 0.17)	0.11 (-0.25 – 0.47)	0.19
AQLQ score	5.44 ± 0.99	5.05 ± 0.99	5.71 ± 0.90	4.88 ± 1.34	0.27 (-0.01 – 0.55)	-0.17 (-0.48 – 0.14)	0.036
Pre-bronchodilator FEV ₁ (L)	2.33 ± 0.87	2.26 ± 0.97	2.44 ± 0.82	2.27 ± 0.96	0.11 (0.02 – 0.19) §	0.01 (-0.14 – 0.17)	0.31
Pre-bronchodilator FVC (L)	3.54 ± 0.89	3.42 ± 1.18	3.57 ± 0.91	3.41 ± 1.19	0.03 (-0.08 – 0.15)	-0.01 (-0.15 – 0.14)	0.68
Pre-bronchodilator FEV ₁ /FVC (%)	64.9 ± 14.4	64.0 ± 11.3	67.4 ± 11.7	64.6 ± 11.2	2.6 (0.8 – 4.3) §	0.6 (-1.0 – 2.2)	0.09
Post-bronchodilator FEV ₁ (L)	2.55 ± 0.89	2.62 ± 1.04	2.66 ± 0.83	2.58 ± 0.95	0.11 (0.05 – 0.17) §	-0.10 (-0.22 – 0.02)	0.004
Post-bronchodilator FVC (L)	3.68 ± 0.87	3.71 ± 1.19	3.73 ± 0.89	3.70 ± 1.07	0.04 (-0.06 – 0.14)	-0.08 (-0.20 – 0.03)	0.10
Post-bronchodilator FEV ₁ /FVC (%)	68.1 ± 14.1	68.7 ± 11.6	70.8 ± 12.8	68.5 ± 10.8	2.7 (0.7 – 4.7) §	-1.0 (-2.8 – 0.9)	0.008

Table 3.17b: Outcome Measures at Baseline and Post-Treatment in the Per-Protocol Population

Outcome	Baseline values		Post-treatment values		Change from baseline to post-treatment values		
	QAW039 (n = 25)	Placebo (n = 29)	QAW039 (n = 25)	Placebo (n = 29)	QAW039 (n = 25)	Placebo (n = 29)	P value†
RV (L)	2.74 ± 1.18	2.91 ± 1.27	2.52 ± 1.18	2.91 ± 1.31	-0.22 (-0.52 – 0.08)	0.01 (-0.16 – 0.17)	0.16
TLC (L)	6.43 ± 1.46	6.48 ± 1.53	6.37 ± 1.33	6.45 ± 1.45	-0.06 (-0.40 – 0.28)	-0.03 (-0.19 – 0.13)	0.86
RV/TLC (%)	42.0 ± 12.4	44.5 ± 13.9	38.8 ± 12.7	44.8 ± 15.0	-3.2 (-5.9 – 0.6) §	0.3 (-1.8 – 2.4)	0.036
VA (L)	5.06 ± 1.18	4.81 ± 1.34	5.10 ± 1.12	4.73 ± 1.43	0.04 (-0.18 – 0.26)	-0.08 (-0.30 – 0.13)	0.43
VA/TLC (%)	79.2 ± 11.3	74.9 ± 13.9	80.7 ± 11.0	73.8 ± 15.9	1.5 (-2.5 – 5.5)	-1.1 (-4.8 – 2.6)	0.33
Kco (mmol•min ⁻¹ •kPa ⁻¹ •L ⁻¹)	1.67 ± 0.38	1.64 ± 0.27	1.63 ± 0.27	1.68 ± 0.25	-0.04 (-0.12 – 0.04)	0.04 (-0.01 – 0.10)	0.06
DLco (mmol•min ⁻¹ •kPa ⁻¹)	8.30 ± 2.17	7.82 ± 2.42	8.25 ± 2.00	7.90 ± 2.54	-0.05 (-0.29 – 0.18)	0.08 (-0.24 – 0.39)	0.51
LCI	8.94 ± 1.66	9.18 ± 1.90	8.40 ± 1.46	8.89 ± 2.00	-0.66 (-1.05 – 0.27) §	-0.29 (-0.81 – 0.23)	0.26
LCI _{vent}	1.34 ± 0.11	1.39 ± 0.17	1.30 ± 0.11	1.39 ± 0.19	-0.04 (-0.08 – 0.00) §	0.00 (-0.05 – 0.05)	0.19
LCI _{ds}	1.23 ± 0.09	1.24 ± 0.08	1.19 ± 0.07	1.23 ± 0.09	-0.04 (-0.06 – 0.01) §	-0.01 (-0.03 – 0.02)	0.06
S _{cond} (L ⁻¹)	0.068 ± 0.034	0.074 ± 0.038	0.061 ± 0.031	0.071 ± 0.038	-0.008 (-0.027 – 0.011)	-0.002 (-0.016 – 0.011)	0.60
S _{acin} (L ⁻¹)	0.205 ± 0.107	0.219 ± 0.112	0.211 ± 0.095	0.228 ± 0.157	-0.006 (-0.034 – 0.022)	0.009 (-0.019 – 0.037)	0.48

Table 3.17c: Outcome Measures at Baseline and Post-Treatment in the Per-Protocol Population

Outcome	Baseline values		Post-treatment values		Change from baseline to post-treatment values		
	QAW039 (n = 25)	Placebo (n = 29)	QAW039 (n = 25)	Placebo (n = 29)	QAW039 (n = 25)	Placebo (n = 29)	P value†
R5 (kPa•L ⁻¹ •s)	0.55 ± 0.26	0.61 ± 0.20	0.52 ± 0.20	0.64 ± 0.29	-0.03 (-0.10 – 0.03)	0.03 (-0.04 – 0.11)	0.18
R20 (kPa•L ⁻¹ •s)	0.37 ± 0.13	0.42 ± 0.10	0.36 ± 0.10	0.43 ± 0.15	-0.01 (-0.04 – 0.03)	0.01 (-0.03 – 0.06)	0.53
R5-R20 (kPa•L ⁻¹ •s)	0.18 ± 0.15	0.19 ± 0.16	0.16 ± 0.12	0.21 ± 0.20	-0.03 (-0.07 – 0.02)	0.02 (-0.02 – 0.06)	0.11
AX (kPa•L ⁻¹)	2.44 ± 2.24	2.74 ± 2.69	1.96 ± 1.87	2.95 ± 3.45	-0.48 (-1.11 – 0.16)	0.21 (-0.49 – 0.91)	0.15
Inspiratory MLD (HU)	-826 ± 37	-838 ± 35	-839 ± 29	-847 ± 24	-12 (-22 – -2) §	-9 (-19 – 1)	0.67
Expiratory MLD (HU)	-701 ± 65	-719 ± 49	-704 ± 69	-733 ± 48	-1 (-12 – 11)	-13 (-22 – -3) §	0.11
MLD expiratory / inspiratory ratio	0.85 ± 0.07	0.86 ± 0.06	0.84 ± 0.07	0.87 ± 0.05	-0.01 (-0.03 – 0.01)	0.00 (-0.01 – 0.02)	0.19
RB1 wall area (mm ²)	41.6 ± 10.0	37.2 ± 10.6	41.0 ± 13.5	36.1 ± 10.9	-0.3 (-4.3 – 3.7)	-1.1 (-3.6 – 1.3)	0.31
RB1 wall percentage	62.7 ± 5.8	63.9 ± 2.8	63.9 ± 5.3	63.3 ± 3.4	1.3 (0.0 – 2.6)	-0.6 (-1.5 – 0.3)	0.39
RB1 luminal area (mm ²)	26.3 ± 13.5	21.5 ± 7.9	24.7 ± 14.4	21.4 ± 8.4	-1.5 (-4.2 – 1.1)	-0.2 (-1.5 – 1.1)	0.46

Table 3.18a: Outcome Measures at Baseline and Post-Treatment in the Intention-to-Treat Population

Outcome	Baseline values		Post-treatment values		Change from baseline to post-treatment values		
	QAW039 (n = 29)	Placebo (n = 32)	QAW039 (n = 29)	Placebo (n = 32)	QAW039 (n = 29)	Placebo (n = 32)	P value†
Eosinophil count in sputum (%) ‡	4.88 ± 1.27	5.11 ± 1.24	1.15 ± 1.11	3.80 ± 1.23	0.24 (0.14 – 0.39) §	0.77 (0.39 – 1.52)	0.005¶
Eosinophil count in blood (×10 ⁹ /L)	0.38 ± 0.27	0.36 ± 0.23	0.37 ± 0.28	0.36 ± 0.22	-0.01 (-0.08 – 0.06)	0.01 (-0.07 – 0.08)	0.73
FENO ₅₀ (ppb)	30.5 ± 1.4	36.3 ± 1.6	32.2 ± 19.8	46.2 ± 39.6	-5.6 (-12.0 – 0.8)	-3.9 (-12.8 – 5.1)	0.75
ACQ-6 score	1.68 ± 0.95	2.13 ± 0.91	1.45 ± 0.97	2.25 ± 1.27	-0.22 (-0.58 – 0.14)	0.13 (-0.20 – 0.45)	0.14
AQLQ score	5.42 ± 1.04	5.02 ± 0.95	5.65 ± 0.98	4.84 ± 1.31	0.24 (-0.01 – 0.48)	-0.18 (-0.47 – 0.10)	0.028
Pre-bronchodilator FEV ₁ (L)	2.25 ± 0.87	2.21 ± 0.95	2.35 ± 0.82	2.23 ± 0.93	0.10 (0.02 – 0.18) §	0.02 (-0.12 – 0.16)	0.33
Pre-bronchodilator FVC (L)	3.52 ± 0.88	3.34 ± 1.16	3.55 ± 0.90	3.34 ± 1.16	0.03 (-0.07 – 0.13)	0.00 (-0.13 – 0.14)	0.73
Pre-bronchodilator FEV ₁ /FVC (%)	62.9 ± 14.8	64.5 ± 11.6	65.3 ± 12.7	65.0 ± 11.5	2.4 (0.8 – 3.9) §	0.5 (-1.0 – 1.9)	0.08
Post-bronchodilator FEV ₁ (L)	2.46 ± 0.89	2.58 ± 1.00	2.55 ± 0.85	2.51 ± 0.92	0.09 (0.04 – 0.15) §	-0.07 (-0.19 – 0.05)	0.013
Post-bronchodilator FVC (L)	3.67 ± 0.86	3.64 ± 1.15	3.70 ± 0.88	3.60 ± 1.04	0.03 (-0.05 – 0.12)	-0.05 (-0.16 – 0.06)	0.24
Post-bronchodilator FEV ₁ /FVC (%)	66.1 ± 14.7	69.3 ± 11.5	68.5 ± 13.9	68.7 ± 10.7	2.4 (0.6 – 4.1) §	-0.6 (-2.4 – 1.2)	0.017

Table 3.18b: Outcome Measures at Baseline and Post-Treatment in the Intention-to-Treat Population

Outcome	Baseline values		Post-treatment values		Change from baseline to post-treatment values		
	QAW039 (n = 29)	Placebo (n = 32)	QAW039 (n = 29)	Placebo (n = 32)	QAW039 (n = 29)	Placebo (n = 32)	P value†
RV (L)	2.81 ± 1.18	2.86 ± 1.24	2.61 ± 1.20	2.87 ± 1.28	-0.19 (-0.45 – 0.07)	0.00 (-0.15 – 0.15)	0.17
TLC (L)	6.52 ± 1.45	6.38 ± 1.53	6.46 ± 1.35	6.35 ± 1.45	-0.05 (-0.34 – 0.24)	-0.03 (-0.17 – 0.12)	0.87
RV/TLC (%)	42.5 ± 12.7	44.5 ± 13.2	39.8 ± 13.1	44.7 ± 14.3	-2.8 (-5.1 – 0.5) §	0.2 (-1.6 – 2.1)	0.041
VA (L)	5.08 ± 1.18	4.74 ± 1.31	5.11 ± 1.12	4.67 ± 1.38	0.03 (-0.16 – 0.22)	-0.08 (-0.27 – 0.12)	0.42
VA/TLC (%)	78.5 ± 11.3	75.1 ± 13.3	79.8 ± 11.1	74.1 ± 15.3	1.3 (-2.1 – 4.7)	-1.0 (-4.4 – 2.3)	0.33
KCO (mmol•min ⁻¹ •kPa ⁻¹ •L ⁻¹)	1.66 ± 0.36	1.64 ± 0.26	1.63 ± 0.26	1.68 ± 0.25	-0.04 (-0.10 – 0.03)	0.04 (-0.01 – 0.09)	0.06
DLCO (mmol•min ⁻¹ •kPa ⁻¹)	8.29 ± 2.02	7.74 ± 2.35	8.24 ± 1.87	7.81 ± 2.46	-0.05 (-0.25 – 0.15)	0.07 (-0.21 – 0.35)	0.51
LCI	9.05 ± 1.57	9.27 ± 2.24	8.50 ± 1.50	9.01 ± 2.33	-0.55 (-0.88 – 0.21) §	-0.26 (-0.73 – 0.20)	0.33
LCI _{vent}	1.36 ± 0.12	1.40 ± 0.20	1.32 ± 0.12	1.39 ± 0.22	-0.04 (-0.07 – 0.00) §	0.00 (-0.04 – 0.04)	0.19
LCI _{ds}	1.23 ± 0.09	1.24 ± 0.09	1.20 ± 0.07	1.23 ± 0.10	-0.03 (-0.05 – 0.01) §	0.00 (-0.03 – 0.02)	0.06
S _{cond} (L ⁻¹)	0.068 ± 0.032	0.076 ± 0.039	0.061 ± 0.030	0.074 ± 0.039	-0.007 (-0.023 – 0.009)	-0.002 (-0.014 – 0.010)	0.62
S _{acin} (L ⁻¹)	0.215 ± 0.114	0.213 ± 0.112	0.210 ± 0.104	0.222 ± 0.153	-0.005 (-0.028 – 0.018)	0.008 (-0.017 – 0.033)	0.43

Table 3.18c: Outcome Measures at Baseline and Post-Treatment in the Intention-to-Treat Population

Outcome	Baseline values		Post-treatment values		Change from baseline to post-treatment values		
	QAW039 (n = 29)	Placebo (n = 32)	QAW039 (n = 29)	Placebo (n = 32)	QAW039 (n = 29)	Placebo (n = 32)	P value†
R5 (kPa•L ⁻¹ •s)	0.55 ± 0.25	0.60 ± 0.19	0.52 ± 0.20	0.63 ± 0.29	-0.03 (-0.08 – 0.02)	0.03 (-0.04 – 0.10)	0.18
R20 (kPa•L ⁻¹ •s)	0.36 ± 0.12	0.42 ± 0.10	0.36 ± 0.10	0.43 ± 0.15	-0.01 (-0.03 – 0.02)	0.01 (-0.03 – 0.05)	0.53
R5-R20 (kPa•L ⁻¹ •s)	0.19 ± 0.15	0.18 ± 0.15	0.16 ± 0.12	0.20 ± 0.20	-0.02 (-0.06 – 0.01)	0.02 (-0.02 – 0.06)	0.11
AX (kPa•L ⁻¹)	2.53 ± 2.19	2.64 ± 2.60	2.12 ± 1.90	2.83 ± 3.32	-0.41 (-0.95 – 0.13)	0.19 (-0.44 – 0.82)	0.15
Inspiratory MLD (HU)	-831 ± 37	-837 ± 35	-840 ± 28	-845 ± 26	-10 (-18 – -1) §	-8 (-18 – 1)	0.83
Expiratory MLD (HU)	-715 ± 70	-720 ± 48	-716 ± 71	-731 ± 46	-1 (-9 – 8)	-11 (-20 – -2) §	0.08
MLD expiratory / inspiratory ratio	0.86 ± 0.07	0.86 ± 0.06	0.85 ± 0.07	0.87 ± 0.05	-0.01 (-0.02 – 0.00)	0.00 (-0.01 – 0.02)	0.21
RB1 wall area (mm ²)	40.2 ± 10.1	36.5 ± 10.5	39.9 ± 12.5	35.5 ± 10.8	-0.3 (-3.3 – 2.7)	-1.1 (-3.3 – 1.2)	0.66
RB1 wall percentage	63.0 ± 6.1	63.7 ± 3.1	64.0 ± 5.5	63.2 ± 3.5	1.0 (0.0 – 2.0)	-0.6 (-1.4 – 0.3)	0.018
RB1 luminal area (mm ²)	25.2 ± 13.2	21.3 ± 7.9	24.0 ± 13.4	21.2 ± 8.2	-1.2 (-3.2 – 0.8)	-0.2 (-1.4 – 1.0)	0.36

Legend for Tables 3.17 and 3.18

FENO₅₀ denotes the fraction of exhaled nitric oxide in exhaled air at a flow rate of 50 ml/s, ACQ-6 six-point Asthma Control Questionnaire score, AQLQ Asthma Quality of Life Questionnaire score, FEV₁ forced expiratory volume in one second, FVC forced vital capacity, RV residual volume, TLC total lung capacity, VA alveolar volume by single breath helium dilution, KCO carbon monoxide transfer coefficient, DLCO carbon monoxide diffusing capacity, LCI lung clearance index, LCI_{vent} = specific ventilation inequality component of lung clearance index, LCI_{ds} = dead space component of lung clearance index, R5/R20 = resistance at 5Hz/20Hz, AX reactance area, MLD mean lung density, HU Hounsfield Units, and RB1 right upper lobe apical segmental bronchus.

* Plus-minus values are mean \pm standard deviation (SD), and changes from baseline to post-treatment are mean (95% confidence interval), unless otherwise stated.

† P values were calculated with the use of a two-sided unpaired t-test comparing the baseline-to-post-treatment changes between the QAW039 and placebo groups, unless otherwise stated.

‡ Baseline and post-treatment values are geometric means \pm log₁₀ SD. Change from baseline to post-treatment is the geometric mean (95% confidence interval) fold-change in sputum eosinophil percentage.

¶ P value was calculated using a two-sided unpaired t-test comparing the baseline-to-post-treatment changes between the QAW039 and placebo groups with respect to log-transformed sputum eosinophil percentage.

§ Denotes a significant ($p < 0.05$) change from baseline to post-treatment values within a treatment group. P values were calculated using a two-sided paired t-test comparing baseline and post-treatment values in each treatment group. Sputum eosinophil percentage was log-transformed prior to analysis.

Discussion

We found that QAW039 significantly reduced sputum eosinophil percentage compared to placebo in patients with persistent, moderate-to-severe asthma and a sputum eosinophilia. The 5.2-fold reduction seen was comparable to that observed with mepolizumab^{29,30}, and appreciably greater than that observed with montelukast^{287,288}. Unlike mepolizumab^{29,30}, QAW039 did not have any significant effect on the blood eosinophil count. This suggests that CRTH2 receptor blockade attenuates the migration of eosinophils into the airway tissues, but may not affect the release of eosinophils from the bone marrow in humans. We did not observe a significant reduction in FeNO₅₀ with QAW039. Interestingly, reductions in FeNO have been observed with lebrikizumab (anti-IL-13)³¹ but not mepolizumab (anti-IL-5)²⁹, suggesting that the production of FeNO may be partly dependent upon the precise T_H2 cytokine profile.

In this study, QAW039 significantly improved AQLQ(S) scores compared to placebo, with non-significant improvements in ACQ-6 scores. In addition, QAW039 significantly improved expiratory flow limitation (post-bronchodilator FEV₁) and expiratory air trapping (RV/TLC ratio) compared to placebo. Previous interventional studies have shown that anti-eosinophilic treatments or strategies exert their major therapeutic effect through the reduction in asthma exacerbations^{29,30,281}, although effects on FEV₁ have also been observed^{30,31}. The treatment period in this study was not long enough to observe a significant effect on exacerbations, and future studies should examine the hypothesis that QAW039 reduces the frequency of exacerbations in patients with eosinophilic asthma. Following a six-week placebo wash-out period, we noted a prompt rebound effect in the QAW039 group with respect to sputum eosinophil percentage, ACQ-6 and AQLQ(S) scores, and FEV₁. This suggests that the short-term improvements in asthma quality of life and FEV₁ seen with QAW039 were driven by reversible processes such as reductions in airway wall oedema or mucus production. Future studies are required to examine the longer-term effects of QAW039 on airway remodelling.

Two previous clinical trials of CRTH2 receptor antagonists in asthma have yielded mixed results. In a randomized controlled study of OC000459 in patients with asthma not currently receiving ICS, significant improvements were observed in FEV₁ and

asthma quality of life²⁸⁹. However, this compound has not yet been tested in patients with moderate-to-severe asthma who have higher treatment requirements, and it is therefore unknown whether OC000459 would have additional clinical benefit in this important group. The alternative compound AMG853, a dual CRTH2 and D-prostanoid receptor antagonist, was not effective in improving asthma symptoms or FEV₁ in patients with moderate-to-severe asthma²⁹⁰. In these two studies, patient selection was not based upon evidence of eosinophilic airway inflammation. Previous experience has shown that targeting anti-eosinophilic therapies to patients with evidence of uncontrolled T_H2-driven inflammation results in improved efficacy²⁹⁻³¹. The positive results obtained in our study should therefore not be extrapolated to an unselected group of patients with moderate-to-severe asthma.

We utilised a number of novel physiological and imaging outcome measures in this study such as multiple breath inert gas washout (MBW), impulse oscillometry and quantitative CT. These modalities did not appear to be as responsive as standard outcome measures such as FEV₁. However, a number of the MBW outcomes, namely LCI, LCI_{vent} and LCI_{ds}, did show statistically significant improvements within the QAW039 group, and the change in LCI_{ds} from baseline to post-treatment was close to showing a statistically significant difference between the QAW039 and placebo groups ($p = 0.06$). Moreover, a number of these techniques are still at a relatively early stage of development, and improvements may be anticipated in the future. In particular, we assessed changes in airway wall geometry with quantitative CT using the dimensions of a single lobar bronchus. Newer techniques such as computational fluid dynamics, which take into account the morphology of the first six generations of the airway tree, may provide novel insights into the effect of an intervention on airway resistance¹⁶⁹.

We conclude that QAW039 is effective at attenuating eosinophilic airway inflammation in patients with persistent eosinophilic asthma, and has a favourable safety profile. There is evidence that QAW039 improves lung function and asthma-related quality of life. Longer-term studies are required to confirm these findings and to investigate the effect of QAW039 on preventing asthma exacerbations.

4 Conclusions

4.1 Summary of findings

The aim of the work presented in this thesis was to assess the clinical utility and structural correlates of putative non-invasive measurements of small airway obstruction in patients with asthma. The rationale underpinning this aim was the widely-stated hypothesis that small airway disease may represent a cause of disease persistence in asthma, since conventional inhaled therapies do not penetrate to the very distal airways. The accurate measurement of small airway obstruction would potentially enable treatments that targeted the small airway compartment, such as small particle inhalers or systemic therapies, to be selectively administered to the patient group most likely to benefit from them. Moreover, small airway biomarkers could be used to assess the response to these treatments in clinical practice, or within the context of interventional trials. A further possibility, albeit speculative, is that small airway markers may provide an early warning for the incipient development of incompletely reversible airflow obstruction in patients with asthma.

We first undertook a period of methodological validation, particularly focusing on the multiple breath inert gas washout (MBW) technique, since this method is currently less well standardised than spirometry, body plethysmography and impulse oscillometry (IOS). Utilising an acrylic glass lung model, we determined that measurements of functional residual capacity performed using our MBW method are accurate and repeatable *in vitro*, and we also demonstrated good within-visit repeatability *in vivo*. This provided increased confidence in the results presented in the remainder of the thesis using this technique.

The MBW test yields a large amount of data, but only one data point is utilised to derive the lung clearance index (LCI), the most commonly used MBW parameter. Phase III slope analysis had been adequately explored by other investigators, but it did not appear that the information content of the standard washout curve, comprising breath-by-breath exhaled inert gas concentration, had been fully assessed. We therefore derived two novel parameters, LCI_{vent} and LCI_{ds} , based upon a simple two-compartment lung model, which estimated the contribution towards LCI of specific ventilation

inequality and increased respiratory dead space, respectively. These parameters were found to be repeatable in patients with asthma, cystic fibrosis (CF) and non-cystic fibrosis bronchiectasis. Moreover, there was evidence that they could discriminate between different phenotypes of cystic fibrosis, a condition that is characterised by severe ventilation heterogeneity. A further important observation was that in patients with both non-CF bronchiectasis and CF, LCI_{vent} and LCI_{ds} were strongly correlated, suggesting that specific ventilation inequality and increased respiratory dead space are not completely independent. Since these mechanisms are expected to occur mainly in the proximal and the distal airways respectively, it may be surmised that the calibre of the large and small airways are also related to a certain extent. The association between large and small airway obstruction may be purely statistical, in that the two processes may tend to coexist in the same patients due to a common underlying pathological process, or alternatively, the calibre of the large and small airways may interact due to the network properties of the airway tree. In either case, it is clear that attempting to draw a sharp distinction between large and small airway obstruction is somewhat artificial. Nevertheless, this does not preclude the possibility that some patients may have disproportionate small airway disease, and that this characteristic could be measured and used to stratify therapy.

The next study dealt with the repeatability of putative small airway biomarkers, both within-visit and between-visit. We found that IOS parameters exhibited good within-visit repeatability, and were stable over time. With the notable exception of S_{cond} , MBW parameters exhibited good within-visit repeatability, and were moderately stable over time. We then investigated the relationship between putative small airway markers and the clinical expression of asthma. We found that the main physiological predictors of asthma symptoms, quality of life and exacerbations were spirometric measures of expiratory flow limitation and measures of airway resistance using IOS. The most predictive IOS parameter was the resistance at 20Hz (R20), which is often considered to be a marker of large airway disease, although in reality the structural correlates of IOS parameters are not fully understood. Nevertheless, the fact that FEV_1 and R20 are independent predictors of asthma control suggests that they probe two different aspects of asthma pathophysiology or disease expression.

The MBW parameter S_{acin} was introduced as a specific marker of acinar airspace disease, but the structural correlates of this index had not previously been validated using either imaging or histological techniques. We utilised hyperpolarised ^3He magnetic resonance to probe diffusion within the acinar airspaces, in two polar groups of patients with asthma, one of which comprised patients with a normal S_{acin} , and the other of which comprised patients with a raised S_{acin} . We found that long-timescale diffusion of ^3He was less restricted in patients with a high S_{acin} . Moreover, the correlation between S_{acin} and long-timescale ADC could not be accounted for purely by expiratory air trapping and lung hyperinflation. We therefore concluded that there was evidence for a structural abnormality in the pulmonary acinus in patients with asthma causing subtle alterations in diffusion within this compartment.

The final study presented in this thesis was a randomised controlled trial of a novel anti-eosinophilic agent, the CRTH2 receptor antagonist QAW039. The primary outcome of the study was met, in that the drug very effectively reduced sputum eosinophil counts. In addition, there was evidence that QAW039 improves asthma quality of life and FEV₁. It therefore appears that QAW039 is a promising agent for the treatment of persistent eosinophilic asthma. The main relevance of this study to the present thesis was the inclusion of a number of novel exploratory outcome measures in the study design. These included MBW, IOS and quantitative CT parameters. Statistically significant improvements were observed within the QAW039 group for a number of MBW parameters, suggesting their possible utility as outcome measures in future interventional trials.

4.2 Future work

The work presented in this thesis may be built upon in a number of ways in the future. The validation study we performed using the photoacoustic gas analyser-based MBW system suggests that it may be suitable for development into a commercial product for clinical or research use, an undertaking that would benefit from academic input. We utilised a one-compartment lung model to validate our Innocor system, but in future this may be refined to include two parallel compartments subtended by airways with different resistances, in order to simulate ventilation heterogeneity.

Further studies are also required to understand the structural basis of IOS and MBW parameters, including the novel parameters LCI_{vent} and LCI_{ds} . This work is likely to involve a combination of computational modelling, and experiments using physical rapid prototype models of the human airways. With respect to IOS, the prevailing paradigm that R20 reflects large airways and R5-R20 reflects small airways is likely to be overly simplistic. It is now possible to produce patient-specific physical models of the upper airways down to the segmental branches of the bronchial tree, from CT images²⁹¹. The impedance of these models can be measured using IOS or other variants of the forced oscillation technique. Patient-specific computational models of the airway tree utilise CT images to derive the geometry of the first six generations, and the remainder of the bronchial tree, which is beyond the resolution of CT, is ‘grown out’ using an automated algorithm. The impedance of these models may be simulated, and the effects of altering the model, for instance by imposing homogeneous or heterogeneous airway constriction, can then be investigated. These techniques are likely to provide for the first time a true understanding of the structural significance of IOS parameters. A similar approach may be utilised to model gas mixing in the airways, although simulating the interaction between convection and diffusion within the whole airway tree is likely to be computationally intractable. However, it is likely that useful insights can be gained using simplified forward models that incorporate both diffusive and convective effects. Altering the structure of the model and then entering the output of the simulation into the inverse model described in Section 2.7 may yield further insights into the structural correlates of LCI_{vent} and LCI_{ds} .

In this thesis, the diffusive component of ventilation heterogeneity was investigated using hyperpolarised ^3He diffusion MR. Magnetic resonance techniques may also be utilised to quantify the regional fractional ventilation throughout the lungs^{210,292}, and the coupling of this technique with standard MBW is a further potentially fruitful area of research. In particular, this would allow the convective component of ventilation heterogeneity to be better understood.

We examined the clinical significance of small airway biomarkers cross-sectionally, and found that the IOS parameter R20 appeared to independently predict asthma control, quality of life and exacerbations. Longitudinal studies are required to

investigate the possibility that one or more of these markers may predict the future development of spirometric fixed airflow obstruction, which is known to be associated with worse clinical outcomes in patients with asthma⁴. Early intervention at this stage may potentially alter the natural history of the disease. Future work following up our asthma cohort is planned in order to determine the baseline predictors of accelerated lung function decline in this patient group.

References

- 1) Masoli M, Fabian D, Holt S, Beasley R. Global burden of asthma. Global Initiative for Asthma (GINA), 2004. Available from: <http://www.ginasthma.org/>.
- 2) Global Strategy for Asthma Management and Prevention. Global Initiative for Asthma (GINA) 2012. Available from: <http://www.ginasthma.org/>.
- 3) Braman SS. The global burden of asthma. *Chest*. 2006; **130**(Suppl. 1): 4S-12S.
- 4) Contoli M, Baraldo S, Marku B, Casolari P, Marwick JA, Turato G, Romagnoli M, Caramori G, Saetta M, Fabbri LM, Papi A. Fixed airflow obstruction due to asthma or chronic obstructive pulmonary disease: 5-year follow-up. *J Allergy Clin Immunol*. 2010; **125**(4): 830-7.
- 5) Orie NGM, Sluiter HJ, De Vries K, Tammeling GJ, Witkop J. The host factor in bronchitis. In: Orie NGM, Sluiter HJ, editors. *Bronchitis*. Assen, The Netherlands: Royal Van Gorcum; 1961. pp 43-59.
- 6) Kraft M. Asthma and chronic obstructive pulmonary disease exhibit common origins in any country! *Am J Respir Crit Care Med*. 2006; **174**(3): 238-40.
- 7) Barnes PJ. Against the Dutch hypothesis: asthma and chronic obstructive pulmonary disease are distinct diseases. *Am J Respir Crit Care Med*. 2006; **174**(3): 240-3
- 8) Vanfleteren LE, Kocks JW, Stone IS, Breyer-Kohansal R, Greulich T, Lacedonia D, Buhl R, Fabbri LM, Pavord ID, Barnes N, Wouters EF, Agusti A. Moving from the Oslerian paradigm to the post-genomic era: are asthma and COPD outdated terms? *Thorax*. 2014; **69**(1): 72-9.
- 9) Albert P, Agusti A, Edwards L, Tal-Singer R, Yates J, Bakke P, Celli BR, Coxson HO, Crim C, Lomas DA, Macnee W, Miller B, Rennard S, Silverman EK, Vestbo

- J, Wouters E, Calverley P. Bronchodilator responsiveness as a phenotypic characteristic of established chronic obstructive pulmonary disease. *Thorax*. 2012; **67**(8): 701-8.
- 10) Scichilone N, Battaglia S, La Sala A, Bellia V. Clinical implications of airway hyperresponsiveness in COPD. *Int J Chron Obstruct Pulmon Dis*. 2006; **1**(1): 49-60.
 - 11) O'Byrne PM, Pedersen S, Lamm CJ, Tan WC, Busse WW; START Investigators Group. Severe exacerbations and decline in lung function in asthma. *Am J Respir Crit Care Med*. 2009; **179**(1): 19-24.
 - 12) James AL, Palmer LJ, Kicic E, Maxwell PS, Lagan SE, Ryan GF, Musk AW. Decline in lung function in the Busselton Health Study: the effects of asthma and cigarette smoking. *Am J Respir Crit Care Med*. 2005; **171**(2): 109-14.
 - 13) Ebina M, Yaegashi H, Chiba R, Takahashi T, Motomiya M, Tanemura M. Hyperreactive site in the airway tree of asthmatic patients revealed by thickening of bronchial muscles. A morphometric study. *Am Rev Respir Dis*. 1990; **141**(5 Pt 1): 1327-32.
 - 14) Brightling CE, Gupta S, Gonem S, Siddiqui S. Lung damage and airway remodelling in severe asthma. *Clin Exp Allergy*. 2012; **42**(5): 638-49.
 - 15) Evans CM, Kim K, Tuvim MJ, Dickey BF. Mucus hypersecretion in asthma: causes and effects. *Curr Opin Pulm Med*. 2009; **15**(1): 4-11.
 - 16) Wagers SS, Norton RJ, Rinaldi LM, Bates JH, Sobel BE, Irvin CG. Extravascular fibrin, plasminogen activator, plasminogen activator inhibitors, and airway hyperresponsiveness. *J Clin Invest*. 2004; **114**(1): 104-11.
 - 17) Mauad T, Silva LF, Santos MA, Grinberg L, Bernardi FD, Martins MA, Saldiva PH, Dolhnikoff M. Abnormal alveolar attachments with decreased elastic fiber

- content in distal lung in fatal asthma. *Am J Respir Crit Care Med.* 2004; **170**(8): 857-62.
- 18) Lee JH, Haselkorn T, Borish L, Rasouliyan L, Chipps BE, Wenzel SE. Risk factors associated with persistent airflow limitation in severe or difficult-to-treat asthma: insights from the TENOR study. *Chest.* 2007; **132**(6): 1882-9.
- 19) ten Brinke A, Zwinderman AH, Sterk PJ, Rabe KF, Bel EH. Factors associated with persistent airflow limitation in severe asthma. *Am J Respir Crit Care Med.* 2001; **164**(5): 744-8.
- 20) Shaw DE, Berry MA, Hargadon B, McKenna S, Shelley MJ, Green RH, Brightling CE, Wardlaw AJ, Pavord ID. Association between neutrophilic airway inflammation and airflow limitation in adults with asthma. *Chest.* 2007; **132**(6): 1871-5.
- 21) Rackemann FM, Mallory TB. Intrinsic Asthma. *Trans Am Clin Climatol Assoc.* 1941; **57**: 60-73.
- 22) Lötvall J, Akdis CA, Bacharier LB, Bjermer L, Casale TB, Custovic A, Lemanske RF Jr, Wardlaw AJ, Wenzel SE, Greenberger PA. Asthma endotypes: a new approach to classification of disease entities within the asthma syndrome. *J Allergy Clin Immunol.* 2011; **127**(2): 355-60.
- 23) Bhakta NR, Woodruff PG. Human asthma phenotypes: from the clinic, to cytokines, and back again. *Immunol Rev.* 2011; **242**(1): 220-32.
- 24) Agache I, Akdis C, Jutel M, Virchow JC. Untangling asthma phenotypes and endotypes. *Allergy.* 2012; **67**(7): 835-46.
- 25) Wenzel SE. Asthma phenotypes: the evolution from clinical to molecular approaches. *Nat Med.* 2012; **18**(5): 716-25.

- 26) Wenzel S. Severe asthma: from characteristics to phenotypes to endotypes. *Clin Exp Allergy*. 2012; **42**(5): 650-8.
- 27) Lin TY, Poon AH, Hamid Q. Asthma phenotypes and endotypes. *Curr Opin Pulm Med*. 2013; **19**(1): 18-23.
- 28) Flood-Page P, Swenson C, Faiferman I, Matthews J, Williams M, Brannick L, Robinson D, Wenzel S, Busse W, Hansel TT, Barnes NC; International Mepolizumab Study Group. A study to evaluate safety and efficacy of mepolizumab in patients with moderate persistent asthma. *Am J Respir Crit Care Med*. 2007; **176**(11): 1062-71.
- 29) Haldar P, Brightling CE, Hargadon B, Gupta S, Monteiro W, Sousa A, Marshall RP, Bradding P, Green RH, Wardlaw AJ, Pavord ID. Mepolizumab and exacerbations of refractory eosinophilic asthma. *N Engl J Med*. 2009; **360**(10): 973-84.
- 30) Nair P, Pizzichini MM, Kjarsgaard M, Inman MD, Efthimiadis A, Pizzichini E, Hargreave FE, O'Byrne PM. Mepolizumab for prednisone-dependent asthma with sputum eosinophilia. *N Engl J Med*. 2009; **360**(10): 985-93.
- 31) Corren J, Lemanske RF, Hanania NA, Korenblat PE, Parsey MV, Arron JR, Harris JM, Scheerens H, Wu LC, Su Z, Mosesova S, Eisner MD, Bohlen SP, Matthews JG. Lebrikizumab treatment in adults with asthma. *N Engl J Med*. 2011; **365**(12): 1088-98.
- 32) Han MK, Agusti A, Calverley PM, Celli BR, Criner G, Curtis JL, Fabbri LM, Goldin JG, Jones PW, Macnee W, Make BJ, Rabe KF, Rennard SI, Sciruba FC, Silverman EK, Vestbo J, Washko GR, Wouters EF, Martinez FJ. Chronic obstructive pulmonary disease phenotypes: the future of COPD. *Am J Respir Crit Care Med*. 2010; **182**(5): 598-604.
- 33) Burgel PR. The role of small airways in obstructive airway diseases. *Eur Respir Rev*. 2011; **20**(119): 23-33.

- 34) Contoli M, Kraft M, Hamid Q, Bousquet J, Rabe KF, Fabbri LM, Papi A. Do small airway abnormalities characterize asthma phenotypes? In search of proof. *Clin Exp Allergy*. 2012; **42**(8): 1150-60.
- 35) Hamid Q. Pathogenesis of small airways in asthma. *Respiration*. 2012; **84**(1): 4-11.
- 36) Usmani OS. Treating the small airways. *Respiration*. 2012; **84**(6): 441-53.
- 37) van den Berge M, ten Hacken NH, van der Wiel E, Postma DS. Treatment of the bronchial tree from beginning to end: targeting small airway inflammation in asthma. *Allergy*. 2013; **68**(1): 16-26.
- 38) Scichilone N, Contoli M, Paleari D, Pirina P, Rossi A, Sanguinetti CM, Santus P, Sofia M, Sverzellati N. Assessing and accessing the small airways; implications for asthma management. *Pulm Pharmacol Ther*. 2013; **26**(2): 172-9.
- 39) van der Wiel E, ten Hacken NH, Postma DS, van den Berge M. Small-airways dysfunction associates with respiratory symptoms and clinical features of asthma: a systematic review. *J Allergy Clin Immunol*. 2013; **131**(3): 646-57.
- 40) Pedley TJ, Schroter RC, Sudlow MF. The prediction of pressure drop and variation of resistance within the human bronchial airways. *Respir Physiol*. 1970; **9**(3): 387-405.
- 41) Leach CL, Davidson PJ, Hasselquist BE, Boudreau RJ. Lung deposition of hydrofluoroalkane-134a beclomethasone is greater than that of chlorofluorocarbon fluticasone and chlorofluorocarbon beclomethasone: a cross-over study in healthy volunteers. *Chest*. 2002; **122**(2): 510-6.
- 42) Bateman ED, Boushey HA, Bousquet J, Busse WW, Clark TJ, Pauwels RA, Pedersen SE; GOAL Investigators Group. Can guideline-defined asthma control

- be achieved? The Gaining Optimal Asthma Control study. *Am J Respir Crit Care Med.* 2004; **170**(8): 836-44.
- 43) Gamble J, Stevenson M, McClean E, Heaney LG. The prevalence of nonadherence in difficult asthma. *Am J Respir Crit Care Med.* 2009; **180**(9): 817-22.
- 44) Murphy AC, Proeschal A, Brightling CE, Wardlaw AJ, Pavord I, Bradding P, Green RH. The relationship between clinical outcomes and medication adherence in difficult-to-control asthma. *Thorax.* 2012; **67**(8): 751-3.
- 45) Melani AS, Bonavia M, Cilenti V, Cinti C, Lodi M, Martucci P, Serra M, Scichilone N, Sestini P, Aliani M, Neri M; Gruppo Educazionale Associazione Italiana Pneumologi Ospedalieri. Inhaler mishandling remains common in real life and is associated with reduced disease control. *Respir Med.* 2011; **105**(6): 930-8.
- 46) Adcock IM, Ford PA, Bhavsar P, Ahmad T, Chung KF. Steroid resistance in asthma: mechanisms and treatment options. *Curr Allergy Asthma Rep.* 2008; **8**(2): 171-8.
- 47) Carroll N, Elliot J, Morton A, James A. The structure of large and small airways in nonfatal and fatal asthma. *Am Rev Respir Dis.* 1993; **147**(2): 405-10.
- 48) Carroll N, Cooke C, James A. The distribution of eosinophils and lymphocytes in the large and small airways of asthmatics. *Eur Respir J.* 1997; **10**(2): 292-300.
- 49) Faul JL, Tormey VJ, Leonard C, Burke CM, Farmer J, Horne SJ, Poulter LW. Lung immunopathology in cases of sudden asthma death. *Eur Respir J.* 1997; **10**(2): 301-7.
- 50) Hamid Q, Song Y, Kotsimbos TC, Minshall E, Bai TR, Hegele RG, Hogg JC. Inflammation of small airways in asthma. *J Allergy Clin Immunol.* 1997; **100**(1): 44-51.

- 51) Kraft M, Djukanovic R, Wilson S, Holgate ST, Martin RJ. Alveolar tissue inflammation in asthma. *Am J Respir Crit Care Med.* 1996; **154**(5): 1505-10.
- 52) Kraft M, Martin RJ, Wilson S, Djukanovic R, Holgate ST. Lymphocyte and eosinophil influx into alveolar tissue in nocturnal asthma. *Am J Respir Crit Care Med.* 1999; **159**(1): 228-34.
- 53) Wenzel SE, Szeffler SJ, Leung DY, Sloan SI, Rex MD, Martin RJ. Bronchoscopic evaluation of severe asthma. Persistent inflammation associated with high dose glucocorticoids. *Am J Respir Crit Care Med.* 1997; **156**(3 Pt 1): 737-43.
- 54) Balzar S, Wenzel SE, Chu HW. Transbronchial biopsy as a tool to evaluate small airways in asthma. *Eur Respir J.* 2002; **20**(2): 254-9.
- 55) Hauber HP, Gotfried M, Newman K, Danda R, Servi RJ, Christodoulopoulos P, Hamid Q. Effect of HFA-flunisolide on peripheral lung inflammation in asthma. *J Allergy Clin Immunol.* 2003; **112**(1): 58-63.
- 56) Bergeron C, Hauber HP, Gotfried M, Newman K, Dhanda R, Servi RJ, Ludwig MS, Hamid Q. Evidence of remodeling in peripheral airways of patients with mild to moderate asthma: effect of hydrofluoroalkane-flunisolide. *J Allergy Clin Immunol.* 2005; **116**(5): 983-9.
- 57) British Thoracic Society Bronchoscopy Guidelines Committee, a Subcommittee of Standards of Care Committee of British Thoracic Society. British Thoracic Society guidelines on diagnostic flexible bronchoscopy. *Thorax.* 2001; **56** (Suppl 1): i1-21.
- 58) Macklem PT, Mead J. Resistance of central and peripheral airways measured by a retrograde catheter. *J Appl Physiol.* 1967; **22**(3): 395-401.

- 59) Wagner EM, Liu MC, Weinmann GG, Permutt S, Bleecker ER. Peripheral lung resistance in normal and asthmatic subjects. *Am Rev Respir Dis.* 1990; **141**(3): 584-8.
- 60) Wagner EM, Bleecker ER, Permutt S, Liu MC. Direct assessment of small airways reactivity in human subjects. *Am J Respir Crit Care Med.* 1998; **157**(2): 447-52.
- 61) Kaminsky DA, Irvin CG, Gurka DA, Feldsien DC, Wagner EM, Liu MC, Wenzel SE. Peripheral airways responsiveness to cool, dry air in normal and asthmatic individuals. *Am J Respir Crit Care Med.* 1995; **152**(6 Pt 1): 1784-90.
- 62) Kaminsky DA, Bates JH, Irvin CG. Effects of cool, dry air stimulation on peripheral lung mechanics in asthma. *Am J Respir Crit Care Med.* 2000; **162**(1): 179-86.
- 63) Kraft M, Pak J, Martin RJ, Kaminsky D, Irvin CG. Distal lung dysfunction at night in nocturnal asthma. *Am J Respir Crit Care Med.* 2001; **163**(7): 1551-6.
- 64) Gompelmann D, Eberhardt R, Herth FJ. Collateral ventilation. *Respiration.* 2013; **85**(6): 515-20.
- 65) Yanai M, Sekizawa K, Ohru T, Sasaki H, Takishima T. Site of airway obstruction in pulmonary disease: direct measurement of intrabronchial pressure. *J Appl Physiol.* 1992; **72**(3): 1016-23.
- 66) Mead J, Whittenberger JL. Physical properties of human lungs measured during spontaneous respiration. *J Appl Physiol.* 1953; **5**(12): 779-96.
- 67) Ohru T, Sekizawa K, Yanai M, Morikawa M, Jin Y, Sasaki H, Takishima T. Partitioning of pulmonary responses to inhaled methacholine in subjects with asymptomatic asthma. *Am Rev Respir Dis.* 1992; **146**(6): 1501-5.

- 68) Hutchinson J. On the capacity of the lungs, and on the respiratory functions, with a view of establishing a precise and easy method of detecting disease by the spirometer. *Med Chir Trans.* 1846; **29**: 137-252.
- 69) Gaensler EA. An instrument for dynamic vital capacity measurements. *Science.* 1951; **114**(2965): 444-6.
- 70) Hyatt RE, Schilder DP, Fry DL. Relationship between maximum expiratory flow and degree of lung inflation. *J Appl Physiol.* 1958; **13**(3): 331-6.
- 71) Pedersen OF, Butler JP. Expiratory flow limitation. *Compr Physiol.* 2011; **1**(4): 1861-82.
- 72) Dawson SV, Elliot EA. Wave-speed limitation on expiratory flow – a unifying concept. *J Appl Physiol.* 1977; **43**(3): 498-515.
- 73) Polak AG. A model-based method for flow limitation analysis in the heterogeneous human lung. *Comput Methods Programs Biomed.* 2008; **89**(2): 123-31.
- 74) McFadden ER Jr, Linden DA. A reduction in maximum mid-expiratory flow rate. A spirographic manifestation of small airway disease. *Am J Med.* 1972; **52**(6): 725-37.
- 75) Hansen JE, Sun XG, Wasserman K. Discriminating measures and normal values for expiratory obstruction. *Chest.* 2006; **129**(2): 369-77.
- 76) Morris ZQ, Coz A, Starosta D. An Isolated Reduction of the FEV3/FVC Ratio is an Indicator of Mild Lung Injury. *Chest.* 2013; **144**(4): 1117-23.
- 77) Cohen J, Postma DS, Vink-Klooster K, van der Bij W, Verschuuren E, Ten Hacken NH, Koëter GH, Douma WR. FVC to slow inspiratory vital capacity ratio: a potential marker for small airways obstruction. *Chest.* 2007; **132**(4): 1198-203.

- 78) Fish J, Menkes H, Rosenthal R, Summer W, Norman P, Permutt S. The effect of acute bronchospasm on the distribution of transit times during forced expiration. *Am Rev Respir Dis.* 1974; **109**: 700.
- 79) Tockman M, Menkes H, Cohen B, Permutt S, Benjamin J, Ball WC Jr, Tonascia J. A comparison of pulmonary function in male smokers and nonsmokers. *Am Rev Respir Dis.* 1976; **114**(4): 711-22.
- 80) Neuburger N, Levison H, Bryan AC, Kruger K. Transit time analysis of the forced expiratory spirogram in growth. *J Appl Physiol.* 1976; **40**(3): 329-32.
- 81) Macfie AE, Harris EA, Whitlock RM. Transit-time analysis of the forced spirogram in healthy children and adults. *J Appl Physiol.* 1979; **46**(2): 263-7.
- 82) Liang A, Macfie AE, Harris EA, Whitlock RM. Transit-time analysis of the forced expiratory spirogram during clinical remission in juvenile asthma. *Thorax.* 1979; **34**(2): 194-9.
- 83) Miller MR, Pincock AC. Repeatability of the moments of the truncated forced expiratory spirogram. *Thorax.* 1982; **37**(3): 205-11.
- 84) Chinn DJ, Cotes JE. Transit time indices derived from forced expiratory spiograms: repeatability and criteria for curve selection and truncation. *Eur Respir J.* 1994; **7**(2): 402-8.
- 85) Permutt S, Menkes HA. Spirometry. Analysis of forced expiration within the time domain. In: Macklem P, Permutt S, eds. *The lung in the transition between health and disease.* New York, Marcel Decker, 1977; pp. 113-151.
- 86) Miller MR, Grove DM, Pincock AC. Time domain spirogram indices. Their variability and reference values in nonsmokers. *Am Rev Respir Dis.* 1985; **132**(5): 1041-8.

- 87) Nakadate T, Sato T, Kagawa J. Longitudinal changes in time domain spirogram indices and their variability. *Eur Respir J*. 1994; **7**(6): 1062-9.
- 88) Nakadate T, Sato T, Kagawa J, Yagami T. Effect of lifetime cigarette consumption on time domain spirogram indices. *Ind Health*. 1994; **32**(1): 29-40.
- 89) Miller MR, Pincock AC, Grove DM. Patterns of spirogram abnormality in individual smokers. *Am Rev Respir Dis*. 1985; **132**(5): 1034-40.
- 90) Wanger J, Clausen JL, Coates A, Pedersen OF, Brusasco V, Burgos F, Casaburi R, Crapo R, Enright P, van der Grinten CP, Gustafsson P, Hankinson J, Jensen R, Johnson D, Macintyre N, McKay R, Miller MR, Navajas D, Pellegrino R, Viegi G. Standardisation of the measurement of lung volumes. *Eur Respir J*. 2005; **26**(3): 511-22.
- 91) Criée CP, Sorichter S, Smith HJ, Kardos P, Merget R, Heise D, Berdel D, Köhler D, Magnussen H, Marek W, Mitfessel H, Rasche K, Rolke M, Worth H, Jörres RA; Working Group for Body Plethysmography of the German Society for Pneumology and Respiratory Care. Body plethysmography--its principles and clinical use. *Respir Med*. 2011; **105**(7): 959-71.
- 92) Sorkness RL, Bleecker ER, Busse WW, Calhoun WJ, Castro M, Chung KF, *et al*. Lung function in adults with stable but severe asthma: air trapping and incomplete reversal of obstruction with bronchodilation. *J Appl Physiol* 2008; **104**(2): 394-403.
- 93) Mahut B, Peiffer C, Bokov P, Beydon N, Delclaux C. Gas trapping is associated with severe exacerbation in asthmatic children. *Respir Med*. 2010; **104**(8): 1230-3.
- 94) Kraft M, Cairns CB, Ellison MC, Pak J, Irvin C, Wenzel S. Improvements in distal lung function correlate with asthma symptoms after treatment with oral montelukast. *Chest*. 2006; **130**(6): 1726-32.

- 95) Gao JM, Cai F, Peng M, Ma Y, Wang B. Montelukast improves air trapping, not airway remodeling, in patients with moderate-to-severe asthma: a pilot study. *Chin Med J (Engl)*. 2013; **126**(12): 2229-34.
- 96) Spahn JD, Covar RA, Jain N, Gleason M, Shimamoto R, Szeffler SJ, Gelfand EW. Effect of montelukast on peripheral airflow obstruction in children with asthma. *Ann Allergy Asthma Immunol*. 2006; **96**(4): 541-9.
- 97) Filippelli M, Duranti R, Gigliotti F, Bianchi R, Grazzini M, Stendardi L, Scano G. Overall contribution of chest wall hyperinflation to breathlessness in asthma. *Chest*. 2003; **124**(6): 2164-70.
- 98) Roberts CM, MacRae KD, Seed WA. Multi-breath and single breath helium dilution lung volumes as a test of airway obstruction. *Eur Respir J*. 1990; **3**(5): 515-20.
- 99) Hughes JM, Pride NB. Examination of the carbon monoxide diffusing capacity (DL(CO)) in relation to its KCO and VA components. *Am J Respir Crit Care Med*. 2012; **186**(2): 132-9.
- 100) DuBois AB, Brody AW, Lewis DH, Burgess BF Jr. Oscillation mechanics of lungs and chest in man. *J Appl Physiol*. 1956; **8**(6): 587-94.
- 101) Oostveen E, MacLeod D, Lorino H, Farré R, Hantos Z, Desager K, Marchal F; ERS Task Force on Respiratory Impedance Measurements. The forced oscillation technique in clinical practice: methodology, recommendations and future developments. *Eur Respir J* 2003; **22**(6): 1026-1041.
- 102) Smith HJ, Reinhold P, Goldman MD. Forced oscillation technique and impulse oscillometry. *Eur Respir Mon*. 2005; **31**: 72-105.

- 103) Oostveen E, Boda K, van der Grinten CP, James AL, Young S, Nieland H, Hantos Z. Respiratory impedance in healthy subjects: baseline values and bronchodilator response. *Eur Respir J*. 2013; **42**(6): 1513-23.
- 104) Hantos Z, Daróczy B, Suki B, Galgóczy G, Csendes T. Forced oscillatory impedance of the respiratory system at low frequencies. *J Appl Physiol*. 1986; **60**(1): 123-32.
- 105) Lutchen KR, Yang K, Kaczka DW, Suki B. Optimal ventilation waveforms for estimating low-frequency respiratory impedance. *J Appl Physiol*. 1993; **75**(1): 478-88.
- 106) Kaczka DW, Ingenito EP, Suki B, Lutchen KR. Partitioning airway and lung tissue resistances in humans: effects of bronchoconstriction. *J Appl Physiol*. 1997; **82**(5): 1531-41.
- 107) Lutchen KR, Jensen A, Atileh H, Kaczka DW, Israel E, Suki B, Ingenito EP. Airway constriction pattern is a central component of asthma severity: the role of deep inspirations. *Am J Respir Crit Care Med*. 2001; **164**(2): 207-15.
- 108) Otis AB, McKerrow CB, Bartlett RA, Mead J, McIlroy MB, Selver-Stone NJ, Radford EP Jr. Mechanical factors in distribution of pulmonary ventilation. *J Appl Physiol*. 1956; **8**(4): 427-43.
- 109) Navajas D, Maksym GN, Bates JH. Dynamic viscoelastic nonlinearity of lung parenchymal tissue. *J Appl Physiol*. 1995; **79**(1): 348-56.
- 110) Lutchen KR, Gillis H. Relationship between heterogeneous changes in airway morphometry and lung resistance and elastance. *J Appl Physiol*. 1997; **83**(4): 1192-1201.
- 111) Johnson MK, Birch M, Carter R, Kinsella J, Stevenson RD. Use of reactance to estimate transpulmonary resistance. *Eur Respir J*. 2005; **25**(6): 1061-9.

- 112) Horan T, Mateus S, Beraldo P, Araújo L, Urschel J, Urmenyi E, Santiago F. Forced oscillation technique to evaluate tracheostenosis in patients with neurologic injury. *Chest*. 2001; **120**(1): 69-73.
- 113) Goldman MD, Saadeh C, Ross D. Clinical applications of forced oscillation to assess peripheral airway function. *Respir Physiol Neurobiol*. 2005; **148**(1-2): 179-94.
- 114) Kaminsky DA, Irvin CG, Lundblad L, Moriya HT, Lang S, Allen J, Viola T, Lynn M, Bates JH. Oscillation mechanics of the human lung periphery in asthma. *J Appl Physiol*. 2004; **97**(5): 1849-58.
- 115) Hantos Z, Daróczy B, Suki B, Nagy S, Fredberg JJ. Input impedance and peripheral inhomogeneity of dog lungs. *J Appl Physiol*. 1992; **72**(1): 168-78.
- 116) Bates JH, Suki B. Assessment of peripheral lung mechanics. *Respir Physiol Neurobiol*. 2008; **163**(1-3): 54-63.
- 117) Suki B, Yuan H, Zhang Q, Lutchen KR. Partitioning of lung tissue response and inhomogeneous airway constriction at the airway opening. *J Appl Physiol*. 1997; **82**(4): 1349-59.
- 118) Ito S, Ingenito EP, Arold SP, Parameswaran H, Tgavalekos NT, Lutchen KR, Suki B. Tissue heterogeneity in the mouse lung: effects of elastase treatment. *J Appl Physiol*. 2004; **97**(1): 204-12.
- 119) Lutchen KR, Greenstein JL, Suki B. How inhomogeneities and airway walls affect frequency dependence and separation of airway and tissue properties. *J Appl Physiol*. 1996; **80**(5): 1696-707.
- 120) Tgavalekos NT, Tawhai M, Harris RS, Musch G, Vidal-Melo M, Venegas JG, Lutchen KR. Identifying airways responsible for heterogeneous ventilation and mechanical dysfunction in asthma: an image functional modeling approach. *J Appl Physiol*. 2005; **99**(6): 2388-97.

- 121) Campana L, Kenyon J, Zhalehdoust-Sani S, Tzeng YS, Sun Y, Albert M, Lutchen KR. Probing airway conditions governing ventilation defects in asthma via hyperpolarized MRI image functional modeling. *J Appl Physiol.* 2009; **106**(4): 1293-300.
- 122) Tgavalekos NT, Musch G, Harris RS, Vidal Melo MF, Winkler T, Schroeder T, Callahan R, Lutchen KR, Venegas JG. Relationship between airway narrowing, patchy ventilation and lung mechanics in asthmatics. *Eur Respir J.* 2007; **29**(6): 1174-81.
- 123) Mullally W, Betke M, Albert M, Lutchen K. Explaining clustered ventilation defects via a minimal number of airway closure locations. *Ann Biomed Eng.* 2009; **37**(2): 286-300.
- 124) Venegas JG, Winkler T, Musch G, Vidal Melo MF, Layfield D, Tgavalekos N, Fischman AJ, Callahan RJ, Bellani G, Harris RS. Self-organized patchiness in asthma as a prelude to catastrophic shifts. *Nature.* 2005; **434**(7034): 777-82.
- 125) Winkler T, Venegas JG. Complex airway behavior and paradoxical responses to bronchoprovocation. *J Appl Physiol.* 2007; **103**(2): 655-63.
- 126) Shi Y, Aledia AS, Tatavoosian AV, Vijayalakshmi S, Galant SP, George SC. Relating small airways to asthma control by using impulse oscillometry in children. *J Allergy Clin Immunol.* 2012; **129**(3): 671-8.
- 127) Takeda T, Oga T, Niimi A, Matsumoto H, Ito I, Yamaguchi M, Matsuoka H, Jinnai M, Otsuka K, Oguma T, Nakaji H, Chin K, Mishima M. Relationship between small airway function and health status, dyspnea and disease control in asthma. *Respiration.* 2010; **80**(2): 120-6.
- 128) Robinson PD, Goldman MD, Gustafsson PM. Inert gas washout: Theoretical background and clinical utility in respiratory disease. *Respiration.* 2009; **78**(3): 339-55.

- 129) Robertson JS, Siri WE, Jones HB. Lung ventilation patterns determined by analysis of nitrogen elimination rates. Use of the mass spectrometer as a continuous as a continuous gas analyzer. *J Clin Invest.* 1950; **29**(5): 577-90.
- 130) Robinson P, Latzin P, Verbanck S, Hall GL, Horsley A, Gappa M, Thamrin C, Arets HG, Aurora P, Fuchs S, King GG, Lum S, Macleod K, Paiva M, Pillow J, Ranganathan S, Ratjen F, Singer F, Sonnappa S, Stocks J, Subbarao P, Thompson B, Gustafsson PM. Consensus statement for inert gas washout measurement using multiple and single breath tests. *Eur Respir J.* 2013; **41**(3): 507-22.
- 131) Verbanck S, Schuermans D, van Muylem A, Noppen M, Paiva M, Vincken W. Ventilation distribution during histamine provocation. *J Appl Physiol* 1997; **83**(6): 1907-1916.
- 132) Horsley AR, Gustafsson PM, Macleod KA, Saunders C, Greening AP, Porteous DJ, Davies JC, Cunningham S, Alton EW, Innes JA. Lung clearance index is a sensitive, repeatable and practical measure of airways disease in adults with cystic fibrosis. *Thorax* 2008; **63**(2): 135-140.
- 133) Fuchs SI, Buess C, Lum S, Kozłowska W, Stocks J, Gappa M. Multiple breath washout with a sidestream ultrasonic flow sensor and mass spectrometry: a comparative study. *Pediatr Pulmonol.* 2006; **41**(12): 1218-25.
- 134) Singer F, Houtz B, Latzin P, Robinson P, Gustafsson P. A realistic validation study of a new nitrogen multiple-breath washout system. *PLoS One.* 2012; **7**(4): e36083.
- 135) Bouhuys A, Lichtneckert S, Lundgren C, Lundin G. Voluntary changes in breathing pattern and N₂ clearance from lungs. *J Appl Physiol.* 1961; **16**(6): 1039-42.
- 136) Edelman NH, Mittman C, Norris AH, Shock NW. Effects of respiratory pattern on age differences in ventilation uniformity. *J Appl Physiol* **24**(1): 49-53, 1968.

- 137) Paiva M, Engel LA. Pulmonary interdependence of gas transport. *J Appl Physiol*. 1979; **47**(2): 296-305.
- 138) Paiva M, Engel LA. The anatomical basis for the sloping N₂ plateau. *Respir Physiol*. 1981; **44**(3): 325-37.
- 139) Engel LA, Paiva M. Analyses of sequential filling and emptying of the lung. *Respir Physiol*. 1981; **45**(3): 309-21.
- 140) Paiva M, Engel LA. Model analysis of gas distribution within human lung acinus. *J Appl Physiol*. 1984; **56**(2): 418-25.
- 141) Engel LA. Gas mixing within the acinus of the lung. *J Appl Physiol*. 1983; **54**(3): 609-18.
- 142) Crawford AB, Makowska M, Paiva M, Engel LA. Convection- and diffusion-dependent ventilation maldistribution in normal subjects. *J Appl Physiol*. 1985; **59**(3): 838-46.
- 143) Verbanck S, Paiva M, Schuermans D, Hanon S, Vincken W, Van Muylem A. Relationships between the lung clearance index and conductive and acinar ventilation heterogeneity. *J Appl Physiol*. 2012; **112**(5): 782-90.
- 144) Verbanck S, Paiva M, Paeps E, Schuermans D, Malfroot A, Vincken W, Vanderhelst E. Lung clearance index in adult CF patients: the role of convection-dependent lung units. *Eur Respir J*. 2013; **42**(2): 380-8.
- 145) Milic-Emili J, Torchio R, D'Angelo E. Closing volume: a reappraisal (1967-2007). *Eur J Appl Physiol*. 2007; **99**(6): 567-83.
- 146) Aurora P, Kozłowska W, Stocks J. Gas mixing efficiency from birth to adulthood measured by multiple-breath washout. *Resp Physiol Neurobiol*. 2005; **148**(1-2): 125-39.

- 147) Horsley AR, Macleod KA, Robson AG, Lenney J, Bell NJ, Cunningham S, Greening AP, Gustafsson PM, Innes JA. Effects of cystic fibrosis lung disease on gas mixing indices derived from alveolar slope analysis. *Respir Physiol Neurobiol*. 2008; **162**(3): 197-203.
- 148) Stuart-Andrews CR, Kelly VJ, Sands SA, Lewis AJ, Ellis MJ, Thompson BR. Automated detection of the phase III slope during inert gas washout testing. *J Appl Physiol*. 2012; **112**(6): 1073-81.
- 149) Paiva M. Two new pulmonary functional indexes suggested by a simple mathematical model. *Respiration*. 1975; **32**(5): 389-403.
- 150) Verbanck S, Paiva M, Schuermans D, Malfroot A, Vincken W, Vanderhelst E. Acinar and conductive ventilation heterogeneity in severe CF lung disease: Back to the model. *Respir Physiol Neurobiol*. 2013; **188**(2): 124-32.
- 151) Verbanck S, Schuermans D, Noppen M, Van Muylem A, Paiva M, Vincken W. Evidence of acinar airway involvement in asthma. *Am J Respir Crit Care Med*. 1999; **159**(5 Pt 1): 1545-50.
- 152) Verbanck S, Schuermans D, Vincken W. Inflammation and airway function in the lung periphery of patients with stable asthma. *J Allergy Clin Immunol*. 2010; **125**(3): 611-6.
- 153) Verbanck S, Schuermans D, Paiva M, Vincken W. Nonreversible conductive airway ventilation heterogeneity in mild asthma. *J Appl Physiol*. 2003; **94**(4): 1380-6.
- 154) Gustafsson PM. Peripheral airway involvement in CF and asthma compared by inert gas washout. *Pediatr Pulmonol* 2007;**42**:168-176.

- 155) Macleod KA, Horsley AR, Bell NJ, Greening AP, Innes JA, Cunningham S. Ventilation heterogeneity in children with well controlled asthma with normal spirometry indicates residual airways disease. *Thorax*. 2009; **64**(1): 33-7.
- 156) Bourdin A, Paganin F, Préfaut C, Kieseler D, Godard P, Chanez P. Nitrogen washout slope in poorly controlled asthma. *Allergy* 2006; **61**(1): 85-89.
- 157) Farah CS, King GG, Brown NJ, Downie SR, Kermode JA, Hardaker KM, Peters MJ, Berend N, Salome CM. The role of the small airways in the clinical expression of asthma in adults. *J Allergy Clin Immunol* 2012; **129**(2): 381-387.
- 158) Thompson BR, Douglass JA, Ellis MJ, Kelly VJ, O'Hehir RE, King GG, Verbanck S. Peripheral lung function in patients with stable and unstable asthma. *J Allergy Clin Immunol*. 2013; **131**(5): 1322-8.
- 159) Farah CS, King GG, Brown NJ, Peters MJ, Berend N, Salome CM. Ventilation heterogeneity predicts asthma control in adults following inhaled corticosteroid dose titration. *J Allergy Clin Immunol*. 2012; **130**(1): 61-8.
- 160) Verbanck S, Schuermans D, Paiva M, Vincken W. The functional benefit of anti-inflammatory aerosols in the lung periphery. *J Allergy Clin Immunol*. 2006; **118**(2): 340-6.
- 161) Weibel ER. What makes a good lung? *Swiss Med Wkly*. 2009; **139**(27-28): 375-86.
- 162) Weibel ER, Gomez DM. Architecture of the human lung. Use of quantitative methods establishes fundamental relations between size and number of lung structures. *Science*. 1962; **137**(3530): 577-85.
- 163) Horsfield K, Cumming G. Morphology of the bronchial tree in man. *J Appl Physiol*. 1968; **24**(3): 373-83.

- 164) Parker H, Horsfield K, Cumming G. Morphology of distal airways in the human lung. *J Appl Physiol.* 1971; **31**(3): 386-91.
- 165) Hsia CC, Hyde DM, Ochs M, Weibel ER; ATS/ERS Joint Task Force on Quantitative Assessment of Lung Structure. An official research policy statement of the American Thoracic Society/European Respiratory Society: standards for quantitative assessment of lung structure. *Am J Respir Crit Care Med.* 2010; **181**(4): 394-418.
- 166) Litzlbauer HD, Korbel K, Kline TL, Jorgensen SM, Eaker DR, Bohle RM, Ritman EL, Langheinrich AC. Synchrotron-based micro-CT imaging of the human lung acinus. *Anat Rec (Hoboken).* 2010; **293**(9): 1607-14.
- 167) Walker C, Gupta S, Hartley R, Brightling CE. Computed tomography scans in severe asthma: utility and clinical implications. *Curr Opin Pulm Med.* 2012; **18**(1): 42-7.
- 168) Gupta S, Siddiqui S, Haldar P, Entwisle JJ, Mawby D, Wardlaw AJ, Bradding P, Pavord ID, Green RH, Brightling CE. Quantitative analysis of high-resolution computed tomography scans in severe asthma subphenotypes. *Thorax.* 2010; **65**(9): 775-81.
- 169) De Backer JW, Vos WG, Vinchurkar SC, Claes R, Drollmann A, Wulfrank D, Parizel PM, Germonpré P, De Backer W. Validation of computational fluid dynamics in CT-based airway models with SPECT/CT. *Radiology.* 2010; **257**(3): 854-62.
- 170) Busacker A, Newell JD Jr, Keefe T, Hoffman EA, Granroth JC, Castro M, Fain S, Wenzel S. A multivariate analysis of risk factors for the air-trapping asthmatic phenotype as measured by quantitative CT analysis. *Chest.* 2009; **135**(1): 48-56.
- 171) Gono H, Fujimoto K, Kawakami S, Kubo K. Evaluation of airway wall thickness and air trapping by HRCT in asymptomatic asthma. *Eur Respir J.* 2003; **22**(6): 965-71.

- 172) Tunon-de-Lara JM, Laurent F, Giraud V, Perez T, Aguilaniu B, Meziane H, Basset-Merle A, Chanez P. Air trapping in mild and moderate asthma: effect of inhaled corticosteroids. *J Allergy Clin Immunol.* 2007; **119**(3): 583-90.
- 173) Newman KB, Lynch DA, Newman LS, Ellegood D, Newell JD Jr. Quantitative computed tomography detects air trapping due to asthma. *Chest.* 1994; **106**(1): 105-9.
- 174) Ueda T, Niimi A, Matsumoto H, Takemura M, Hirai T, Yamaguchi M, Matsuoka H, Jinnai M, Muro S, Chin K, Mishima M. Role of small airways in asthma: investigation using high-resolution computed tomography. *J Allergy Clin Immunol.* 2006; **118**(5): 1019-25.
- 175) Zeidler MR, Klerup EC, Goldin JG, Kim HJ, Truong DA, Simmons MD, Sayre JW, Liu W, Elashoff R, Tashkin DP. Montelukast improves regional air-trapping due to small airways obstruction in asthma. *Eur Respir J.* 2006; **27**(2): 307-15.
- 176) Gupta S, Hartley R, Khan UT, Singapuri A, Hargadon B, Monteiro W, Pavord ID, Sousa AR, Marshall RP, Subramanian D, Parr D, Entwisle JJ, Siddiqui S, Raj V, Brightling CE. Quantitative computed tomography-derived clusters: redefining airway remodeling in asthmatic patients. *J Allergy Clin Immunol.* 2014; **133**(3): 729-38.
- 177) Galbán CJ, Han MK, Boes JL, Chughtai KA, Meyer CR, Johnson TD, Galbán S, Rehemtulla A, Kazerooni EA, Martinez FJ, Ross BD. Computed tomography-based biomarker provides unique signature for diagnosis of COPD phenotypes and disease progression. *Nat Med.* 2012; **18**(11): 1711-5.
- 178) Yablonskiy DA, Sukstanskii AL, Quirk JD, Woods JC, Conradi MS. Probing lung microstructure with hyperpolarized noble gas diffusion MRI: theoretical models and experimental results. *Magn Reson Med.* 2014; **71**(2): 486-505.

- 179) Mugler JP 3rd, Altes TA. Hyperpolarized ^{129}Xe MRI of the human lung. *J Magn Reson Imaging*. 2013; **37**(2): 313-31.
- 180) Chen XJ, Möller HE, Chawla MS, Cofer GP, Driehuys B, Hedlund LW, Johnson GA. Spatially resolved measurements of hyperpolarized gas properties in the lung in vivo. Part I: diffusion coefficient. *Magn Reson Med*. 1999; **42**(4): 721-8.
- 181) Saam BT, Yablonskiy DA, Kodibagkar VD, Leawoods JC, Gierada DS, Cooper JD, Lefrak SS, Conradi MS. MR imaging of diffusion of $(3)\text{He}$ gas in healthy and diseased lungs. *Magn Reson Med*. 2000; **44**(2): 174-9.
- 182) Yablonskiy DA, Sukstanskii AL, Leawoods JC, Gierada DS, Bretthorst GL, Lefrak SS, Cooper JD, Conradi MS. Quantitative in vivo assessment of lung microstructure at the alveolar level with hyperpolarized ^3He diffusion MRI. *Proc Natl Acad Sci U S A*. 2002; **99**(5): 3111-6.
- 183) Salerno M, de Lange EE, Altes TA, Truwit JD, Brookeman JR, Mugler JP 3rd. Emphysema: hyperpolarized helium 3 diffusion MR imaging of the lungs compared with spirometric indexes--initial experience. *Radiology*. 2002; **222**(1): 252-60.
- 184) Wang C, Altes TA, Mugler JP 3rd, Miller GW, Ruppert K, Mata JF, Cates GD Jr, Borish L, de Lange EE. Assessment of the lung microstructure in patients with asthma using hyperpolarized ^3He diffusion MRI at two time scales: comparison with healthy subjects and patients with COPD. *J Magn Reson Imaging*. 2008; **28**(1): 80-8.
- 185) Gierada DS, Woods JC, Bierhals AJ, Bartel ST, Ritter JH, Choong CK, Das NA, Hong C, Pilgram TK, Chang YV, Jacob RE, Hogg JC, Battafarano RJ, Cooper JD, Meyers BF, Patterson GA, Yablonskiy DA, Conradi MS. Effects of diffusion time on short-range hyperpolarized $(3)\text{He}$ diffusivity measurements in emphysema. *J Magn Reson Imaging*. 2009; **30**(4): 801-8.

- 186) Woods JC, Choong CK, Yablonskiy DA, Bentley J, Wong J, Pierce JA, Cooper JD, Macklem PT, Conradi MS, Hogg JC. Hyperpolarized ^3He diffusion MRI and histology in pulmonary emphysema. *Magn Reson Med.* 2006; **56**(6): 1293-300.
- 187) Kaushik SS, Cleveland ZI, Cofer GP, Metz G, Beaver D, Nouls J, Kraft M, Auffermann W, Wolber J, McAdams HP, Driehuys B. Diffusion-weighted hyperpolarized ^{129}Xe MRI in healthy volunteers and subjects with chronic obstructive pulmonary disease. *Magn Reson Med.* 2011; **65**(4): 1154-65.
- 188) Chen XJ, Hedlund LW, Möller HE, Chawla MS, Maronpot RR, Johnson GA. Detection of emphysema in rat lungs by using magnetic resonance measurements of ^3He diffusion. *Proc Natl Acad Sci U S A.* 2000; **97**(21): 11478-81.
- 189) Peces-Barba G, Ruiz-Cabello J, Cremillieux Y, Rodríguez I, Dupuich D, Callot V, Ortega M, Rubio Arbo ML, Cortijo M, Gonzalez-Mangado N. Helium-3 MRI diffusion coefficient: correlation to morphometry in a model of mild emphysema. *Eur Respir J.* 2003; **22**(1): 14-9.
- 190) Mata JF, Altes TA, Cai J, Ruppert K, Mitzner W, Hagspiel KD, Patel B, Salerno M, Brookeman JR, de Lange EE, Tobias WA, Wang HT, Cates GD, Mugler JP 3rd. Evaluation of emphysema severity and progression in a rabbit model: comparison of hyperpolarized ^3He and ^{129}Xe diffusion MRI with lung morphometry. *J Appl Physiol.* 2007; **102**(3): 1273-80.
- 191) Boudreau M, Xu X, Santyr GE. Measurement of ^{129}Xe gas apparent diffusion coefficient anisotropy in an elastase-instilled rat model of emphysema. *Magn Reson Med.* 2013; **69**(1): 211-20.
- 192) Fain SB, Panth SR, Evans MD, Wentland AL, Holmes JH, Korosec FR, O'Brien MJ, Fountaine H, Grist TM. Early emphysematous changes in asymptomatic smokers: detection with ^3He MR imaging. *Radiology.* 2006; **239**(3): 875-83.

- 193) Bartel SE, Haywood SE, Woods JC, Chang YV, Menard C, Yablonskiy DA, Gierada DS, Conradi MS. Role of collateral paths in long-range diffusion in lungs. *J Appl Physiol*. 2008; **104**(5): 1495-503.
- 194) Verbanck S, Paiva M. Determinants of the long-range apparent diffusion coefficient in the human lung: collateral channels or intra-acinar branching? *J Appl Physiol*. 2009; **106**(3): 1023.
- 195) Costella S, Kirby M, Maksym GN, McCormack DG, Paterson NA, Parraga G. Regional pulmonary response to a methacholine challenge using hyperpolarized (3)He magnetic resonance imaging. *Respirology*. 2012; **17**(8): 1237-46.
- 196) Waters B, Owers-Bradley J, Silverman M. Acinar structure in symptom-free adults by Helium-3 magnetic resonance. *Am J Respir Crit Care Med*. 2006; **173**(8): 847-51.
- 197) Yablonskiy DA, Sukstanskii AL, Woods JC, Gierada DS, Quirk JD, Hogg JC, Cooper JD, Conradi MS. Quantification of lung microstructure with hyperpolarized 3He diffusion MRI. *J Appl Physiol*. 2009; **107**(4): 1258-65.
- 198) Quirk JD, Lutey BA, Gierada DS, Woods JC, Senior RM, Lefrak SS, Sukstanskii AL, Conradi MS, Yablonskiy DA. In vivo detection of acinar microstructural changes in early emphysema with (3)He lung morphometry. *Radiology*. 2011; **260**(3): 866-74.
- 199) Altes TA, Powers PL, Knight-Scott J, Rakes G, Platts-Mills TA, de Lange EE, Alford BA, Mugler JP 3rd, Brookeman JR. Hyperpolarized 3He MR lung ventilation imaging in asthmatics: preliminary findings. *J Magn Reson Imaging*. 2001; **13**(3): 378-84.
- 200) Samee S, Altes T, Powers P, de Lange EE, Knight-Scott J, Rakes G, Mugler JP 3rd, Ciambotti JM, Alford BA, Brookeman JR, Platts-Mills TA. Imaging the lungs in asthmatic patients by using hyperpolarized helium-3 magnetic resonance:

- assessment of response to methacholine and exercise challenge. *J Allergy Clin Immunol*. 2003; **111**(6): 1205-11.
- 201) de Lange EE, Altes TA, Patrie JT, Gaare JD, Knake JJ, Mugler JP 3rd, Platts-Mills TA. Evaluation of asthma with hyperpolarized helium-3 MRI: correlation with clinical severity and spirometry. *Chest*. 2006; **130**(4): 1055-62.
- 202) de Lange EE, Altes TA, Patrie JT, Parmar J, Brookeman JR, Mugler JP 3rd, Platts-Mills TA. The variability of regional airflow obstruction within the lungs of patients with asthma: assessment with hyperpolarized helium-3 magnetic resonance imaging. *J Allergy Clin Immunol*. 2007; **119**(5): 1072-8.
- 203) Fain SB, Gonzalez-Fernandez G, Peterson ET, Evans MD, Sorkness RL, Jarjour NN, Busse WW, Kuhlman JE. Evaluation of structure-function relationships in asthma using multidetector CT and hyperpolarized He-3 MRI. *Acad Radiol*. 2008; **15**(6): 753-62.
- 204) de Lange EE, Altes TA, Patrie JT, Battiston JJ, Juersivich AP, Mugler JP 3rd, Platts-Mills TA. Changes in regional airflow obstruction over time in the lungs of patients with asthma: evaluation with ³He MR imaging. *Radiology*. 2009; **250**(2): 567-75.
- 205) Cadman RV, Lemanske RF Jr, Evans MD, Jackson DJ, Gern JE, Sorkness RL, Fain SB. Pulmonary ³He magnetic resonance imaging of childhood asthma. *J Allergy Clin Immunol*. 2013; **131**(2): 369-76.
- 206) Svenningsen S, Kirby M, Starr D, Leary D, Wheatley A, Maksym GN, McCormack DG, Parraga G. Hyperpolarized ³He and ¹²⁹Xe MRI: Differences in asthma before bronchodilation. *J Magn Reson Imaging*. 2013; **38**(6): 1521-30.
- 207) Svenningsen S, Kirby M, Starr D, Coxson HO, Paterson NA, McCormack DG, Parraga G. What are ventilation defects in asthma? *Thorax*. 2014; **69**(1): 63-71.

- 208) Tzeng YS, Lutchen K, Albert M. The difference in ventilation heterogeneity between asthmatic and healthy subjects quantified using hyperpolarized ³He MRI. *J Appl Physiol*. 2009; **106**(3): 813-22.
- 209) Deninger AJ, Månsson S, Petersson JS, Pettersson G, Magnusson P, Svensson J, Fridlund B, Hansson G, Erjefeldt I, Wollmer P, Golman K. Quantitative measurement of regional lung ventilation using ³He MRI. *Magn Reson Med*. 2002; **48**(2): 223-32.
- 210) Deppe MH, Parra-Robles J, Ajraoui S, Wild JM. Combined measurement of pulmonary inert gas washout and regional ventilation heterogeneity by MR of a single dose of hyperpolarized ³He. *Magn Reson Med*. 2011; **65**(4): 1075-83.
- 211) Tawhai M, Clark A, Donovan G, Burrowes K. Computational modeling of airway and pulmonary vascular structure and function: development of a "lung physiome". *Crit Rev Biomed Eng*. 2011; **39**(4): 319-36.
- 212) Burrowes KS, De Backer J, Smallwood R, Sterk PJ, Gut I, Wirix-Speetjens R, Siddiqui S, Owers-Bradley J, Wild J, Maier D, Brightling CE, AirPROM Consortium. Multiscale computational models of the airways to unravel the pathophysiological mechanisms in asthma and chronic obstructive pulmonary disease (AirPROM). *Interface Focus*. 2013; **3**(2): 20120057.
- 213) Mitchell JH, Hoffman EA, Tawhai MH. Relating indices of inert gas washout to localised bronchoconstriction. *Respir Physiol Neurobiol*. 2012; **183**(3): 224-33.
- 214) Leary D, Winkler T, Braune A, Maksym GN. Effects of airway tree asymmetry on the emergence and spatial persistence of ventilation defects. *J Appl Physiol*. 2014; **117**(4): 353-62.
- 215) Miller MR, Hankinson J, Brusasco V, Burgos F, Casaburi R, Coates A, Crapo R, Enright P, van der Grinten CP, Gustafsson P, Jensen R, Johnson DC, MacIntyre N, McKay R, Navajas D, Pedersen OF, Pellegrino R, Viegi G, Wanger J;

- ATS/ERS Task Force. Standardisation of spirometry. *Eur Respir J* 2005; **26**(2): 319-338.
- 216) Quanjer PhH. Standardized lung function testing. *Eur Respir J*. 1993; **6**(Suppl 16): 3-120s.
- 217) Macintyre N, Crapo RO, Viegi G, Johnson DC, van der Grinten CP, Brusasco V, Burgos F, Casaburi R, Coates A, Enright P, Gustafsson P, Hankinson J, Jensen R, McKay R, Miller MR, Navajas D, Pedersen OF, Pellegrino R, Wanger J. Standardisation of the single-breath determination of carbon monoxide uptake in the lung. *Eur Respir J* 2005; **26**(4): 720-735.
- 218) Innovision A/S 2007. Innocor Service Manual. Available from www.innovision.dk
- 219) Darling RC, Cournand A, Richards DW. Studies on the intrapulmonary mixture of gases III. An open circuit method for measuring residual air. *J Clin Invest*. 1940; **19**(4): 609-18.
- 220) Gustafsson PM, Robinson PD, Gilljam M, Lindblad A, Houlitz BK. Slow and fast lung compartments in cystic fibrosis measured by nitrogen multiple-breath washout. *J Appl Physiol*. 2014; **117**(7): 720-9.
- 221) Fowler WS, Cornish ER, Kety SS. Lung function studies VIII. Analysis of alveolar ventilation by pulmonary N₂ clearance curves. *J Clin Invest*. 1952; **31**(3): 40-50.
- 222) Dirksen A, Dijkman JH, Madsen F, Stoel B, Hutchison DC, Ulrik CS, Skovgaard LT, Kok-Jensen A, Rudolphus A, Seersholm N, Vrooman HA, Reiber JH, Hansen NC, Heckscher T, Viskum K, Stolk J. A randomized clinical trial of alpha(1)-antitrypsin augmentation therapy. *Am J Respir Crit Care Med*. 1999; **160**(5 Pt 1): 1468-72.

- 223) Hashemi RH, Bradley WG, Lisanti CJ. MRI: The basics. 3rd edition. Philadelphia: Lippincott, Williams & Wilkins, 2010.
- 224) Durand D, Guillot G, Darrasse L, Tastevin G, Nacher PJ, Vignaud A, Vattolo D, Bittoun J. CPMG measurements and ultrafast imaging in human lungs with hyperpolarized helium-3 at low field (0.1 T). *Magn Reson Med.* 2002; **47**(1): 75-81.
- 225) Wang C, Miller GW, Altes TA, de Lange EE, Cates GD Jr, Mugler JP 3rd. Time dependence of ³He diffusion in the human lung: measurement in the long-time regime using stimulated echoes. *Magn Reson Med.* 2006; **56**(2): 296-309.
- 226) Stolz E, Meyerhoff M, Bigelow N, Leduc M, Nacher PJ, Tastevin G. High nuclear polarization in ³He and ³He-⁴He gas mixtures by optical pumping with a laser diode. *Appl Phys B.* 1996; **63**(6): 629-33.
- 227) Bland JM, Altman DG. Statistical methods for assessing agreement between two methods of clinical measurement. *Lancet* 1986; **1**(8476): 307-10.
- 228) Pittman JE, Johnson RC, Jones PW, Davis SD. Variability of a closed, rebreathing setup for multiple breath wash-out testing in children. *Pediatr Pulmonol.* 2012; **47**(12): 1242-50.
- 229) Seitz AE, Olivier KN, Adjemian J, Holland SM, Prevots R. Trends in bronchiectasis among medicare beneficiaries in the United States, 2000 to 2007. *Chest.* 2012; **142**(2): 432-9.
- 230) Weycker D, Edelsberg J, Oster G, Tino G. Prevalence and economic burden of bronchiectasis. *Clin Pulm Med.* 2005; **12**(4): 205-9.
- 231) McShane PJ, Naureckas ET, Tino G, Strek ME. Non-cystic fibrosis bronchiectasis. *Am J Respir Crit Care Med.* 2013; **188**(6): 647-56.

- 232) De Soyza A, Brown JS, Loebinger MR; Bronchiectasis Research & Academic Network. Research priorities in bronchiectasis. *Thorax*. 2013; **68**(7): 695-6.
- 233) Horsley A. Lung clearance index in the assessment of airways disease. *Resp Med*. 2009; **103**(6): 793-9.
- 234) Amin R, Subbarao P, Jabar A, Balkovec S, Jensen R, Kerrigan S, Gustafsson P, Ratjen F. Hypertonic saline improves the LCI in paediatric patients with CF with normal lung function. *Thorax*. 2010; **65**(5): 379-83.
- 235) Amin R, Subbarao P, Lou W, Jabar A, Balkovec S, Jensen R, Kerrigan S, Gustafsson P, Ratjen F. The effect of dornase alfa on ventilation inhomogeneity in patients with cystic fibrosis. *Eur Respir J*. 2011; **37**(4): 806-12.
- 236) Horsley AR, Davies JC, Gray RD, Macleod KA, Donovan J, Aziz ZA, Bell NJ, Rainer M, Mt-Isa S, Voase N, Dewar MH, Saunders C, Gibson JS, Parra-Leiton J, Larsen MD, Jeswiet S, Soussi S, Bakar Y, Meister MG, Tyler P, Doherty A, Hansell DM, Ashby D, Hyde SC, Gill DR, Greening AP, Porteous DJ, Innes JA, Boyd AC, Griesenbach U, Cunningham S, Alton EW. Changes in physiological, functional and structural markers of cystic fibrosis lung disease with treatment of a pulmonary exacerbation. *Thorax*. 2013; **68**(6): 532-9.
- 237) Rowan SA, Bradley JM, Bradbury I, Lawson J, Lynch T, Gustafsson P, Horsley A, O'Neill K, Ennis M, Elborn JS. Lung clearance index is a repeatable and sensitive indicator of radiological changes in bronchiectasis. *Am J Respir Crit Care Med*. 2014; **189**(5): 586-92.
- 238) Lee TW, Brownlee KG, Conway SP, Denton M, Littlewood JM. Evaluation of a new definition for chronic *Pseudomonas aeruginosa* infection in cystic fibrosis patients. *J Cyst Fibros*. 2003; **2**(1): 29-34.
- 239) Belessis Y, Dixon B, Hawkins G, Pereira J, Peat J, MacDonald R, Field P, Numa A, Morton J, Lui K, Jaffe A. Early cystic fibrosis lung disease detected by

- bronchoalveolar lavage and lung clearance index. *Am J Respir Crit Care Med*. 2012; **185**(8): 862-73.
- 240) Martínez-García MA, Soler-Cataluña JJ, Perpiñá-Tordera M, Román-Sánchez P, Soriano J. Factors associated with lung function decline in adult patients with stable non-cystic fibrosis bronchiectasis. *Chest*. 2007; **132**(5): 1565-72.
- 241) Larsson A, Jonmarker C, Werner O. Ventilation inhomogeneity during controlled ventilation. Which index should be used? *J Appl Physiol*. 1988; **65**(5): 2030-9.
- 242) Wagner PD. Information content of the multibreath nitrogen washout. *J Appl Physiol*. 1979; **46**(3): 579-87.
- 243) Kapitan KS. Information content of the multibreath nitrogen washout: effects of experimental error. *J Appl Physiol*. 1990; **68**(4): 1621-7.
- 244) Whiteley JP, Gavaghan DJ, Hahn CE. A mathematical evaluation of the multiple breath nitrogen washout (MBNW) technique and the multiple inert gas elimination technique (MIGET). *J Theor Biol*. 1998; **194**(4): 517-39.
- 245) Safonoff I, Emmanuel GE. The effect of Pendelluft and dead space on nitrogen clearance: mathematical and experimental models and their application to the study of the distribution of ventilation. *J Clin Invest*. 1967; **46**(10): 1683-93.
- 246) Verbanck S, Thompson BR, Schuermans D, Kalsi H, Biddiscombe M, Stuart-Andrews C, Hanon S, Van Muylem A, Paiva M, Vincken W, Usmani O. Ventilation heterogeneity in the acinar and conductive zones of the normal ageing lung. *Thorax*. 2012; **67**(9): 789-95.
- 247) Prisk GK, Elliott AR, Guy HJ, Verbanck S, Paiva M, West JB. Multiple-breath washin of helium and sulfur hexafluoride in sustained microgravity. *J Appl Physiol*. 1998; **84**(1): 244-52.

- 248) British Guideline on the Management of Asthma. British Thoracic Society/Scottish Intercollegiate Guidelines Network 2008. Available from: <http://www.brit-thoracic.org.uk/guidelines/asthma-guidelines.aspx>.
- 249) Balbi B, Pignatti P, Corradi M, Baiardi P, Bianchi L, Brunetti G, Radaeli A, Moscato G, Mutti A, Spanevello A, Malerba M. Bronchoalveolar lavage, sputum and exhaled clinically relevant inflammatory markers: values in healthy adults. *Eur Respir J*. 2007; **30**(4): 769-81.
- 250) Juniper EF, Svensson K, Mörk AC, Ståhl E. Measurement properties and interpretation of three shortened versions of the asthma control questionnaire. *Respir Med*. 2005; **99**(5): 553-8.
- 251) Kirkwood BR, Sterne JAC. *Essential Medical Statistics*, 2nd ed. Oxford: Blackwell Publishing Ltd., 2003. pp 420-421.
- 252) Yamaguchi M, Niimi A, Ueda T, Takemura M, Matsuoka H, Jinnai M, Otsuka K, Oguma T, Takeda T, Ito I, Matsumoto H, Hirai T, Chin K, Mishima M. Effect of inhaled corticosteroids on small airways in asthma: investigation using impulse oscillometry. *Pulm Pharmacol Ther*. 2009; **22**(4): 326-32.
- 253) Heaney LG, Brightling CE, Menzies-Gow A, Stevenson M, Niven RM; British Thoracic Society Difficult Asthma Network. Refractory asthma in the UK: cross-sectional findings from a UK multicentre registry. *Thorax*. 2010; **65**(9): 787-94.
- 254) Pellegrino R, Viegi G, Brusasco V, Crapo RO, Burgos F, Casaburi R, Coates A, van der Grinten CP, Gustafsson P, Hankinson J, Jensen R, Johnson DC, MacIntyre N, McKay R, Miller MR, Navajas D, Pedersen OF, Wanger J. Interpretative strategies for lung function tests. *Eur Respir J*. 2005; **26**(5): 948-68.
- 255) LaPrad AS, Lutchen KR. Respiratory impedance measurements for assessment of lung mechanics: Focus on asthma. *Respir Physiol Neurobiol*. 2008; **163**(1-3): 64-73.

- 256) Thorpe CW, Bates JH. Effect of stochastic heterogeneity on lung impedance during acute bronchoconstriction: a model analysis. *J Appl Physiol*. 1997; **82**(5): 1616-25.
- 257) Reddel HK, Taylor DR, Bateman ED, Boulet LP, Boushey HA, Busse WW, Casale TB, Chanez P, Enright PL, Gibson PG, de Jongste JC, Kerstjens HA, Lazarus SC, Levy ML, O'Byrne PM, Partridge MR, Pavord ID, Sears MR, Sterk PJ, Stoloff SW, Sullivan SD, Szeffler SJ, Thomas MD, Wenzel SE; American Thoracic Society/European Respiratory Society Task Force on Asthma Control and Exacerbations. An official American Thoracic Society/European Respiratory Society statement: asthma control and exacerbations: standardizing endpoints for clinical asthma trials and clinical practice. *Am J Respir Crit Care Med*. 2009; **180**(1): 59-99.
- 258) Juniper EF, Buist AS, Cox FM, Ferrie PJ, King DR. Validation of a standardized version of the Asthma Quality of Life Questionnaire. *Chest* 1999; **115**(5): 1265-1270.
- 259) Moy ML, Israel E, Weiss ST, Juniper EF, Drazen JM; NHBLI Asthma Clinical Research Network. Clinical predictors of health-related quality of life depend on asthma severity. *Am J Respir Crit Care Med*. 2001; **163**(4): 924-9.
- 260) Scichilone N, Marchese R, Soresi S, Interrante A, Togias A, Bellia V. Deep inspiration-induced changes in lung volume decrease with severity of asthma. *Respir Med*. 2007; **101**(5): 951-6.
- 261) Farah CS, Kermode JA, Downie SR, Brown NJ, Hardaker KM, Berend N, King GG, Salome CM. Obesity is a determinant of asthma control independent of inflammation and lung mechanics. *Chest*. 2011; **140**(3): 659-66.
- 262) Shim YM, Burnette A, Lucas S, Herring RC, Weltman J, Patrie JT, Weltman AL, Platts-Mills TA. Physical deconditioning as a cause of breathlessness among obese adolescents with a diagnosis of asthma. *PLoS One*. 2013; **8**(4): e61022.

- 263) Thomas M, McKinley RK, Freeman E, Foy C, Price D. The prevalence of dysfunctional breathing in adults in the community with and without asthma. *Prim Care Respir J*. 2005; **14**(2): 78-82.
- 264) Balkissoon R, Kenn K. Asthma: vocal cord dysfunction (VCD) and other dysfunctional breathing disorders. *Semin Respir Crit Care Med*. 2012; **33**(6): 595-605.
- 265) Yii AC, Koh MS. A review of psychological dysfunction in asthma: affective, behavioral and cognitive factors. *J Asthma*. 2013; **50**(9): 915-21.
- 266) Chrystyn H. Anatomy and physiology in delivery: can we define our targets? *Allergy*. 1999; **54** (Suppl 49): 82-7.
- 267) Pavord ID, Pizzichini MM, Pizzichini E, Hargreave FE. The use of induced sputum to investigate airway inflammation. *Thorax*. 1997; **52**(6): 498-501.
- 268) American Thoracic Society. Proceedings of the ATS workshop on refractory asthma: current understanding, recommendations and unanswered questions. *Am J Respir Crit Care Med*. 2000; **162**(6): 2341-51.
- 269) Lahzami S, Schoeffel RE, Pechey V, Reid C, Greenwood M, Salome CM, Berend N, King GG. Small airways function declines after allogeneic haematopoietic stem cell transplantation. *Eur Respir J*. 2011; **38**(5): 1180-8.
- 270) Barnes N, Price D, Colice G, Chisholm A, Dorinsky P, Hillyer EV, Burden A, Lee AJ, Martin RJ, Roche N, von Ziegenweidt J, Israel E. Asthma control with extrafine-particle hydrofluoroalkane-beclometasone vs. large-particle chlorofluorocarbon-beclometasone: a real-world observational study. *Clin Exp Allergy*. 2011; **41**(11): 1521-32.

- 271) Usmani OS, Biddiscombe MF, Barnes PJ. Regional lung deposition and bronchodilator response as a function of beta2-agonist particle size. *Am J Respir Crit Care Med.* 2005; **172**(12): 1497-504.
- 272) Vos W, De Backer J, Poli G, De Volder A, Ghys L, Van Holsbeke C, Vinchurkar S, De Backer L, De Backer W. Novel functional imaging of changes in small airways of patients treated with extrafine beclomethasone/formoterol. *Respiration.* 2013; **86**(5): 393-401.
- 273) Leach CL, Bethke TD, Boudreau RJ, Hasselquist BE, Drollmann A, Davidson P, Wurst W. Two-dimensional and three-dimensional imaging show ciclesonide has high lung deposition and peripheral distribution: a nonrandomized study in healthy volunteers. *J Aerosol Med.* 2006; **19**(2): 117-26.
- 274) Leach CL, Kuehl PJ, Chand R, Ketai L, Norenberg JP, McDonald JD. Characterization of respiratory deposition of fluticasone-salmeterol hydrofluoroalkane-134a and hydrofluoroalkane-134a beclomethasone in asthmatic patients. *Ann Allergy Asthma Immunol.* 2012; **108**(3): 195-200.
- 275) Newman S, Salmon A, Nave R, Drollmann A. High lung deposition of ^{99m}Tc-labeled ciclesonide administered via HFA-MDI to patients with asthma. *Respir Med.* 2006; **100**(3): 375-84.
- 276) Verbanck S, Paiva M. Effective axial diffusion in an expansile alveolar duct model. *Respir Physiol.* 1988; **73**(2): 273-8.
- 277) Verbanck S, Paiva M. Simulation of the apparent diffusion of Helium-3 in the human acinus. *J Appl Physiol.* 2007; **103**(1): 249-54.
- 278) Verbanck S, Paiva M. Acinar determinants of the apparent diffusion coefficient for Helium-3. *J Appl Physiol.* 2010; **108**(4): 793-9.

- 279) Hajari AJ, Yablonskiy DA, Sukstanskii AL, Quirk JD, Conradi MS, Woods JC. Morphometric changes in the human pulmonary acinus during inflation. *J Appl Physiol*. 2012; **112**(6): 937-43.
- 280) McDonough JE, Yuan R, Suzuki M, Seyednejad N, Elliott WM, Sanchez PG, Wright AC, Gefter WB, Litzky L, Coxson HO, Paré PD, Sin DD, Pierce RA, Woods JC, McWilliams AM, Mayo JR, Lam SC, Cooper JD, Hogg JC. Small-airway obstruction and emphysema in chronic obstructive pulmonary disease. *N Engl J Med*. 2011; **365**(17): 1567-75.
- 281) Green RH, Brightling CE, McKenna S, Hargadon B, Parker D, Bradding P, Wardlaw AJ, Pavord ID. Asthma exacerbations and sputum eosinophil counts: a randomised controlled trial. *Lancet*. 2002; **360**(9347): 1715-21.
- 282) Hirai H, Tanaka K, Yoshie O, Ogawa K, Kenmotsu K, Takamori Y, Ichimasa M, Sugamura K, Nakamura M, Takano S, Nagata K. Prostaglandin D2 selectively induces chemotaxis in T helper type 2 cells, eosinophils, and basophils via seven-transmembrane receptor CRTH2. *J Exp Med*. 2001; **193**(2): 255-61.
- 283) Xue L, Barrow A, Pettipher R. Novel function of CRTH2 in preventing apoptosis of human Th2 cells through activation of the phosphatidylinositol 3-kinase pathway. *J Immunol*. 2009; **182**(12): 7580-6.
- 284) Xue L, Gyles SL, Wetley FR, Gazi L, Townsend E, Hunter MG, Pettipher R. Prostaglandin D2 causes preferential induction of proinflammatory Th2 cytokine production through an action on chemoattractant receptor-like molecule expressed on Th2 cells. *J Immunol*. 2005; **175**(10): 6531-6.
- 285) Gervais FG, Cruz RP, Chateaufneuf A, Gale S, Sawyer N, Nantel F, Metters KM, O'Neill GP. Selective modulation of chemokinesis, degranulation, and apoptosis in eosinophils through the PGD2 receptors CRTH2 and DP. *J Allergy Clin Immunol*. 2001; **108**(6): 982-8.

- 286) Kips JC, Inman MD, Jayaram L, Bel EH, Parameswaran K, Pizzichini MM, Pavord ID, Djukanović R, Hargreave FE, Sterk PJ. The use of induced sputum in clinical trials. *Eur Respir J Suppl.* 2002; **37**: 47s-50s.
- 287) Pizzichini E, Leff JA, Reiss TF, Hendeles L, Boulet LP, Wei LX, Efthimiadis AE, Zhang J, Hargreave FE. Montelukast reduces airway eosinophilic inflammation in asthma: a randomized, controlled trial. *Eur Respir J.* 1999; **14**(1): 12-8.
- 288) Jayaram L, Duong M, Pizzichini MM, Pizzichini E, Kamada D, Efthimiadis A, Hargreave FE. Failure of montelukast to reduce sputum eosinophilia in high-dose corticosteroid-dependent asthma. *Eur Respir J.* 2005; **25**(1): 41-6.
- 289) Barnes N, Pavord I, Chuchalin A, Bell J, Hunter M, Lewis T, Parker D, Payton M, Collins LP, Pettipher R, Steiner J, Perkins CM. A randomized, double-blind, placebo-controlled study of the CRTH2 antagonist OC000459 in moderate persistent asthma. *Clin Exp Allergy.* 2012; **42**(1): 38-48.
- 290) Busse WW, Wenzel SE, Meltzer EO, Kerwin EM, Liu MC, Zhang N, Chon Y, Budelsky AL, Lin J, Lin SL. Safety and efficacy of the prostaglandin D2 receptor antagonist AMG 853 in asthmatic patients. *J Allergy Clin Immunol.* 2013; **131**(2): 339-45.
- 291) Giesel FL, Mehndiratta A, von Tengg-Kobligk H, Schaeffer A, Teh K, Hoffman EA, Kauczor HU, van Beek EJ, Wild JM. Rapid prototyping raw models on the basis of high resolution computed tomography lung data for respiratory flow dynamics. *Acad Radiol.* 2009; **16**(4): 495-8.
- 292) Horn FC, Deppe MH, Marshall H, Parra-Robles J, Wild JM. Quantification of regional fractional ventilation in human subjects by measurement of hyperpolarized ³He washout with 2D and 3D MRI. *J Appl Physiol.* 2014; **116**(2): 129-39.